Bending moment resistance of UHPFRC-to-UHPFRC interlocking connection

A numerical, experimental and analytical study

Alef Termeer

TU Delft Delft University of Technology

Master Thesis

Bending moment resistance of UHPFRC-to-UHPFRC interlocking connection

A numerical, experimental and analytical study

by

Alef Termeer

To obtain the degree of Master of Science
In structural Engineering
at the Delft University of Technology
To be defended publicly on Thursday, June 20th, 2024, at 15:30

Student number	5415497
Master	Structural Engineering
Track	Concrete

Thesis committee	Dr. M. Luković (chair + daily supervisor)	TU Delft – Concrete Structures
	Dr. B. Šavija	TU Delft – Materials, Mechanics, Management & Design (3MD)
	Dr. Y. Xu	TU Delft – Materials, Mechanics, Management & Design (3MD)

Acknowledgements

This thesis is the product of several months of research in the final stage of the master's degree in Civil engineering at the faculty of Civil Engineering and Geosciences – Delft University of Technology. I am grateful to all those who supported me during this research.

First of all, the members of my thesis committee, helped me a lot with their critical questions and guidance during the thesis. Many thanks to my chair member, professor Mladena Luković, her interest in my thesis project has been stimulating throughout the project. Furthermore, her advice gave me confidence that I was in the right direction during this thesis. I appreciated the advice of Branko Šavija where I could always come by for some questions about the master thesis. I furthermore want to thank Yading Xu who helped me prepare the 3D printed parts.

For casting the specimens and execution of the experiments I want to thank Tom Blom, Ake Blom and Giorgos Stamoulis. They helped me with preparing the materials, casting equipment, preparing the test setup and making the DIC pattern.

Furthermore, I want to thank my professors and my fellow students. They helped me get a grasp of challenging subjects and made my time on the TU-Delft overall pleasant.

Also, I thank my family and my parents. I appreciate all the (financial) help and assistance they gave me during my time at university in Delft.

Abstract

In the realm of civil engineering, projects often entail the assembly of diverse components at various stages of construction. This introduces interfaces between elements, where load transfer has to be considered. This load transfer is governed by dowel action (reinforcement), mechanical interlock, adhesive bonding and friction (1). Without reinforcement, most concrete interfaces are brittle and weak (2). However, these interfaces do not have to be brittle and weak. Several naturally occurring hard materials have interfaces that exhibit tough failures, such as bone, tooth and sea shells (3). This toughness arises from geometric interlock and friction between the materials. Implementing these natural occurring interlocks could enhance the performance of connection, making them more ductile.

In this study, the focus is on applying one of these naturally occurring interface designs into a concrete-to-concrete connection subjected to bending conditions. This naturally occurring design is based on jigsaw-like contours built from a series of arcs of circles with radii R_1 and R_2, which are blended tangentially at locations defined by angles θ_1 and θ_2 (3). This interlock exhibits two distinctive stable positions during pullout, making the interlocking design bistable (3). In this thesis, the attempt is made to make a similar interlocking connection from a cement-based material. In order to enhance ductility without implementing reinforcement, Ultra-High Performance Fiber-Reinforced Concrete (UHPFRC) is used. UHPFRC is a fibre-reinforced concrete known for its higher tensile strength compared to traditional concrete and strain-hardening behaviour (4).

The performed literature study was focused on three areas; The jigsaw-like interlock with bistable behaviour reported for different type of materials, the behaviour of the interlocks under three-point bending and the UHPFRC, and its composition and mechanical properties.

After the literature study, a numerical study is conducted. The interface is loaded in a three-point bending test. This model is then used to design and optimize the interface profile, which results in three designs where two UHPFRC specimens are connected with five interlocks. With these three designs, a parametric study is made, where the role of the following parameters is investigated:

- E-modulus
- Strength of the material (both elastic and plastic strength)
- Friction coefficient
- Plastic strain at peak resistance

The fracture behaviour of the interlocking connection under a bending moment in the numerical analyses consists of several phases: First a relatively linear loading phase occurs, where some geometric hardening behaviour is observed. The tabs slide out slightly without significant plastic deformation. Then, the lowest (half) tab of the sequence shows plastic deformation, causing a small change in the force-displacement curve. At the peak load, the middle tabs break, leading to a drop in total resistance. After this drop, the force-displacement curve shows a rather horizontal trend.

Of the three designs tested, the smoothest interlocking design, where the surface between interfaces has minimal deviation, yields the most ductile response. This design is achieved by a low θ_1 and θ_2 and radii close to a quarter of the width of the interlocking tab. Furthermore, the conducted parameter study reveals that a more ductile behaviour of the interlocking connection is obtained when a material is used that has a low elastic modulus, higher tensile strength, lower friction coefficient or more plastic strain. This increase in ductility was accompanied by a decrease in strength.

In order to improve the ductility of the connection, apart from material properties of UHPFRC, two additional designs where investigated: one where the interlock itself is composed of one circle instead of two, and one that includes a gap in the interlock.

The interlocking design composed of a single circle exhibits a more ductile response than the bistable interlocking design with two circles. This can be attributed to the tab having two contact points instead of four, resulting in increased pull out.

Incorporating a gap in the interlocking design slightly improves the ductility of the connection, while causing a small decrease in strength. This is because the interlocking tabs become easier to compress. The depth of this gap plays a critical role. A shallow gap results in a failure similar to the bistable design, while a deeper gap leads to a bending failure in the tips of the design.

From this numerical study, three designs are selected for experimental research. These designs are scaled with a factor of 1/3 to align with current research, and ease of fabrication. These designs are:

1. A bistable interlocking design with two circles.
2. The same interlocking design, but the second circle (denoted with a radii of R_2) is removed.
3. The same interlocking design as the first, but with the incorporation of a gap.

All designs are created in two stages. Initially, a 3D printed mould is placed within a rectangular mould. Concrete is cast against the walls of the rectangular mould and the 3D printed mould, thereby forming the first half of the interlocking connection. After the specimen has hardened, UHPFRC is poured against the surface of the casted specimen. Before pouring, a layer of oil has been applied to the surface of the casted specimen, creating a layer of oil between the interfaces and thus preventing any chemical bond.

The measured strength ranges from approximately 3% to 9.5% compared to that of a monolithic connection, whereas the numerical model predicts a range of 30% to 32%. This discrepancy is likely due to poor fibre distribution, fabrication issues with the small design and the oil lowering the friction coefficient. Closer alignment between experiments and the numerical model is observed when the friction coefficient in the numerical model is lowered.

Regarding the failure sequence, Design 1 aligns well with expectations, with the lowest (half) tab failing first, followed by cracks in the middle tabs. Design 2 does not align with the numerical model, as the connection fail before the tabs pullout, with a vertical crack through the interface and interlocking tabs. Design 3 aligns well with the numerical model, as for both the cracks congregates near the gaps.

In all designs, both in the experimental and numerical studies, it was observed that the tabs break with minimal pullout of the interlocks for two main reasons. First, the material used (UHPFRC) has a high elastic modulus compared to its tensile strength. This high elastic modulus means that more force is required to compress the interlocking tabs, resulting in high tensile stress and thus cracks with minimal pullout. Second, due to the rotation introduced by the bending moment the individual interlocking tabs experience an off-centre force, where the frictional and contact forces are higher on either the top or bottom. This introduces a bending moment in addition to the tensile force, weakening the tabs, leading to faster failure and reduced pullout.

Finally, an analytical model is developed to approximate the behaviour of the connection. While this approximation comes close to the numerical model, it deviates when the total top displacement increases (for example when the elastic modulus is decreased). This is probably caused by the following assumptions made:

1. No bending moment in the tabs, only a full tensional force
2. No plastic hardening with a linear plastic softening phase
3. Rigid body movement
4. Compressive point and the rotation points stay the same

To conclude, it was observed that a lower elastic modulus, reduced friction coefficient, higher strength or smoother design increases ductility of the interlocking connection but decreases the bending resistance. Experimental investigations of the selected designs reveals discrepancies with numerical predictions, attributed to factors such as poor fibre distribution, lower friction and fabrication issues due to the small designs. It is argued that a lower friction coefficient in the numerical model, and an increase in size of the experiments would solve these discrepancies.

For the researched interlocking design, where the connection is made out of UHPFRC, an optimal design is achieved with a very smooth interlocking design. This is accomplished by a low θ_1 and θ_2 and radii close to a quarter of the width of the interlocking tab.

For further research, a different design is recommended. As previously mentioned, this interlocking design does not seem to behave optimally under bending conditions, as it introduces an off-centre force due to the rotation. To address this, a bent interlocking tab is suggested. This bent interlocking tab follows the rotation, thereby decreasing the inequality of the frictional and contact forces and thus reducing the introduced bending moment. This design showed a more ductile response without significantly decreasing the strength.

Additionally, the developed analytical could be used for further research, as it showed promise but exhibited limitations with higher displacements. To enhance this model, the assumptions made should be revised and corrected in the calculation. This could include incorporating a bending moment in the tabs, adding a plastic hardening phase or accounting for non-rigid movement.

Contents

List of symbols and abbreviations

R_1, R_2	The radius of interlocking circles
f, μ_k	Friction coefficient
P	Contact force
E	Elastic Modulus
ε_{tc}	Elastic strain
ε_{tp}	Plastic strain
$Delta$	Compression of the interlocking tabs
θ_i	The local angle of the interlocking tabs
$\theta_{1,2}$	Interlocking angle
σ_{tc}	Maximum elastic stress
σ_{tp}	Maximum plastic stress
L	Length of the tabs
W	Width of the tabs
z_n	Distance between interlocking tabs and compressive zone
F_{max}	Maximum tensional resistance for a tab
UHPFRC	Ultra-high-performance fibre-reinforced concrete

1. Introduction

1.1. Background and problem definition

In the realm of civil engineering, projects often involve the assembly of diverse components at various stages of construction. When it comes to concrete-to-concrete connections, the most common connections are precast-to-precast connections and precast-to-in-situ connections. Examples of these types of connections are:

- repair and strengthening of existing reinforced concrete members using new concrete layers.
- supplement of precast elements with additional concrete cast at the site.
- all situations at the site where, due to interruptions in the erection process, new concrete is cast against already completely hardened concrete.
- post-installed concrete elements attached to existing elements.

For all of these examples, load transfer between interfaces has to be considered. This load transfer is governed by dowel action (reinforcement), mechanical interlock, adhesive bonding and friction (1). Without reinforcement, most concrete interfaces are rigid and weak (2). However, these interfaces do not have to be rigid and weak. Several naturally occurring hard materials have interfaces that exhibit tough failures, such as bone, tooth and sea shells (3). The microstructures with these interfaces are illustrated in Figure 1. The toughness of these interfaces arises from the geometric interlock of the materials. By interlocking in a certain way, the interfaces become strong and tough.

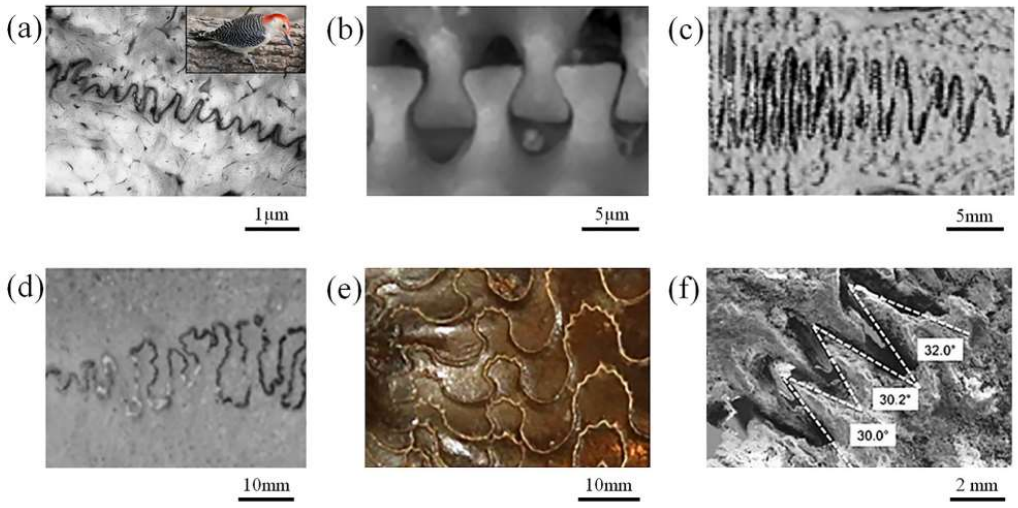

Figure 1 Examples of sutured interfaces in nature: (a) red-bellied woodpecker (Melanerpes carolinus) beak (adapted from (5)), (b) linking girdles of diatoms (adapted from (6)), (c) marine threespine stickleback (Gasterosteus aculeatus) (adapted from (7)), (d) Pan troglodytes cranial sutures (adapted from (8)), (e) Ammonite shell (Ceratitic ammonoid) with intricate suture e lines (6) (f) osteoderms of a leatherback sea turtle shell (adapted from (9)).

The implementation of these naturally occurring interlocking interfaces into concrete-to-concrete connections holds immense promise. These interlocks could spread deformation and dissipate energy (3), potentially creating a ductile and strong connection without the need for reinforcement.

Recent research efforts have delved into the exploration and testing of various shapes of naturally occurring interlocks. One of these interlocking designs is based on jigsaw-like contours built from a series of arcs of circles with radii R_1 and R_2, which are blended tangentially at locations defined by angles θ_1 and θ_2 (3). This interlock exhibits two distinctive stable positions during pullout, making the interlocking design bistable. The design of this interlock is seen in Figure 2.

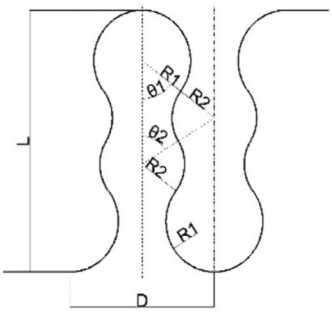

Figure 2 example of a bistable interlock between 2 elements (10)

In this study, the focus is on applying this jigsaw-like interlocking design into a connection subjected to a bending moment, as for example seen in Figure 3. This interlocking connection is made with a cement-based material. Traditional concrete cannot be used because of its low tensile strength, this will make the interlocking design break before pullout. So, Ultra-High Performance Fiber-Reinforced Concrete (UHPFRC) is used. UHPFRC is a fibre-reinforced concrete known for its higher tensile strength and strain-hardening behaviour compared to traditional concrete (4).

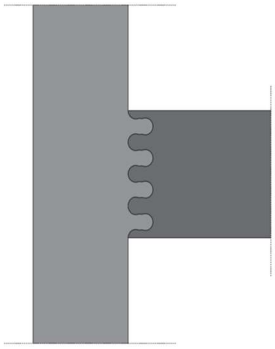

Figure 3 Design of a beam with bistable interlocking

While the implementation of these interlocks in connections shows theoretical promise, practical implementation and empirical validation are lacking. This research seeks to bridge this gap by exploring the mechanical behaviours and structural performance of an interface made with interlocks between UHPFRC elements.

1.2. Objective and Research questions

This research aims to investigate the performance of interlocked connections made with Ultra-High-Performance Fiber-Reinforced Concrete under a bending moment. The design of the interlocking tabs is based on a bistable design.

The research questions in this study are:

1. What are the governing parameters that influence the ductility and strength of the interlocking connection?
2. How closely does the numerical model correlate with the experimental results?
3. Which is the type of failure mechanism that occurs?
4. Is an analytical solution applicable in assessing the behaviour of the interlocking connection?

1.3. Research Methodology

To realize the goal of the research, a numerical study has been made with Abaqus. This model is verified by earlier experimental research. After the model is verified, three bistable designs are chosen to model numerically. These designs are again verified with a hand calculation and according to earlier research. Then, a parametric analysis is done for these three designs, where the following parameters are varied:

- E-modulus
- Strength of the material (both elastic and plastic strength)
- Friction coefficient
- Plastic strain at peak resistance
- One circle instead of two
- Incorporating a gap in the design

The best-performing designs (based on strength and toughness) from this parameter study was chosen for an experimental test. This experimental test is a three-point bending test. The results were documented via Digital Image Correlation (DIC) and Linear Variable Differential Transformers (LVDTs).

Then, an analytical solution is tried to approximate the behaviour of the bistable interlocking connection loaded with a bending moment. This is done to give insights into the failure mechanism of the interlocking connection.

1.4. Outline of master thesis

Besides the introduction (chapter 1), the report is divided into 7 chapters. These are in order:

- Chapter 2 introduces and explains the (bistable) interlocking design, discussing what to expect from a (partly) clamped connection made with interlocking tabs and the properties of Ultra-High-Performance Fiber-Reinforced-Concrete (UHPFRC)
- Chapter 3 presents the methods and approach to this research.
- Chapter 4 presents a numerical study of the designs with a parameter study. Alternative designs are made, modelled, and studied in this chapter.
- Chapter 5 presents the experimental results from the lab.
- Chapter 6 presents an analytical approach to this design.
- Chapter 7 provides a discussion regarding the research questions.
- Chapter 8 provides conclusions drawn from this study and gives recommendations for further research

The outline of this thesis is seen in Figure 4.

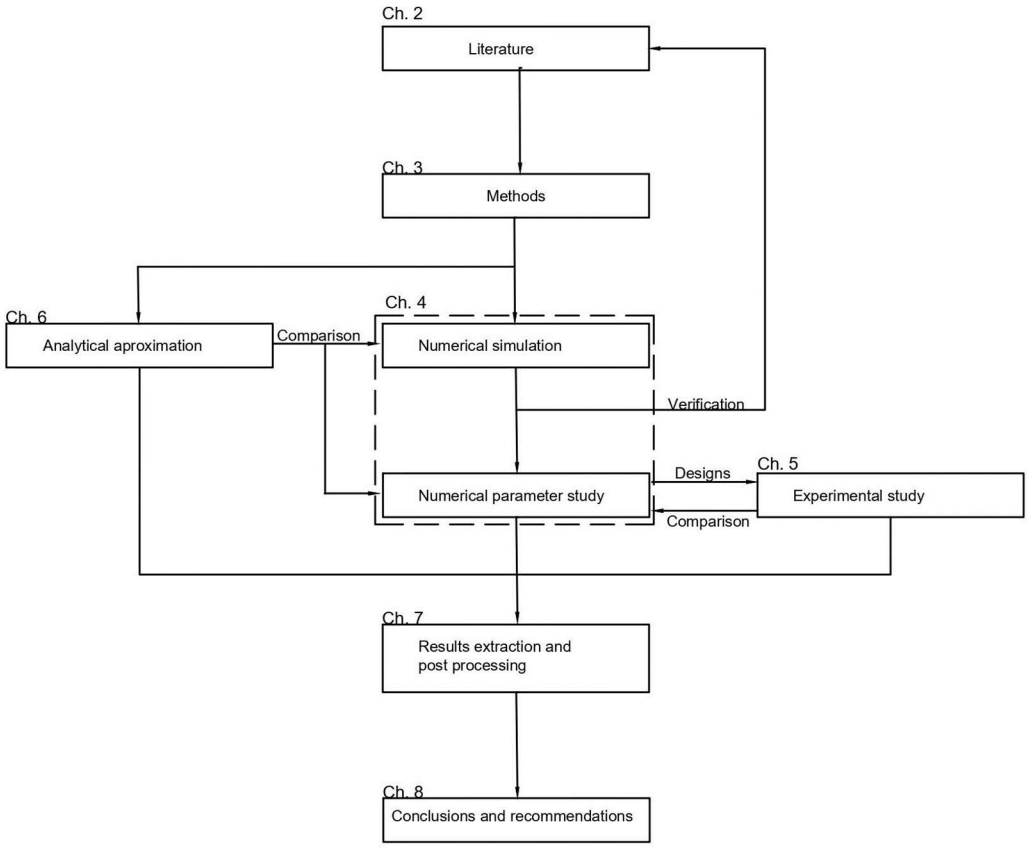

Figure 4 outline of the master thesis

2. Literature review

2.1. Introduction

Several unknown parameters are crucial for the calculation of the interlocking joints. These parameters are needed for both the finite element analyses, experimental testing and the analytical approximation. These parameters are:

1. The properties and design of the jigsaw-like, bistable interlocking design.
2. Interlocking structures under a 3-point bending test.
3. The properties of the material used UHPFRC (Ultra-High Performance Fiber-Reinforced Concrete).

Firstly, the interlocking shape is defined and researched. This is the tensile behaviour of this interlock and how to calculate the interlock analytically. Secondly, the usage of interlocks with a 3-point bending test is researched. What to expect of the connection and how to design it. Furthermore, an analytical solution is discussed for a connection under a bending moment and tension. Finally, the material used is shortly discussed. These are the tensile properties of UHPFRC, elastic modulus and compressive strength.

2.2. The interlocking design

The new bistable interlocked materials (BIMs) are based on controlled separation and pullout of sutures with well-controlled geometries. The design of the suture is based on jigsaw-like contours built from a series of arcs of circles with radii R_1 and R_2, which are blended tangentially at locations defined by angles θ_1 and θ_2 seen in Figure 5. Round features were chosen for their simplicity and also because they reduce stress concentrations in the solid. (3).

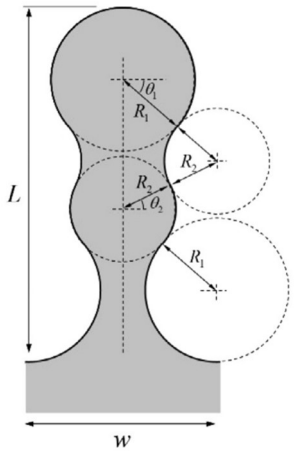

Figure 5 Overview of the design of bistable interlocked tabs; The profile of the tab consists of arcs of circles or radii R1 and R2 which blend according to angle ϑ1. Angle ϑ2 is dependent on R1, R2 and ϑ1 (3).

To illustrate a typical sequence of a pull-out test and traction-displacement curves, a graph can be seen in Figure 6. This graph demonstrates that a proper design of bistable interlocking can spread deformation and frictional energy dissipation throughout an otherwise brittle material (3).

The pull-out mechanism can be described in 3 stages, these are:

An initial configuration is the first stable configuration (stage I). From this stage the tab are pulled out due to a tensile stress (stage I→II), the pull-out is resisted by geometric interface, contact stress and friction acting at two pairs of contact points (11).

If a certain threshold of pull-out stress is applied the tabs move to the second stable phase. This phase is stage II inFigure 6. If compression is applied the tab could go back to the initial configuration (stage I). Alternatively, if more tension would be applied (stage II→III) it will be pulled out completely (stage III).

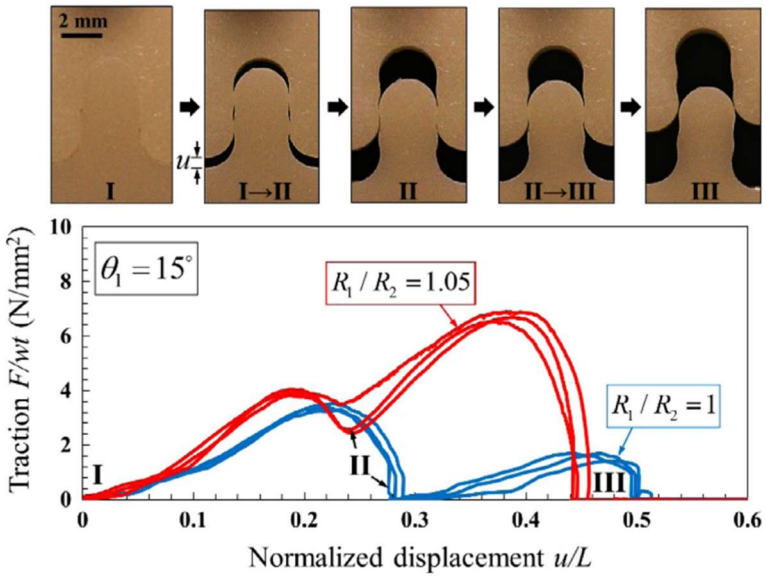

Figure 6 . Tensile behaviour of individual bistable interlocked tabs; Typical sequence of a pullout test and traction–displacement curves of the bistable interlocked tab. The shape of the pullout curve can be tuned with R1/R2 and ϑ1. In particular, the second peak can be made stronger by increasing R1/R2. (11)

The traction against normalized displacement of a numerical model is seen in Figure 7 and shows excellent agreement between the finite elements and analytical predictions in terms of pullout response and maximum tensile stress within the material. (11). This indicates that the bistable interlocking joint can be modelled with a numerical model.

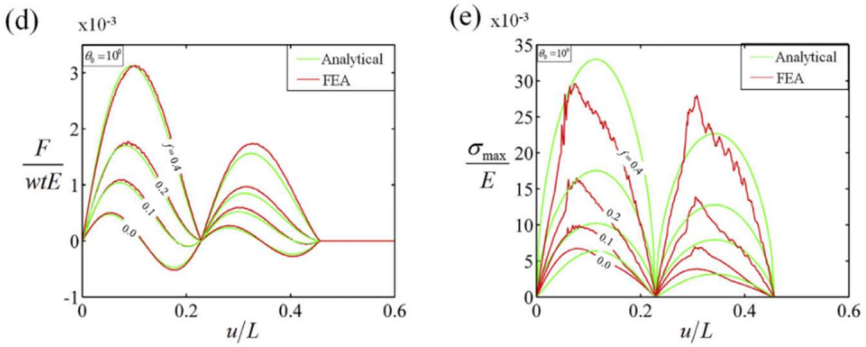

Figure 7 traction and stresses as a function of pullout distance showing a good agreement between the analytical and finite elements results (11).

To indicate what the important parameters are, a parametric study is done (12). This parametric study is done with the design of one circle instead of two. The results of this parameter study are seen in Figure 8. In these results, it can be noted that a high $\frac{\sigma}{E}$ ($\frac{resistance}{elastic\ modulus}$) ratio gives an overall stronger and tougher structure with a higher maximum extension. An overall smoother tab (a low-angle θ) gives an overall higher energy absorption with a relatively low impact on the total strength.

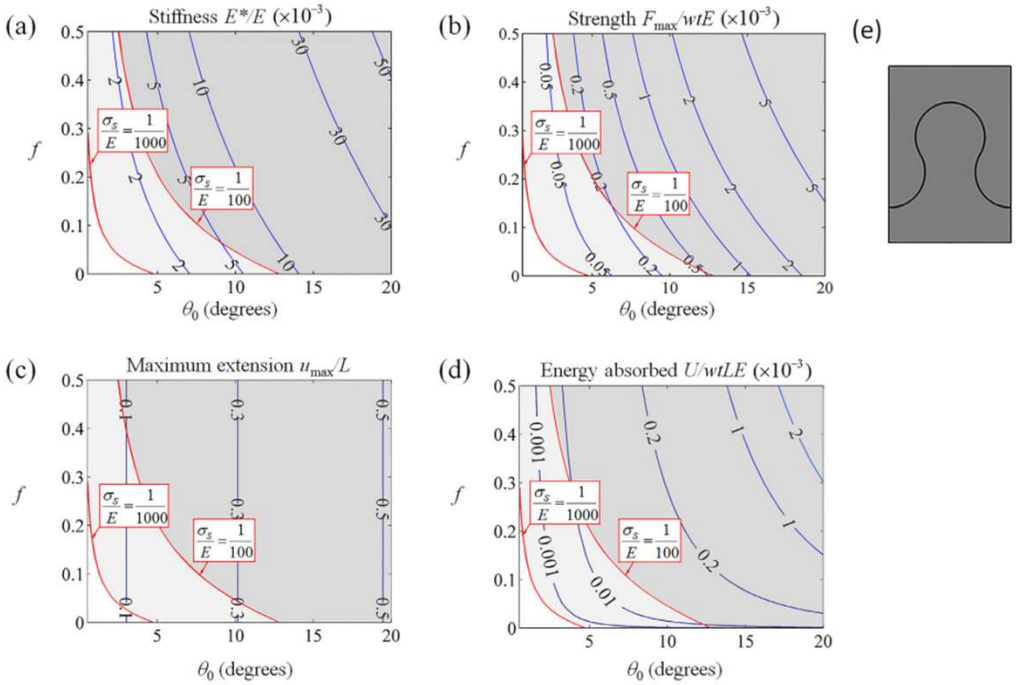

Figure 8 Mechanical properties of the jigsaw suture as a function of interlocking angle ϑ 0 and friction coefficient f. The properties are plotted as blue contour lines on each of the diagrams. (a) stiffness; (b) strength; (c) maximum extension and (d) energy absorbed. In each case, the red lines show limit designs for which the tensile strength of the material is reached (σs /E = 1/100 and σs/E = 1/1000). (e) A sketch of the interlocking suture. (12)

The mechanical force needed for a pullout should not be higher than the resistance of the tab. If this were the case the interlocking tabs would break. This can be avoided by changing the interlocking angle of the tab as seen in Figure 9. This means that if the properties of the material itself introduce a high mechanical resistance (a high $\frac{resistance}{elastic\ modulus}$ ratio) the interlocking angle (θ) should be low.

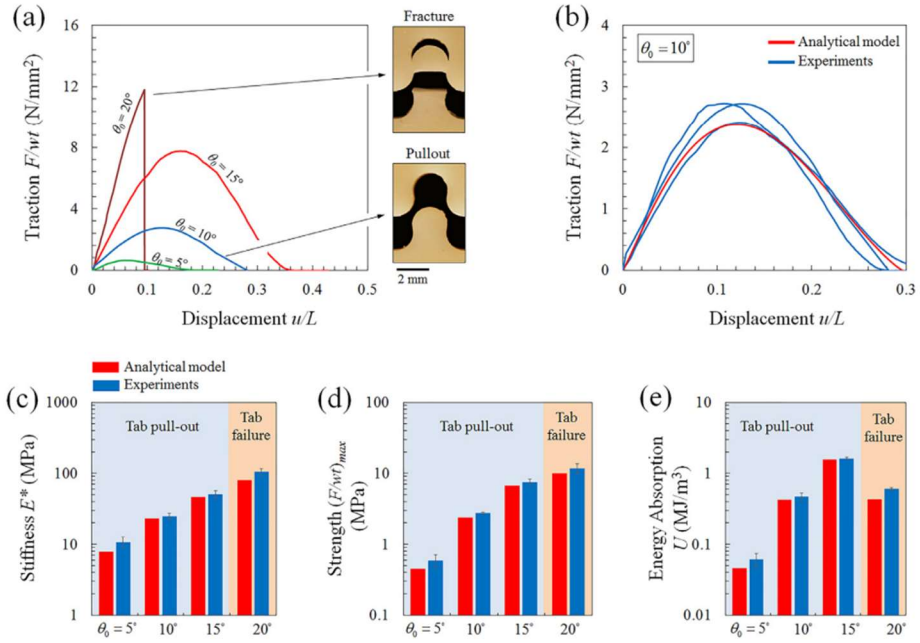

Figure 9 Experiments on the jigsaw interlocked tabs. (a) representative pullout curves with different interlocking angles (ϑ 0 = 5°, 10°, 15°, 20°), with representative pictures showing two different failure modes: tab pullout and fracture. (b) comparison between simulation and experimental pullout curves for sutures with ϑ 0 = 10°. (c) stiffness, (d) strength, and (e) energy absorption of the suture as a function of interlocking angle, with comparisons from models. (12).

These interlocking tabs can be analytically calculated using the formula for the non-Euclidian contact force of 2 disks (13). This formula describes the total compression (δ in mm) in relation to the force, radius, elastic modulus and thickness. The formula is seen below, here it is noted that this formula ignores the poison ratio, It is argued that this should not influence the results significantly (12).

$$\delta = \frac{a^2}{2R}\left[2\ln\left(\frac{4R}{a}\right) - 1\right] \quad 2.1$$

$$a^2 = \frac{4PR}{\pi tE} \quad 2.2$$

Where:

- δ= Total compression of the discs in mm
- R= Radius of the discs. It is suggested that with 2 circles with different radius, the adjusted radius is $R = \frac{1}{R_1} + \frac{1}{R_2}$ (3)
- t= the thickness of the tab.
- P= contact force.
- E= elastic modulus

The contact force P can be calculated numerically in relation to δ. After this the δ can be expressed in θ (the angle the two circles have). Here θ_0 is the original angle.

$$\delta = 2R\left(1 - \frac{\cos(\theta_0)}{\cos(\theta)}\right) \quad 2.3$$

Then the pullout force can be calculated. A design with one circle has two contact points, so the force has to be doubled. A design with two circles has four contact points so here it has to be quadrupled. The formula is seen below, here f is the friction coefficient.

$$F_{single} = 2P\big(\sin(\theta) + f\cos(\theta)\big) \quad 2.4$$

$$F_{double} = 4P\big(\sin(\theta) + f\cos(\theta)\big) \quad 2.5$$

A sketch is made and can be seen in Figure 10.

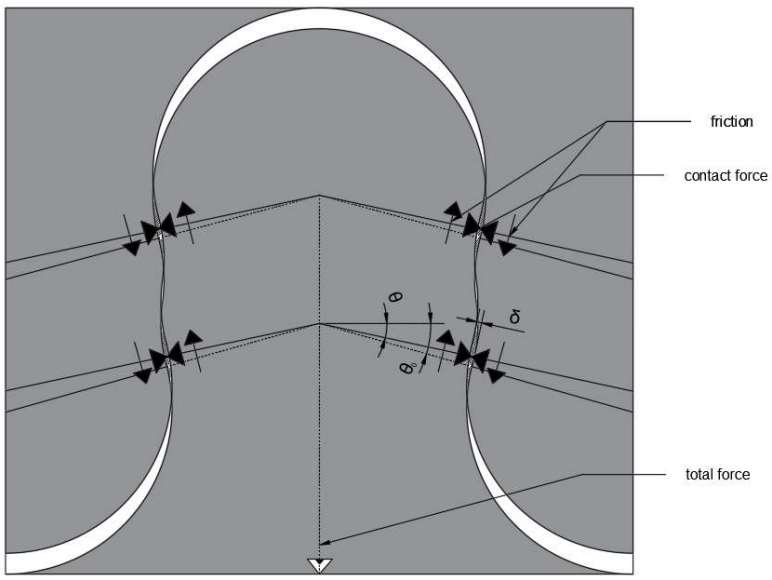

Figure 10 sketch of the forces in the tab

2.3. Interlocking structures under a 3-point bending test

It is noted that the experiments in chapter 2.2 where only tested in tension. The interlocking shapes are likely to behave differently when loaded with a bending moment. To indicate how these interlocking connections will act under a bending moment, prior experiments of 3-point bending tests with interlocks are discussed, the test setup can be seen in Figure 11.

Figure 11 3 three-point bending setup with specimen (14)

The first test that is discussed is with PLA (polylactic acid thermoplastic). This is one of the most popular thermoplastic materials used in FDM (Fused Deposition Modelling) printing due to their biodegradability and ease of printing, good strength, and stiffness (14).

The outcome of these tests is seen in Figure 13. The tests S1, S2 and S3 are for different tab sizes. The sizes and shapes of the tabs are described in Figure 12 and Table 1. The tabs are also tested on an angle. These angles are noted in Figure 13.

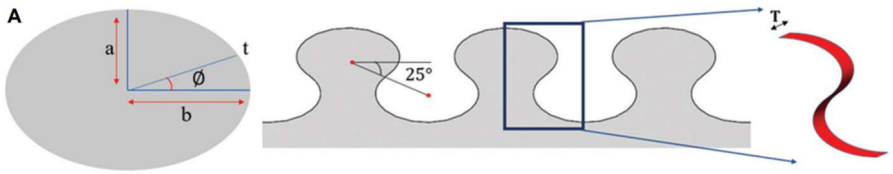

Figure 12 schematic design of the suture tabs (14)

Specimen	Length (mm)	Width (mm)	Thickness (mm)	Minor radius, a (mm)	Major radius, b (mm)	Print layer height (mm)	Infill density	Number of print layers
S1	200	44	4	1.5	2.7	0.2	100%	20
S2	200	44	4	2	3.6	0.2	100%	20
S3	200	44	4	2.5	4.5	0.2	100%	20

Table 1 dimensions of the 3D printed PLA (polylactic acid thermoplastic) specimens (14)

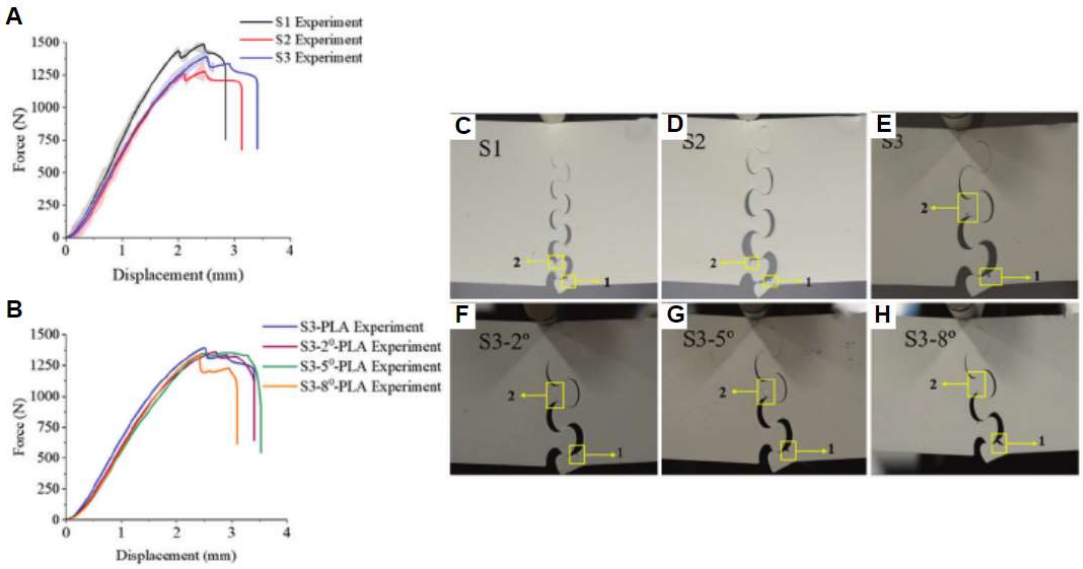

Figure 13 (A) Force-displacement curves of S1, S2, and S3. (B) Force- displacement curves of S3, S3-2°, S3-5°, and S3-8°; the failure points highlighted in yellow for (C) S1- first & second points, (D) S2 - first & second points, (E) S3 - first & second points (F) S3-2, (G) S3-5°, (H) S3-8° (14)

Here it is seen that the angle of the tabs has some influence on the total strength of the structure but not a significant amount. The modes of failure are also seen. It is suspected that the design with the bistable interlocking tabs fails in the same manner. Where the lowest tab fails first and then the 4th lowest tab noted as 2. In the same picture, it is noted that in design S3 the middle tab fails due to a bending moment.

Several parameters are compared. These are flexural strength, bending stiffness and energy absorption. These values are seen in Figure 14. The bending stiffness of each design is calculated using the force-displacement curve slope. Energy absorption is calculated using the area under the force-displacement curve. Here it seems that S1 has a higher flexural strength but the energy absorption of S3 is higher. The total bending stiffness is about the same.

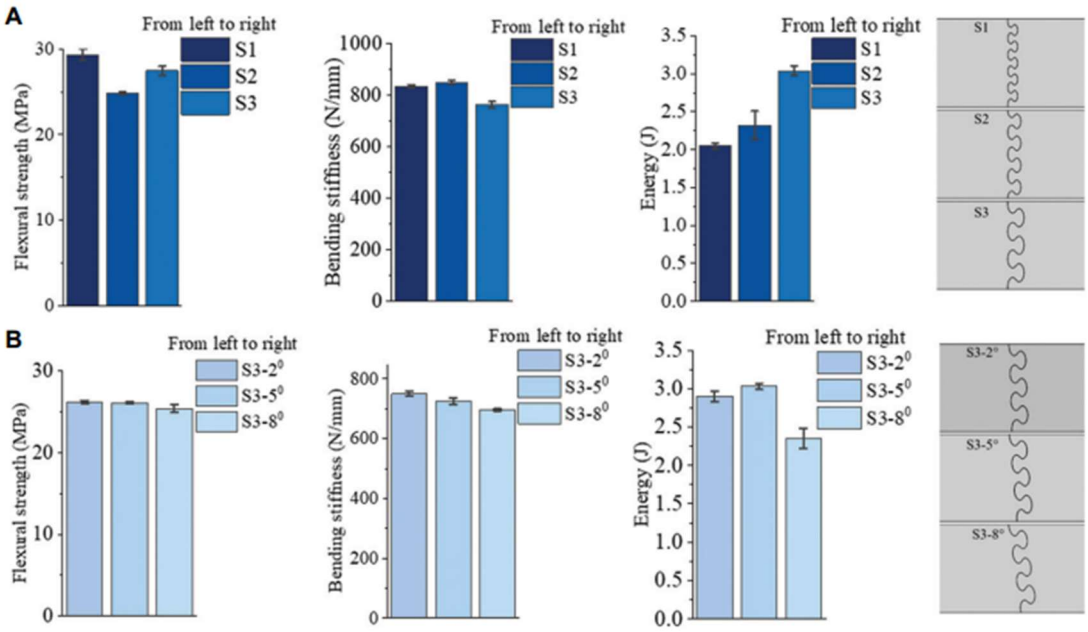

Figure 14 Flexural strength, bending stiffness and energy absorption of S1, S2 and S3. (B) Flexural strength, bending stiffness and energy absorption of S3-2º, S3-5º and S3-8º (14)

The second test that is discussed is a 3-point bending test made with VeroWhitePlus (VWP) with a soft interface layer made of TangoBlackPlus (TBP). VWP is a rigid material, and TBP is a rubbery material (15). The schematic of this specimen is seen in Figure 15. The thickness of the interface layer is noted as ST (suture thickness). The results of this 3-point bending test are seen in Figure 16. A good agreement could be observed between the experimental results and the simulation up to the first peak point (15).

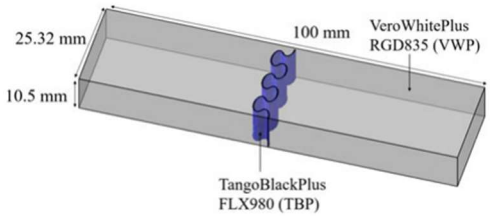

Figure 15 Schematic of a 3-point bending specimen including (15)

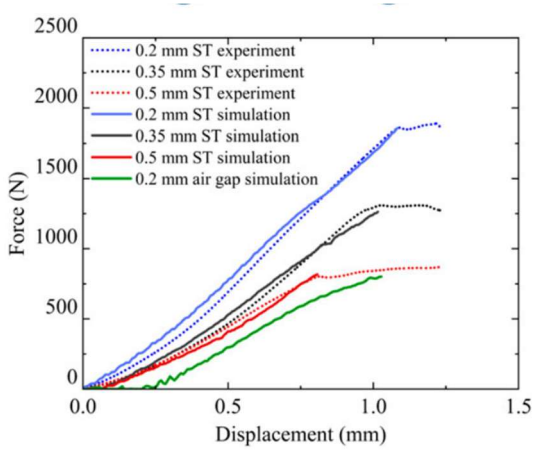

Figure 16 Experimental and simulation force-displacement results comparison, the results when 0.2 mm ST () TBP is removed and left with an air gap is also given for the comparison. (15)

With the same design, a parametric study has been done. The results of the parametric study are seen in Figure 17. The influence of changing the a:b ratio and the interlocking angle on the design are seen in Figure 18. Here It is noted that the total width of the interlocking tabs changes when the shape of the interlocks changes.

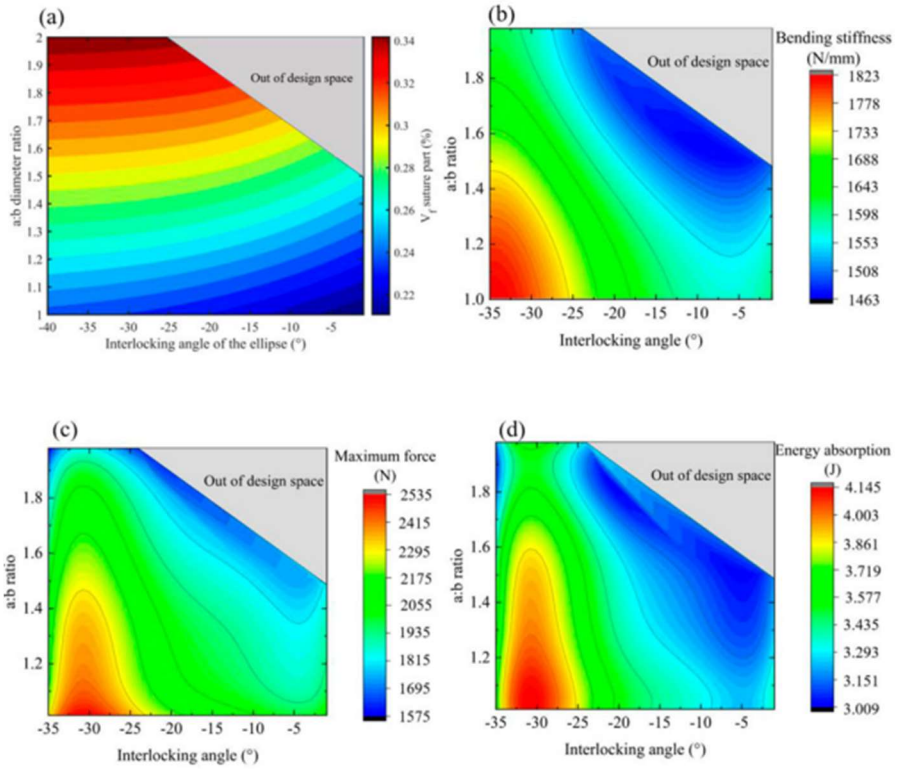

Figure 17 (a) Volume fraction of the TBP suture part when varying a:b ratios and interlocking angles, Results from the Design of Experiment (DoE), considering both TBP volume fraction and sample height conditions (b) Bending stiffness (N/mm), (c) maximum reaction force (N), (d) energy absorption (J). (15)

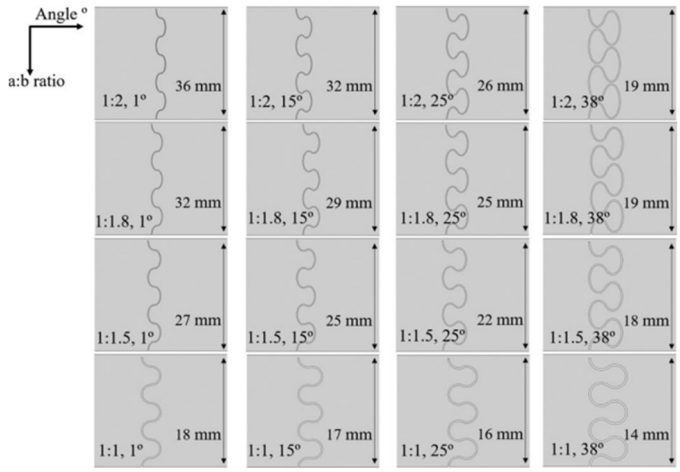

Figure 18 Effect of changing the a:b ratio and interlocking angle on the shape of the suture (15)

In summary, it can be said that with a low a:b ratio, the bending stiffness, energy absorption and the maximum reaction force increase. When decreasing the interlocking angle, the bending stiffness, energy absorption and maximum reaction force are reduced. When smaller interlocking angles are combined with larger a:b ratios, the structure becomes more flexible and deformable (15).

A similar test is analytically modelled with glass (16). In this analytical model, coordinates are given to each of these interlocking tabs. These coordinates are rotated with a rotation matrix so every tab has a given coordinate based on the rotation. This is seen in Figure 19.

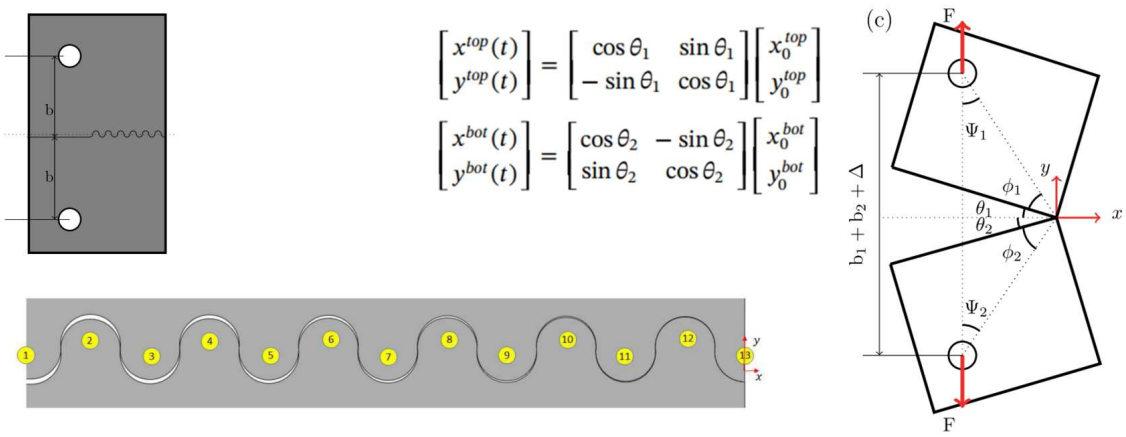

Figure 19 dimensions of the analytical solution with the formulas for positioning (16)

Then the change in distance between the tabs are calculated (δ) and the local angle of the force at the contact point(θ).

$$\delta_i = 2R - \sqrt{(y_{i+1} - y_i)^2 - (x_{i+1} - x_i)^2} \quad 2.6$$

$$\theta_i = abs\left(\tan^{-1}\left(\frac{y_{i+1} - y_i}{x_{i+1} - x_i}\right)\right) \quad 2.7$$

After this, the total contact force is calculated with the formula for the non-Euclidian contact force of 2 disks (13) (equation 2.1 and 2.2). Then, the bending resistance of the structure is calculated with the formula seen below.

$$M_z^{contact} = \sum_{i=1}^{11} p_i(\mu_k \cos(\theta_i) + \sin(\theta_i))(x_{13} - c_{xi}) \quad 2.8$$

For the design of the paper with glass (16) the force-displacement curve is plotted and seen in Figure 20

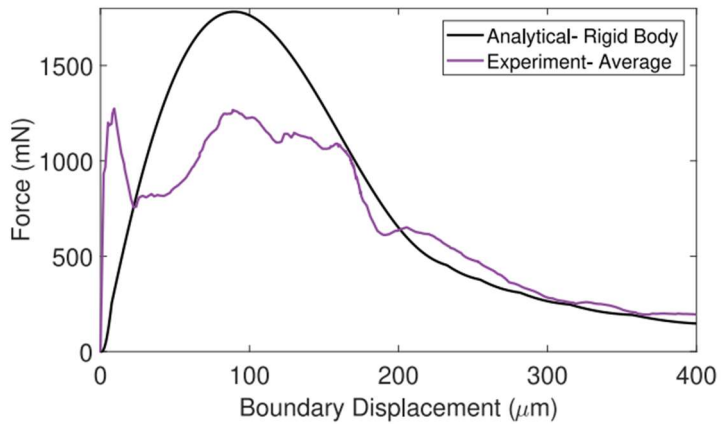

Figure 20 analytical solution of the curve without any second-order effects (16)

2.4. Properties UHPFRC

The material used in this thesis is UHPFRC (ultra-high performance fibre-reinforced concrete). UHPFRC has different properties and mix design than traditional concrete. The UHPFRC mixes typically contain 650 to 900kg/m^3 cement as well as micro silica and fine particles with a maximum grain size not

exceeding 1mm. The water/binder ratio is between 0.13 and 0.17. The components are mixed using a superplasticizer. This matrix is typically strengthened with straight steel fibres of 13mm to 15mm length (4).

The tensile behaviour of UHPFRC consists of three phases. These are (17):

- First an elastic phase up to the elastic limit stress
- Second, it goes into a strain hardening phase characterized by fibre activation accompanied by multiple fine micro-cracking of the matrix; the material still behaves like a continuum.
- The third phase starts upon the formation of a discrete macro-crack at ultimate resistance and strain softening begins. The maximum crack opening $w_{Ut,max}$ uals about half of the fiber length, i.e. 6 to 8mm. At these crack openings, no more tensile stress is transferred.

The tensile hardening and softening behaviour of UHPFRC depends on the bond, aspect ratio, content and orientation of the steel fibres (18) (19). The characteristic tensile behaviour of UHPFRC is seen in Figure 21.

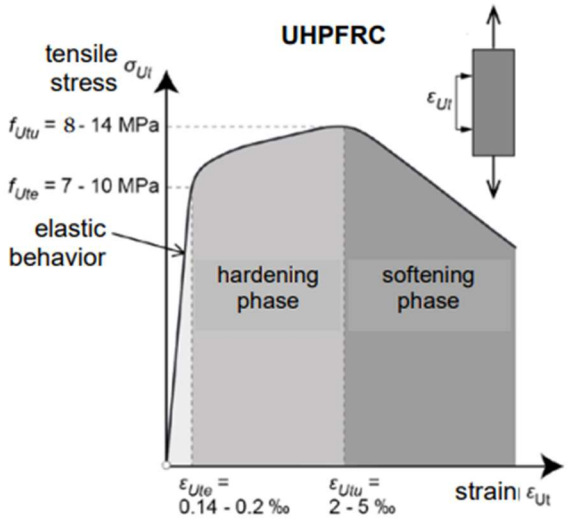

Figure 21 Characteristic tensile behaviour of UHPFRC (4)

For the numerical model, the constitutive relation can be simplified in accordance with Figure 22 (20). Where the plastic hardening and softening are linear.

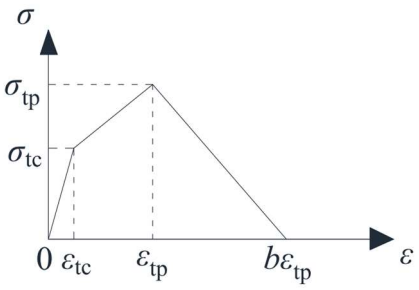

Figure 22 Simplified constitutive tensile relation of UHPFRC (20)

The tensional behaviour of UHPFRC could deviate quite a lot in relation to its mixture design. In this thesis, a mixture is used that gives the tensional behaviour described in Figure 23and Table 2 (21). The E-modulus of the UHPFRC resulting from this mixture is 45.2 GPa.

Mixture	Compressive strength (MPa)		Tensile strength (MPa)			Elastic modulus (GPa)
	0 FT cycle	30 FT cycles	f_{sp}	f_{ct}	f_{pt}	
Concrete	35.2 ± 1.5	33.8 ± 5.3	3.4 ± 0.7	-	-	35.3 ± 1.5
UHPFRC	122.4 ± 5.1	125.4 ± 8.7	-	6.9 ± 2.0	9.2 ± 2.1	45.2 ± 1.1

Table 2 Properties of the UHPFRC and traditional concrete (21)

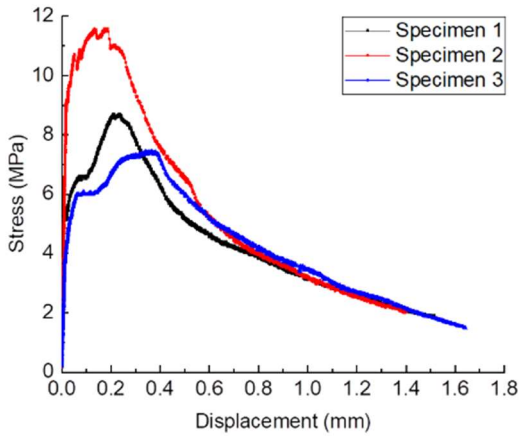

Figure 23 tensile Stress-displacement behaviour of UHPFRC, note that the LVDT displacement is obtained over 80 mm (21)

The behaviour of UHPFRC under a compressive force is characterized by a rather linear stress-strain relation until the compressive strength is reached (10).

3. Methods

3.1. Introduction

With the information described in the literature review, the design depicted in Figure 24is investigated. This design consists of 5 interlocking tabs that are placed in sequence till a connection has been created with a height of 5*w (width of the tab). 5 tabs have been chosen because when less interlocking tabs are used, the middle tab fails due to a bending moment (see Figure 13).

The shape of the interlocking tabs is designed with two circles with a certain diameter (R_1 and R_2). These circles are intersected by two other "void" circles with the same diameter. The placement of the upper void circle is determined by the angles θ_1 and θ_2 and the diameters. The lower void circle is positioned below the upper void circle and is not displaced horizontally compared to the upper void circle, and is placed on the lowest part of the interlocking shape. The total height of the interlocking tab is L.

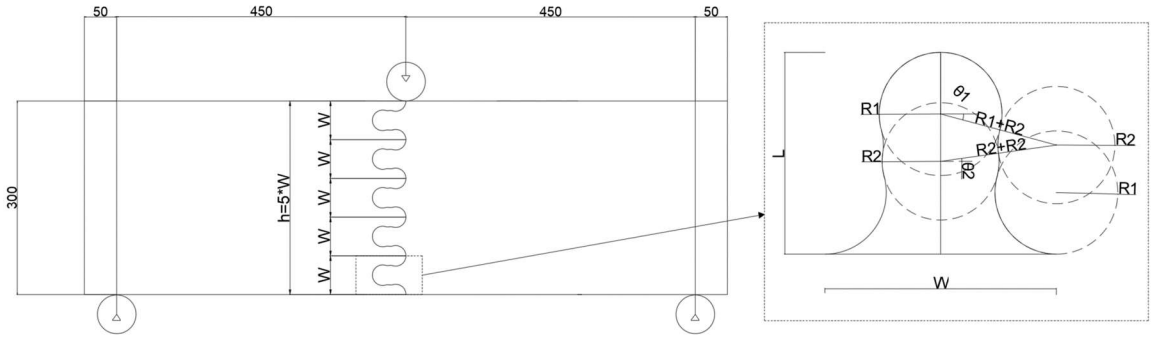

Figure 24 Design of the researched interlocking connection.

Three variations of these interlocks (the design seen in Figure 24) are researched numerically. These variations are seen in Figure 25. The parameters of these designs are described in Table 3. A sketch of the numerical model is illustrated in Figure 26. This model is based on a 3-point bending test, with a total span of 900mm. These designs are chosen for the following reasons:

- Design 1 is chosen for its stronger second stable position. Because R1 is bigger than R2, a second stronger position can occur during the pullout sequence (as indicated in Figure 6)
- Design 2 is chosen because Ultra High Performance Reinforced Concrete (UHPFRC) has a high $\frac{\sigma}{E}$ ratio. The literature suggests that a high $\frac{\sigma}{E}$ ratio the interlocking angle should be low. In this design, this is the case.
- Design 3 is chosen because it is seen that the tabs fail in the neck of the interlock. If this part would be wider, the total resistance could increase.

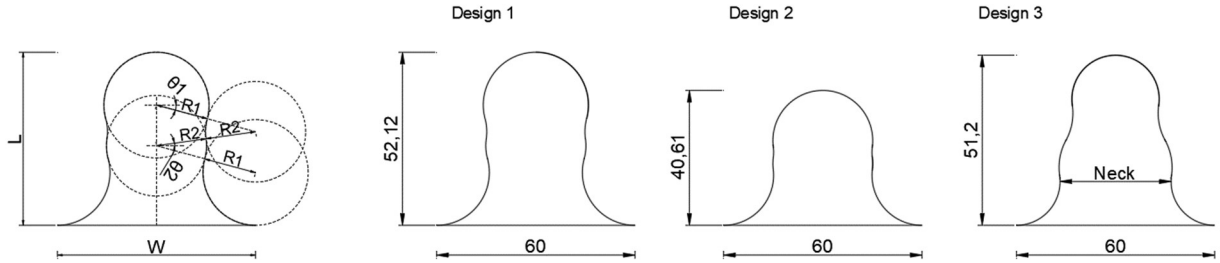

Figure 25 designs of the interlocking tabs modelled in the numerical model

	Design 1	Design 2	Design 3
θ_1	15°	6°	8°
θ_2	8°	6°	8°
R_1	15.91mm	15.1mm	13.2mm
R_2	15.15mm	15.1mm	17.1mm
L	64.64mm	40.61mm	51.2mm
W	60mm	60mm	60mm

Table 3 parameters of the designed tabs

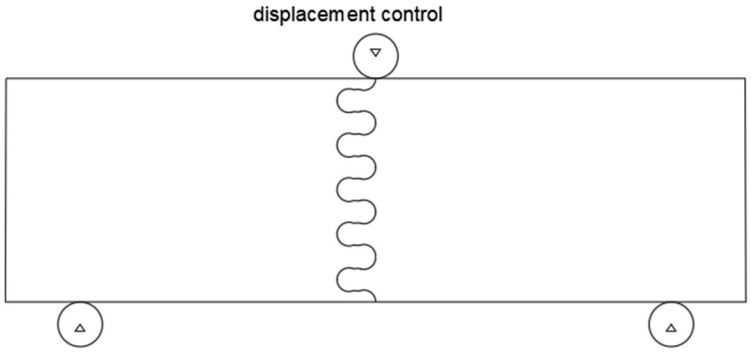

Figure 26 design of the numerical simulation

This model is verified by previous experiments and a hand calculation. After verification, a parameter/variation study is conducted to examine the effects of various parameter adjustments. The parameters that are investigated are as follows:

- E-modulus
- Strength of the material (both elastic and plastic strength)
- Friction coefficient
- Plastic strain at peak resistance

Additionally, different variations of the designs are modelled. These are:

- One circle instead of two circles
- 4-point bending test instead of a 3-point bending test
- Incorporating a gap in the design

After this, three designs are selected for experimental testing. This test is a 3-point bending test. Furthermore, the bending resistance and compressive resistance of the chosen UHPFRC mixture are measured.

3.2. Research methodology- Numerical modelling

A finite element model was made using ABAQUS/Explicit 2023 (Dassault Systems Simulia Corp., Providence, RI) to simulate the bistable interlocking structure under a three-point bending test. The parameters of this numerical model are seen in Figure 27, where the dimensions of the interlocks are described in Table 3.

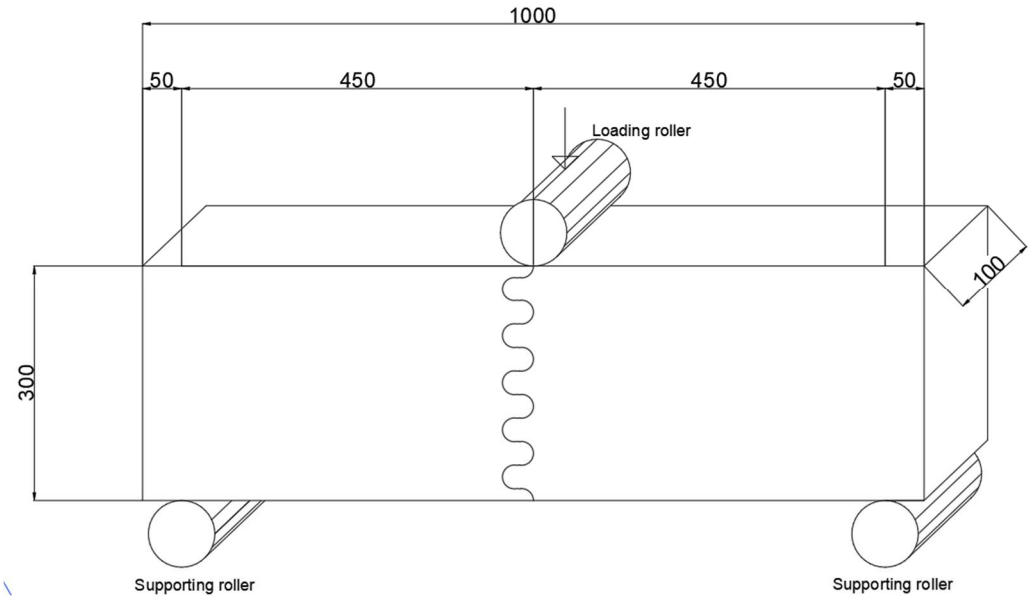

Figure 27 Parameters of the numerical model

The model consists of 5 parts; 2 beams with bistable interlocks and 3 rollers. All these individual parts are modelled as 2D planar deformable parts with a thickness of 100mm. interactions between parts are modelled with a penalty contact method. The supporting rollers are fully encastered, meaning that these rollers can't move. The load on the structure is given in displacement control. This is done by giving the loading roller a displacement of -5mm in the y direction over a certain time.

The constitutive behaviour of the material is considered to be elastic-plastic-based (20), so considering the data presented in Table 2 and the material behaviour of Figure 22, the material behaviour in the model is as illustrated in Figure 28. The compressive behaviour is modelled as perfectly elastic. It is not suspected that the compressive forces will exceed the maximum, so an elastic behaviour is accurate. These parameters are put in as concrete-damaged plastic material. This material model can accurately model UHPFRC (22).

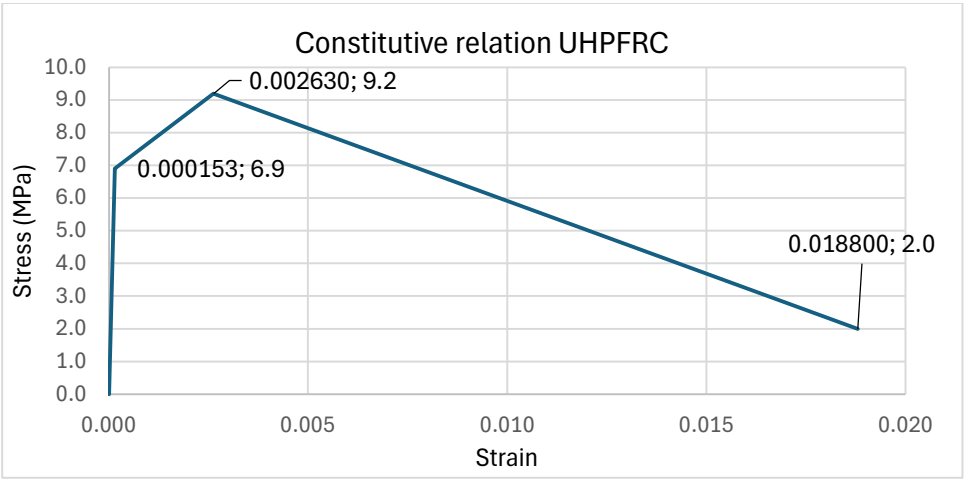

Figure 28 graph of the simplified constitutive relation based on Table 2 and the simplified constitutive behaviour(Yang, 2022)

The geometry is calculated as if the geometry is uniform, this means that any localized defects that occur during the casting process (for example bad fibre distribution) are not considered.

In Appendix A Abaqus model parameters the steps and properties of the finite element analyses are explained according to the element tree. Every parameter for the basic three designs are discussed.

3.3. Research methodology-Experimental

3.3.1. Design, materials and mix design used

One of the three designs described in the numerical model are used in the experimental research. The chosen design from the numerical model is design 2, along with 2 variations of design 2, as these designs exhibit the best results. Overall, this design seems the most ductile without losing a lot of strength.

The chosen designs are illustrated in Figure 29, and the corresponding parameters are found in Table 4. Here it is noted that these designs are smaller than in the numerical model. This is to be more in line with current research and the ease of testing and casting. The mix design used in this experiment is seen in Table 5.

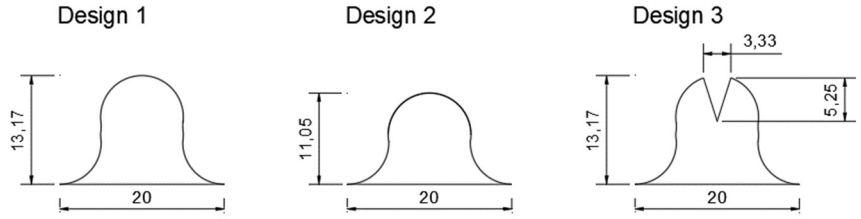

Figure 29 designs of the tabs for the experimental test.

	Design 1	Design 2	Design 3
θ_1	6	6	6
θ_2	6	6	6
R_1	5.033	-	5.033
R_2	5.033	5.033	5.033
L	13.17	11.05	13.17

Table 4 parameters of the tabs for the experimental test

Ultra-High Strength Concrete (UHSC) **w/c : 0.23** **Casting date: 23rd April 2019**		**25L**
Ingredients	**Density (kg/m3)**	**(in kg)**
CEM I 52,5 R	800.4	20.01
CEM I 42,5	69.6	1.74
Blast furnace slag	104.4	2.61
Silica fume	43.8	1.095
Water	219.945	5.49863
Superplasticizer	26.6	0.665
Sand 0,5-1,0	529.1	13.2275
Sand 0,25-0,5	318.7	7.9675
Sand 0.125-0,25	213.3	5.3325
Fibers (13 mm in length, 0.2 mm in diameter)	156.25	3.90625

Table 5 Mixture design of the UHPFRC

3.3.2. Testing procedure

3.3.2.1. 3-point bending test with bistable interlocking

To evaluate the behaviour of the interlocking structure under flexural loading, a three-point bending test was conducted following NEN-EN 14651+A1, except for the fact that the prism was 100x100x400 instead of 150x150x550-700 as specified in the NEN-standers. A span of 300 mm is adopted. The test was performed using the Instron machine in the Macrolab-TU delft, with a speed of 5 microns/sec. This test setup has a capacity of 85kN. Both supporting conditions are sliding hinges. 150x50x10 mm^3 steel

support plates are placed at the bottom of the concrete beam to prevent stress localizations in the concrete. LVDTs and Digital Image Correlation (DIC) is used to make measurements during the tests. A sketch of the setup is seen in Figure 30. The setup of the performed test is seen in Figure 31.

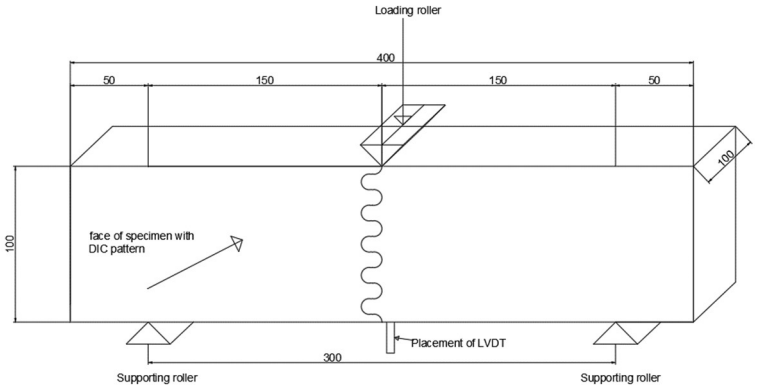

Figure 30 sketch of the 3-point bending test for the bistable interlocking joint

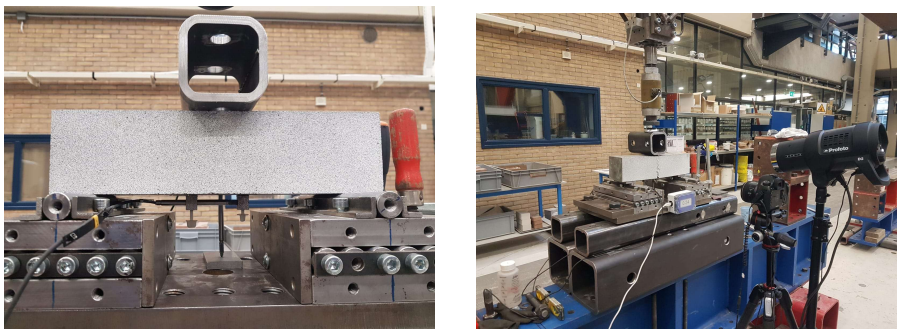

Figure 31 test setup of the 3-point bending test for the bistable interlocking joint

3.3.2.2. Bending resistance

The bending resistance is calculated with a 3-point bending test following NEN-EN 14651+A1, except for the fact that the prism was 150x40x40 instead of 150x150x550-700 as specified in the NEN-standers. The test has been performed using the Cybertronic in the Macrolab-TU delft, with a loading rate of 6.5 kN/sec. The support-to-support distance is 100mm.

3.3.2.3. Compressive strength

The compressive strength test has been performed following NEN-EN 12390-3, however, cube specimens of 40x40x40 mm3 were used. The cube specimens are reused specimens from the bending resistance test. The tests have been performed using the CYBER-TRONIC machine in the TU Delft Macrolab, with a loading rate of 6.5 kN/sec. All cube specimens have been positioned so that the load is applied perpendicularly to the direction of casting. The compressive strength of the concrete was then obtained from the maximum load sustained by the specimen, divided by the cross-sectional area of the concrete specimen.

3.3.3. Casting, demoulding and curing progress

Firstly, for the casting process, the 3D printed parts are produced. The designs are seen in Figure 32. These designs include the parts to create the gaps. The results and procedure of this printing are seen in Figure 33.

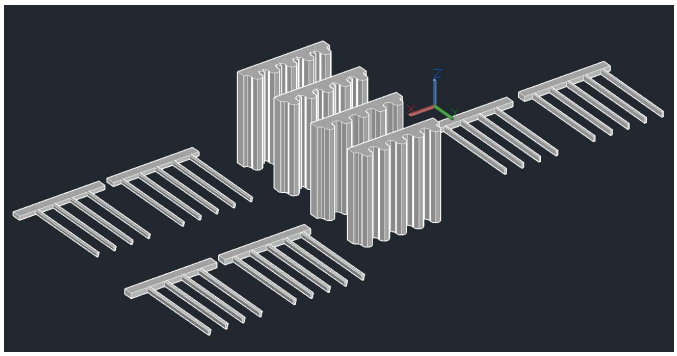

Figure 32 designs of the 3D-printed parts

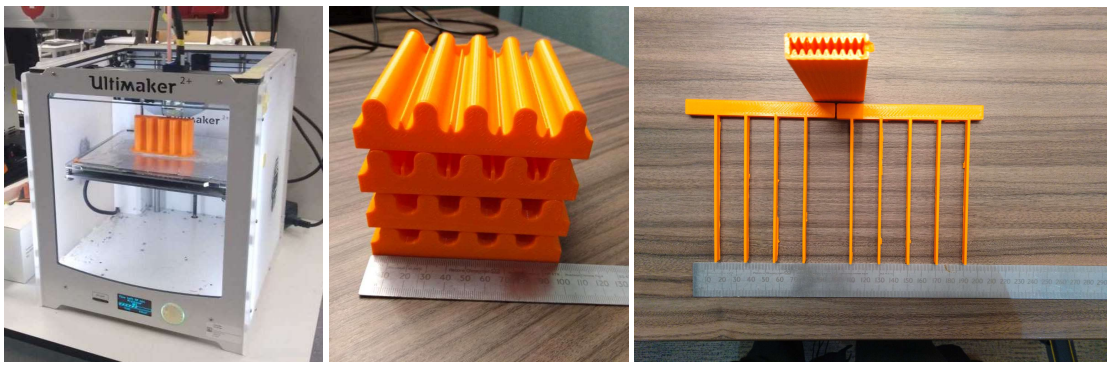

Figure 33 Production and results of the 3D printed mould. Left is the 3D printer, in the middle are the moulds for the tabs and right are the moulds for the gaps.

Then, the 3D-printed part is placed in a 400x100x100 mould, and the first element is cast. Once this has been sufficiently hardened the second part is cast against the first part. This is done using casting oil to prevent any bond between elements. The holes are created with small parts that can be pulled out. A sketch of the total process is illustrated in Figure 34. Pictures of the casting procedure are seen in Figure 35.

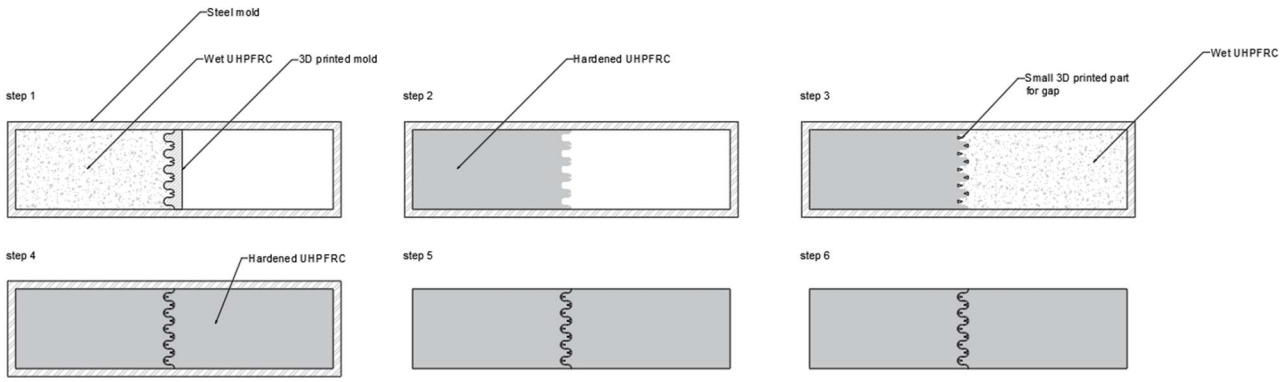

Figure 34 casting procedure of the elements

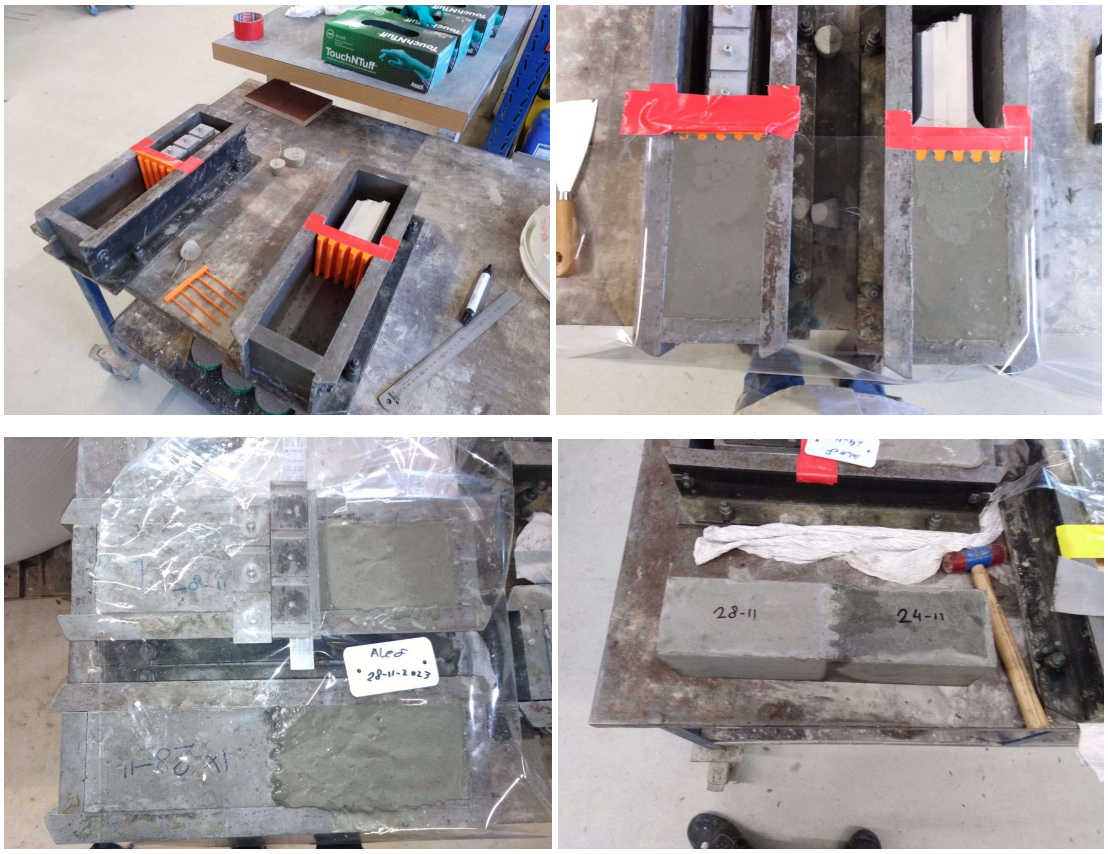

Figure 35 casting steps of the bistable interlocking joint

Additionally, prisms of 140x40x40 are cast. These prisms are made to calculate the bending resistance and the compressive resistance of the UHPFRC mixture. These prisms are seen in Figure 36.

Figure 36 small prisms for compressive and bending resistance tests

4. Numerical results

In this section, the results of the numerical simulation are presented. This simulation is made with the parameters described in the methods. Where the strength of the material are based on Ultra-High-Performance-Fibre-Reinforced Concrete (UHPFRC). This model is verified by a comparison of prior papers and a hand calculation.

After the numerical simulation, a parameter study is done. This is to examine the effects of various parameter adjustments. In this parameter study the material properties of UHPFRC is taken as a basis, where the differences are increments of these properties.

Lastly, the results are discussed and conclusions are made.

4.1. Numerical model

First, the numerical model is verified, this is done by recreating the model of Sachini (15), and comparing it to the model made with Abaqus. Then the three interlocking designs are simulated, presenting the results by force-displacement curves and snapshots from the model. Finally, the bistable design is verified by a hand calculation.

4.1.1. Verification of the Abaqus model

The connection with a 0.2mm air gap from Sachini's paper (15) is replicated using the model described in paragraph 3.2 and Appendix A. Subsequently. the force-displacement curve of this replicated model is compared to the results of the paper, as depicted in Figure 37.

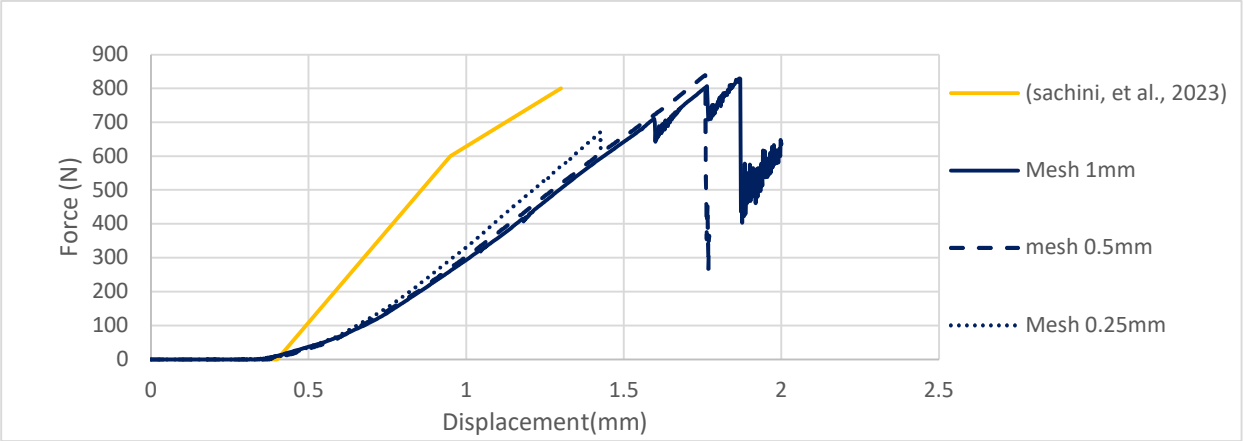

Figure 37 Comparison of the model from the paper (15) and a remake of the model from the paper with the properties of the model of this paper.

In this force-displacement curve, the behaviour of the models seems to align with the results of the paper (15). The maximum force is about the same, and the difference between displacement is negligible. This small difference could be explained by the way interactions are modelled. The made model uses the penalty contact method as a mechanical constraint formulation. The compared paper could have used the kinematic contact method (this is not stated in the paper). The penalty contact method allows some penetration of materials which could increase the total top displacement.

The von Mises stress at the point of failure can also be compared. This comparison is seen in Figure 38 and Figure 39. Here it is seen that the von Mises stresses in the paper and the made model of this paper align closely. This further indicates that the model is satisfactory.

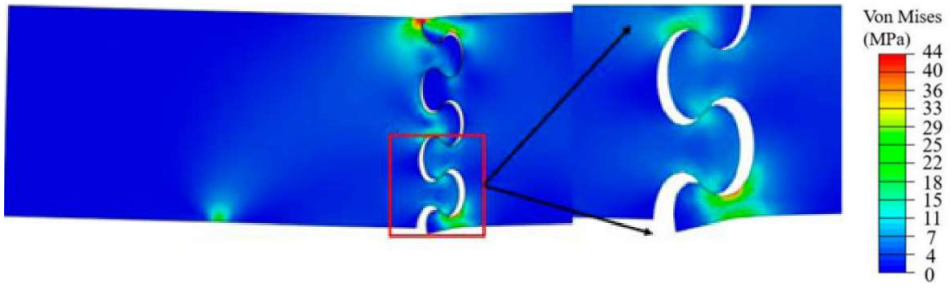

Figure 38 the Von Mises stresses of the design with a 0.2mm air gap (15) .

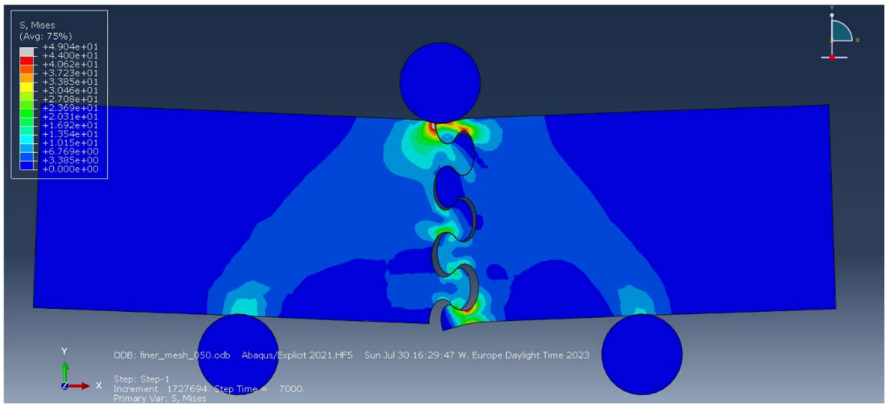

Figure 39 the Von Mises stress from the made model.

4.1.2. Results of the numerical model

Using the geometry of Figure 25 and Table 3, along with the material properties from Figure 28, numerical models of the three designs are constructed and simulated in Abaqus. The parameters of these three designs are seen in Figure 40.

Parameters of the designs

	Design 1	Design 2	Design 3
θ_1	15°	6°	8°
θ_2	8°	6°	8°
R_1	15.91mm	15.1mm	13.2mm
R_2	15.15mm	15.1mm	17.1mm
L	64.64mm	40.61mm	51.2mm
W	60mm	60mm	60mm

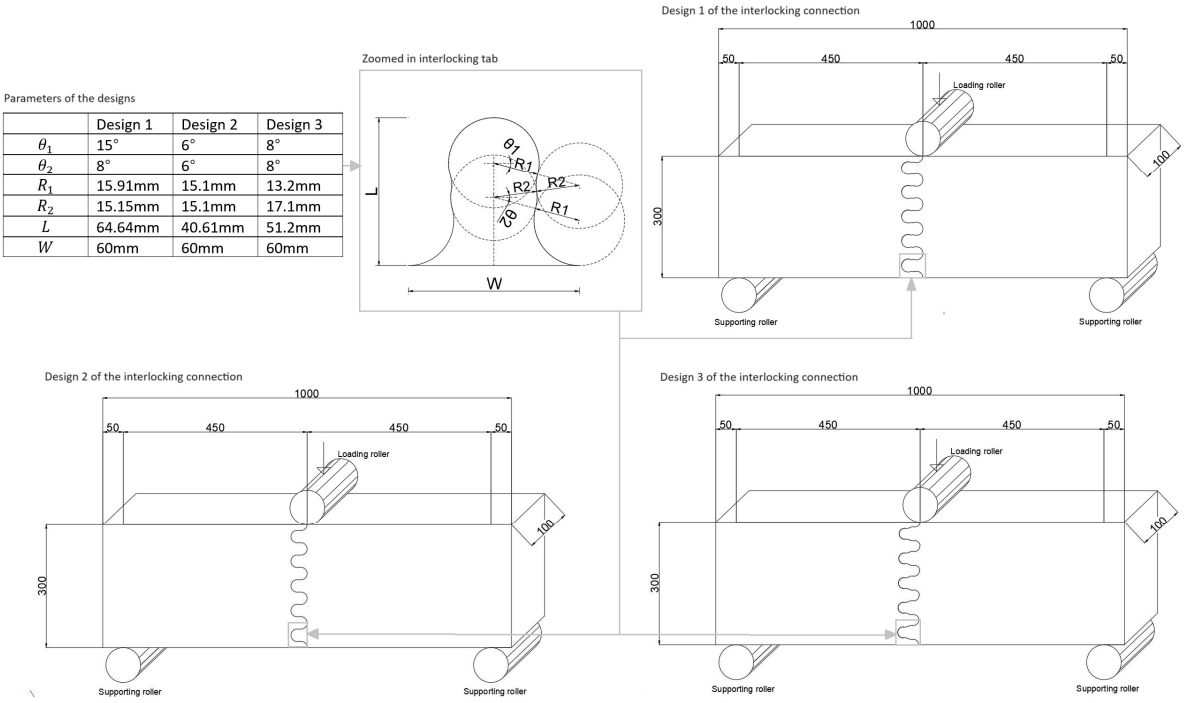

Figure 40 designs of the interlocking connection

From this, a force-displacement curve is plotted, where the force is the reaction force of the 2 lower circles, and the displacement is the total displacement of the loading roller. This force-displacement curve is seen in Figure 41.

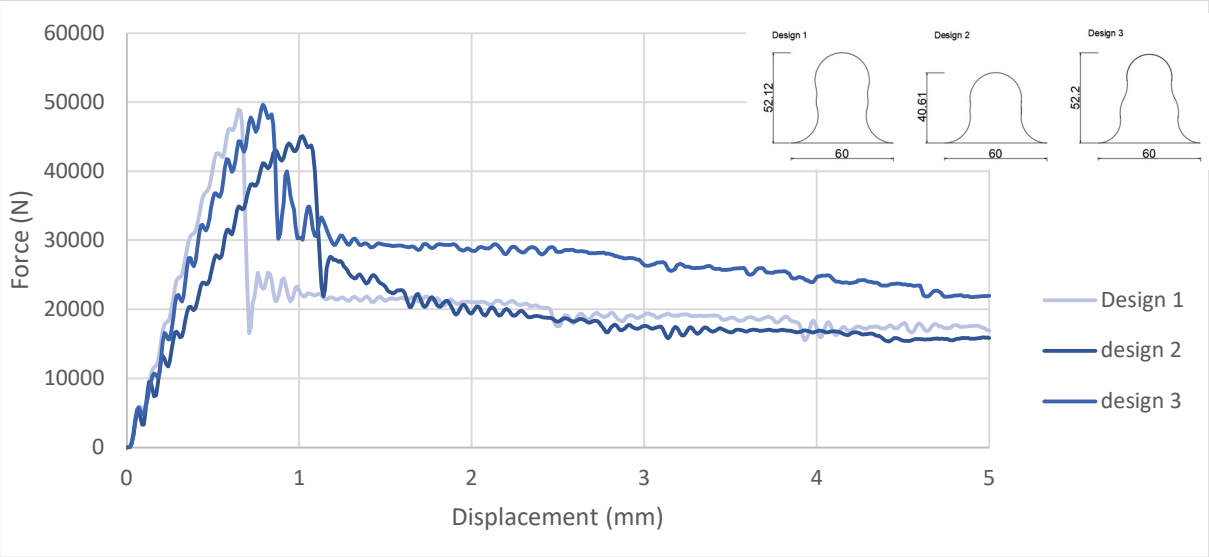

Figure 41 Force displacement curve of the 3 designed tabs with a mesh of 1mm for the tabs. Displacement is the displacement of the top support. The force is the sum of the reaction forces of the bottom supports

The loading sequence is quite clear, first a relatively linear loading sequence occurs where some geometric hardening behaviour (pullout of the interlocking tabs) is seen. Then the lowest (half) tab breaks and a small change in the curve is observed (especially in design 2). After the peak, which is 48.9kN for design 1, 46.8kN for design 2 and 49.6kN for design 3, the resistance suddenly drops and the plastic softening behaviour of the material becomes governing.

It seems that design 1 and 3 reaches their maximum resistance quite fast. Design 2 has the highest displacement at failure, indicating that the tabs pull out more. This is suspected because the interlocking design is smoother than designs 1 and 2.

The cracking pattern of design 1 is seen in Figure 42. This figure shows that the first tab to fail is the lower (half) tab. The second tab to fail is the third full tab from the bottom. The damage then propagates to the top. This is the same as seen in the paper (14).

The von Mises stresses are plotted in Figure 43 with the force-displacement curve. This figure depicts a high amount of stress at the top of the beam. This is because there are a lot of compressive forces at the top. Furthermore, compression is seen in the interlocking tabs themselves. Indicating that the tabs are being compressed.

The plastic deformation of design 2 is seen in Figure 44. It appears that this connection fails similarly to design 1, except for the absence of plastic deformation in the lowest tab of the right element. This absence can be explained by the difference between designs 1 and 2. It seems that for design 1, the bigger circle still has some contact with the left element, which is not the case for design 2. The stress distribution is similar to design 1 as illustrated in Figure 45.

The plastic deformation of design 3 is depicted in Figure 46. This plastic deformation is similar to design 2, but notably, design 3 displays the highest total resistance, likely due to the design. The tabs mostly fail at the smallest point of the first circle known as the neck. Given that this design has the thickest neck among the three, it is logical that the design has the highest strength. The von Mises stress is seen in Figure 47. These stresses do not deviate from the other design and are about the same.

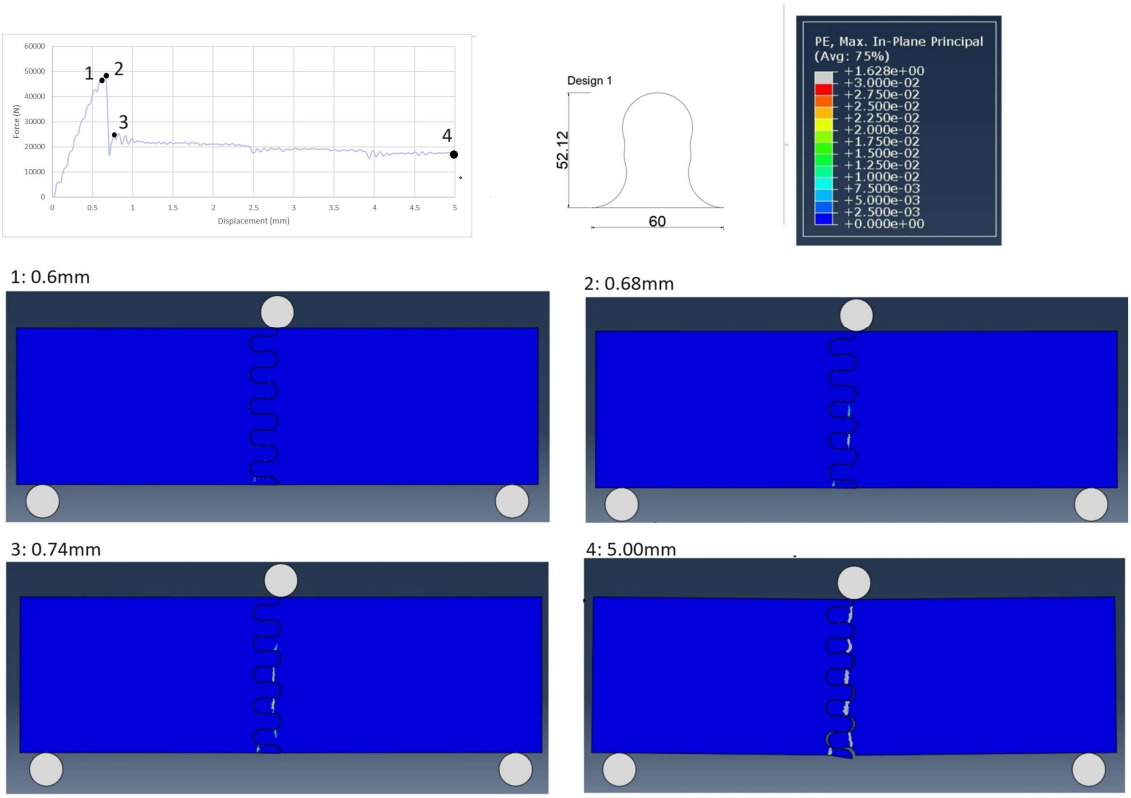

Figure 42 Force displacement curve of design 1 with the plastic deformation taken at a top displacement of 0.6, 0.68, 0.74 and 5.0mm

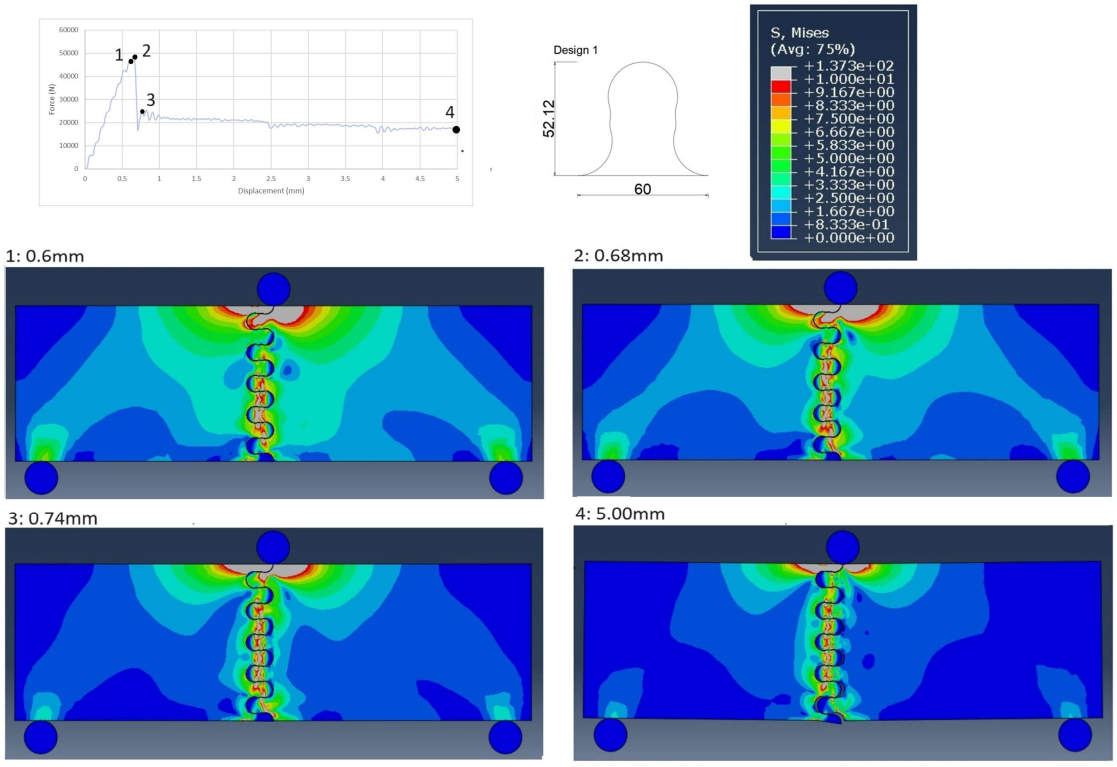

Figure 43 Force displacement curve of design 1 with the von Mises stresses taken at a top displacement of 0.6, 0.68, 0.74 and 5.0mm

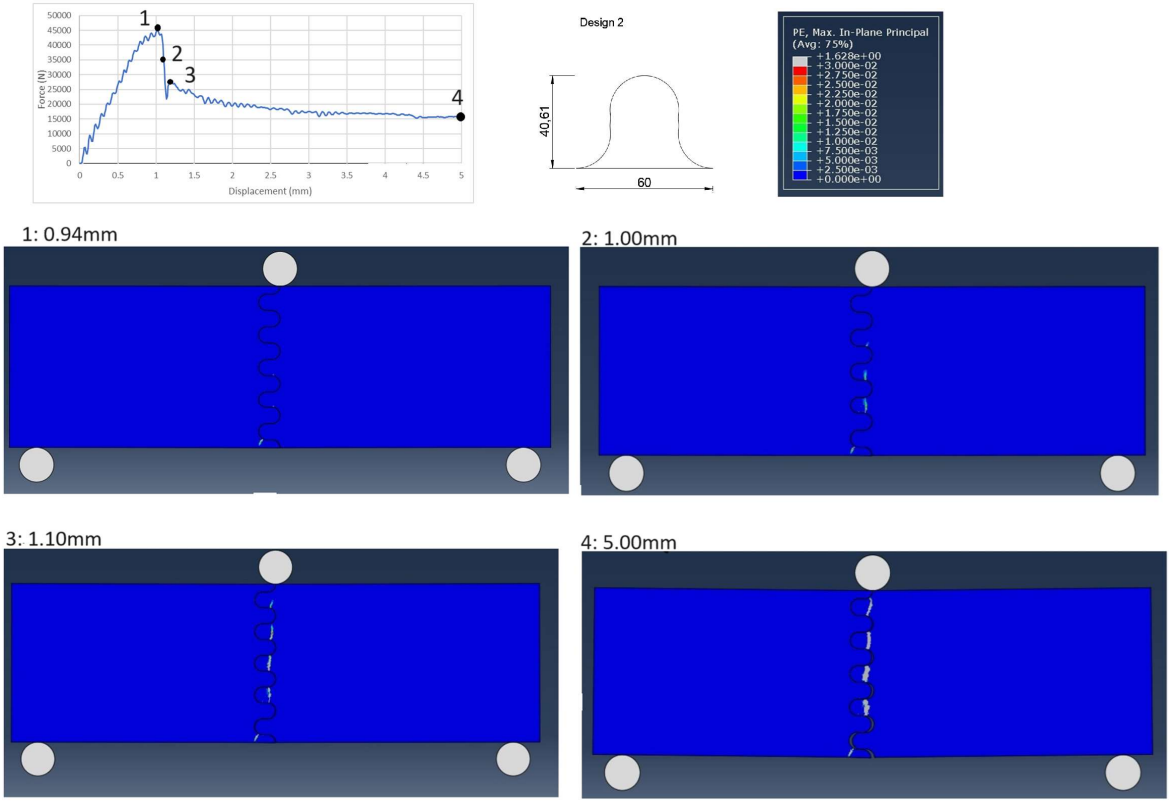

Figure 44 Force displacement curve of design 2 with the plastic deformation taken at a top displacement of 1.0, 1.1, 1.2 and 5.0mm

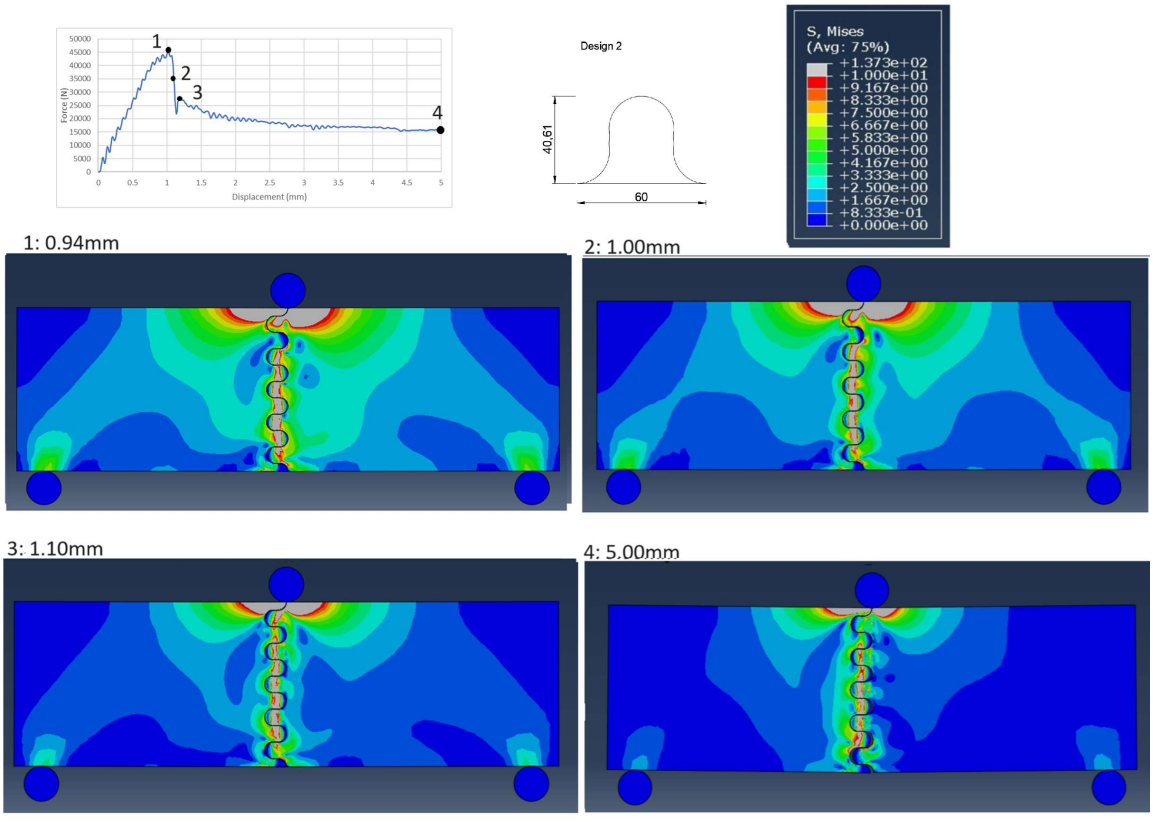

Figure 45 Force displacement curve of design 2 with the von Mises stresses taken at a top displacement of 1.0, 1.1, 1.2 and 5.0mm

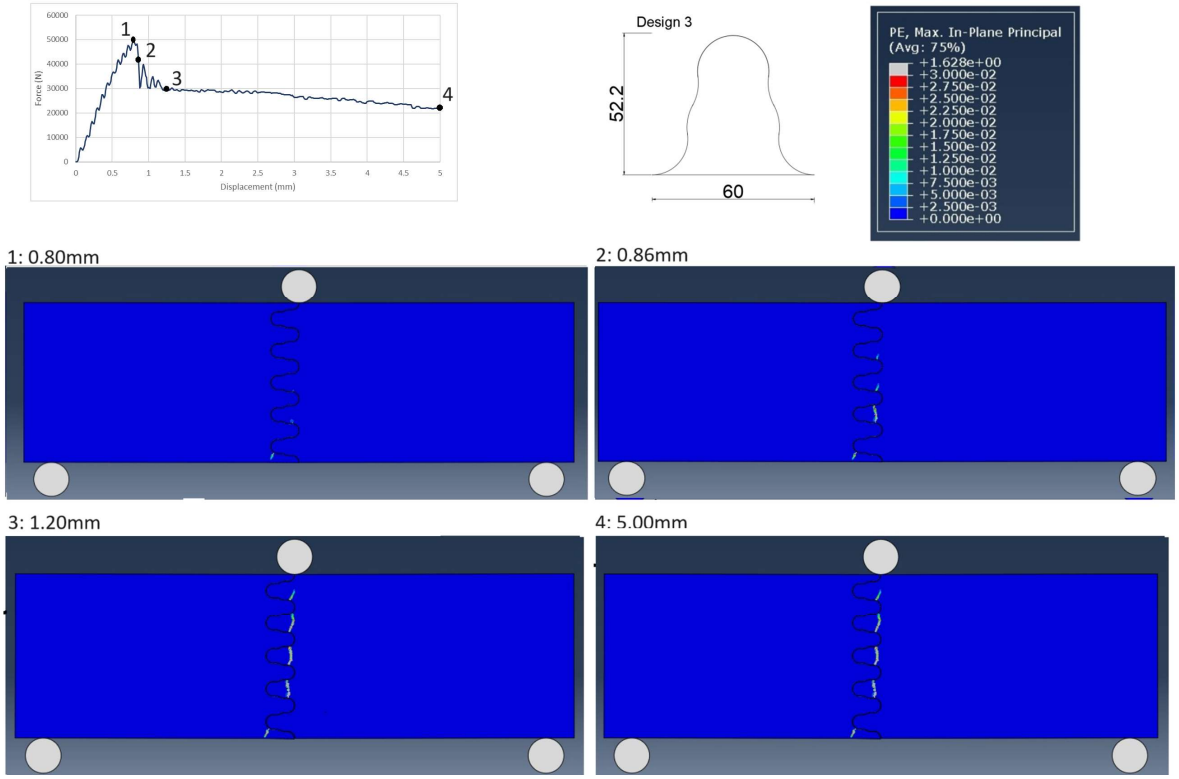

Figure 46 Force displacement curve of design 3 with the plastic deformation taken at a top displacement of 0.80, 0.86, 1.20 and 5.0mm

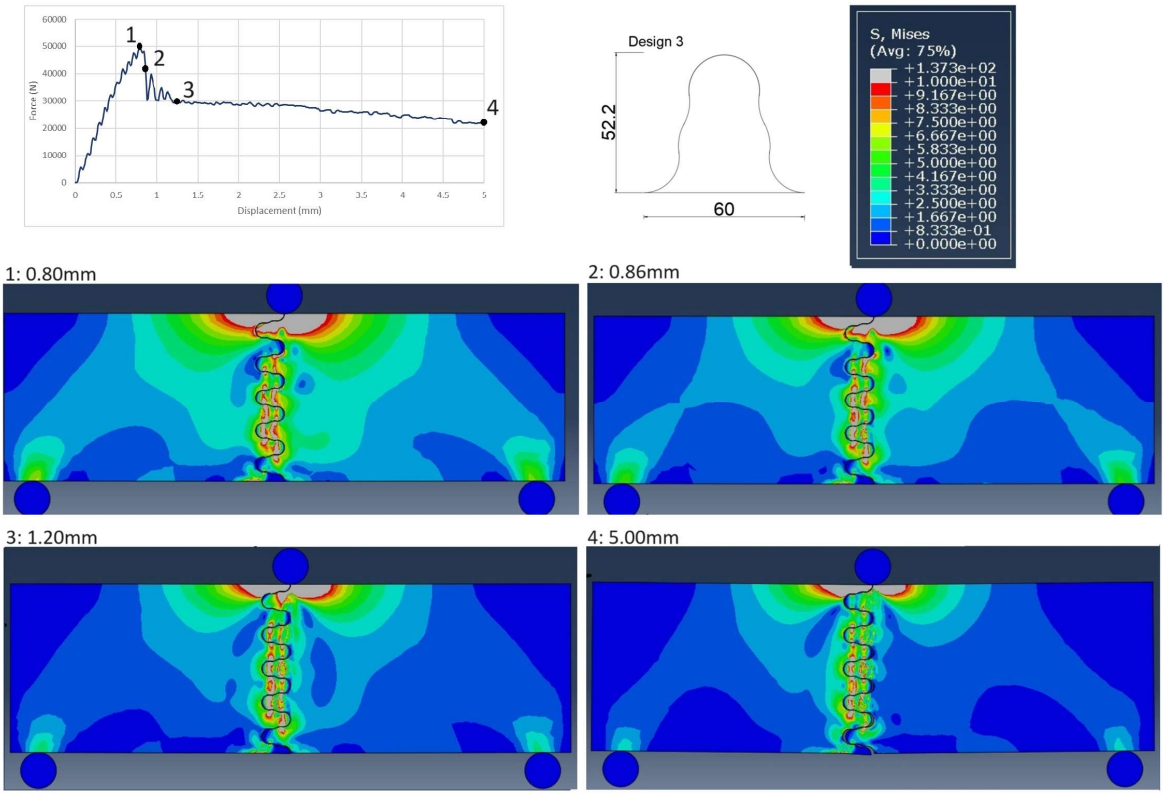

Figure 47 Force displacement curve of design 3 with the von Mises stresses taken at a top displacement of 0.80, 0.86, 1.20 and 5.0mm

4.1.3. Verification of the design with bistable interlocks

To verify this model, a simple hand calculation is made. In this hand calculation, the tabs are seen as a spring (see Figure 48). This spring exerts a force that is equal to the smallest area of the tab times the acting stress.

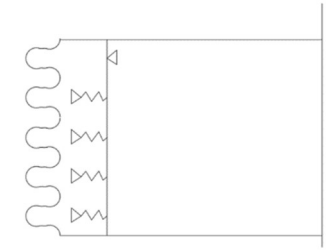

Figure 48 simplified model of the tab structure

This model is refined with the observations of the Abaqus model. As seen in Figure 49 the lowest tab does not experience a full axial force. In the horizontal stresses (s1) it is seen that the lowest point of the beam has a compressive force. This indicates that the lowest tab experiences a bending moment. The plastic deformation of the tab starts at the top which also indicates that the tab experiences a bending moment. So this indicates that the model of Figure 48 is as seen in Figure 50, with a bending moment at the bottom.

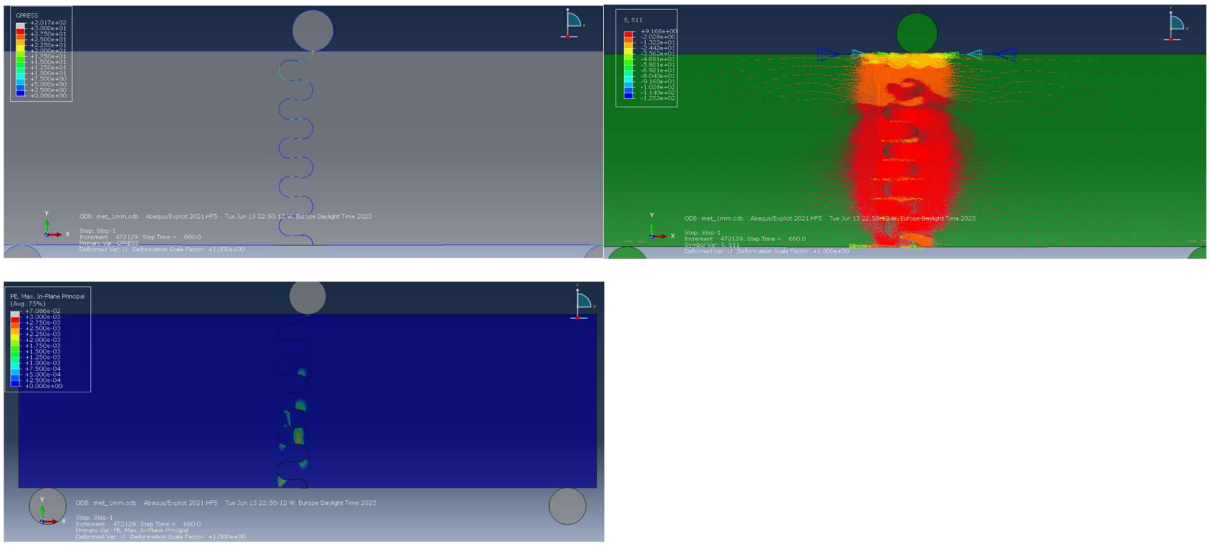

Figure 49 Snapshots of the Abaqus model design 1. The top left shows the interaction forces between the tabs. The top right shows the horizontal forces (S1) of the total structure. The bottom left shows the plastic deformation of the total structure. Each of these snapshots is made at the point of failure (at a top displacement of 1mm).

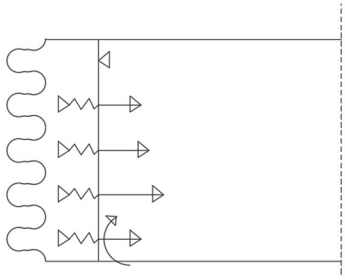

Figure 50 simplified model of the tab structure. In this model the lowest tensional force is reduced due to the bending moment.

To determine this bending moment, it is assumed that the lowest tab does not have any contact with the lowest half tab but only with the tab immediately above. The point where the force is applied is seen in Figure 51. For design 1 it is assumed that the lowest tab fails plastically. For designs 2 and 3 it is assumed that the lowest tab fails elastically. This is because in design 1 plastic deformation is seen, this is not the case for designs 2 and 3.

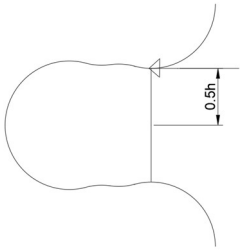

Figure 51 place where the force is applied on the lowest tab

For the stresses, linear strain is assumed, so based on the stress-strain behaviour of Figure 28 the stresses is as depicted in Figure 52. Additionally, it is assumed that the compressive zone is the full height of the highest tab. This is assumed because it is in line with what is seen in Figure 49.

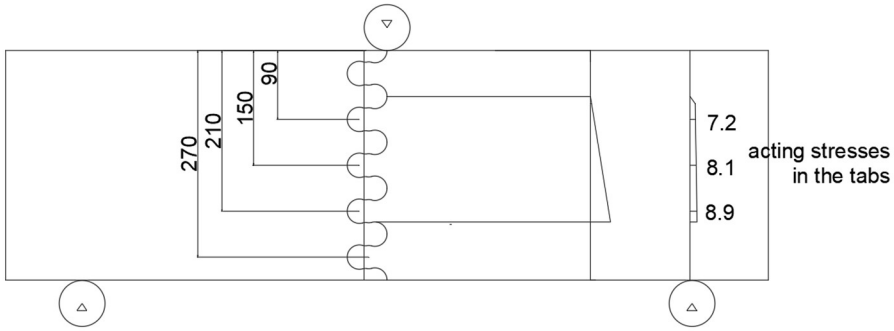

Figure 52 acting stresses in the tabs

The full calculation is seen in Appendix B hand calculations . The results of these calculations are presented in Figure 53 and appear to align the numerical model. This suggests that the model is satisfactory.

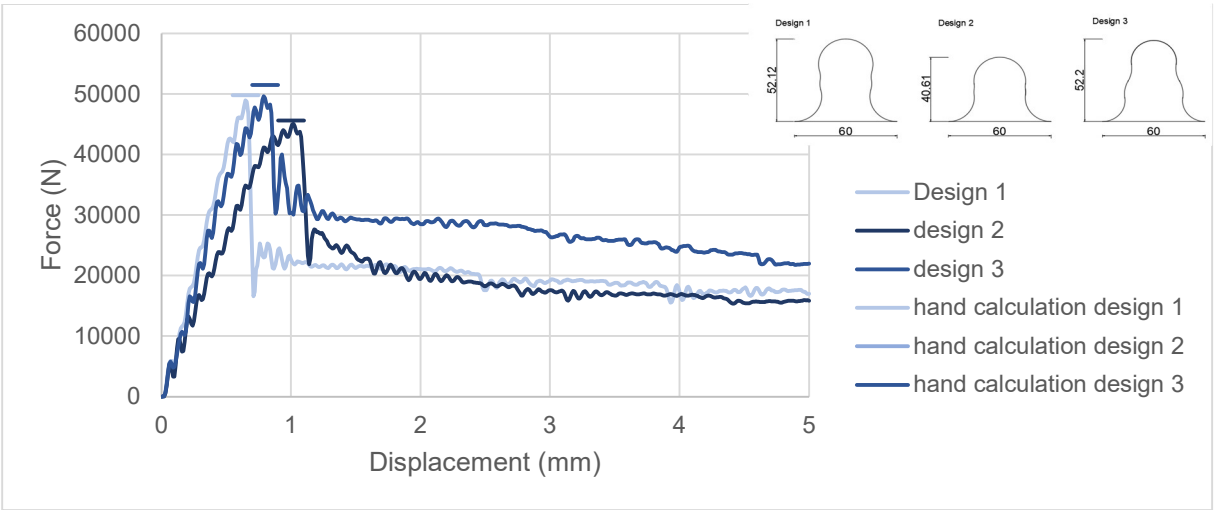

Figure 53 Force-displacement curve of designs 1, 2 and 3 with the calculated maximum force according to the hand calculations.

Furthermore, the maximum resistance is compared to the maximum resistance found in earlier tested interlocking designs. This is done by dividing the total resistance of the interlocking designs by the strength of a homogenous connection. For the bistable interlocking design in this report, the resistance is 30%-33% of a homogenous connection. In the researched papers (14) (15) it is 14%-46% indicating that the resistance of the numerical model is in line with the expectations of previous testing.

4.2. Parameter study and variations of the design

To examine the effects of various parameter adjustments on the designs, specific changes are made to individual parameters. These changes are increments of the material properties of ultra-high performance fibre-reinforced concrete (UHPFRC). The parameters that are analysed are:

- E-modulus
- Elastic and plastic tensile strength
- Friction coefficient
- Plastic strain at peak resistance

Additionally, different variations of the total design are explored, these are:

- One circle instead of two
- 4-point bending test instead of a 3-point bending test
- Incorporating a gap in the design

Each parameter adjustment is analysed through a force-displacement curve, where the force represents the reaction force of the two supporting rollers, and the displacement indicates the total displacement of the loading roller. Furthermore, snapshots of the model are captured to visually depict the changes

4.2.1. E-modulus

The E-modules have a significant influence on the total applied force. A decrease in the elastic modulus relative to the tensional strength is likely to increase the toughness, strength, energy absorbed and maximum extension (12).

In this study, five increments of E-modulus are simulated. These are 100%, 50%, 25%, 10% and 5% of the E-modulus of UHPFRC (22.5GPa, 11.3GPa, 4.51GPa and 2.25Gpa). The force-displacement curve for all 3 designs is shown in Figure 54, Figure 55 and Figure 56.

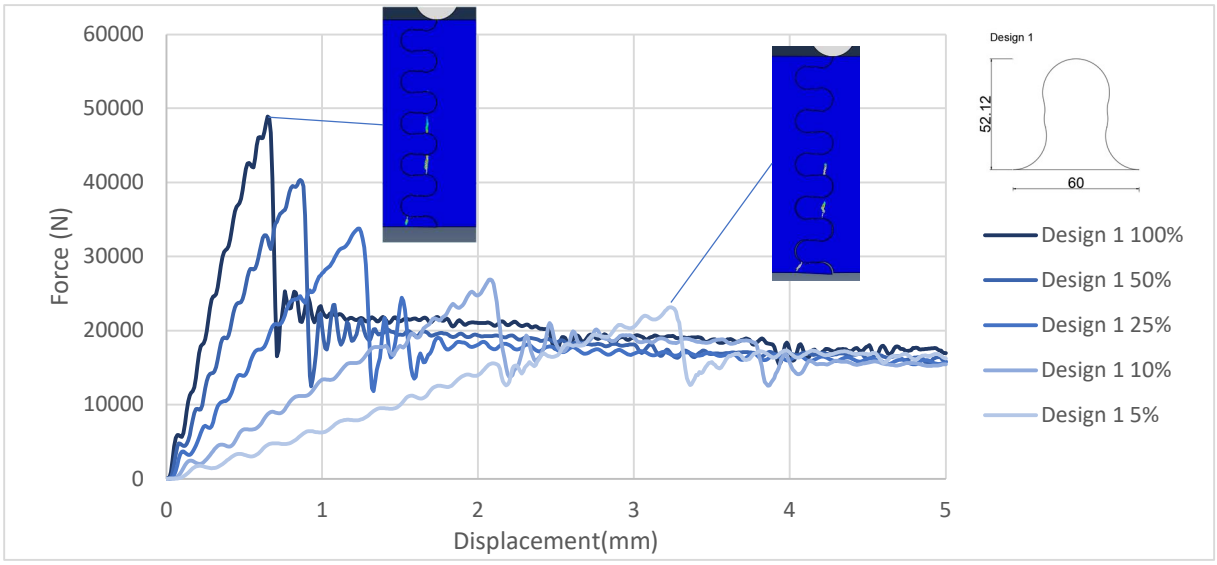

Figure 54 force-displacement curves of design 1 with variations in elastic modulus. The figures are captured at the peak load, with an elastic modulus of 100% and 5%.

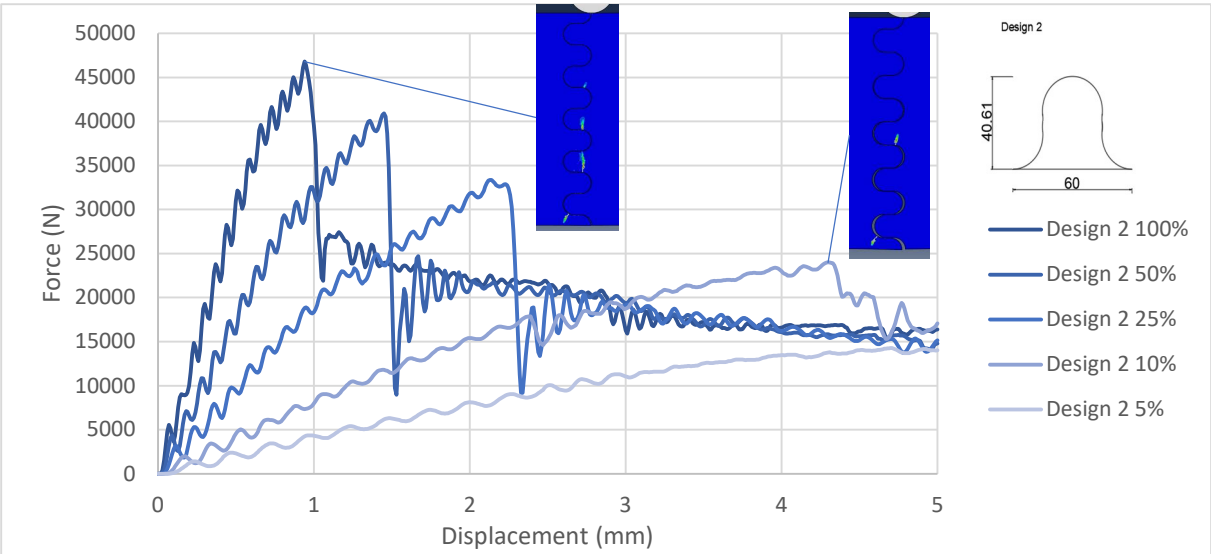

Figure 55 force-displacement curves of design 2 with variations in elastic modulus. The figures are captured at the peak load, with an elastic modulus of 100% and 10%.

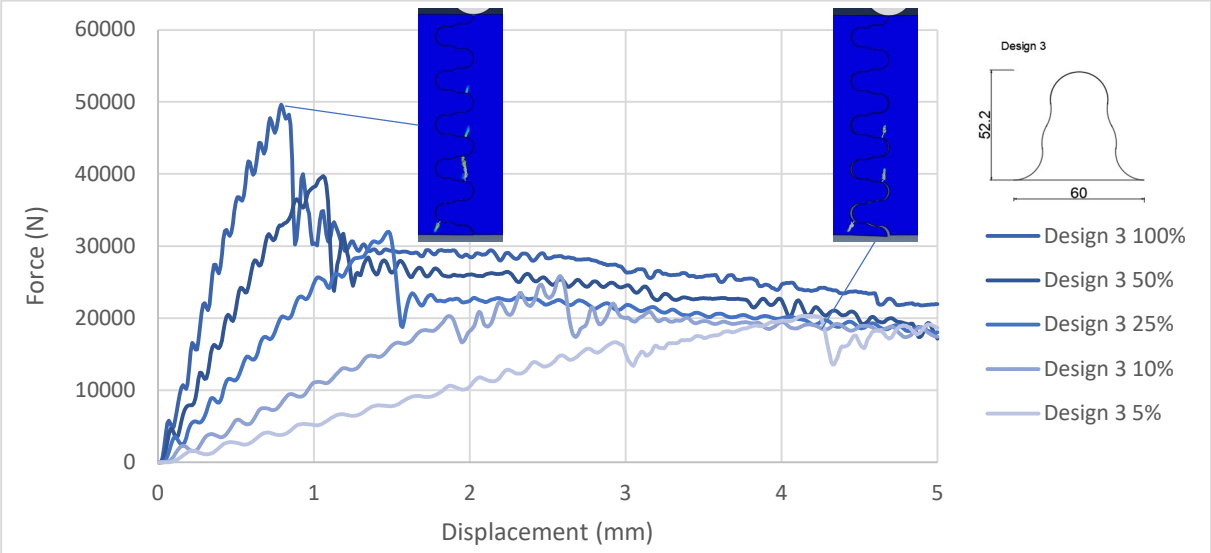

Figure 56 force-displacement curves of design 3 with variations in elastic modulus. The figures are captured at the peak load, with an elastic modulus of 100% and 5%.

These results align with the expectations. A lower elastic modulus would lead to more compression of the interlocking tabs compared to a higher elastic modulus. Consequently, this would result in more tab pullout during the loading of the interlocking connection, resulting in a peak load at a higher displacement. However, an unexpected observation was the reduction in the total resistance (peak load), despite the material strength remaining constant.

Design 2 is further discussed with an elastic modulus of 0.1. Snapshots from Abaqus are captured and presented in Figure 57. These snapshots are taken at a top displacement of 2.39mm, 4.35mm and 5mm. Notably, the tabs fail differently compared to the original E-modulus. While the first plastic deformation still occurs at the lowest half tab, the second plastic deformation (at the peak load) is observed in the middle tab of the right element.

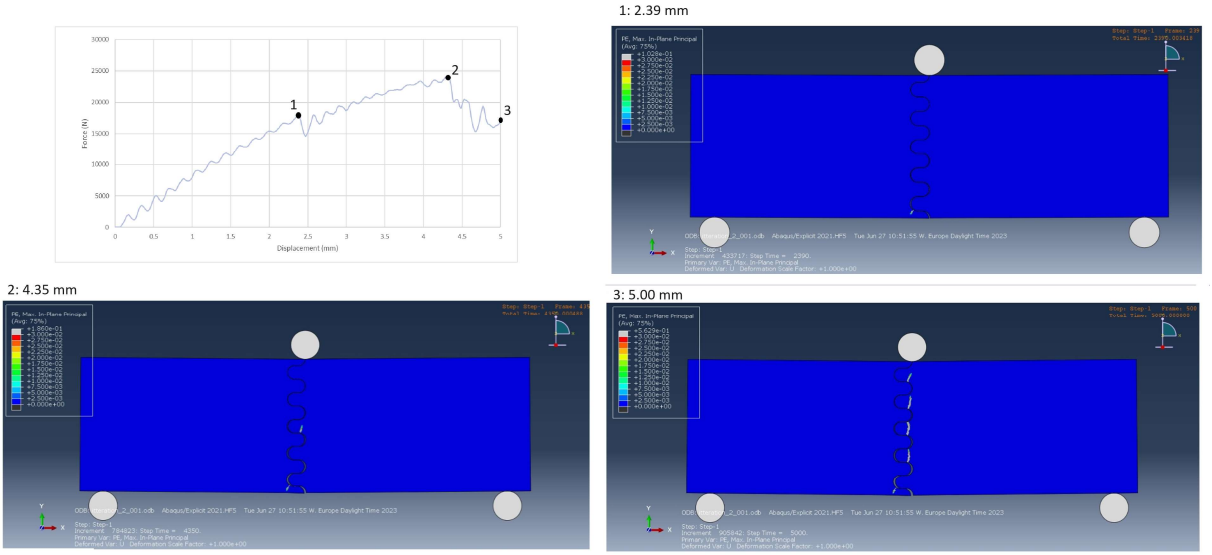

Figure 57 damage propagation of design 2 with 10% elastic modulus. The snapshot is taken at a top displacement of 2.39, 4.35 and 5.00mm respectively.

The total pullout of design 2 with an elastic modulus of 10% of UHPFRC is compared to the original elastic modulus at the peak load. This comparison is illustrated in Figure 58, where it is seen that the tabs will pull out more with a lower elastic strength.

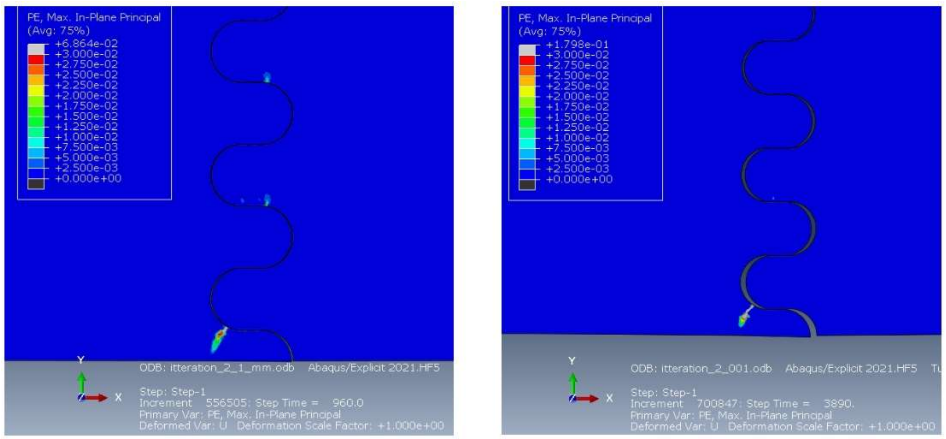

Figure 58 comparison of the plastic deformation of 100% elastic modulus and 10% elastic modulus at peak load (a top displacement of 0.96mm and 4.35mm).

These findings hold across all variations in E-modulus. The crack propagation remains consistent, with the lowest half tab failing first, followed by cracks in the middle tabs of the right element. Overall it can be concluded that with a lower E-modulus, the tabs become easier to compress, exhibiting more pullout, and thus the peak load is reached later.

4.2.2. Tensile resistance

As previously mentioned, the $\frac{\sigma_{max}}{E}$ ratio significantly influences the behaviour of the interlocking tabs. In this study, three increments of tensile strength are simulated, these are 100%, 200% and 400% of the strength of UHPFRC (6.9, 13.8 and 27.6MPa elastic strength and 9.2, 18.4 and 36.8MPa plastic strength). The constitutive relation of these changes can be seen in Figure 59. The force-displacement curves for each design are seen in Figure 60, Figure 61 and Figure 62.

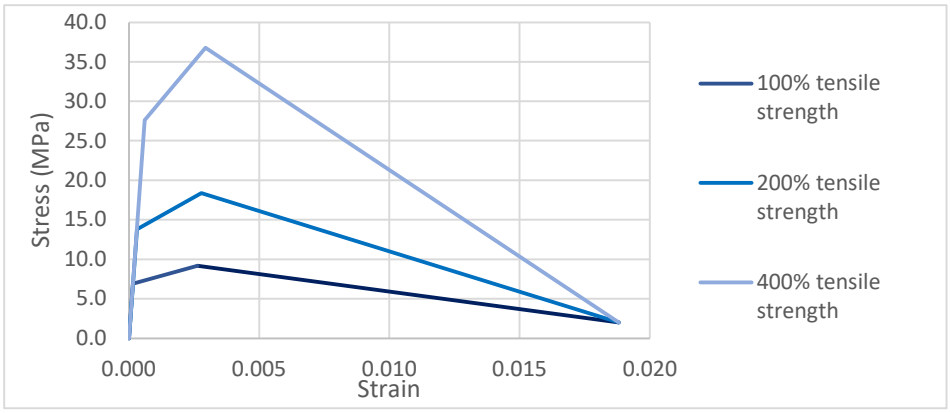

Figure 59 Constitutive relations of the UHPFRC with an increase in tensile resistance.

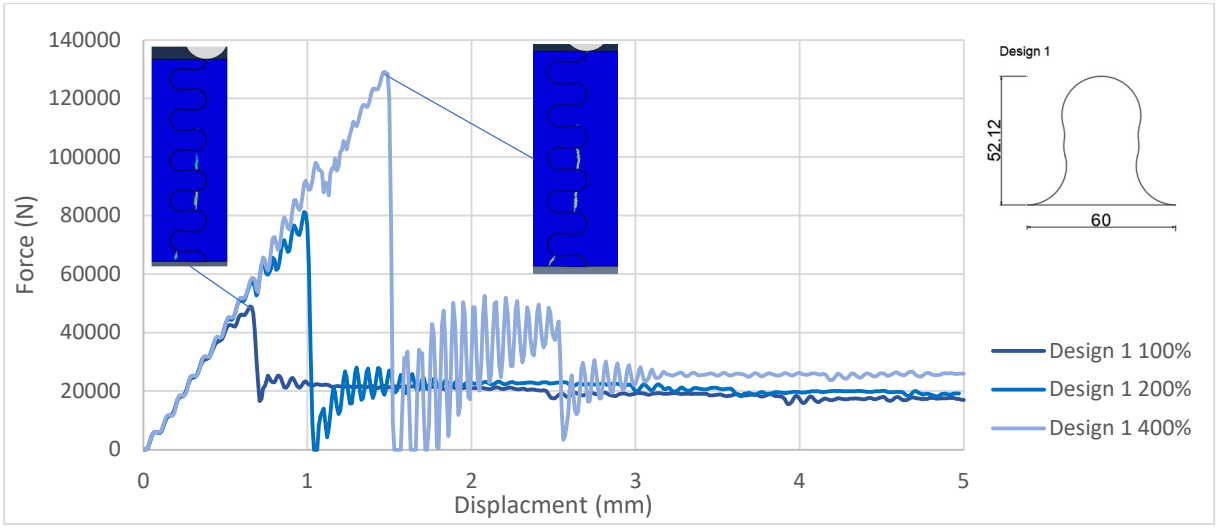

Figure 60 force-displacement curves of design 1 with variations in tensile strength. The figures are captured at the peak load, with a tensile resistance of 100% and 400%.

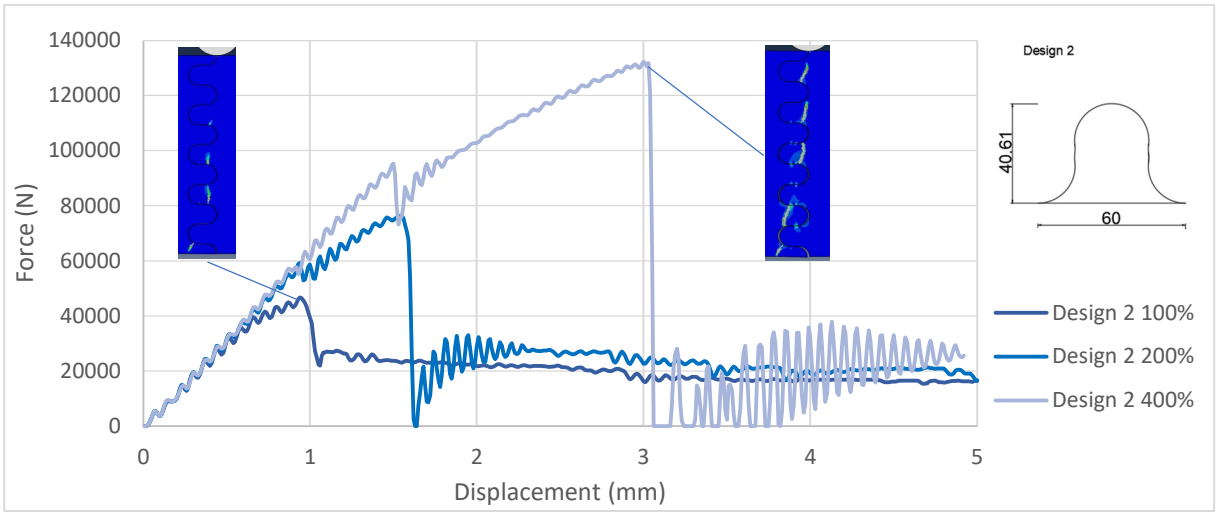

Figure 61 force-displacement curves of design 2 with variations in tensile strength. The figures are captured at the peak load, with a tensile resistance of 100% and 400%.

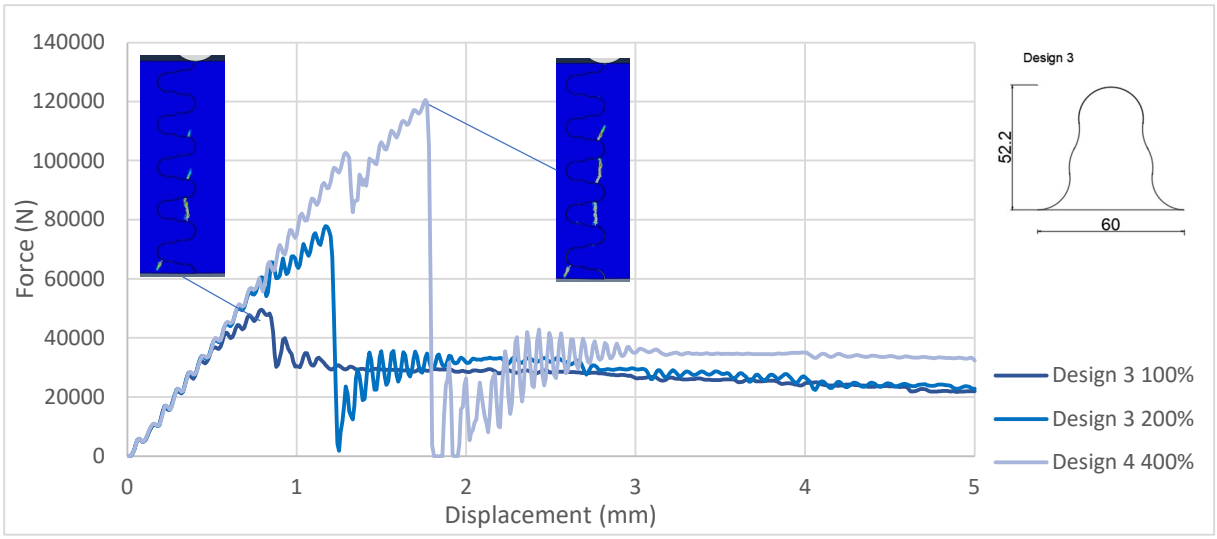

Figure 62 force-displacement curves of design 3 with variations in tensile strength. The figures are captured at the peak load, with a tensile resistance of 100% and 400%.

These results show that the displacement at peak load increases as the strength of the material increases. With higher tensional strength, more force can be applied to the tabs, leading to more compression, so an increased tab pullout.

The tabs still fail in the same manner, with a crack occurring at the neck (smallest section) of the tab. Design 2 400% tensional resistance shows a big “toughening stage” in the force-displacement curve. The damage propagation of this design is seen in Figure 63. The snapshots are taken at a displacement of 1.60mm, 3.04mm and 5.00mm respectively.

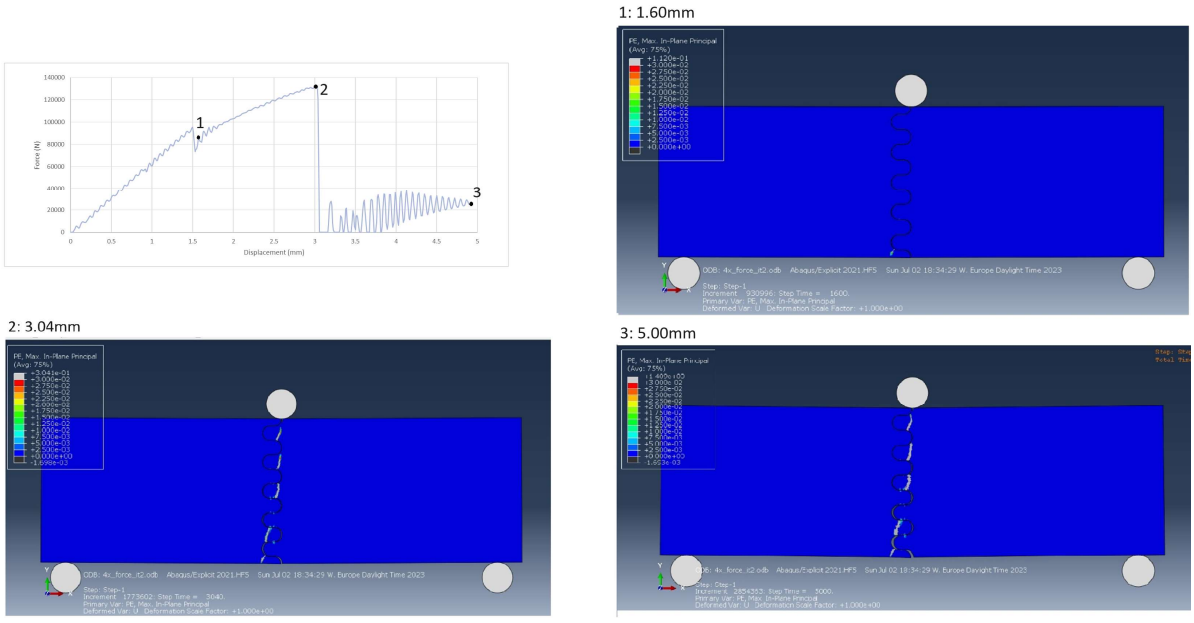

Figure 63 design 2 damage propagation 400% strength. These snapshots are taken at a top displacement of 1.60, 3.04, and 5.00mm respectively.

A comparison of the total pullout of the tabs is presented in Figure 64. Here, it is observed that there is more space between interlocking tabs. This space (tab pullout) gives the connection a more ductile response.

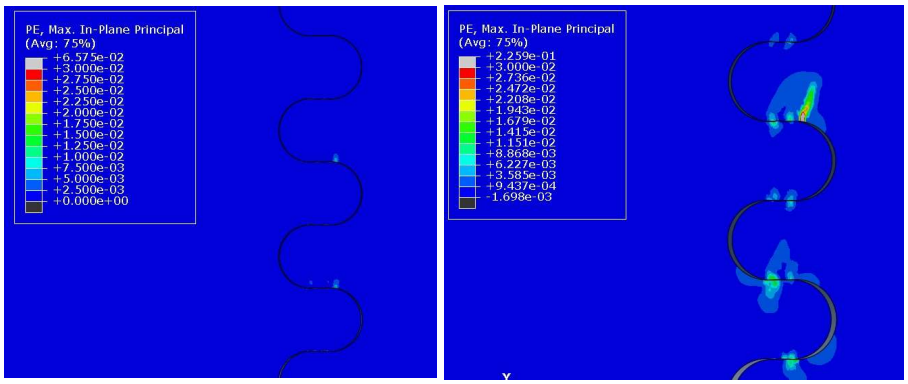

Figure 64 comparison pullout between original strength and 400% strength at the peak load of design 2. This is for the original strength a top displacement of 0.95mm and 3.04mm for the 4x strength.

Less pullout is observed for designs 1 and 3. Due to the shape, more force is required to pull the tabs out. However, the tabs still experience more pullout compared to the original strength of UHPFRC, but it is less pronounced. The damage propagation of design 1 with an increased strength (400%) is seen in Figure 65. These snapshots are taken at a top displacement of 1.09mm, 1.49mm and 5.00mm respectively

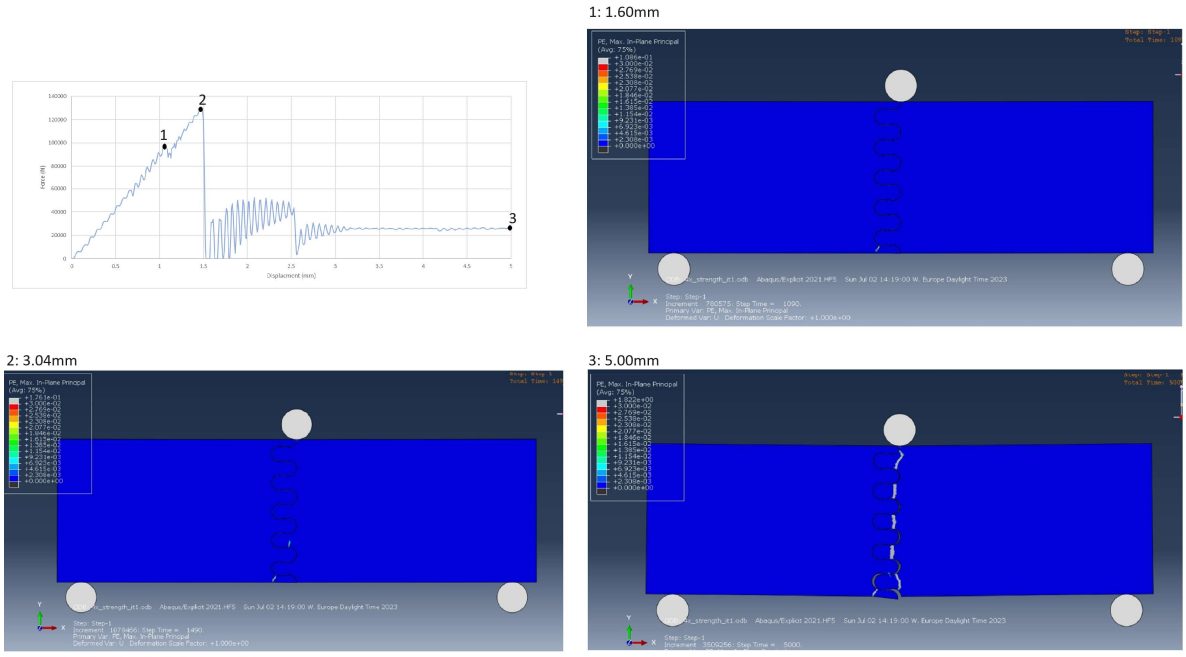

Figure 65 design 1 damage propagation 400% strength. These snapshots are taken at a top displacement of 1.09, 1.49, and 5.00mm respectively.

In conclusion, an increase in tensile strength leads to increased pullout of the interlocks. This increase in pullout would result in a peak load at a later displacement.

4.2.3. Plastic resistance

There may be a difference between increasing both the elastic and plastic tensile resistance versus only increasing the plastic tensile resistance. Therefore, three increments of the plastic strengths are modelled and compared to the previous results of increasing both the plastic and elastic tensile resistance. The increment of plastic strength is 100%, 200% and 400% of UHPFRC (9.2, 18.4 and 36.8MPa respectively), the constitutive relation of these changes can be seen in Figure 66. The results are seen in Figure 67, Figure 68 and Figure 69.

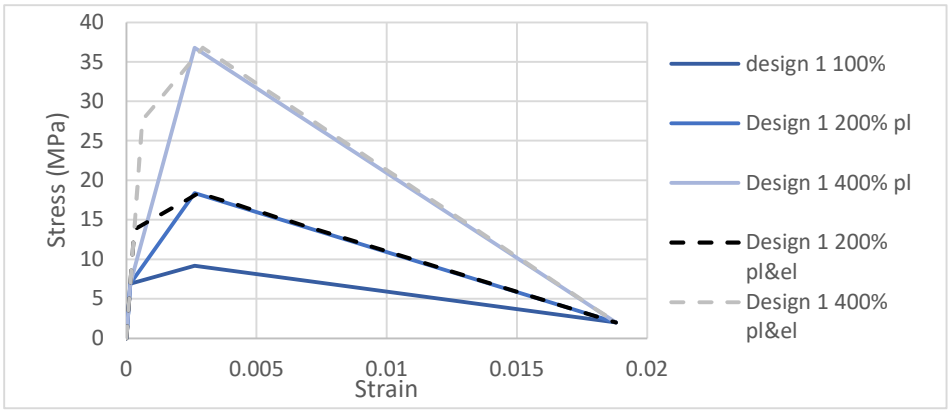

Figure 66 Constitutive relations of the UHPFRC with an increase in plastic and elastic resistance.

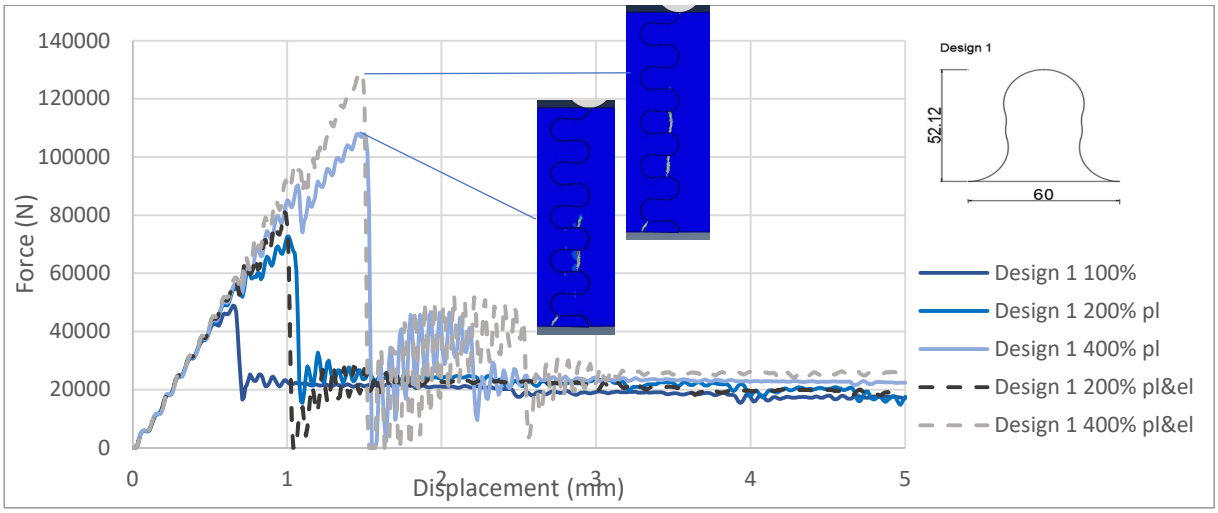

Figure 67 comparison of increasing the elastic (el) resistance and the plastic (pl) resistance of design 1. The figures are captured at the peak load, with a pl and pl & el resistance of 400%

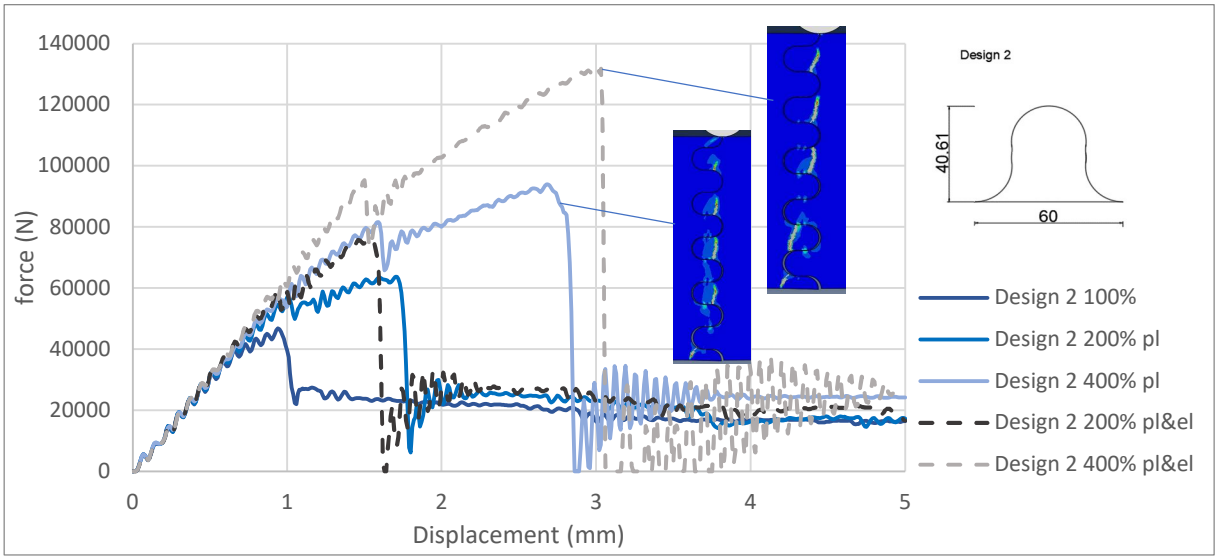

Figure 68 comparison of increasing the elastic (el) resistance and the plastic (pl) resistance of design 2. The figures are captured at the peak load, with a pl and pl & el resistance of 400%

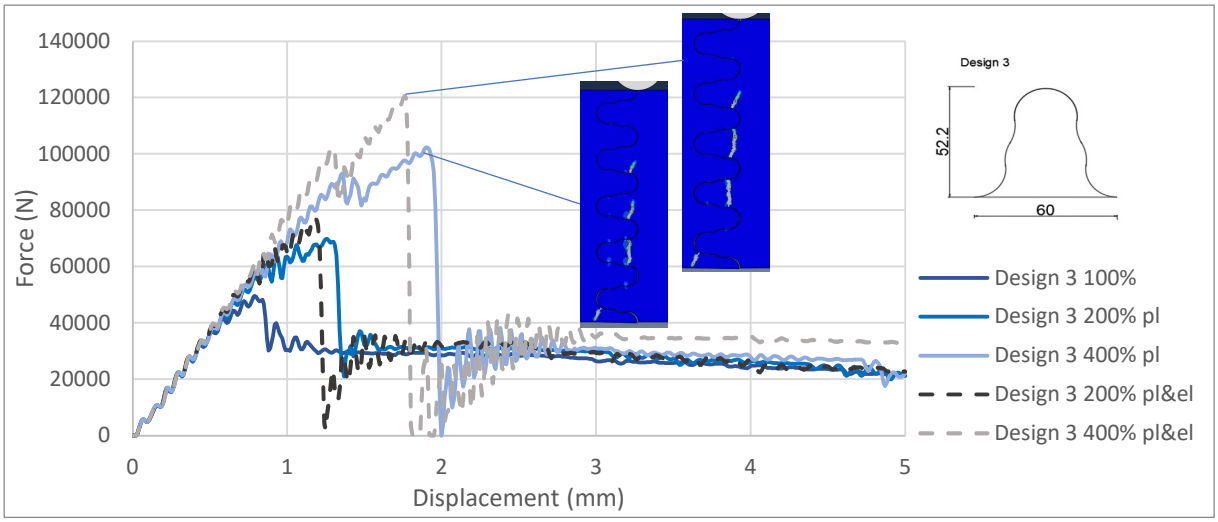

Figure 69 comparison of increasing the elastic (el) resistance and the plastic (pl) resistance of design 3. The figures are captured at the peak load, with a pl and pl & el resistance of 400%

It appears that increasing only the plastic strength reduces the total bending resistance of the structure. This could be due to the tabs not experiencing the same displacement at the same time. Because of this, different strains are observed at different tabs. Because the elastic strength is reached with a lower strain, the total stress in each interlocking tab would be higher with increasing both the elastic and plastic resistance. This would thus result in a higher bending resistance for a material with a higher elastic strength.

4.2.4. Friction coefficient

Changing the friction coefficient will most likely decrease the amount of force needed to pull out the interlocking tabs. This is because the resistance of the interlocks is a sum of contact force and friction (see equation 2.4 and 2.5). If the friction is less, the total resistance of the interlocks would be less, and so, the tabs would pull out more. For this study, the friction coefficient deviates from 0.3 to 0. The force-displacement graphs for these deviations are seen in Figure 70, Figure 71 and Figure 72.

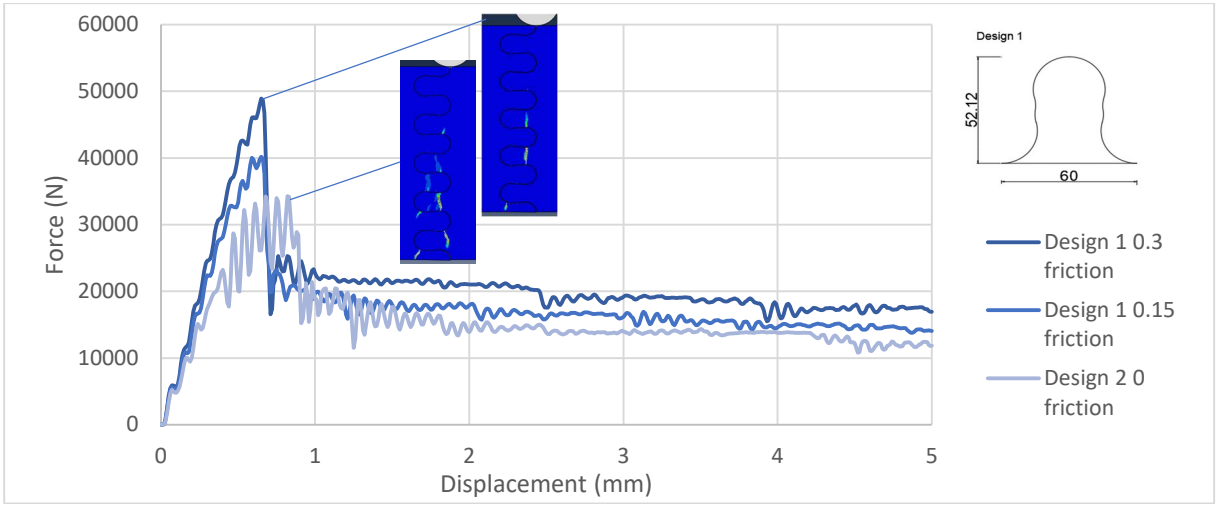

Figure 70 force-displacement curves of design 1 with variations in friction coefficients. The figures are captured at the peak load, with a friction coefficient of 0.3 and 0.

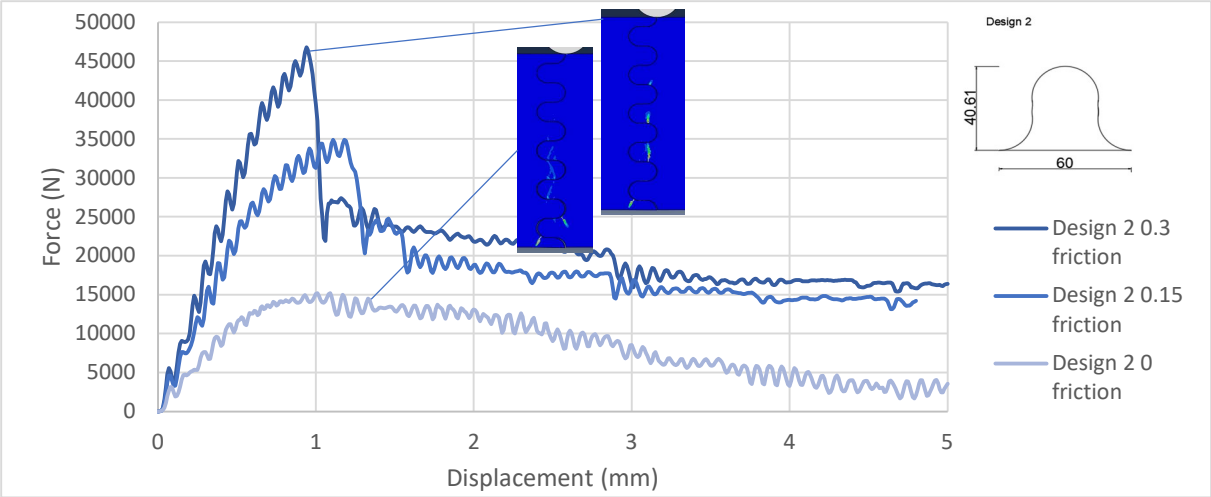

Figure 71 force-displacement curves of design 2 with variations in friction coefficients. The figures are captured at the peak load, with a friction coefficient of 0.3 and 0.

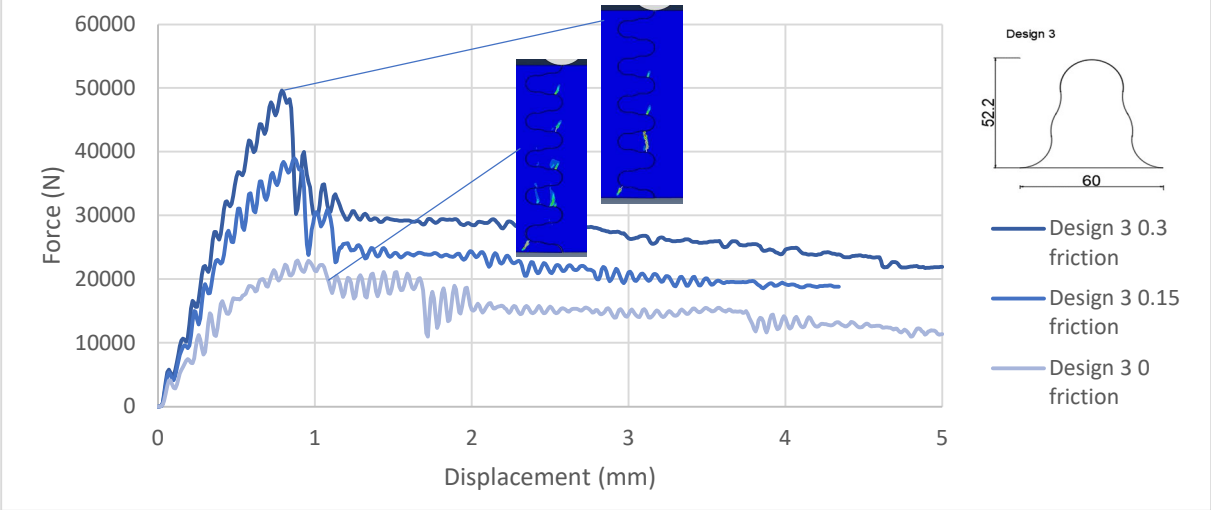

Figure 72 force-displacement curves of design 3 with variations in friction coefficients. The figures are captured at the peak load, with a friction coefficient of 0.3 and 0.

It appears that decreasing the friction coefficient increases the ductility of the connection but decreases the total resistance. Design 2 with a friction coefficient of 0 seems quite interesting. According to these graphs, the tabs pull out completely. However, In the model itself (seen in Figure 73), there does not appear to be a total pullout. While there is an increase in the pullout, the tabs still crack before the complete pullout.

It is noted that the full tab at the bottom fails differently. There seems to be a failure due to a bending moment. This bending moment could arise because the tabs cannot transfer horizontal forces. Due to a friction coefficient of 0, there are only vertical forces in the lower tab.

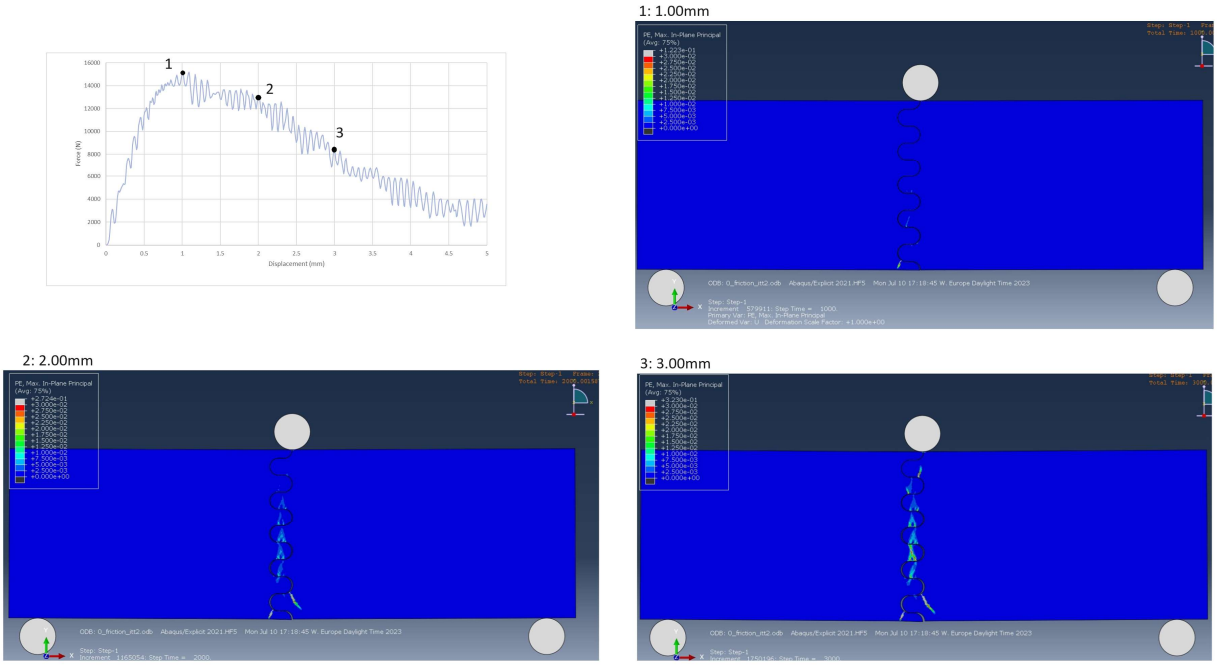

Figure 73 damage propagation of design 2 with a friction coefficient of 0. These snapshots are taken at a top displacement of 1.00, 2.00 and 3.00.

The difference in failure between 0.15 friction and 0.3 friction is less pronounced (see Figure 74). Overall, the structure fails later, but the cracks seem to be the same.

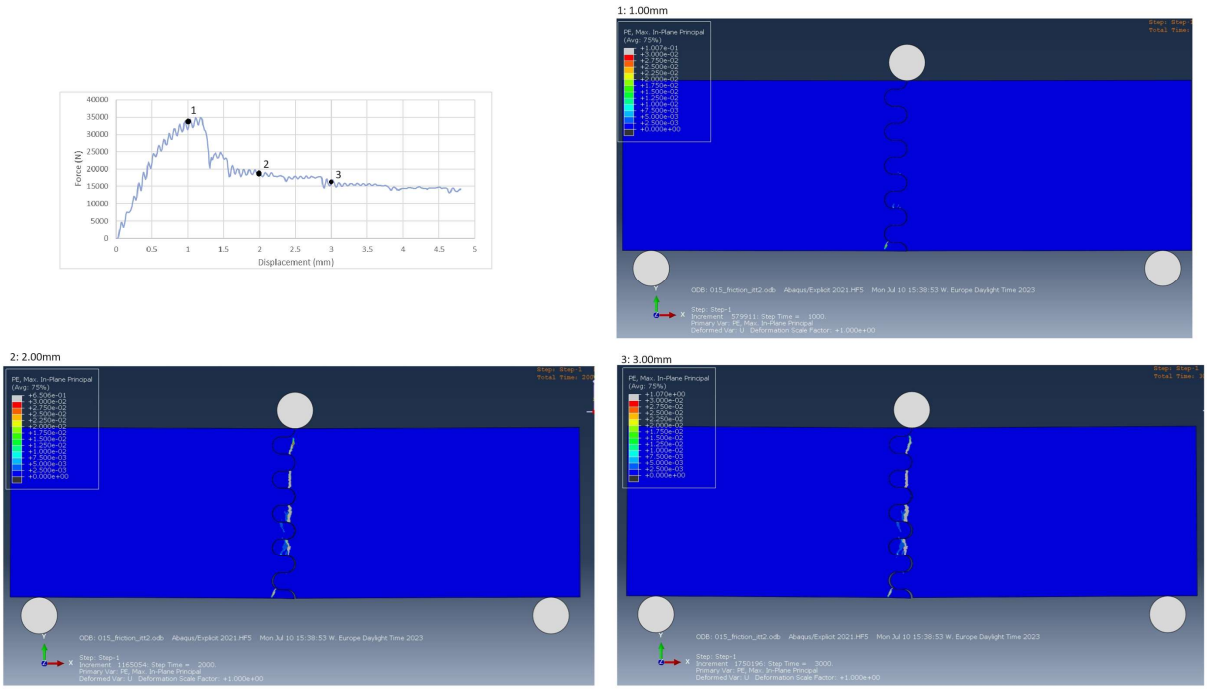

Figure 74 damage propagation of design 2 with a friction coefficient of 0.15. These snapshots are taken at a top displacement of 1.00, 2.00 and 3.00.

4.2.5. Plastic strain at peak tensile resistance

Another property of the material is the plastic strain at failure. In this study, the plastic toughening phase is elongated without increasing the maximum resistance. Specifically, The plastic toughening

stage are increased to 400% and 800% of UHPFRC. The constitutive relation of these increases is seen in Figure 75.

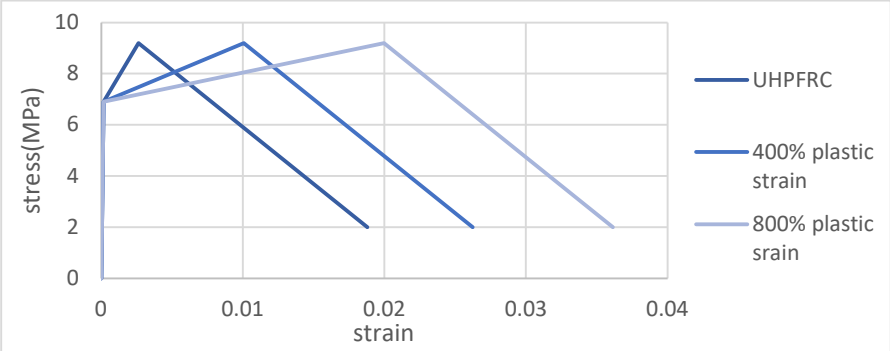

Figure 75 Constitutive relations of the UHPFRC with an increase in toughness.

The plastic strain variants have been simulated in Abaqus. The force-displacement graphs are visible in Figure 76, Figure 77 and Figure 78. It appears that with each increase in toughness, the total top displacement at peak load increases. Furthermore, the total resistance of the structure increases.

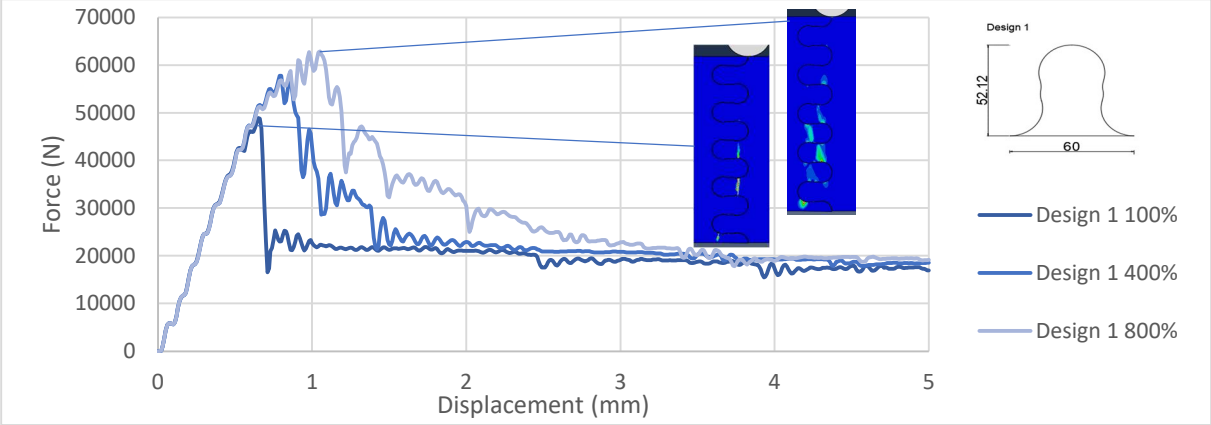

Figure 76 force-displacement curves of design 1 with different toughness. The figures are captured at the peak load, with a plastic strain at peak resistance of 100% and 400%

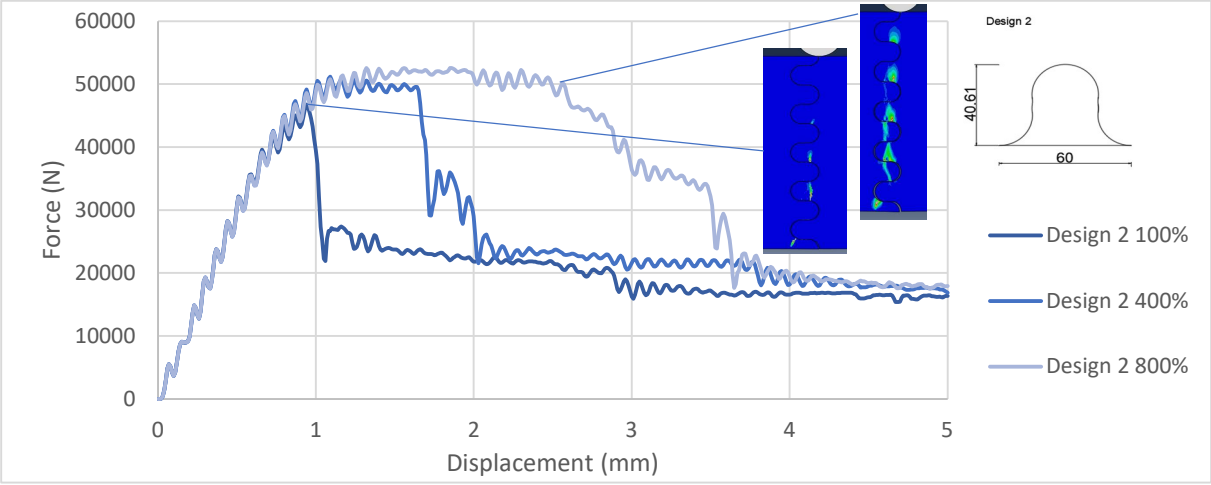

Figure 77 force-displacement curves of design 2 with different toughness. The figures are captured at the peak load, with a plastic strain at peak resistance of 100% and 400%

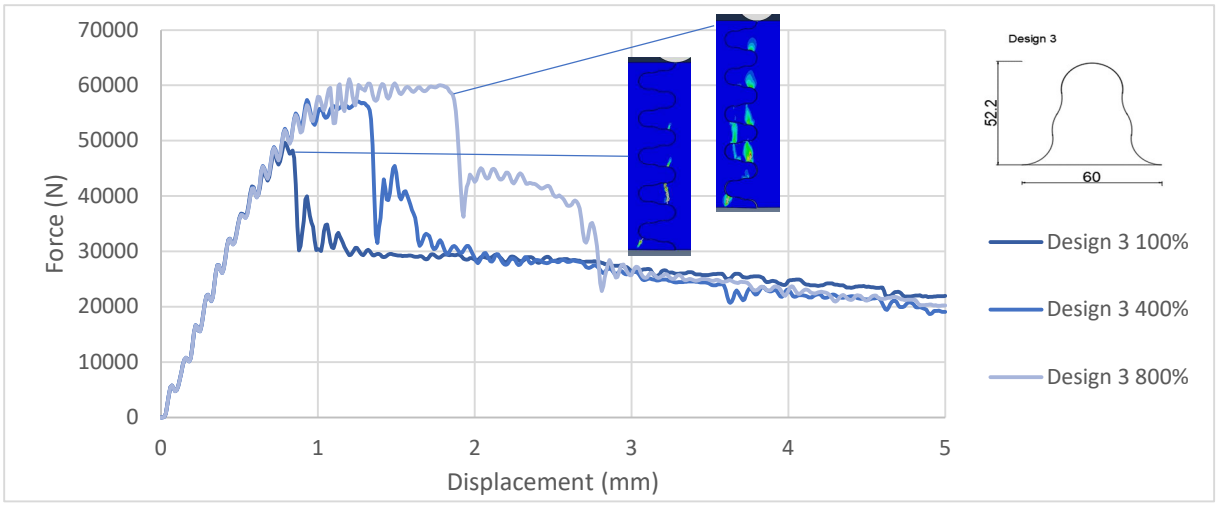

Figure 78 force-displacement curves of design 3 with different toughness. The figures are captured at the peak load, with a plastic strain at peak resistance of 100% and 400%

The plastic deformation in the connection is seen in Figure 79 and Figure 80. In Figure 79 , design 2 is shown at a top displacement of 1.95, 2.83, 3.48 and 5mm, with an increase in plastic strain to 800% of UHPFRC. In Figure 80, design 3 is seen with a top displacement of 1.32, 1.48, 2.00 and 5,00mm, with an increase to 400% of UHPFRC.

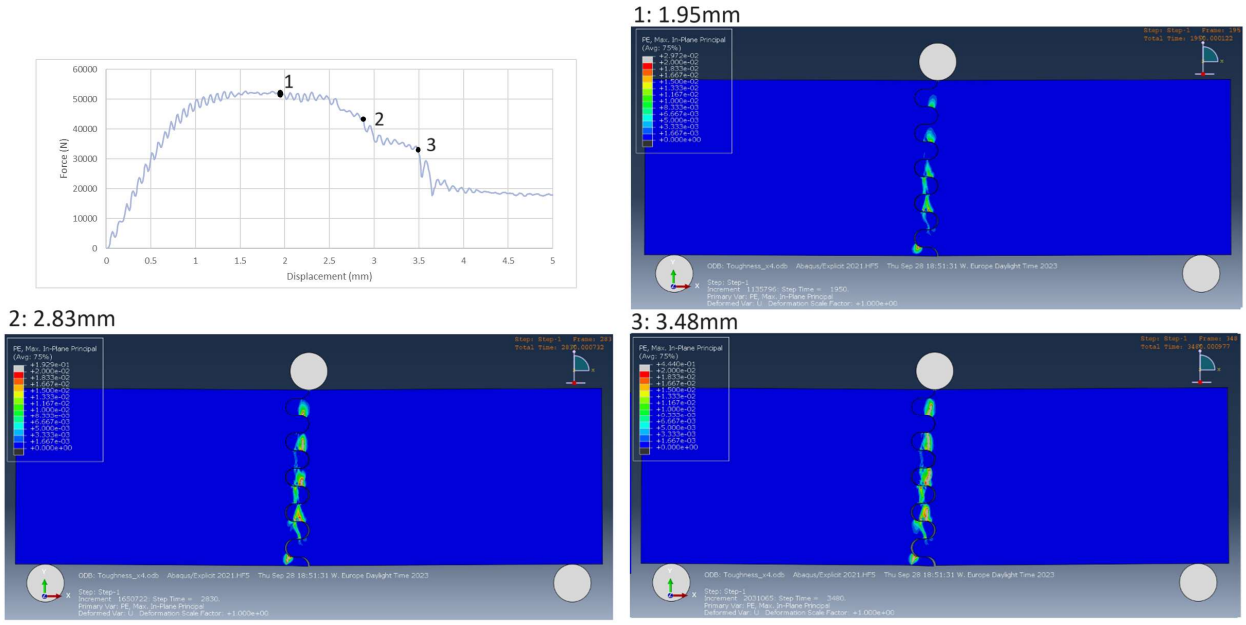

Figure 79 plastic deformation of design 2 with 800% plastic strain at peak tensile resistance at 1.95, 2.83, 3.48 and 5.00mm respectively.

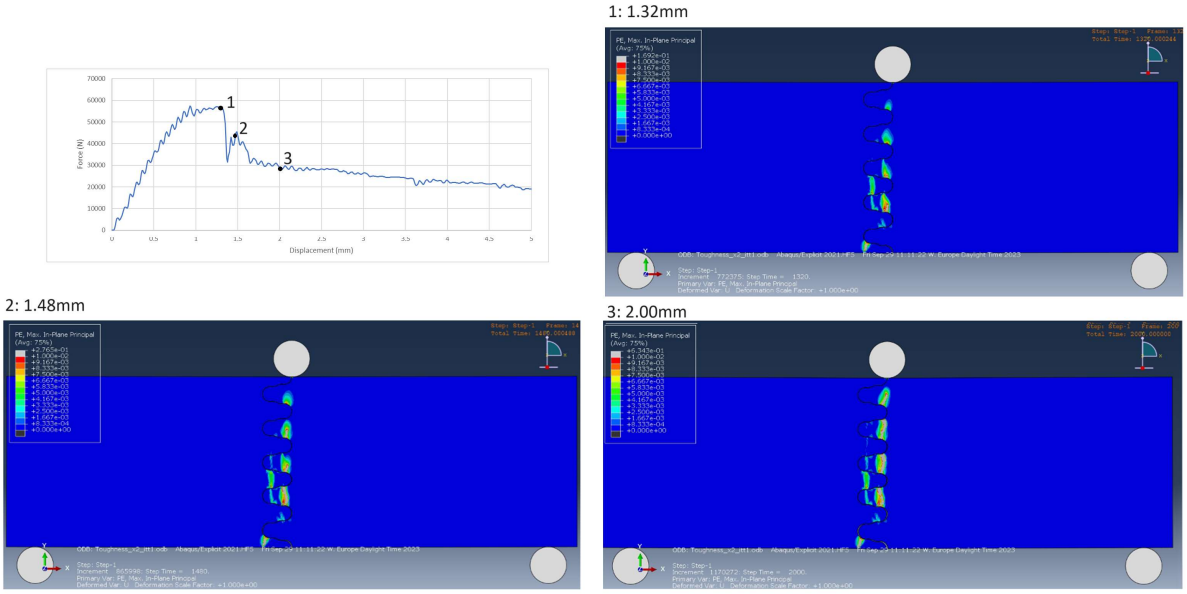

Figure 80 plastic deformation of design 3 with 400% plastic strain at peak tensile at 1.32, 1.48, 2.00 and 5.00mm respectively.

In these figures, it is clear that there is more plastic deformation compared to the structure with each increase in plastic strain capacity. This indicates that there is more cracking when the toughness increases of the material increases.

4.2.6. One circle instead of two

The same test was conducted using a simpler design consisting of only one circle. This was done because it appeared that the extended interlocking design damaged the tabs by creating an additional bending moment/force, thereby making them weaker and fail faster. The designed tabs are shown in Figure 81, where design 1 and 2 are the same as previous chapters. The parameters of these designs are described in Table 6. The force-displacement graph of these designs is seen in Figure 82.

	Design 1	Design 1a	Design 2	Design 2a
θ_1	15°	15°	6°	6°
θ_2	8°	8°	6°	6°
R_1	15.91mm	15.91mm	15.1mm	15.1mm
R_2	15.15mm	-	15.1mm	-
L	64.64mm	38.1mm	40.61mm	33.44mm
W	60mm	60mm	60mm	60mm

Table 6 parameters of the design with one circle

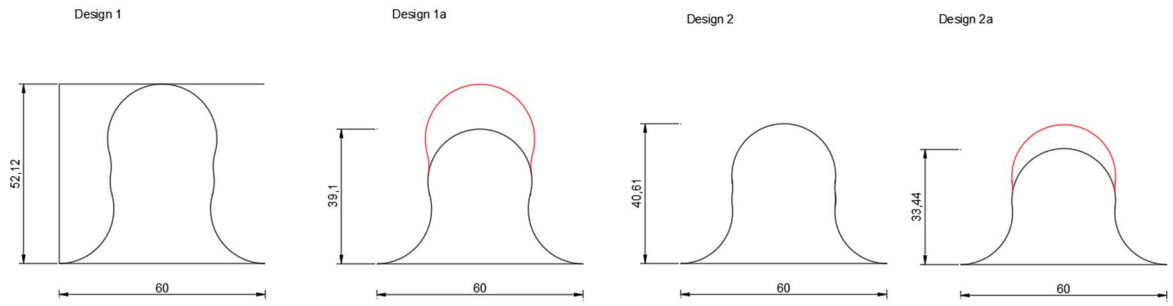

Figure 81 Simpler designs of the interlocking tabs where the top circle (seen in red) is taken away.

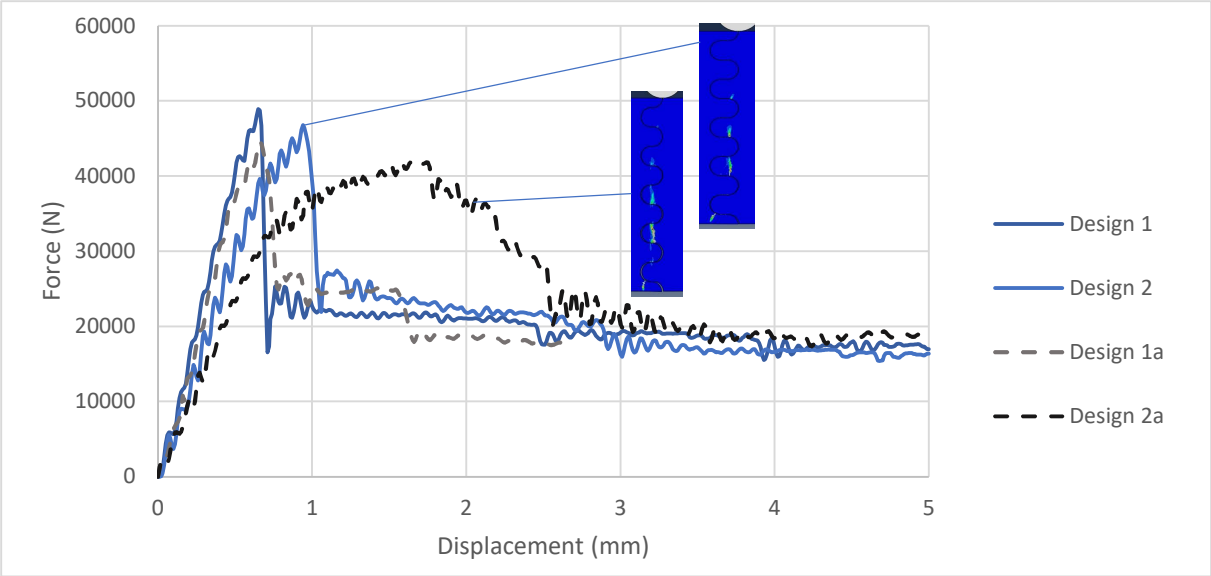

Figure 82 Force displacement curves of the simpler designs with a comparison to the original design.

The designs with one circle appear to exhibit better properties, particularly design 2a. The damage propagation of this design is seen in Figure 83. It appears that this design fails similarly to the bistable designs, but each tab fails individually rather than in rapid succession. It seems that this design has more “stable” positions where first the lower tabs fail and then the next one on top.

Additionally, more pullout is observed. This is due to the decrease in contact points of the design. The bistable design (designs 1 and 2) has four contact points, whereas this design has two contact points. This reduction in contact points decreases the friction and contact force, thereby reducing the force needed to pull out the interlock.

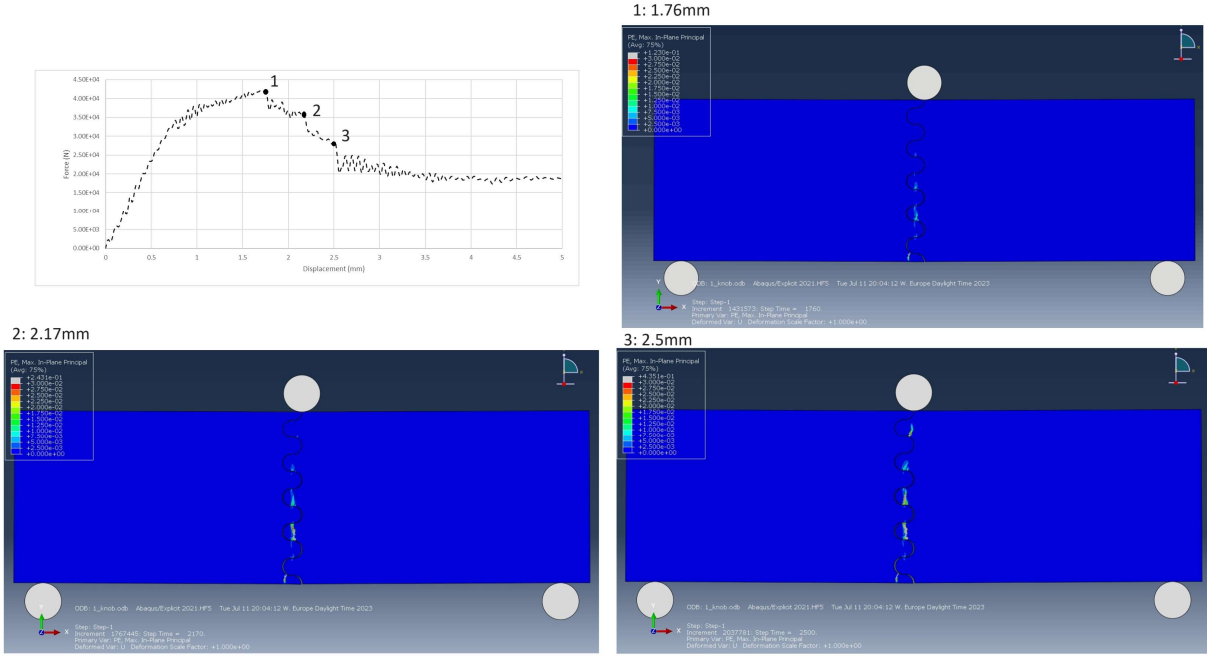

Figure 83 damage propagation of the simpler design 2. These are at a top displacement of 1.76, 2.17, 2.50 and 5.00mm respectively.

4.2.7. 4-point bending test

The behaviour of the interlocking connection may vary when subjected to a 4-point bending test. This could be the case because there are some shear forces in the tabs due to the 3-point bending test. The total span is increased to 1800mm and the top supports are 400mm from each other. A sketch of the test setup is seen in Figure 84. The bending moment-displacement graph of the simulation is seen in Figure 85. Where the bending moment is calculated with the reaction forces at the supports and a forget me not.

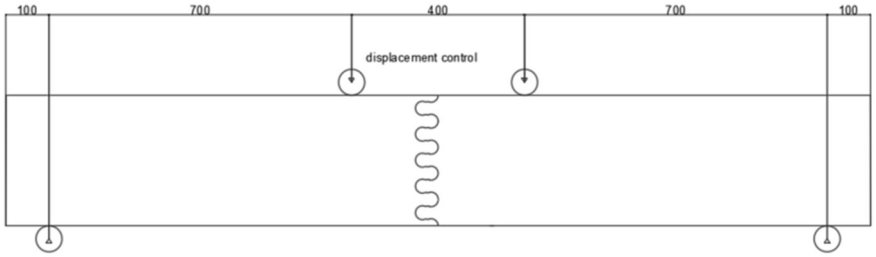

Figure 84 model of the 4-point bending test

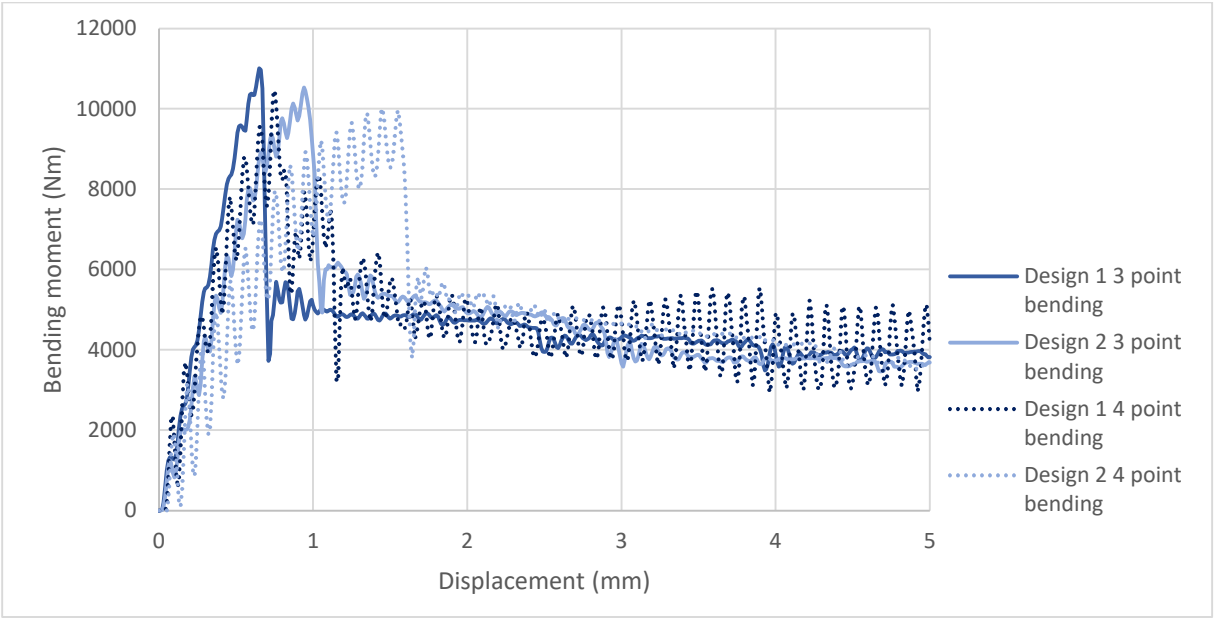

Figure 85 Force displacement curves of the 3-point bending test and the 4-point bending test

It appears that the testing method does not significantly influence the total resistance of the structure. The structure fails with more displacement compared to the three-point bending test, but this is most likely due to the increased span allowing for greater displacement. Overall, the assumption that the three-point bending test measures the connection only loaded with a bending moment is correct.

4.2.1. Design with a gap

In this study, the incorporation of a gap in the three designs is investigated. The introduction of this gap is aimed at increasing the pullout of the interlocks, thereby increasing the ductility of the connection. The interlocking designs corresponding to this investigation are illustrated in Figure 86.

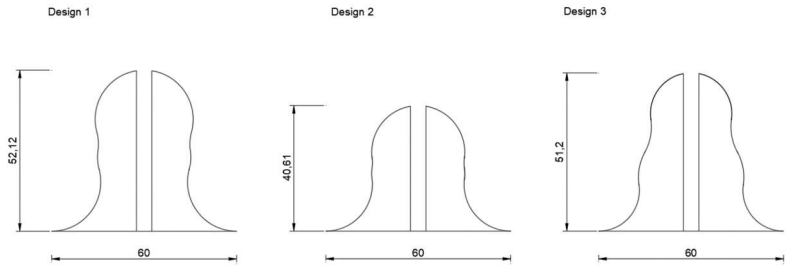

Figure 86 designs of bistable interlocking tabs with gap

The force-displacement curves of these designs are shown in Figure 87, and are compared with the designs without a gap in Figure 88. The results suggest an increase in structural ductility but a notable decrease in overall strength. This could be because the tabs are failing due to a bending moment instead of a pullout or tensional force. This failure mode is generally weaker than the failure mode in the original design. In Figure 87, it is observed that design 3 with a gap exhibits unstable results after reaching its peak. This instability is attributed to the enforced displacement being applied too rapidly for the model.

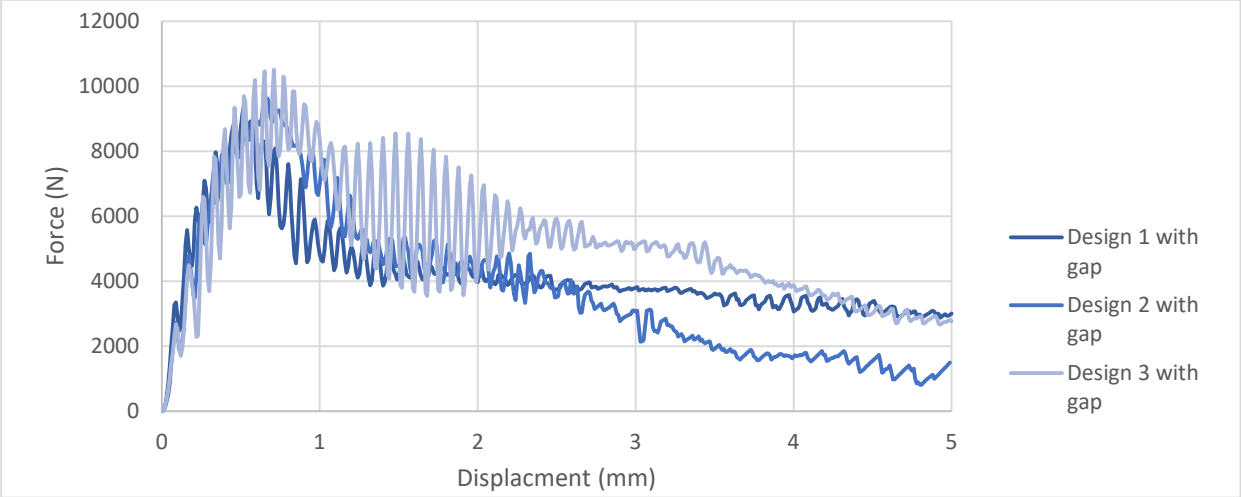

Figure 87 Force displacement curves of the tabs with a gap

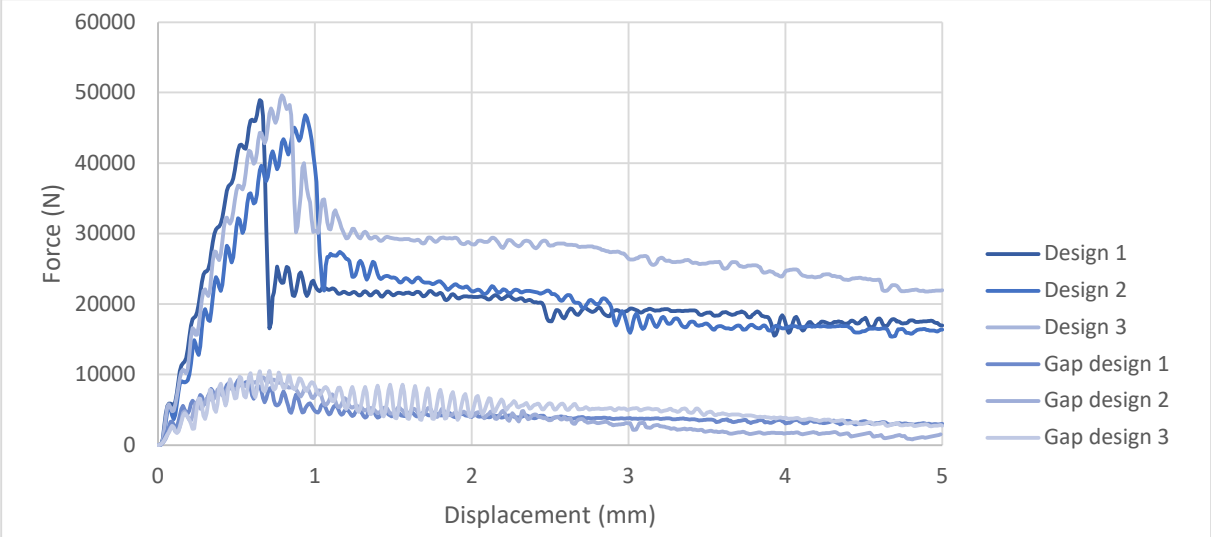

Figure 88 Force displacement curves of the tabs with a gap compared with the original design.

The damage propagation of these interlocking designs with a gap is illustrated in Figure 89. The interlocking tabs seem to fail due to a bending moment, as illustrated by the damage propagation at the bottom of the tabs. The snapshots of the Abaqus model are taken at the peak load and the last calculated point (5mm).

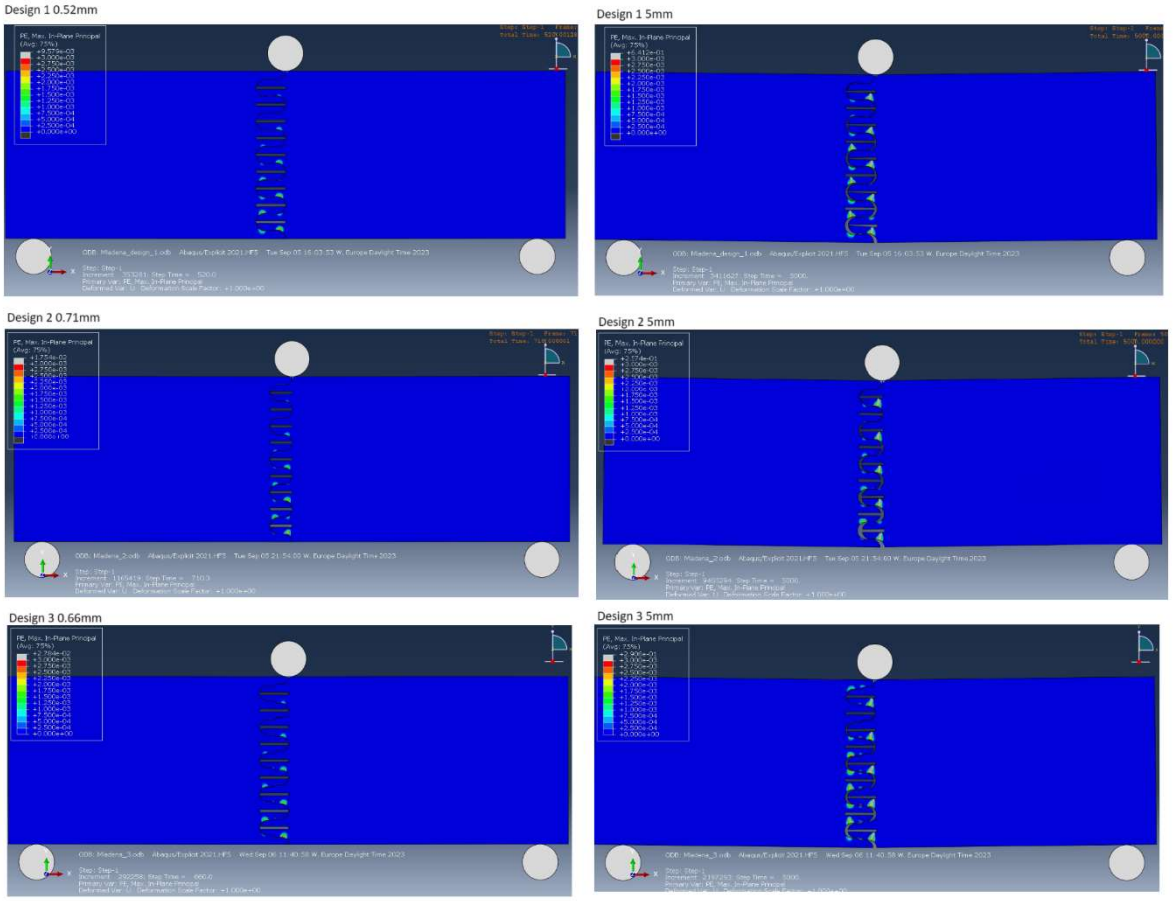

Figure 89 damage at peak load design 1 (0.52mm), design 2 (0.71mm), design 3 (0.66mm) and 5mm

There may be a difference between gap thicknesses, so variations of thicknesses are modelled. The thinner gap designs are seen in Figure 90 and the force-displacement graph of these designs is seen in Figure 91. Here it is noted that the interaction between the inner edges of the tab (seen in red in Figure 90) is not modelled. This is fine because the tab will already have failed before these interact.

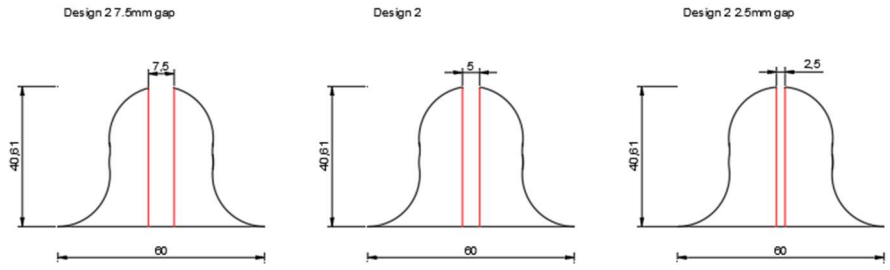

Figure 90 designs of the gaps with a 7.5mm, 5.0mm and 2.5mm gap

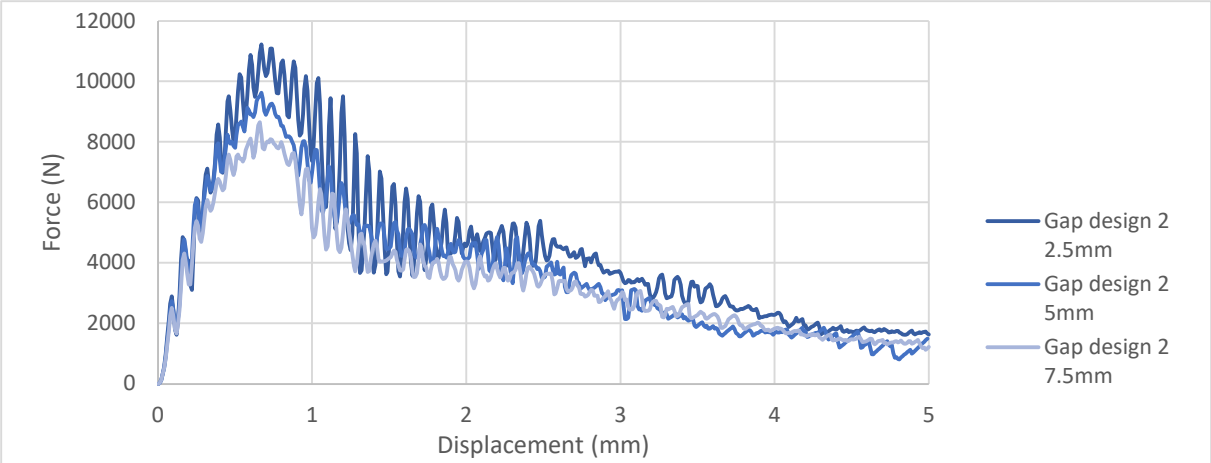

Figure 91 comparison force-displacement curves of a thinner gap design

It seems that the gap thickness does not have a significant influence on the force-displacement curves. The thinner gaps are a bit stronger, due to less material being taken away, and the wider gaps are a bit weaker, due to more material being taken away.

The failure modes observed in the plastic deformation snapshots do not seem to differ much between the thicknesses of the gaps. The cracking pattern seems to be the same. The plastic deformation is seen in Figure 92. These plastic deformations are taken at the peak load 0.5mm and 0.67mm for designs 1 and 2 respectively and at 5mm.

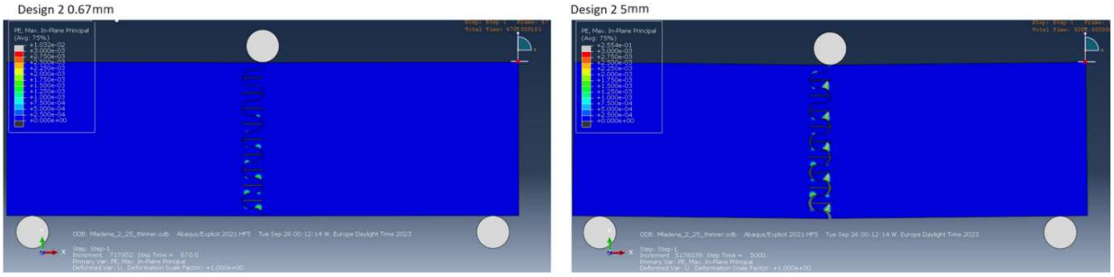

Figure 92 Plastic deformation of interlocking design with a gap of 2.5mm taken at the highest applied force and 5mm.

Another variation of the design with a gap is to have these gaps in one element (so on the right or the left). This configuration allows the tabs to still deform and will likely have less influence on the total strength. The designs are seen in Figure 93.

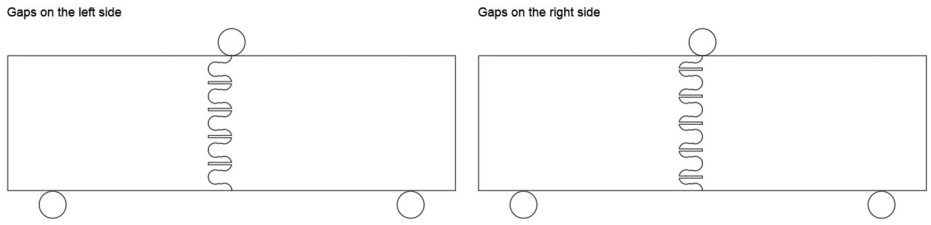

Figure 93 designs of the structure with gaps on the left or right side

The force-displacement curves of the designs depicted in Figure 94 and Figure 95. In these force-displacement curves, there is a significant increase in the total resistance compared to the design with gaps on all sides. However, there is still a notable decrease in strength compared to the design with no gaps. In design 2, it is observed that the gaps on the left result in a resonating behaviour after failure.

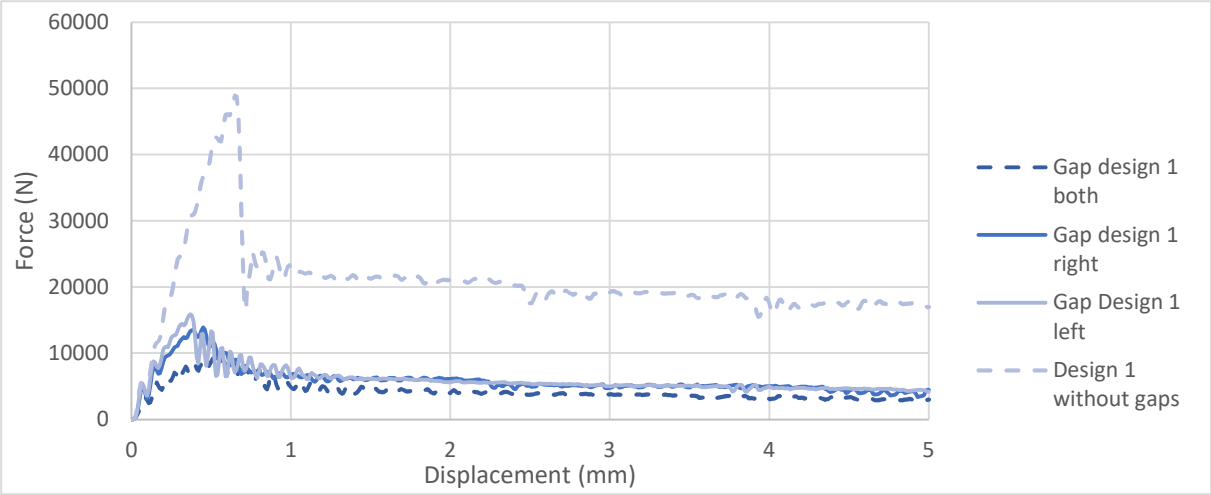

Figure 94 Comparison of the force-displacement graphs for gaps on the right side or left side of design 1

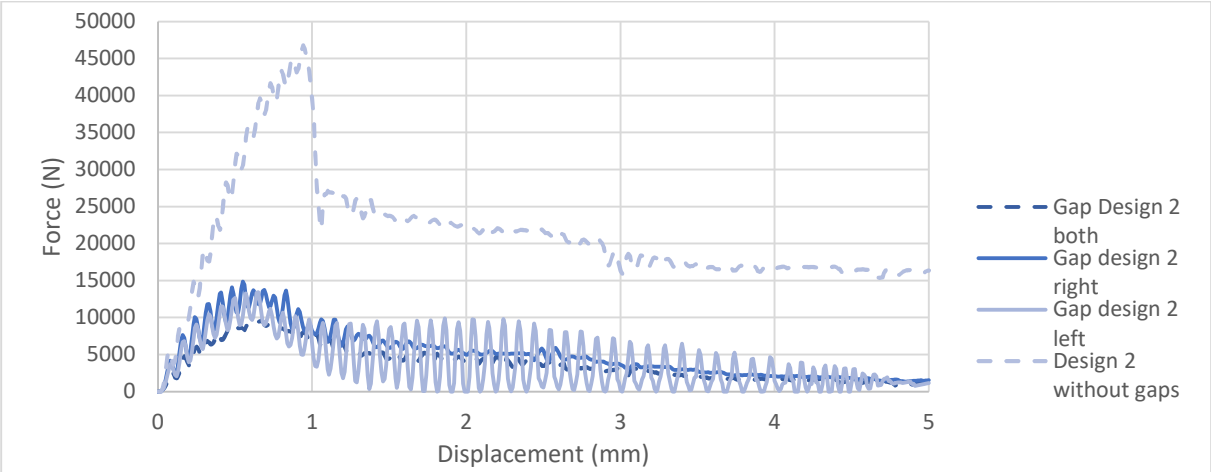

Figure 95 Comparison of the force-displacement graphs for gaps on the right side or left side of design 2

The plastic deformation of design 1 is depicted in Figure 96. As expected, the plastic deformation occurs at the smallest section of the interlocking tabs with a gap. The tabs can pull out completely due to the gap providing room to deform.

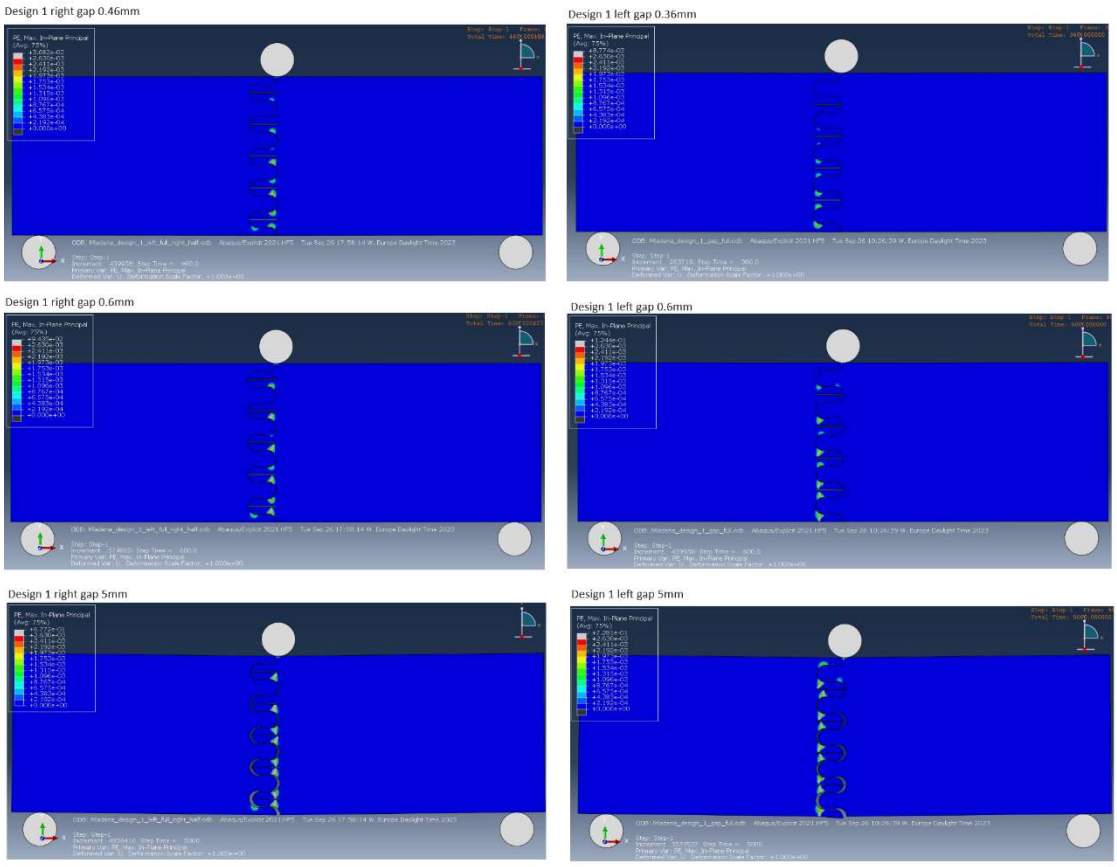

Figure 96 damage propagation of design 1 with gaps either on the right or left side. These are taken just before failure, at 0.6mm top displacement and 5mm top displacement.

There could also be a difference in resistance with different gap depths, so a couple of designs are calculated with different depths. These designs are seen in Figure 97 and Figure 98 and are a variation of designs 1 and 2. It is suspected that the designs with lower depths will act more like the original design. The force-displacement graphs for these designs are seen in Figure 99 and Figure 100.

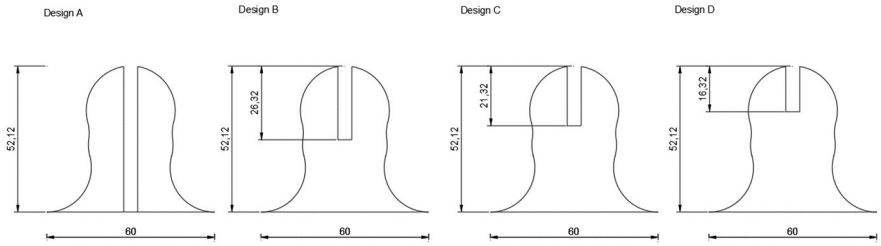

Figure 97 design 1 with different depths of gaps

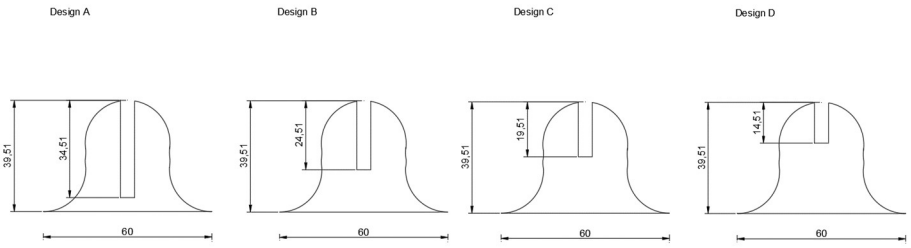

Figure 98 Design 2 with different depths of gaps

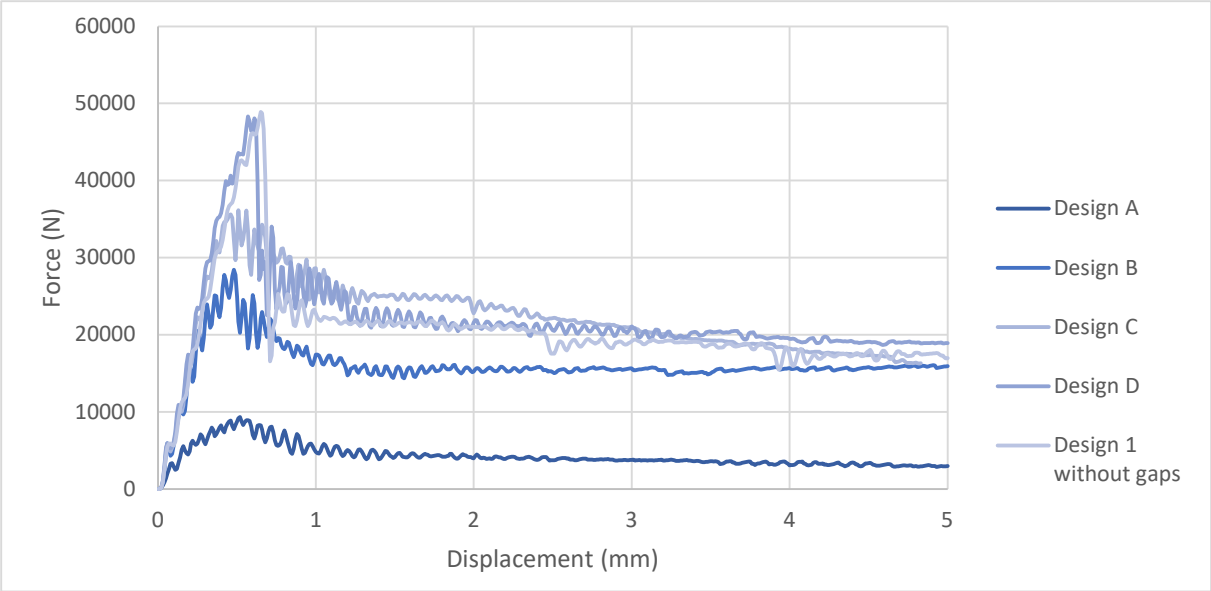

Figure 99 force-displacement curves of design 1 with variations of gap depths. The variations are seen in Figure 94.

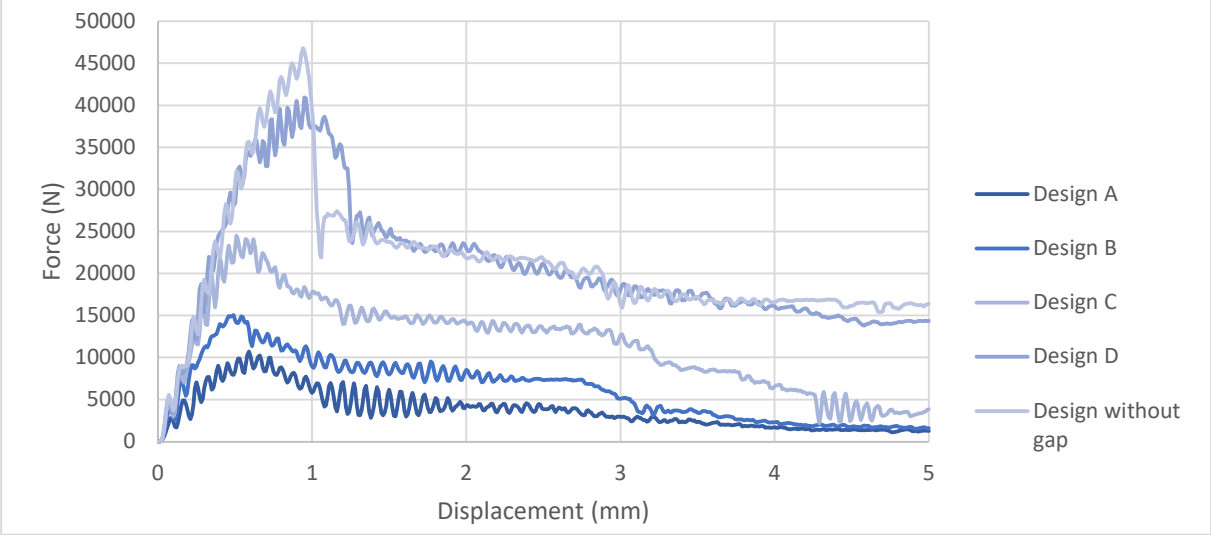

Figure 100 force-displacement curves of design 2 with variations of gap depths. The variations are seen in Figure 95.

To explore the failure mode of design 2 with a shallower gap, the damage propagation for design 2 variant D is plotted at a top displacement of 0.57, 0.96, 1.19 and 5 seen in Figure 101, Figure 103. A zoomed-in picture of the damage propagation at the highest point of reaction force is plotted in Figure 102. The damage propagation of design 1 variant C is plotted in Figure 105 at 0.58, 0.6 and 1mm.

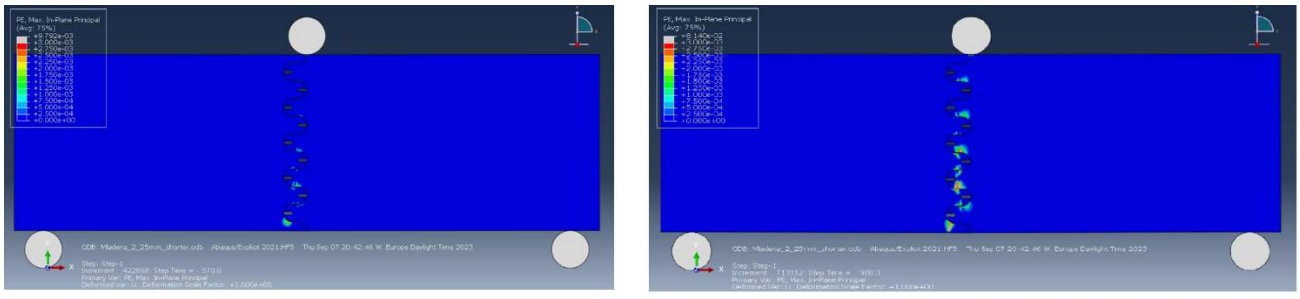

Figure 101 damage propagation of design 2 variant D at a top displacement of 0.57 mm and 0.96mm

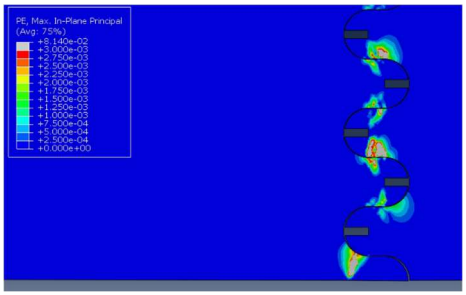

Figure 102 zoomed in damage propagation of design 2 variant D at a top displacement of 0.96mm

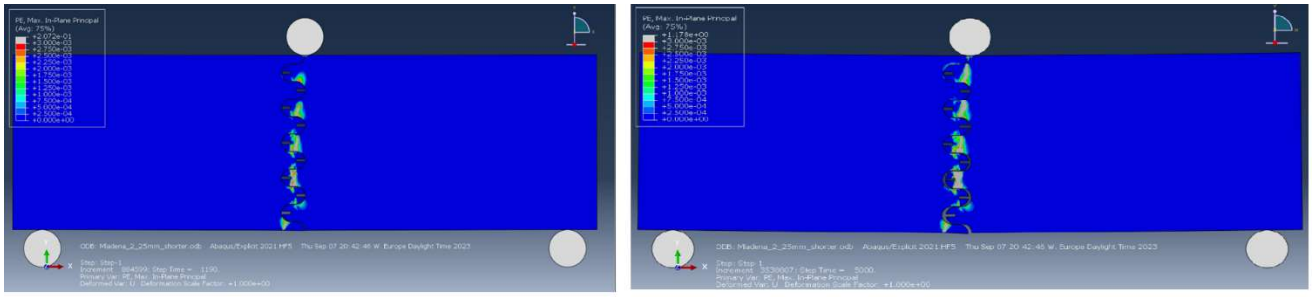

Figure 103 damage propagation of design 2 variant D at a top displacement of 1.19mm and 5.00mm

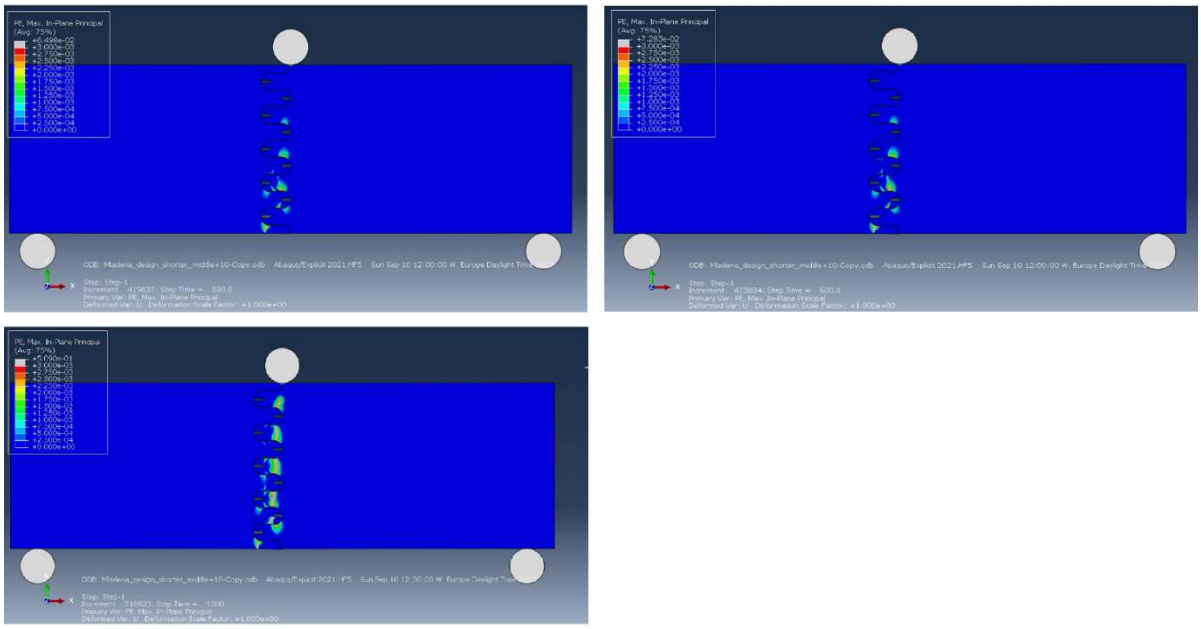

Figure 104 damage propagation of design 1 variant C at a top displacement of 0.58, 0.60 and 5.00mm

Overall, it is observed that there is more plastic deformation in the interlocking connection when applying a gap. The plastic deformation for this design either congregates near the gaps or the neck. It appears that the depth of this gap influences where this plastic deformation occurs. A shallow gap results in plastic deformation occurring in the neck, and a deeper gap leads to deformation near the tips.

A better design could involve a different type of gap. Instead of a square gap, a triangular gap could be applied. The depth of the gap is in between design C and D of design 2, as seen in Figure 98. The triangular gap designs are seen in Figure 105. The force-displacement graphs are seen in Figure 106.

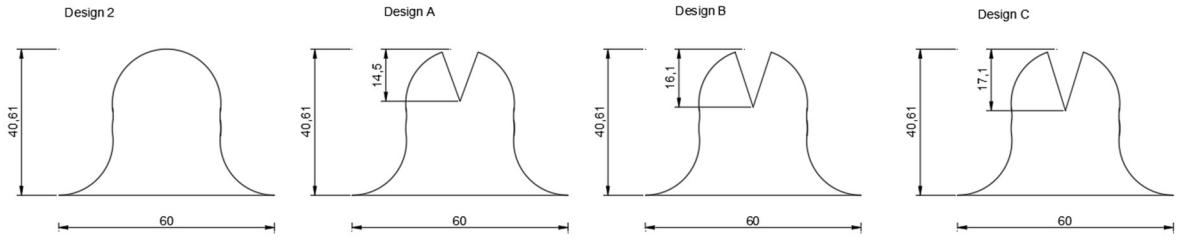

Figure 105 Designs of the tabs with a triangular gap

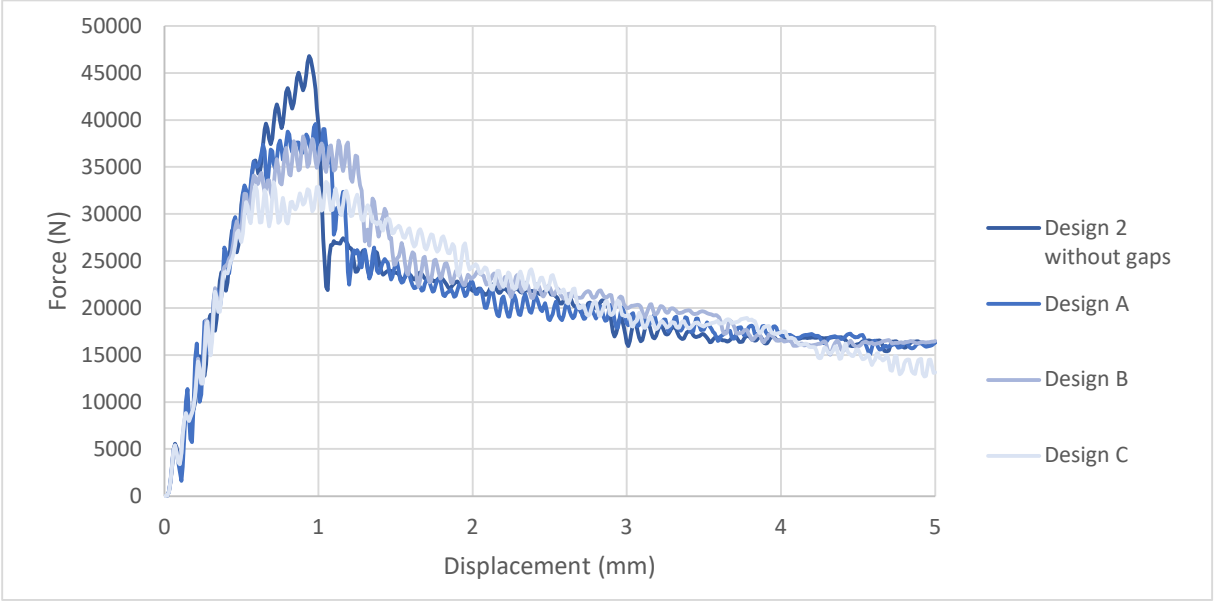

Figure 106 force-displacement curves of design 2 with variations of triangular gap depths. The variations are seen in Figure 97.

The plastic deformation at the displacements of 1mm and 1.5mm are illustrated in Figure 107 and Figure 108 respectively. In both of these pictures, two distinct failure modes are seen: one where the upper part of the tab fails due to a bending moment and one where the neck fails due to tension. It seems that the failure at the top part produces more cracking and fails later.

In summary, the interlocking design with a gap has the potential to increase the ductility of the connection with a small influence on the resistance of the connection. The depth of this gap seemed the most important parameter, as this influences the failure mode of the connection.

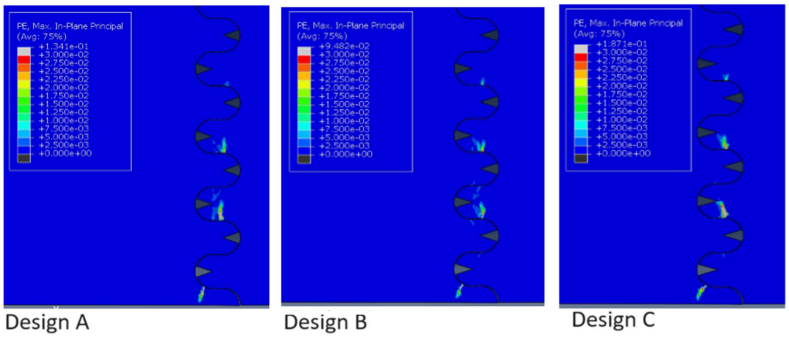

Figure 107 plastic deformation of the designs with a triangular gap at 1mm

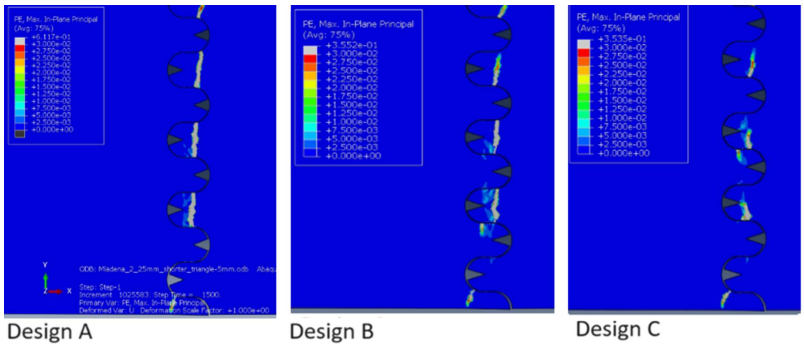

Figure 108 plastic deformation of the designs with a triangular gap at 1.5mm

4.3. Discussion and conclusion of the numerical simulations

The numerical model seems to simulate the interlocking tabs satisfactorily. The experiments from prior papers are modelled satisfactorily, and the researched interlocking designs have a bending resistance that falls in line with prior papers. Additionally, the suggested hand-calculated model seems to align with the numerical model. It is not fully clear when the lowest tab of the right element acts plastically or elastically. A more complex calculation is needed to provide a real answer to these questions. This is explored in chapter 6.

Overall, it is observed that achieving the desired bistable interlocking effect of the interlocks is hard. Some geometric toughening effects are observed when a high-strength material is used in combination with a smooth design. It seems that due to the bending moment on the connection, the tabs do not experience a full axial force, but more force on either the top or bottom of the tab, introducing a bending moment. This is an overall weaker failure mode and makes the bistable behaviour almost impossible.

The loading sequence is quite clear, first a relatively linear loading sequence occurs where some geometric hardening behaviour (pullout of the interlocking tabs) is seen. Then the lowest (half) tab breaks and a small change in the curve is observed. After the peak, the resistance suddenly drops and the plastic softening behaviour of the material becomes governing.

In the parameter study, the results followed the trend described in the papers. Where a higher $\frac{\sigma}{E}$ ratio (reached by increasing the tensile strength or decreasing the elastic modules) made the structure more ductile. It is noted that Ultra-high performance fibre-reinforced concrete does not have a high $\frac{\sigma}{E}$, making it not the best material for an interlocking connection.

The friction coefficient seems to have a significant influence on the design by making it more ductile at the cost of the maximum resistance. The increase in plastic strain at peak resistance seems to affect the structure positively, and an increase in toughness and strength is observed.

The design with one circle (design 2a) had a significant improvement in the total ductility of the interlocking connection. It seemed that the failure was prolonged with a small influence on the total strength of the connection.

Results of the peak load and displacement at the peak load are seen in Figure 109, Figure 110 and Figure 111.

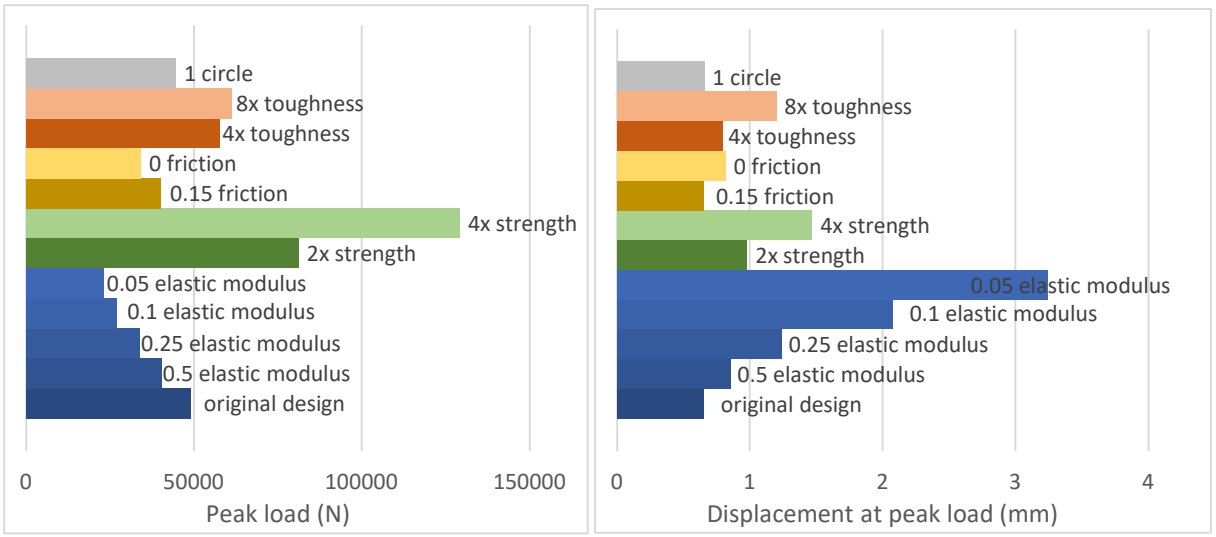

Figure 109 results of the parameter study of design 1, with left the maximum load and right the displacement at this maximum load

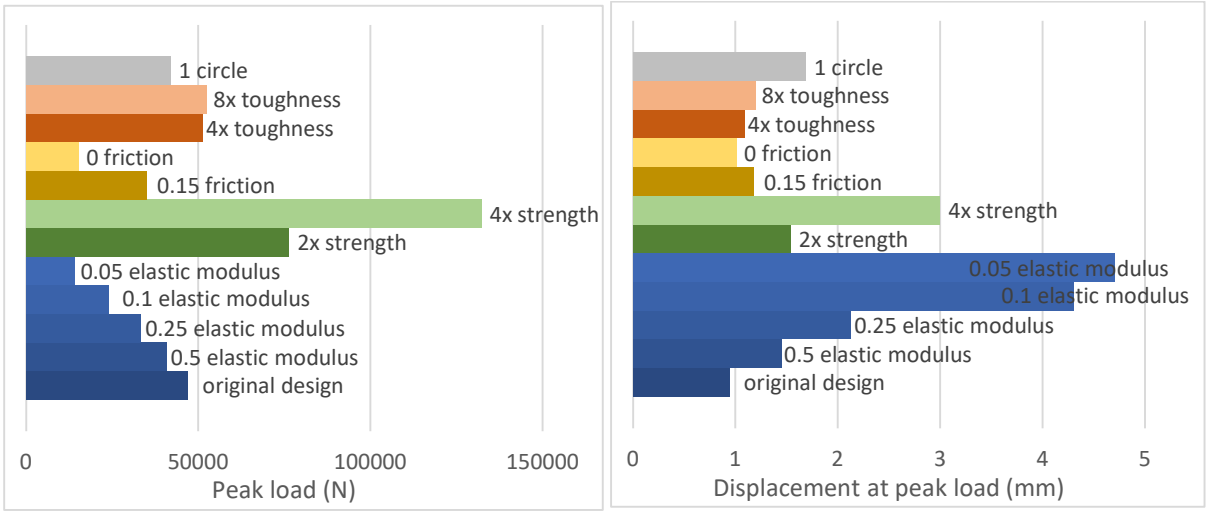

Figure 110 results of the parameter study of design 2, with left the maximum load and right the top displacement at this maximum load

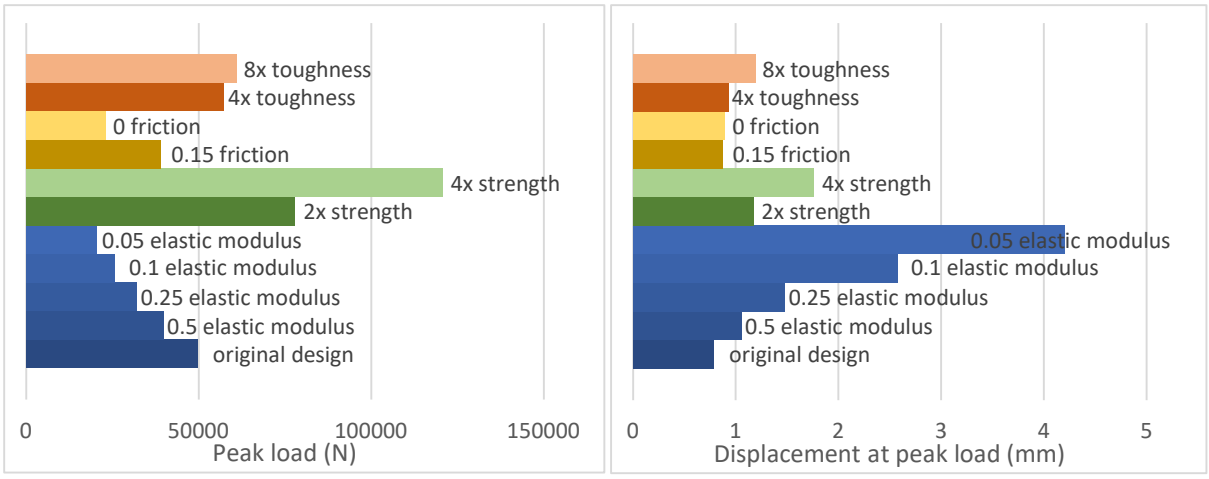

Figure 111 results of the parameter study of design 3, with left the maximum load and right the displacement at this maximum load

In these figures, it is noted that the displacement at the peak load does not fully show the ductility of the structure. The displacements could be greater after the max reaction force, but a comparison point has to be made.

The interlocking design with a gap has the potential to increase the ductility of the connection with a small influence on the resistance of the connection. The depth of this gap seemed the most important parameter, as this influences the failure mode of the connection.

Overall, it appears that design 2 has the most favourable properties for a connection loaded with a bending moment. Specifically, the design with one circle (design 2a) and the design 2 with a (triangular) gap. These designs exhibit the most ductile failure while minimizing the impact on the total bending resistance of the structure. Therefore, these designs are chosen for the experimental study.

5. Experimental results

In this section, an analysis of the specimens under a bending load is performed. This is done by presenting the force-displacement curve for each specimen and analysing the cracking using digital image correlation. Additionally, the compressive strength and bending resistance of the UHPFRC mixture are tested.

5.1. Bending resistance

The results of the conducted bending resistance test are presented in Table 7. The first column gives the sample number, while the second column shows the total load on the specimen. Below the results, the average is calculated along with the standard deviation.

	Load
	kN
Sample 1	11.6
Sample 2	10.644
Sample 3	8.532
Sample 4	10.131
Sample 5	12.831
Sample 6	12.975
Sample 7	17.73
Sample 8	12.616
Sample 9	15.093
Sample 10	13.794
Sample 11	15.095
Sample 12	15.244
average	13.024
standard deviation	2.571

Table 7 results of the bending resistance test

With the average load of 13.024kN, the bending resistance is calculated. This is done in accordance with the paper “Reinforced hybrid concrete beams with a U-shaped SHCC mould” (23). The calculation is seen in Appendix D Bending resistance calculation and results in a bending resistance of 14.9MPa. Assumptions have been made in this calculation, including an elastic modulus of 45000MPa, max elastic resistance of 8.9 MPa and a plastic strain at max plastic resistance of 0.263%.

5.2. Compressive strength

The results of the compression test are seen in Table 8. Where side 1 is the compressive resistance on one side, and side 2 is the compressive resistance on the other side (see Figure 112). The average resistance is 141.9N/mm^2 with a standard deviation of 11.5.

Compressive strength	Side 1		Side 2	
	Load (kN)	Stress (MPa)	Load (kN)	Stress (MPa)
Sample 1	219.22	137.012	226.814	141.794
Sample 2	206.94	129.325	207.029	129.393
Sample 3	190.837	119.273	200.734	125.459
Sample 4	207.502	129.689	203.272	127.045
Sample 5	217.427	135.892	234.214	146.384
Sample 6	220.817	138.01	222.616	139.135
Sample 7	237.204	148.252	233.577	145.985
Sample 8	222.963	139.352	237.822	148.639
Sample 9	237.611	148.507	239.549	149.718
Sample 10	229.261	143.288	235.54	147.212
Sample 11	254.937	159.335	254.335	159.335
Sample 12	254.962	159.335	254.95	159.343
	Load (kN)		Stress (MPa)	
average	227.089		141.946	
standard deviation	18.325		11.477	

Table 8 results of the compression test. Each side of the specimens is tested. The average and standard deviation of all the tested specimens and sides are seen at the bottom of the table.

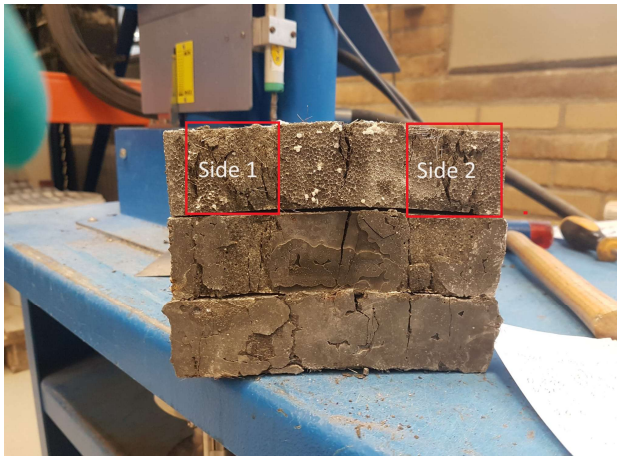

Figure 112 compressive zones for each sample

5.3. 3-point bending test

The force-displacement curves of the specimens are seen in Figure 113. Where samples 1 and 2 are derived from design 1, sample 3 and 4 from design 2 and sample 5, 6 and 7 from design 3.

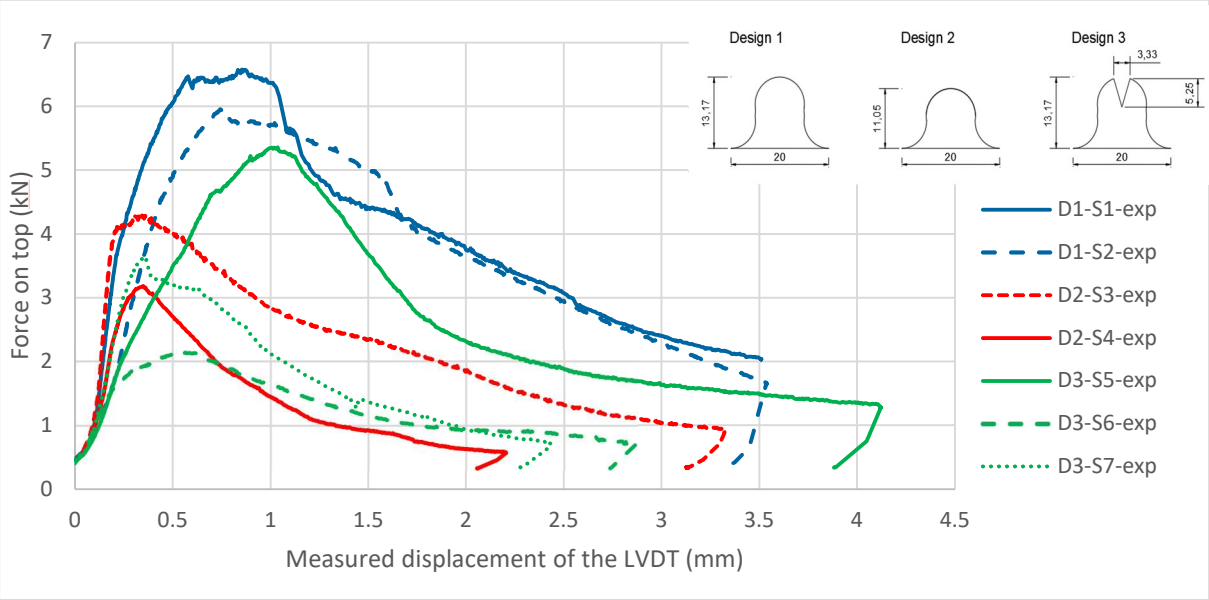

Figure 113 force-displacement curves of the experimental research.

In Figure 113 it is noted that the total resistance of the experiments is lower than expected. Scaling the resistance of the numerical model to match the experimental values yields the following (expected) values: 15.6kN for design 1, 14.09kN for design 2 and 12.71kN for design 3. This means that design 1 is reduced to 40% of the numerical model, Design 2 25% and design 3 deviates from 44% to 17%.

The total strength compared to a monolithic connection is compared. For the test results, this is in $\approx 9.5\%$ for design 1, $\approx 5.0\%$ for design 2 and 7.6% to 3% for design 3. For the numerical model (where the material properties are assumed weaker, 9.6MPa instead of 14.9MPa) this was about 30% to 32%. This reduction in strength compared to the numerical model could have multiple reasons;

- The fibres are not distributed well.
- Due to the oil used the friction coefficient is lower.
- The pattern of the interlocking radius of the made tabs could deviate from the designed radius. Due to the small size, this could have a big influence on the reaction of the joint.

Design 1 emerges as the most effective interlocking design among the three. It exhibits the most toughening and has the highest maximum strength. Design 2 seems to fail faster, and has less hardening behaviour and less bending resistance. Design 3 seems to deviate quite a bit, sample 4 shows decent results but samples 5 and 6 do not. It is suggested that there are small deviations in gap depths, as seen in the parameter study, small increments have a big influence on the total strength.

The DIC analyses of design 1 sample 1 is seen in Figure 115 and Figure 116. The DIC analyses of design 1 sample 2 are seen in Figure 117 and Figure 118. The bending failure of design 1 can be described in 3 stages, these are;

Stage 1: As the tensile force increases, the bending moment is resisted by normal and frictional stresses between the interlocking tabs. Some cracks seem to appear in the interlocking tabs themselves.

Stage 2: After point 1 a small strain-hardening regime occurs until point 3, after which there is a small plateau. This stems from the formation of cracks in the UHPFRC and the pullout of the interlocks. The forces peak at point 4 (6,0-6.6kN). During these phases, the interfaces are completely debonded, and the forces between tabs are transferred by mechanical interlock and friction.

Stage 3: After point 5, there is a gradual loss in bending resistance related to the gradual plastic softening phases of the material itself combined with the pullout of the tabs.

After testing the interlocking connection is taken apart and is seen in Figure 114.

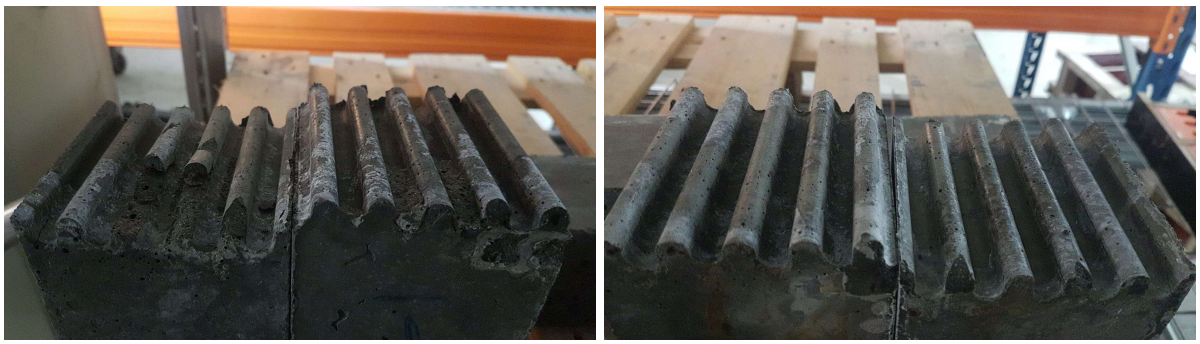

Figure 114 Design 1 taken apart after testing. Where the picture on the left is sample 1 and the picture on the right is sample 2.

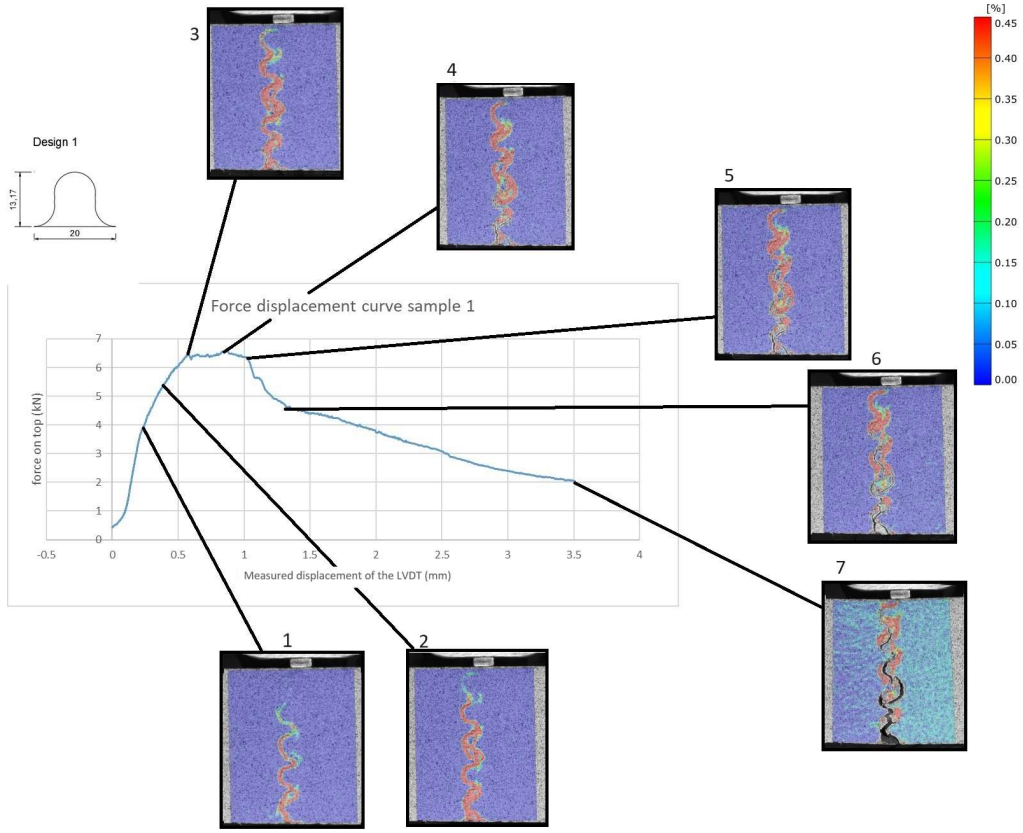

Figure 115 force-displacement diagram illustrating the bending response of design 1 sample 1.

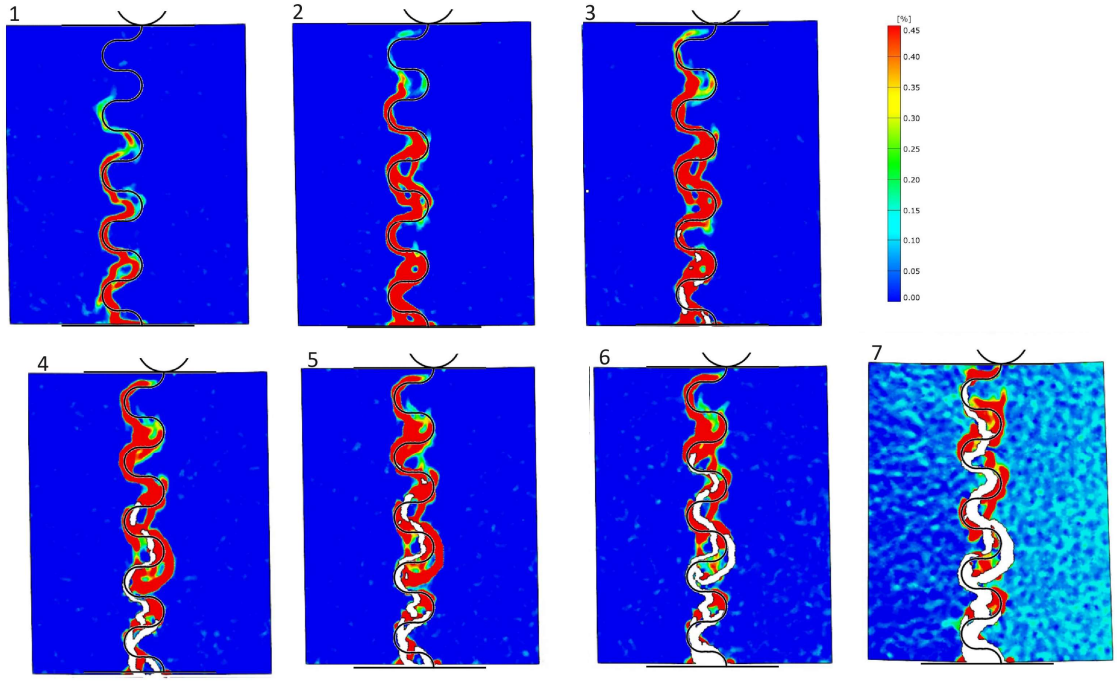

Figure 116 Strain contours of design 1 sample 1.

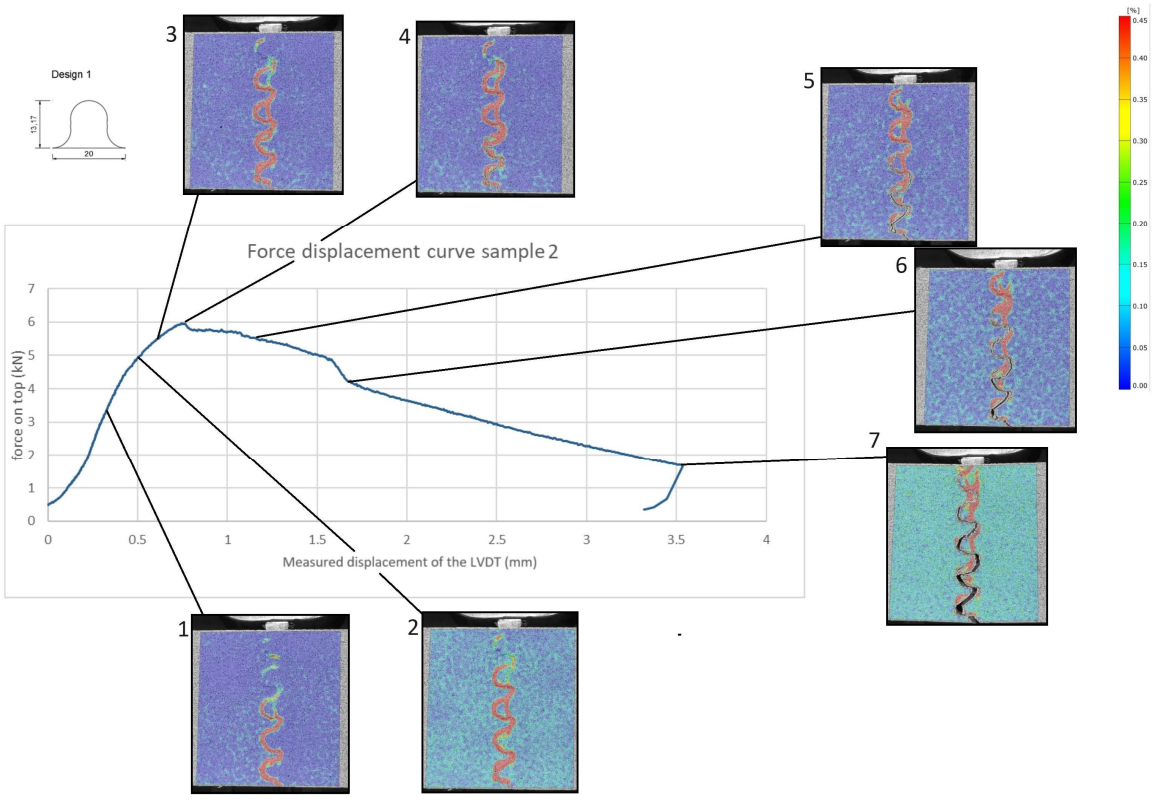

Figure 117 force-displacement diagram illustrating the bending response of design 1 sample 2.

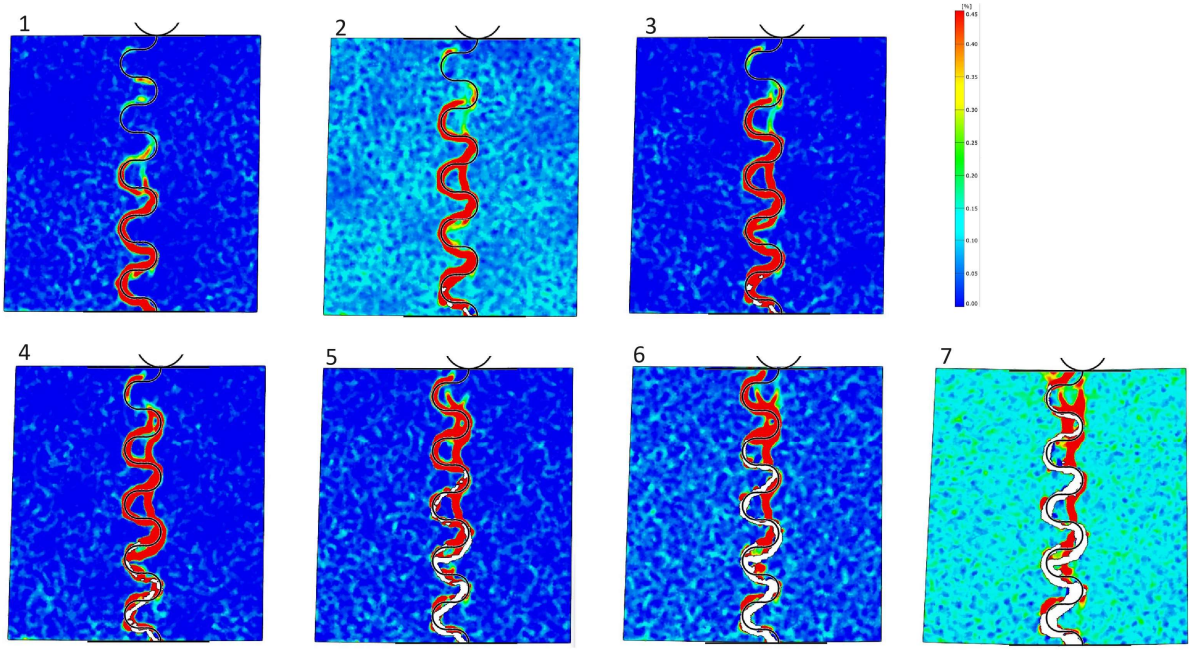

Figure 118 Strain contours of design 1 sample 1.

The DIC analyses of design 2 sample 3 are seen in Figure 120 and Figure 121, design 2 sample 3 is seen in Figure 122 and Figure 123.

In design 2, the peak resistance is reached earlier than in design 1, indicating that the design is a bit less ductile. The first crack that appears seems to be rather linear, running through the interlocking tabs and interface. This design can be divided into 3 stages;

Stage 1: From the start of loading to point 1, an elastic regime occurs. After point 1 There seems to be a rather vertical crack propagated from the bottom to the highest full tab of the left element. These cracks are present in both the interface and the tabs. This crack appears to increase in size until the onset point 3.

Stage 2: After point 3, the total resistance seems to plateau. This arises from the formation of cracks in the UHPFRC and some pull out of the interlocks. The forces peak at point 4 (3.18-5.36kN). During this stage, cracks also seem to appear in the right element through the interface and interlocking tabs.

Stage 3 A strain-softening phase after point 5 and onward. This phase is dominated by the plastic softening of the material itself and the pull out of the interlocks.

After testing, the specimens are opened, this is seen in Figure 119.

Figure 119 Design 2 taken apart after testing. Where the picture on the left is sample 3 and the picture on the right is sample 4.

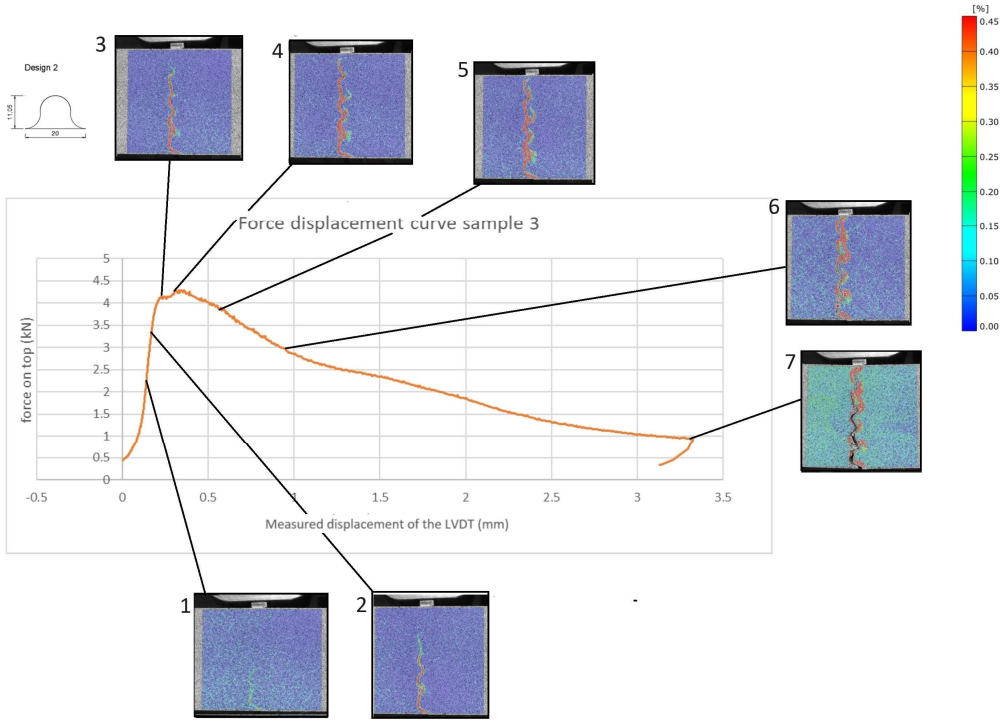

Figure 120 force-displacement diagram illustrating the bending response of design 2 sample 3.

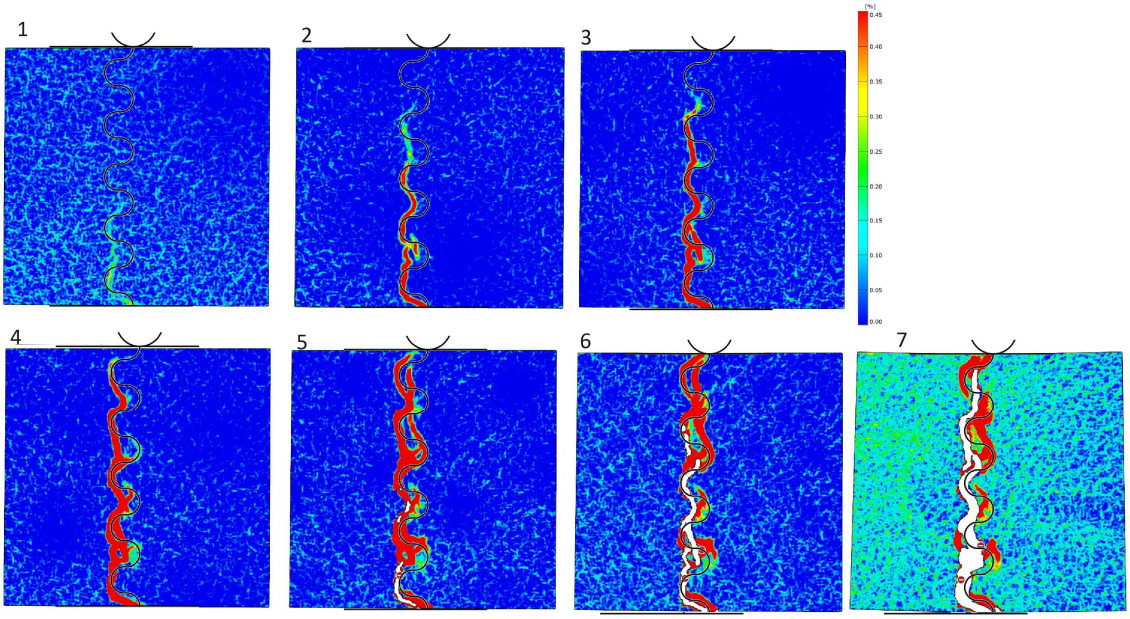

Figure 121 Strain contours of design 2 sample 3.

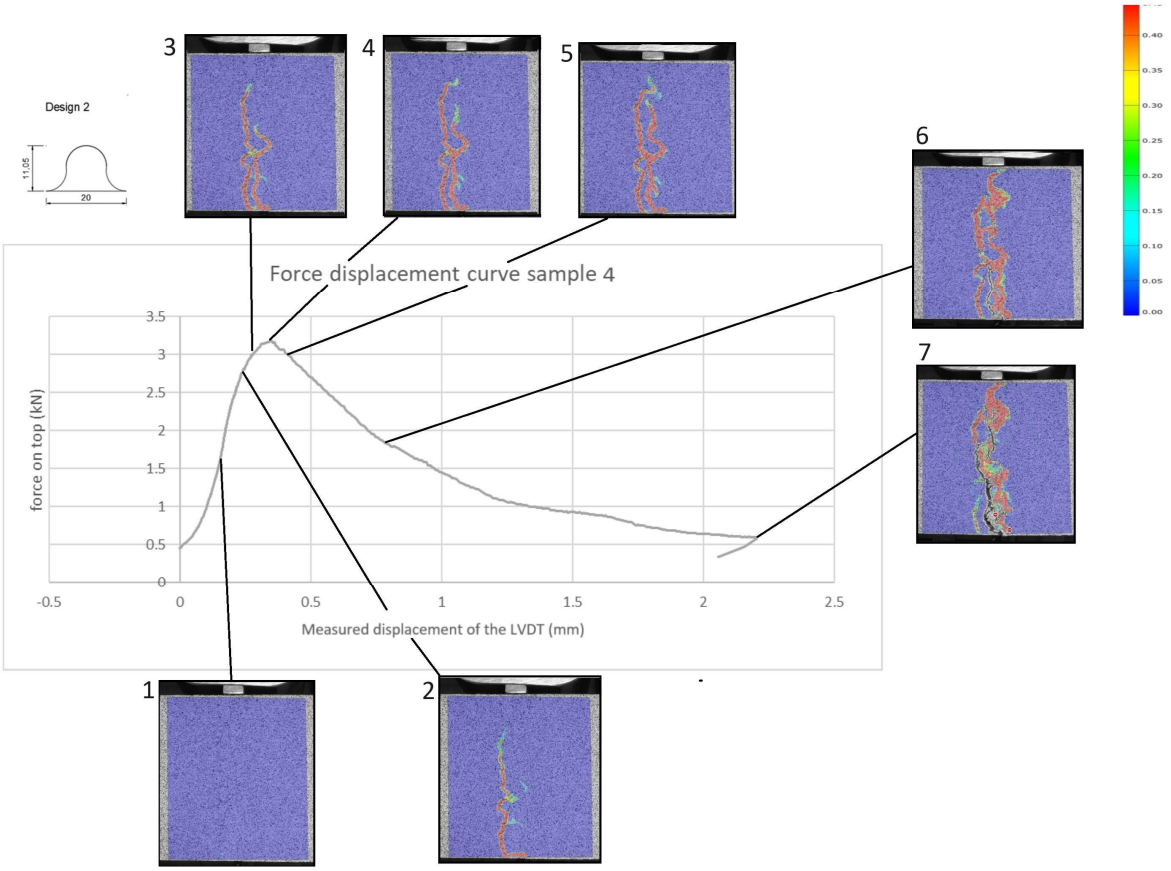

Figure 122 force displacement diagram illustrating the bending response of design 2 sample 3.

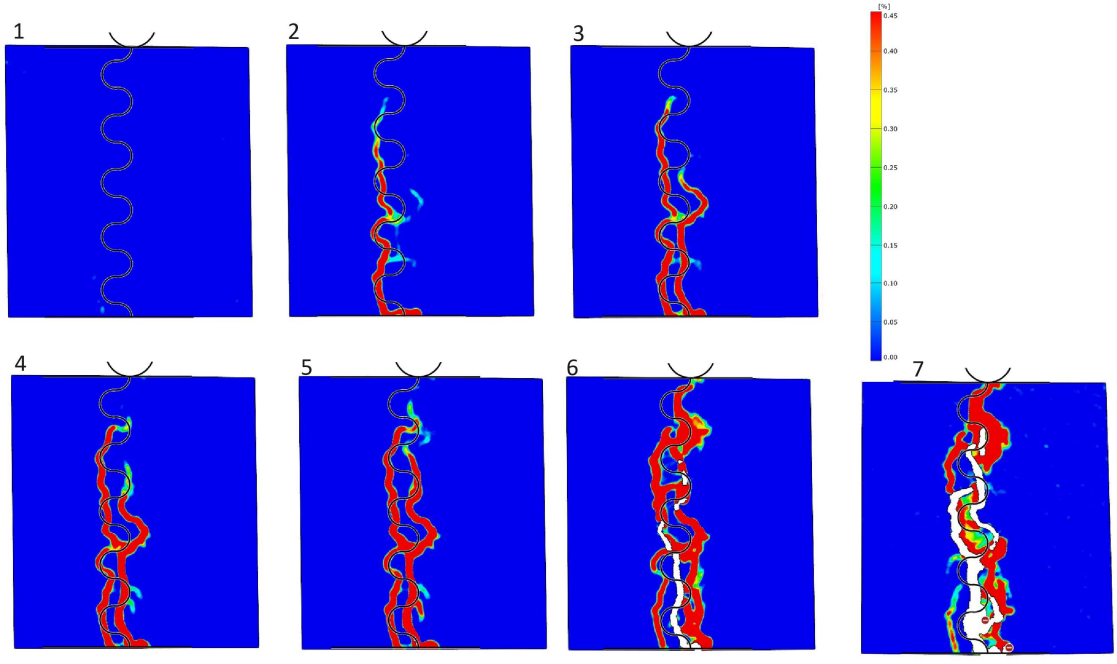

Figure 123 Strain contours of design 2 sample 3.

The DIC analyses of design 3 sample 5 are seen in Figure 125 and Figure 126, design 3 sample 6 is seen in Figure 127 and Figure 128, design 3 sample 7 is seen in Figure 129 and Figure 130.

In these designs, the cracks congregate near the triangular gaps. Indicating that the failure mode is due to a bending moment in the tips of the bistable interlocks. This design can be divided into 3 stages, these stages are;

Stage 1: From start loading to point 1, The tabs pull out. Some cracks are spotted near the gaps.

Stage 2: after point 1, the increase in total resistance with each displacement is less. This is due to the pullout of interlocking tabs and the plastic behaviour of the material itself. The force peaks at point 4 (2.13-5.96kN).

Stage 3 A strain-softening phase after point 4 and onward. This phase is dominated by the plastic softening of the material itself and pulls out of the interlocks

After testing the specimens are opened and seen in Figure 124.

Figure 124 Design 3 taken apart after testing. Where the picture on the top left is sample 5, the picture on the top right is sample 6 and the picture on the bottom left is sample 7.

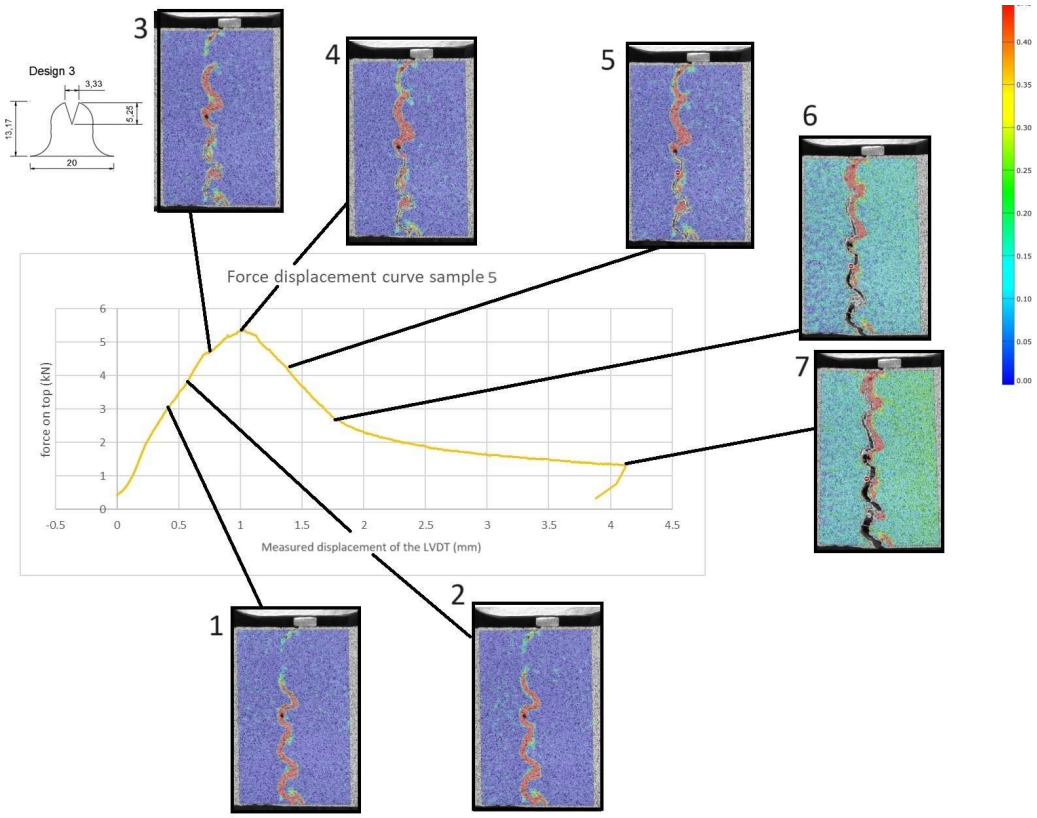

Figure 125 force displacement diagram illustrating the bending response of design 3 sample 5.

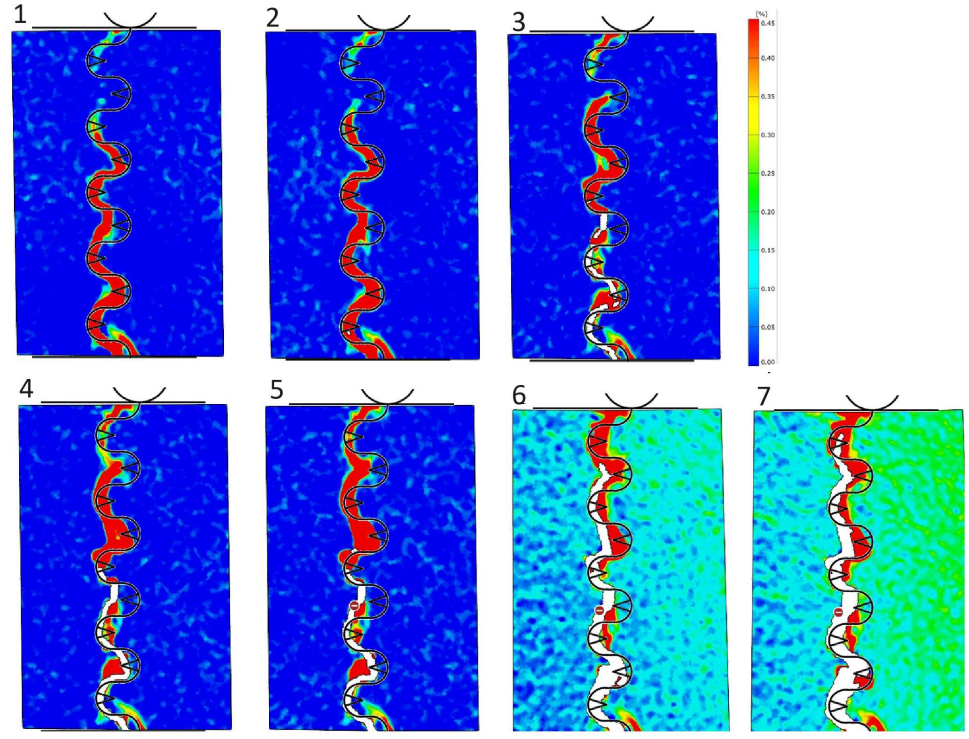

Figure 126 Strain contours of design 3 sample 5.

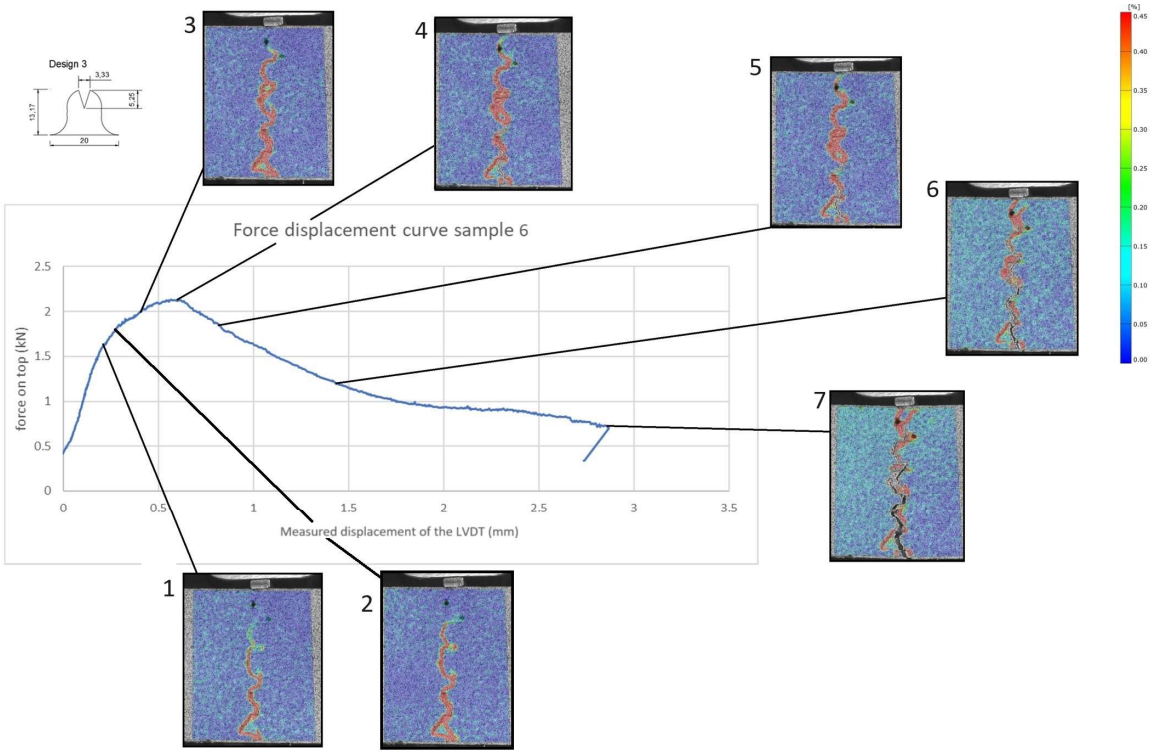

Figure 127 force-displacement diagram illustrating the bending response of design 3 sample 6.

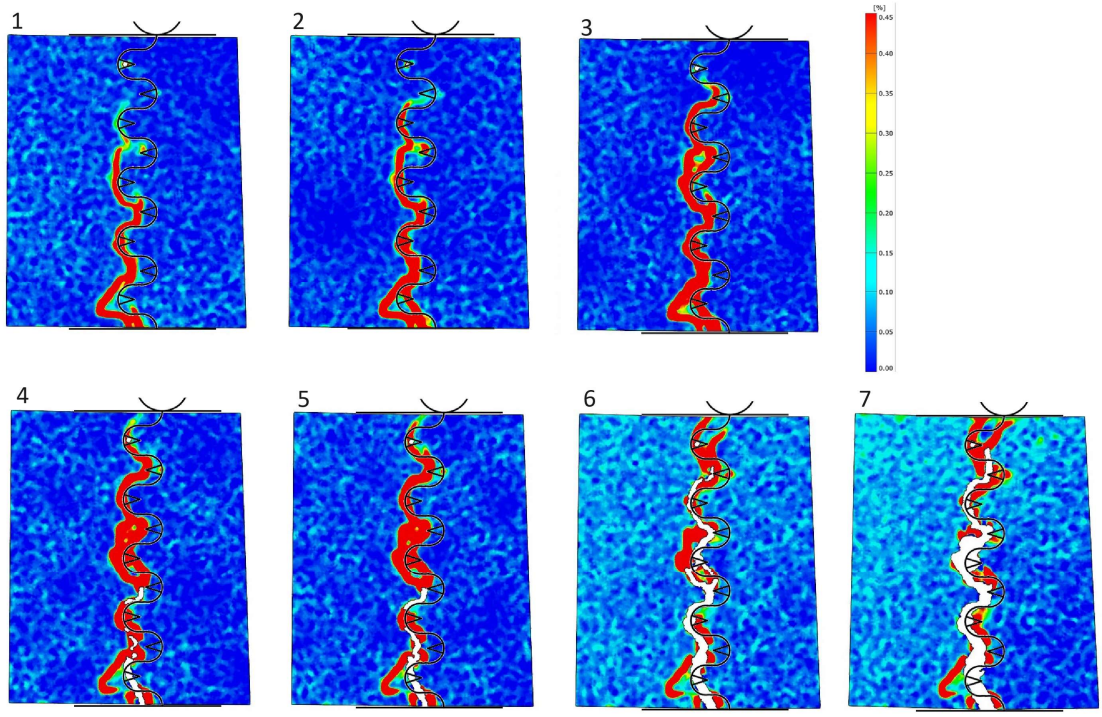

Figure 128 Strain contours of design 3 sample 6.

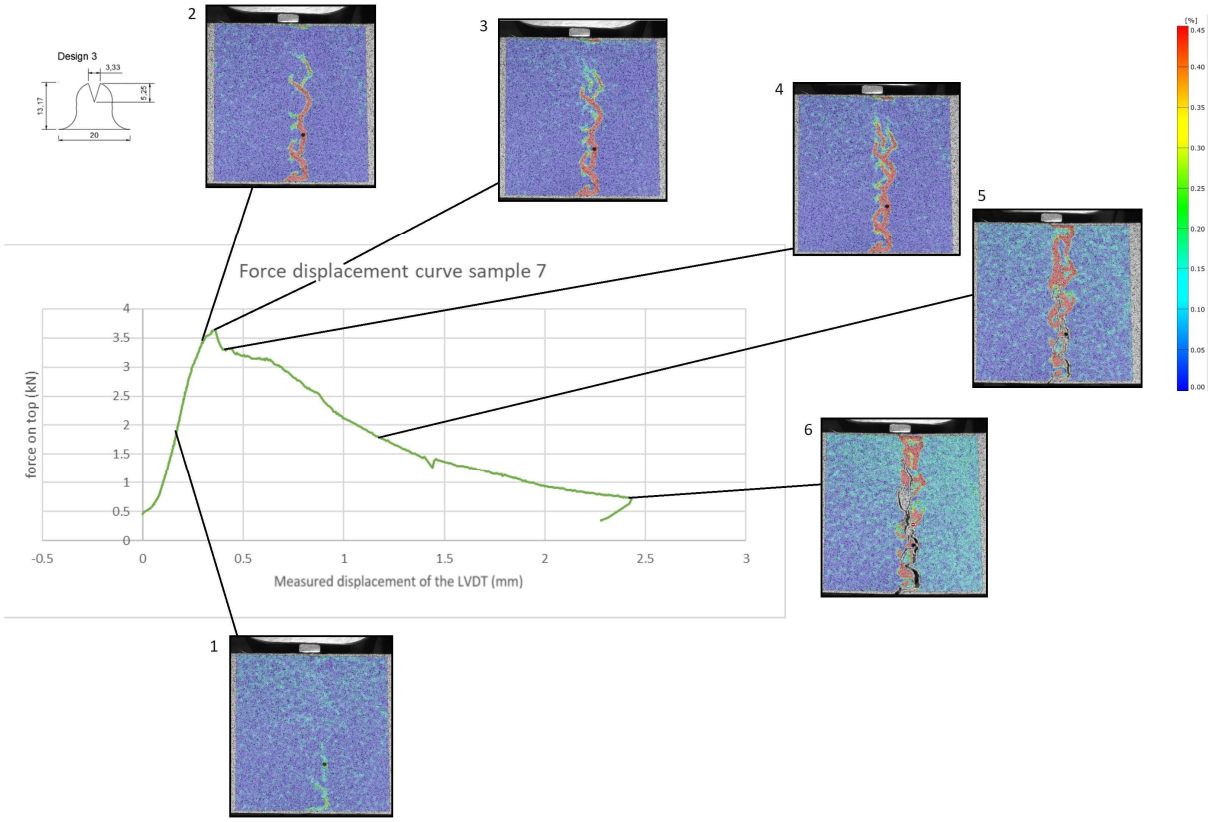

Figure 129 force displacement diagram illustrating the bending response of design 3 sample 7.

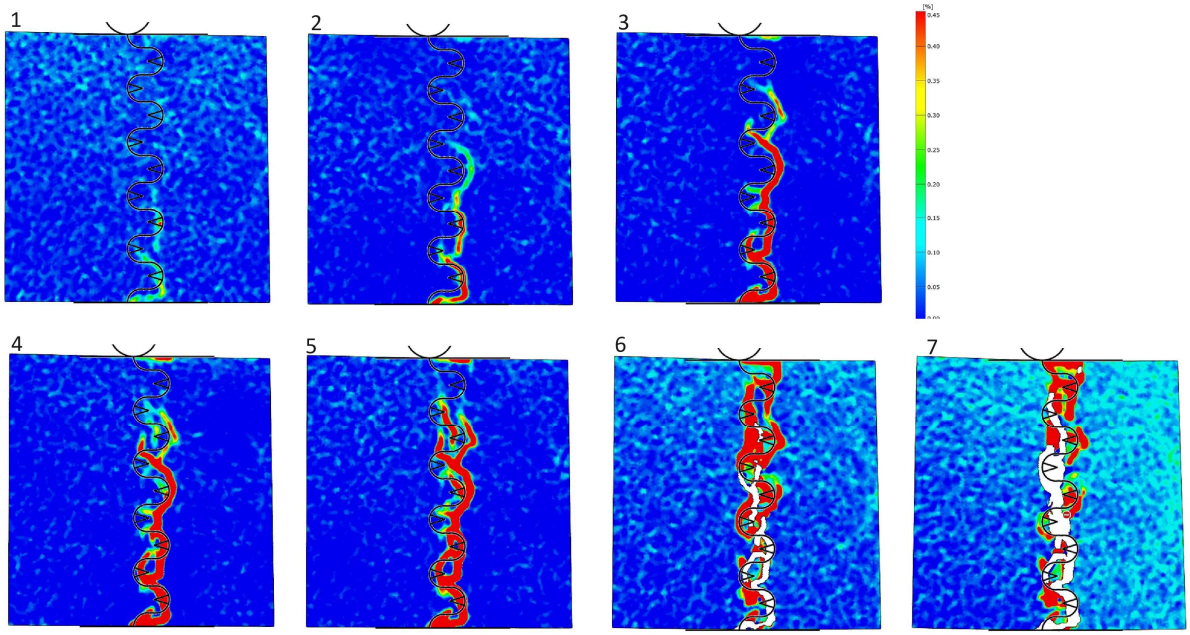

Figure 130 Strain contours of design 3 sample 7.

6. Analytic approximation of the bistable interlocking connection

An analytic approach is made to get a better understanding of the failure mode and validate the numerical analyses. The analytic approach is based on the paper “Interface fracture of micro-architectured glass: Inverse identification of interface properties and a novel analytical model” (16), where interlocks are designed with one circle. Therefore, design 2a with one circle is approximated first.

To simplify the approximation, four assumptions have been made. Firstly, it is assumed that there is no bending moment acting on the tabs, meaning they only break due to full tensional force. Consequently, any vertical forces resulting from frictional or contact forces are ignored. Secondly, it is assumed that the tabs break after the maximum force is reached, without undergoing plastic deformation. Thirdly, the connection is treated as a rigid body. Lastly, it is assumed that the compressive zone and rotation point stay the same. Where the rotation point is 60mm from the top, and the centre of compression 30mm from the top (places seen in Figure 131).

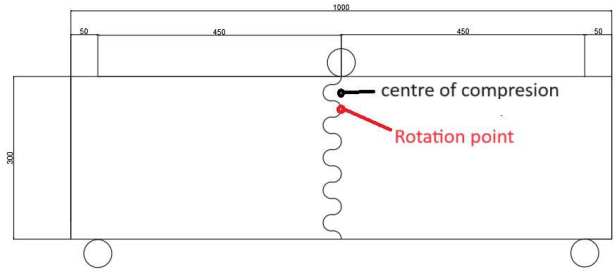

Figure 131 centre of compression and rotation point for the calculation

The approximation starts by assigning coordinates to the centre of each tab. These coordinates are then rotated with an angle of Θ around the rotation point. This rotation results in four contact points where the tabs compress. The total amount of compression is determined by the change in distance between the coordinates. The steps and formulas involved are seen in Figure 132. These formulas are from the literature review, the formula for the total compression (δ_i) is labelled as 2.6.

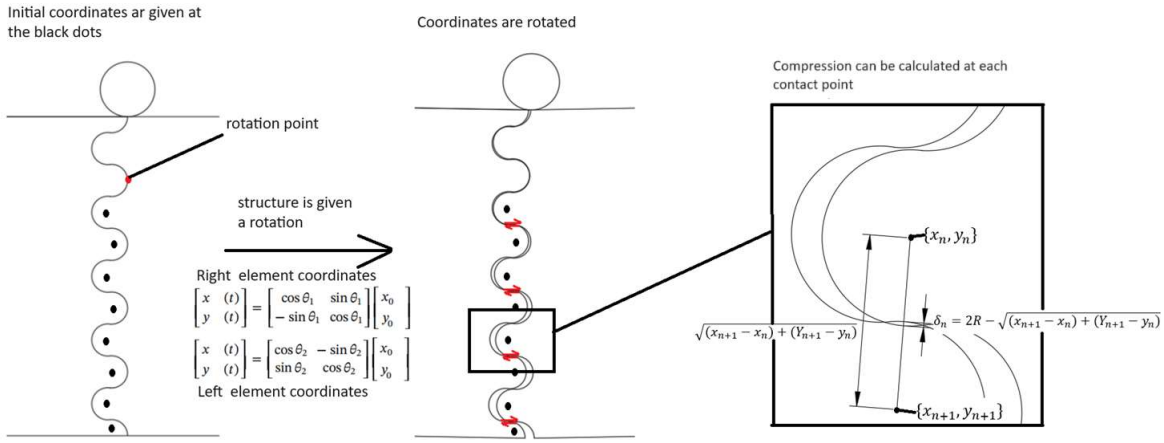

Figure 132 The steps taken to calculate the total compression at the contact points.

With the total compression, the contact force is determined using formulas 2.1 and 2.2 from the literature review, which is also provided below and referred to as 6.1 and 6.2.

$$\delta_n = \frac{a^2}{2R}\left[2\ln\left(\frac{4R}{a}\right) - 1\right] \quad 6.1$$

$$a^2 = \frac{4PR}{\pi tE} \quad 6.2$$

Then, the local angle of the force is calculated, which determines the direction of the contact force. It is calculated with the formula provided in Figure 133 (formula 2.7). With this local angle, the horizontal forces are calculated, using the formula labelled as 6.3. In this formula, the vertical forces are ignored.

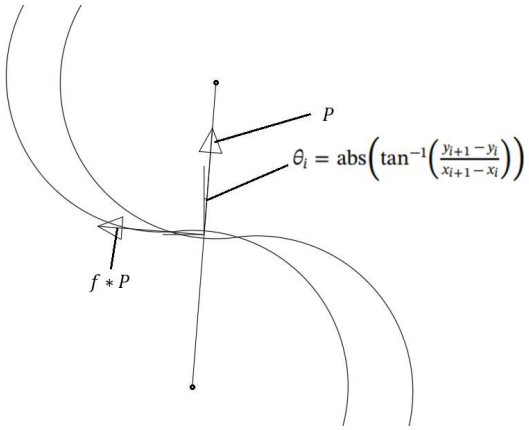

Figure 133 The resultant forces due to the contact force and the local angle of this contact force

$$P_n\left(\sin(\theta_n) + f\cos(\theta_n)\right) \quad 6.3$$

These horizontal forces all have a distance to the assumed compressive point. When the force is multiplied by this distance, the total resistance is calculated with a given angle. The formula for this is seen below, With z_n being the distance to the assumed compressive point from the contact points.

$$M = \sum_{n=1}^{4} P_n\left(\sin(\theta_n) + f\cos(\theta_n)\right) * z_n \quad 6.4$$

It is important to note that the individual tabs could break at different times. To model this, it is assumed that a tab will break when the maximum tensional force is reached in the tab. This means that the maximum tensional force (seen in the equation 6.5) shouldn't be higher than the equation 6.3.

$$F_{max} = \sigma_{tp} * A_n \quad 6.5$$

This maximum force (equation 6.5) is plotted with the forces in each tab (equation 6.3). The points where these lines intersect are read and placed in a Heavyside function to simulate failure. This formula is seen below (equation 6.6) where $u_{f,n}$ is the displacement where this maximum force is reached.

$$M = \sum_{n=1}^{4} P_n\left(\sin(\theta_n) + f\cos(\theta_n)\right) * z_n - \left(P_n\left(\sin(\theta_n) + f\cos(\theta_n)\right) * z_n\right) * Heavyside(-u_{f,n} + u) \quad 6.6$$

With this formula, a graph is plotted incorporating all the dimensions of design 2a with 1 circle. For a better comparison, the angle of the connection (Θ) is translated to the displacement at the top with the formula $tan(\Theta) * \frac{1}{2}l = u$, and the bending moment is translated to applied force with $\frac{M}{l} * 4 = N$. This graph is seen in Figure 134.

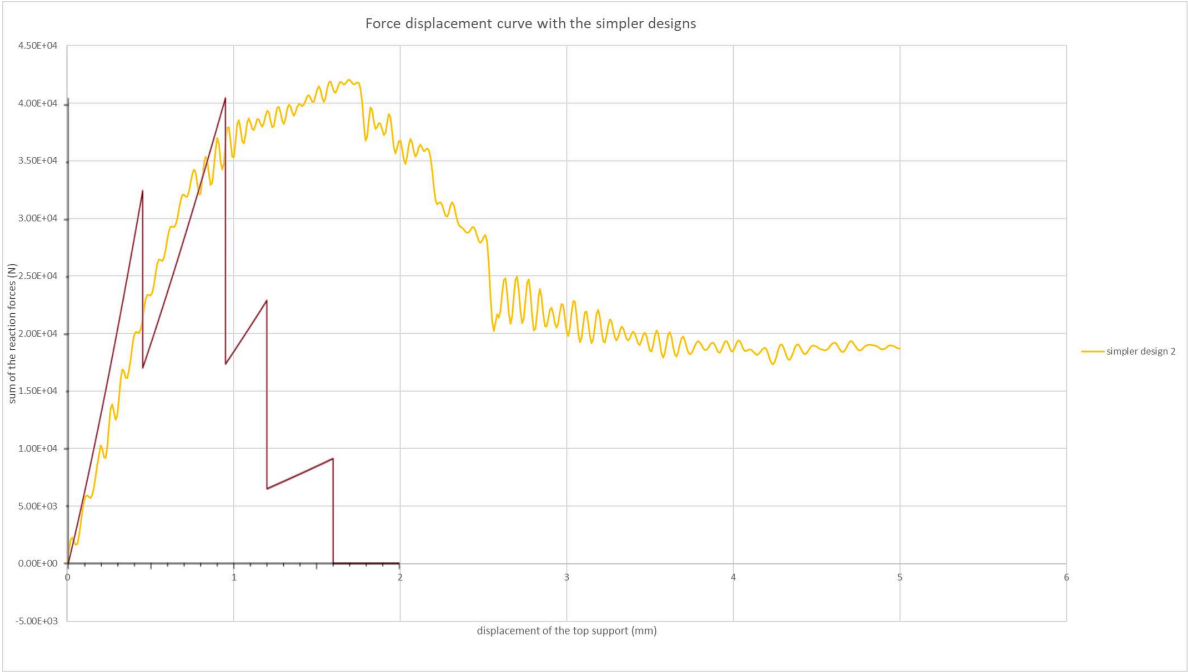

Figure 134 the novel analytical solution (16) in comparison to the numerical simulation of the design with one circle.

In Figure 134, it is observed that the force-displacement curve follows the numerical model initially, but after failure, it deviates. A more accurate model could involve plasticity after failure. To model this plastic failure, a plastic zone needs to be assumed. This assumed plastic zone, in Figure 135, is based on the numerical model, where cracks consistently form within this zone. The length of this zone (l_{pl}) is about 11mm, here it is noted that this could deviate. The plastic strain (ε_{pl}) at failure is modelled as 0.025% (so in total the base would expand 0.275mm).

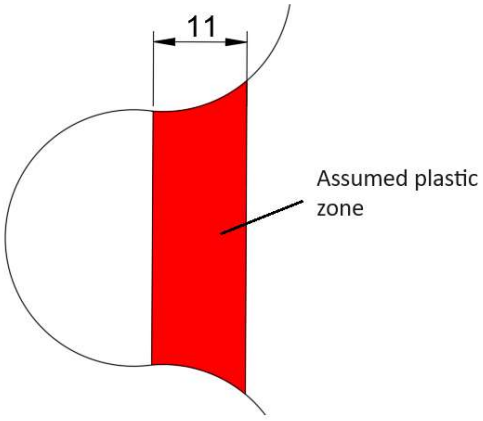

Figure 135 picture of the assumed plastic zone

This plastic failure is added in a Heavyside function, as shown below, where $u_{pl,n}$ represents the total plastic deformation that can occur in the tab. $u_{pl,n}$ is calculated with the equation 6.7 where z_r is the distance from the interlocking tab to the rotation point. By doing this the plastic strain is coupled with the displacement at the top, so it can be coupled with the equation 6.6. The total function will become as described in 6.8

$$u_{pl,n} = \frac{l_{pl} * \varepsilon_{pl}}{z_r} * \frac{1}{2} L \qquad 6.7$$

$$M = \sum_{n=1}^{4} P_n\left(\sin(\theta_n) + f\cos(\theta_n)\right) * z_n - \left(\left(P_n\left(\sin(\theta_n) + f\cos(\theta_n)\right) - F_{max} * \left(1 - \frac{u-u_{fn}}{u_{pl,n}}\right)\right) * z_n\right) * Heavyside\left(-u_{f,n} + u\right) - \left(F_{max} * \left(1 - \frac{u-u_{fn}}{u_{pl,n}}\right) * z_n\right) * Heavyside\left(-u_{f,n} - u_{pl,n} + u\right) \quad 6.8$$

This formula is plotted in Figure 136 for every tab individually and the sum of all tabs (total resistance). This figure demonstrates that the force in the interlocking tabs increases quadratically and decreases linearly.

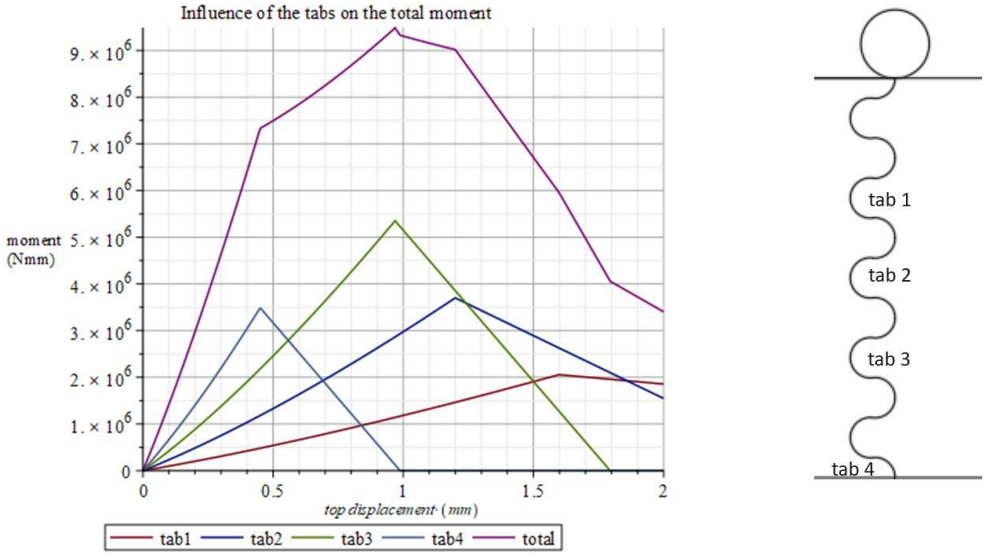

Figure 136 Influence of each tab on the bending resistance of the connection according to the adjusted novel analytical solution (16).

This solution is compared to the force-displacement curve discussed in paragraph 4.2.6. This comparison is illustrated in Figure 137. In this figure, the maximum load is similar to the numerical results. However, the displacement at the peak differs. This variance could be attributed to the fact that neither elastic nor plastic deformation is modelled during the loading of the tabs, only plastic deformation being modelled after failure.

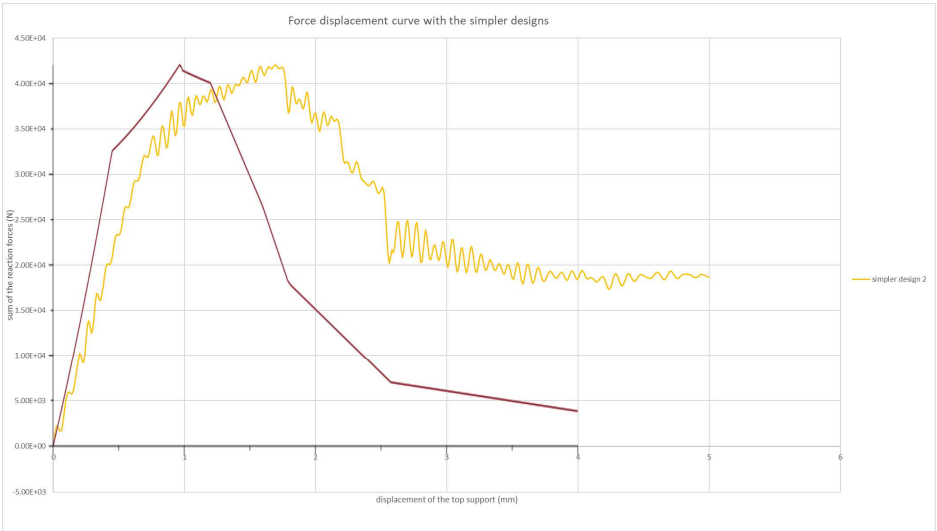

Figure 137 the adjusted novel analytical solution (16) in comparison to the numerical simulation of the design with one circle.

The same can be done with the bistable interlocking design 2, which features two circles. The key difference is that there are more contact points. An illustration of the total assumed contact points is provided in Figure 138. The comparison between the analytical approach and numerical results is illustrated in Figure 139.

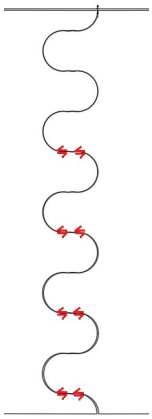

Figure 138 the contact points of design 2

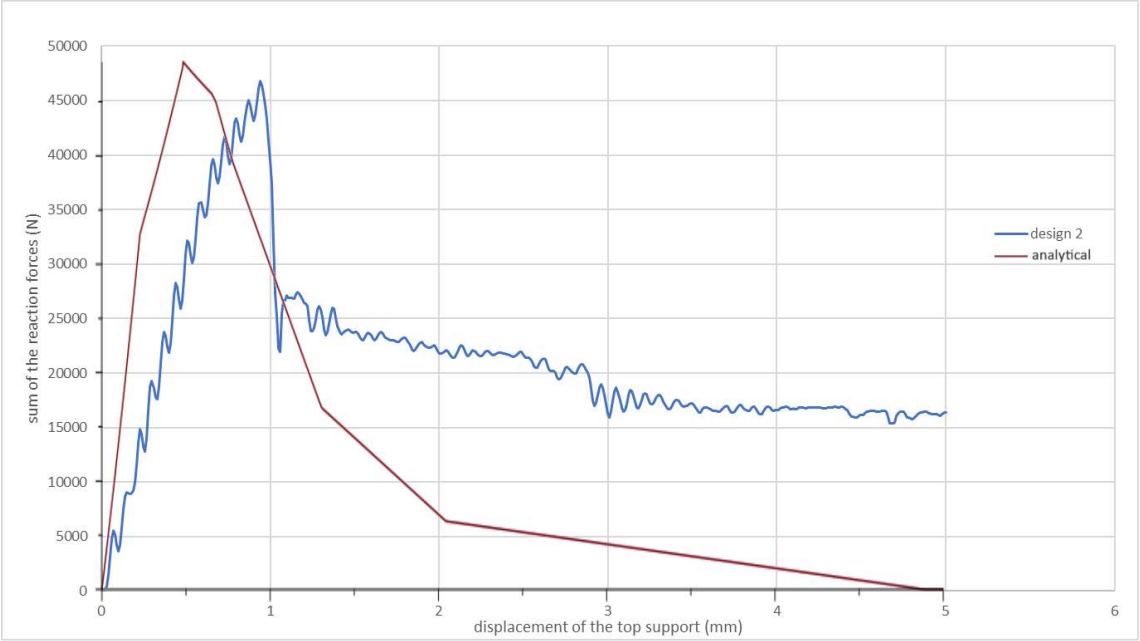

Figure 139 the adjusted novel analytical solution (16) in comparison to the numerical simulation of design 2 (with two circles).

The analytical approximation was also performed with a reduced elastic modulus. Specifically, a reduction of 25% of the original elastic modulus. The results are depicted in Figure 140, where it is observed that the maximum force deviates quite a bit. It suggests that the assumptions made may not be valid when the elastic modulus is lower.

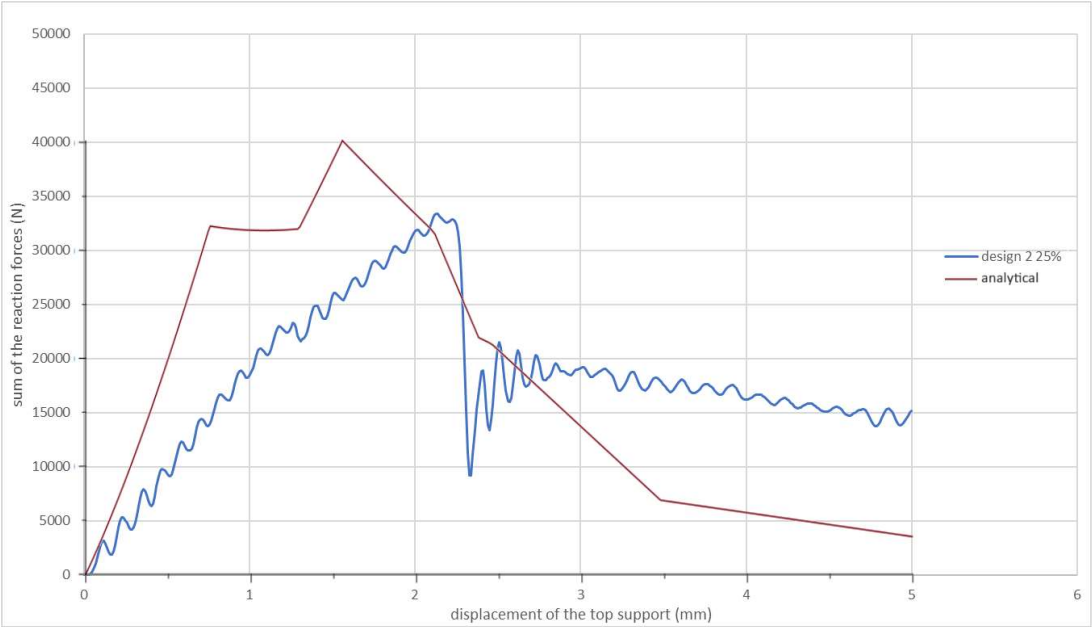

Figure 140 the adjusted novel analytical solution (16) in comparison to the numerical simulation of design 2 with the elastic modulus being 25% of UHPFRC

In summary, the analytical solution shows some resemblance to the force-displacement curves of the numerical model. However, refinements are necessary to achieve closer alignment with the numerical simulation. These refinements may involve incorporating non-rigid behaviour or accounting for plastic/elastic deformation before failure.

These approximations are done with Maple, and the Maple sheets are seen in Appendix C Analytical approximation of the interlocking connection.

7. Discussion of the research questions

In this chapter, the acquired results are reviewed with respect to the sub-research questions. The sub-research questions are discussed and answered.

7.1. What are the governing parameters that influence the ductility and strength of the interlocking connection?

To investigate the influence of the parameters on the interlocking connection, the results of the parameter study are discussed. It is evident that for these interlocking connections, material properties play a crucial role in determining their performance. This includes the elastic modulus, tensile resistance (either plastic or elastic), friction coefficient and plastic strain at failure. The results of the parameter study are summarized in Figure 141.

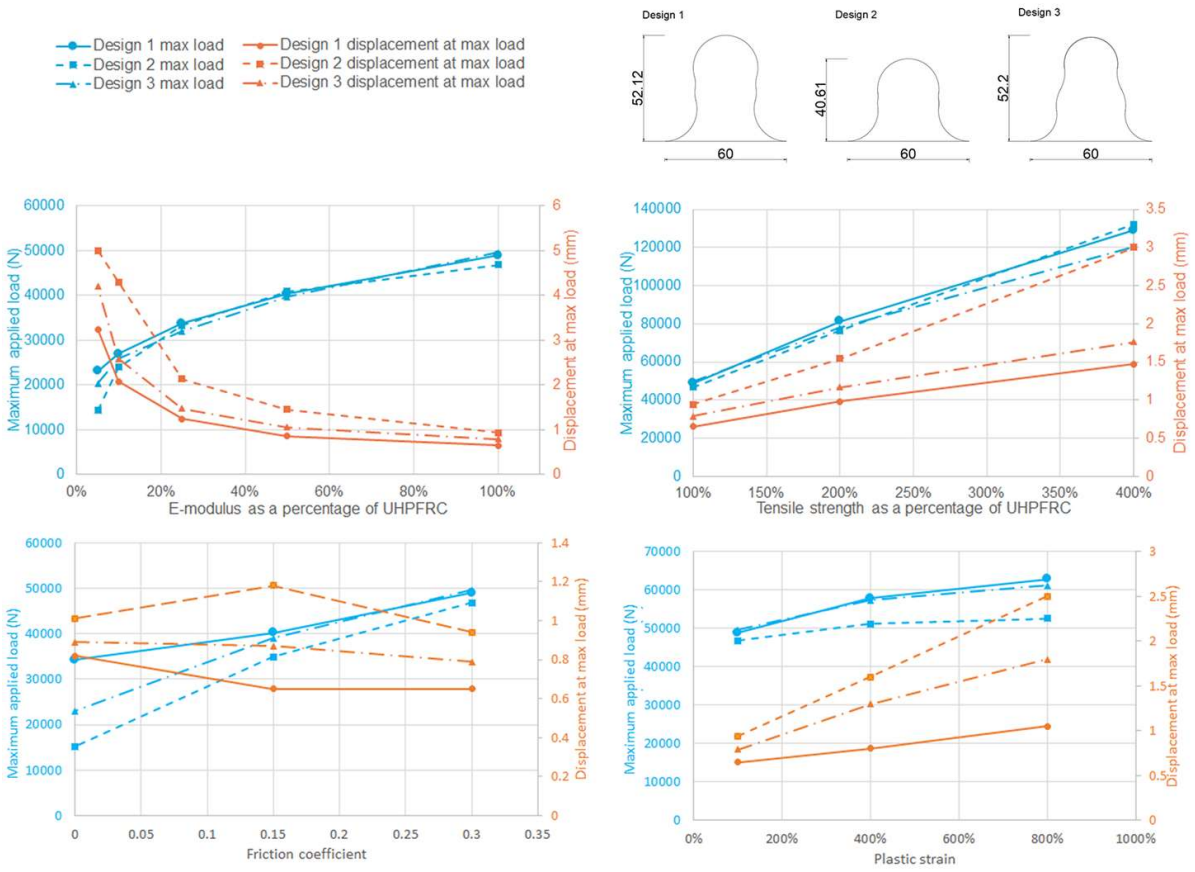

Figure 141 results of the parameter study on Elastic-modulus, Tensile strength, Friction coefficient and Plastic strain. Where in blue the max applied force is seen and in orange the displacement at this max load.

Lowering the elastic modulus increases the displacement at failure, indicating that the connection is more ductile. This increase in ductility could be explained by the interlocking tabs becoming easier to compress, resulting in more tab pullout, and thus failure at a higher displacement. Furthermore, each decrease in elastic modulus also decreases the strength of the connection.

Increasing the tensile strength appears to increase both the strength and displacement at failure. The increase in resistance is self-explanatory (the material is stronger). The greater displacement can be attributed to the increase in force in each tab. If more force is applied, the tabs will pull out further, so there is more displacement.

Decreasing the friction coefficient tends to increase ductility but decreases the resistance of the connection. A lower friction coefficient reduces the force required to pull out the tabs, this is because there is less friction, thereby increasing the displacement at failure. It is suggested that the decrease in total resistance is explained by the increase in vertical forces.

Explanations of these three causes are sketched in Figure 142.

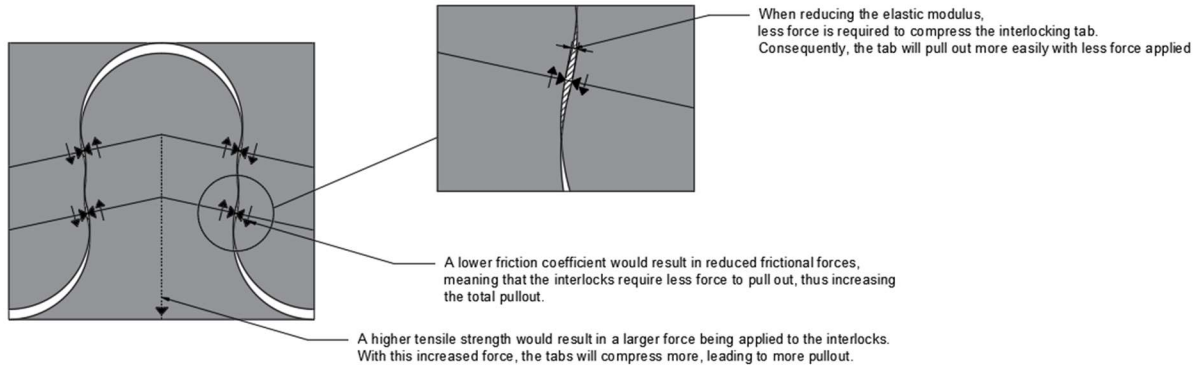

Figure 142 explanation of the effects of the parameters with a sketch.

The increase in plastic strain at the peak tensile strength both increases the strength and displacement at failure. The increase in displacement occurs because the material can deform more. The increase in strength can be explained by the analytical solution. From this analytical solution, the influence of each tab on the total resistance of the connection is plotted, as illustrated in Figure 143. Here, it can be seen that indeed the total strength slightly increases caused by the elongated failure of the tabs. This is because the reduction in strength during failure is less steep, so the failed tabs have more influence on the total strength.

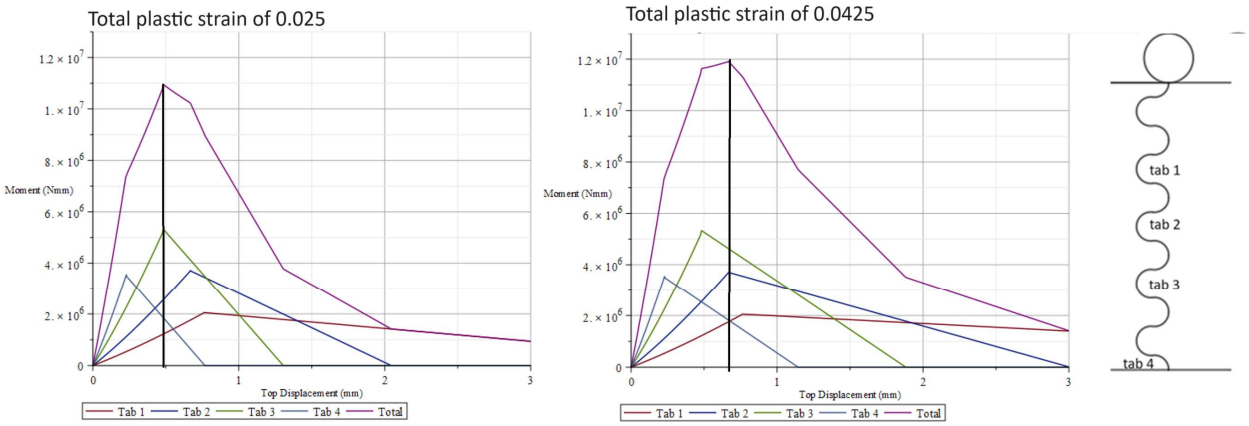

Figure 143 comparison of the analytically calculated resistance of the interlocking connection with different total plastic strains. The design of the tabs of the interlocking connection is the same as design 2.

It is also observed that design 2 has overall the highest displacement at failure. This is attributed to the design of the tab itself. This design has a low interlocking angle in combination with circles being close to 1/4th of the width of the interlocking tab. This makes the tabs smoother, resulting in less material to compress during pullout, and thus causing more displacement at failure.

In all these parameters, a trend can be observed: An increase in ductility (displacement at failure) is accompanied by a decrease in strength. A reason could be that each tab fails individually, meaning that the peak resistance of each tab is observed at different stages. With higher displacements, the failures are more spread out, which means that the residual strength of each tab has less influence on the total

resistance of the structure. This behaviour is evident in the analytical approximation when comparing the behaviour of the connection with an elastic modulus of 45.2GPa (100%) and 11.3GPa (25%) as seen in Figure 144.

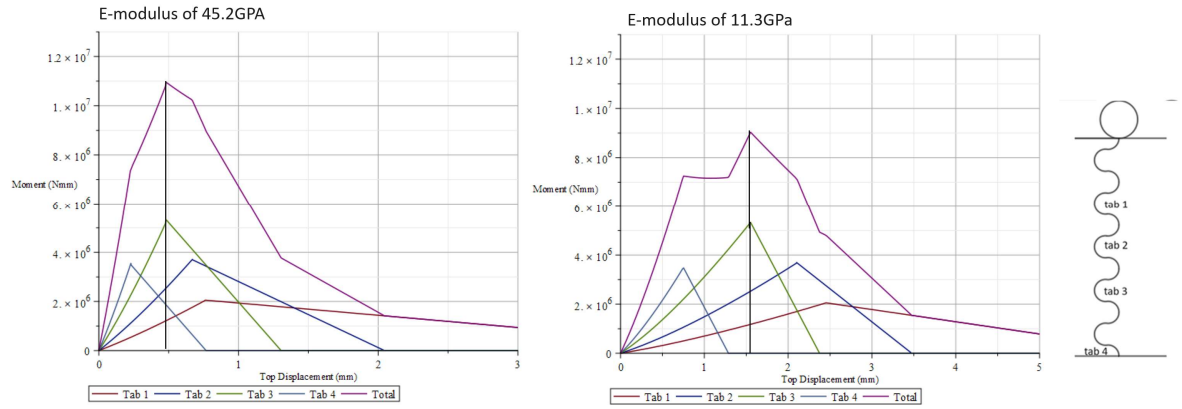

Figure 144 comparison of the analytically calculated bending resistance of the interlocking connection with the different elastic modulus (45.2GPa and 11.3GPa) of design 2. With the purple line being the total bending resistance with a given displacement and the red, blue, green and light blue being the influence of each tab on the total bending resistance.

When designing the tabs with a gap, the most important parameter is the depth of this gap, as it impacts the failure mode. A shallower gap makes the tab fail due to a tensional force in the base, while a deeper gap causes the tabs to fail due to a bending moment at the tips of the tab. Both of these failure modes are illustrated in Figure 145, where design A fails due to a tensional force and B due to a bending moment at the tips.

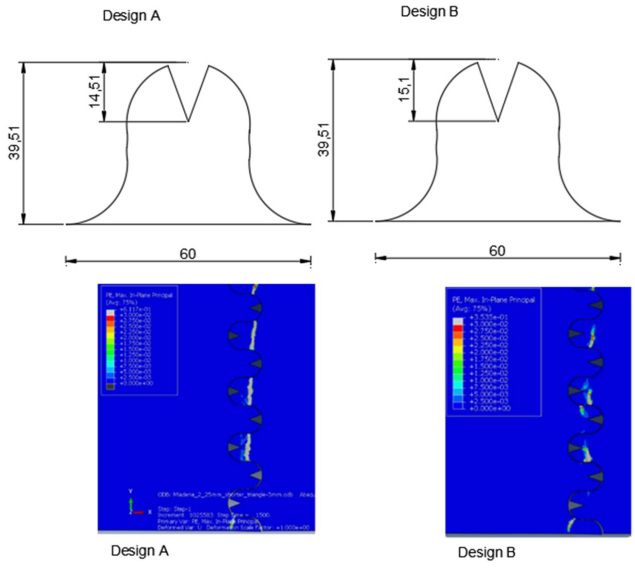

Figure 145 failure modes of the tabs with a gap

7.2. Does the numerical model align with an experimental research

First, the force-displacement curves of the numerical and experimental results are compared, as illustrated in Figure 146. The numerical model is scaled to the size of the experiments.

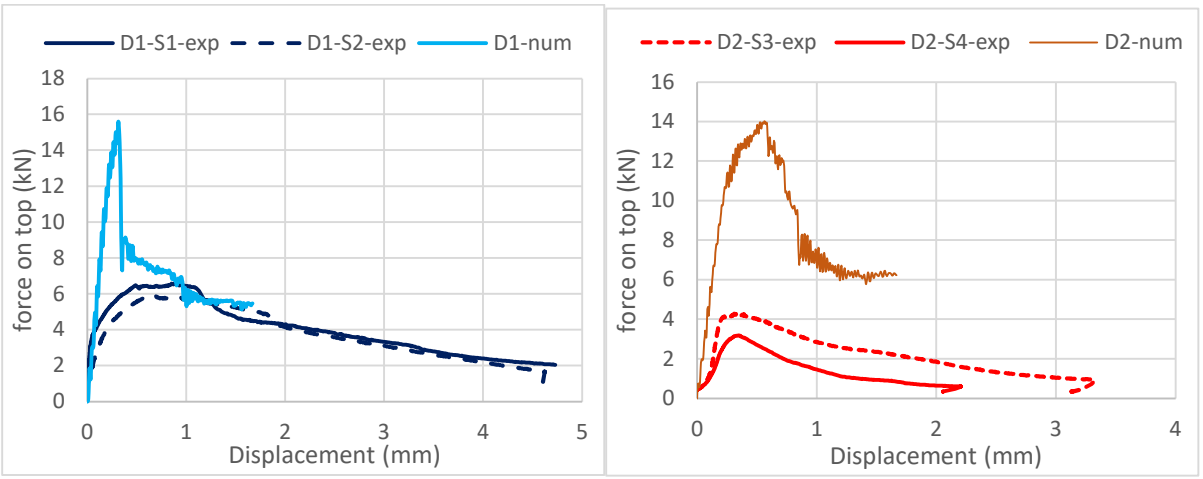

Figure 146 comparison force-displacement curves of the numerical model and experimental model. Design 1 is seen on the left and design 2 is seen on the right.

The force-displacement curve does not seem to align with the experimental results. The total bending resistance is higher in the numerical model and the peak strength is reached earlier. The reduced strength in the experimental results is not expected, because the tested tensile strength of UHPFRC (14.9MPa) is stronger than the numerically modelled strength (9.6MPa). It is hypothesized that this reduction has 3 main causes, these are;

1. The fibres are not distributed well.
2. The friction coefficient could be lower due to the applied oil.
3. The pattern of the interlocking radius of the made tabs could deviate from the design radius. Due to the small size, this could have a big influence on the reaction of the joint.

First, The fibres are in total 13mm long. The total width of each tab is about 20mm with the narrowest part being 9.93mm. This means that the fibres could not flow well in the tabs, resulting in a lower tensional strength. The designs of the experiments with their narrowest parts measured are seen in Figure 147.

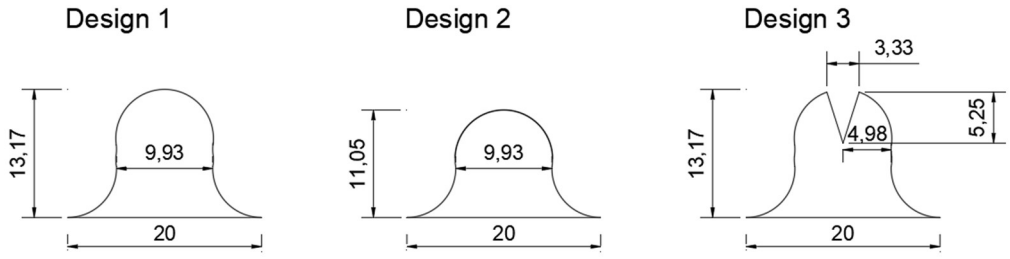

Figure 147 experimental designs with the narrowest parts measured

The second reason that the design in the experiment experiences a lower resistance is that the friction coefficient could be lower than the assumed 0.3. There may be some residual oil left in between the tabs that influences the friction coefficient. The experimental research comes closer to the numerical simulation with a friction coefficient of 0.15 and 0 (seen in Figure 148) than the assumed friction coefficient of 0.3. It seems that the friction coefficient of UHPFRC is significantly lower than expected.

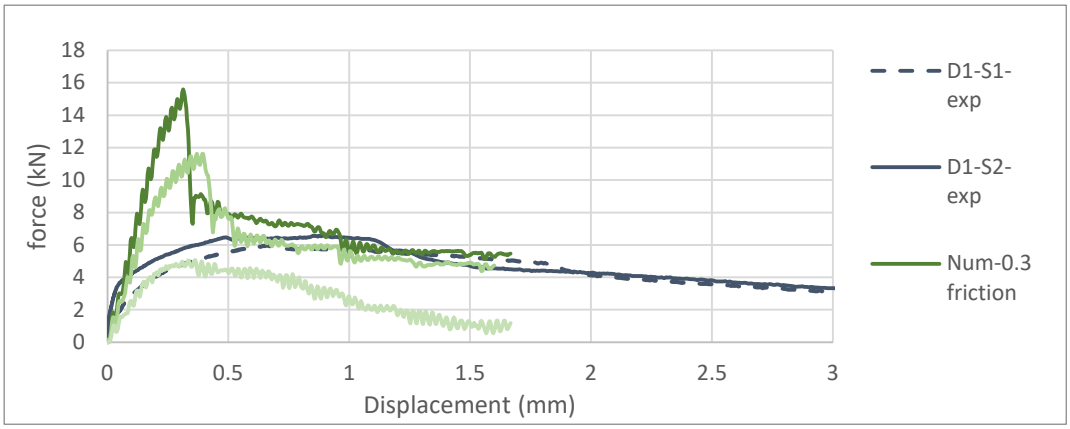

Figure 148 Comparison between experimental research and numerical model with a lower friction coefficient. The numerical model is scaled to the same dimension of the experimental research by hand calculations.

The third and final reason is that the radii of the circles are not cast well. The change in the pattern is about 0.1mm as seen in Figure 149. This is quite small and thus this pattern cannot be guaranteed.

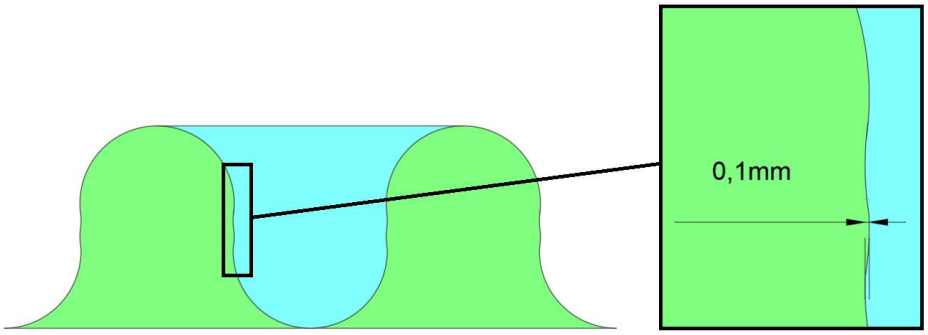

Figure 149 visualization of the pattern in between tabs

For a better comparison, a numerical model is made with the tensile strength of the experiments (14.9MPa) and a friction coefficient of 0.06. The results are presented with a force-displacement curve in Figure 150. The numerical model with these properties comes closer to the experimental results, but there is still a difference. This could be explained by the bad fibre distribution lowering the total resistance of UHPFRC.

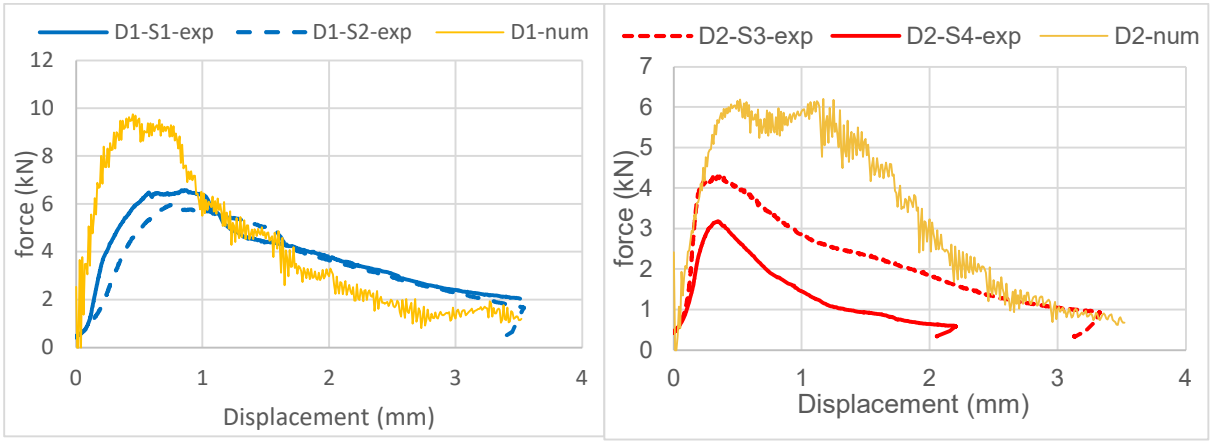

Figure 150 force-displacement curves obtained from the numerical model of design 1 (left) and design 2 (right) with a friction coefficient of 0.06 and a (plastic) tensile strength of 14.9MPa compared to the experimental results.

To compare the damage in the interlocking connection, strains from the digital image correlation (DIC) analyses are taken and compared to the plastic strains of the numerical analyses. These images are taken at the peak resistance (where the highest load is measured). This comparison point is taken because the numerical analyses are bigger and fail at different places. These comparisons are seen in Figure 151.

Design 1 seems to be in accordance with expectations. The cracks in the numerical analyses seem to occur in the neck of the tab, which is the same for the experiments. There are small differences in the shape of the crack, this is due to the way material is modelled in the numerical analyses. UHPFRC is a heterogeneous material, but in the numerical analyses, it is assumed to be homogeneous, making the cracks rather straight.

Design 2 seems to be less in accordance with the numerical analyses. It seems that in the experiments the tabs fail before the pullout of the interlocks occurs. The cracks seem to propagate through the tabs and interfaces.

Design 3 seems to be more in line with the numerical analyses. For both the numerical and experimental analyses, the cracks seem to congregate near the gaps. The only difference is that for the experiments the cracks are in the interlocking part with the half tabs (left element), while the numerical analyses show cracks in the interlocking part with only full tabs (right element). This is explained by that the total strength of each element could differ. Because the total strength of each element is about the same, the heterogeneity of UHPFRC could make either element fail. In the numerical analysis, the slightly weaker (right) side would always fail first.

In summary, the experiments deviate quite a bit when compared to the numerical results. This is due to the friction coefficient being lower in the experiments, bad fibre distribution and the pattern of the interlocks deviating a bit from the numerical analyses. Better results are expected when the interlocking tabs are fabricated bigger, so the fibres can distribute well, and when the friction coefficient is lowered in the numerical model.

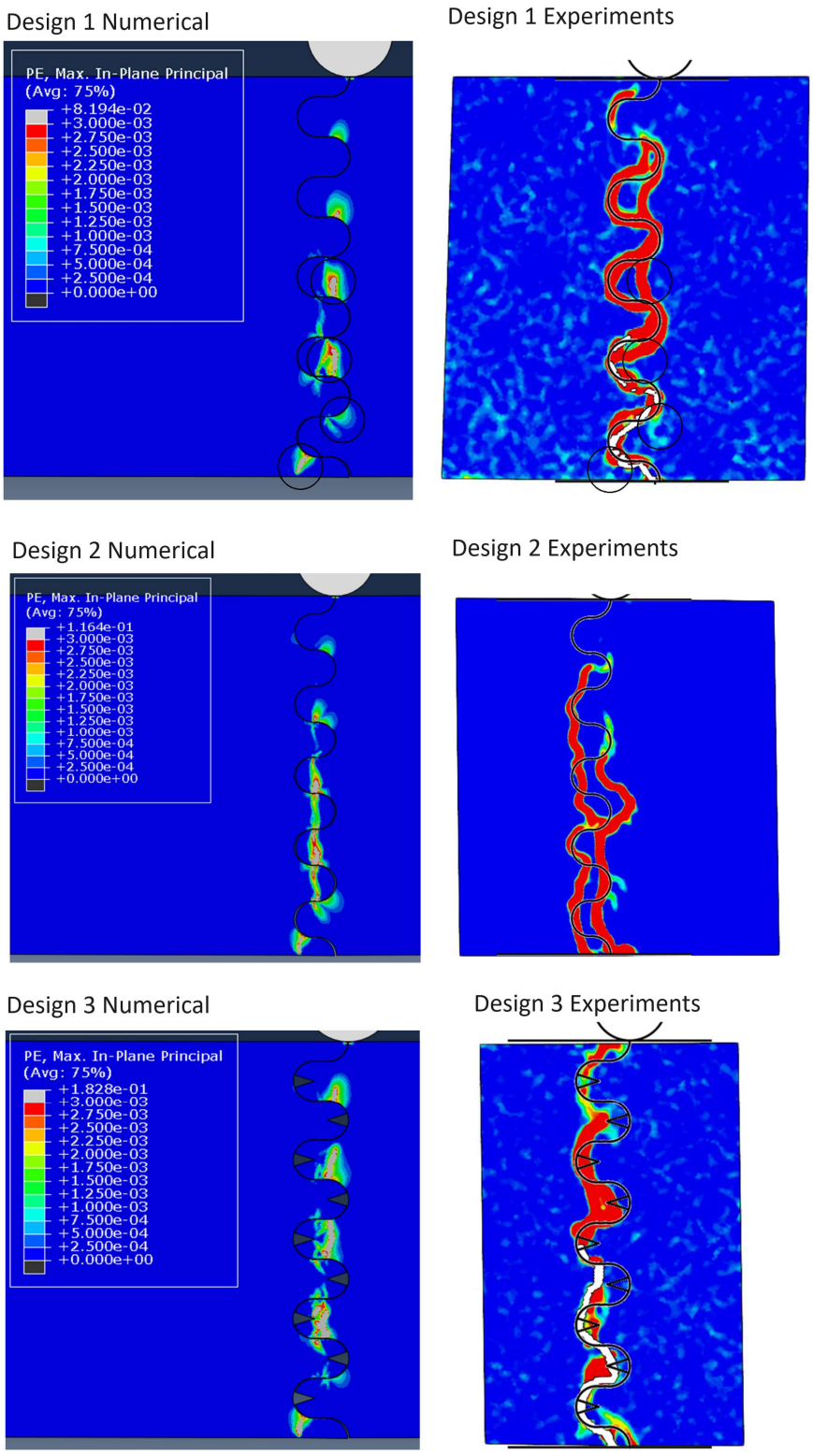

Figure 151 (plastic) strains for the numerical analyses and the experiment, where the strains from the experiments are obtained with Digital Image Correlation (DIC).

7.3. Which is the type of failure mechanism that occurs?

The loading sequence for the interlocking connection in the numerical analyses is quite clear, first a relatively linear loading sequence occurs where some geometric hardening behaviour (pullout of the interlocking tabs) is seen. Then the lowest half tab (denoted as 1 in Figure 152) breaks and a small change in the curve is observed. At the peak load the middle tabs (denoted as 2 and 3 in Figure 152) break and the total resistance suddenly drops. After this drop, the force displacement curve shows a rather horizontal line.

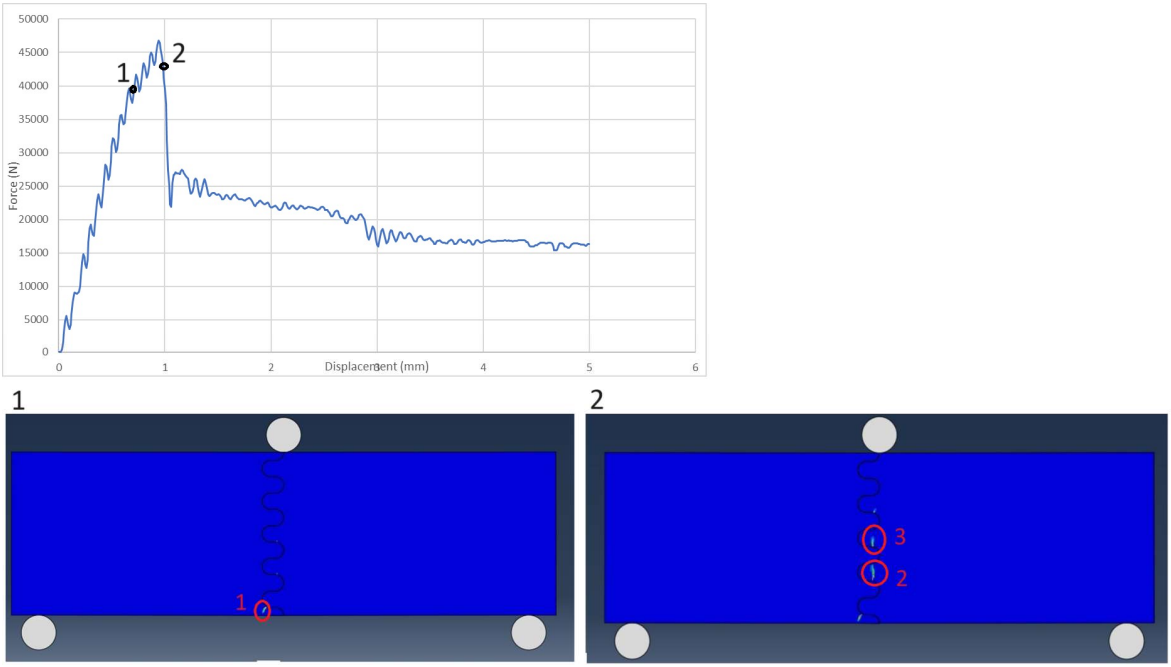

Figure 152 damage propagation in the numerical model

There is some resemblance in the cracking behaviour observed in the experiments and the numerical model for design 2, as depicted in Figure 153. The main difference lies in that the interlocking tabs pull out more, but still, the lowest half tab breaks first, followed by the middle tabs. After these fail, the total force on the connection decreases. This is not a sudden drop as seen in the numerical simulation.

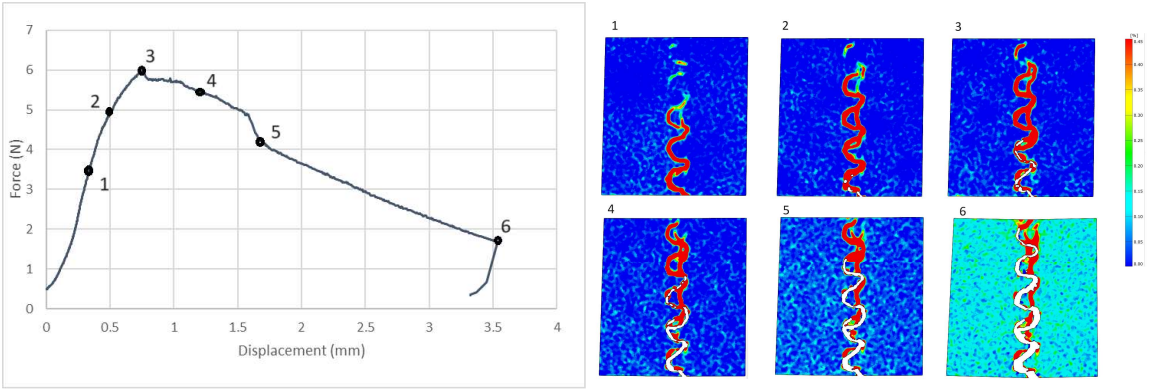

Figure 153 damage propagation of design 1 sample 2

Both in the numerical and plastic study, the interlocking tabs do not seem to pullout a lot at peak load. Additionally, no bistable behaviour is spotted in the (bistable) interlocking connection. The lack of pullout and bistable behaviour could have two reasons:

Firstly, concrete has a rather high elastic modulus in relation to its tensile resistance which makes the interlocking phases hard to reach. The high elastic modulus makes the tabs harder to compress and the low tensile strength makes it so the needed force cannot occur. So, the tab always breaks before the tab can be in its second interlocking phase.

This theory is backed by the results of the numerical simulation of changing the E-modulus and changing the strength (see chapter 4.2.1 and 4.2.2). Here it is seen that when the E-modulus is decreased or the tensile strength is increased, the tabs will pull out more.

The second reason why the interlocking phases do not seem to act may be attributed to the rotation. For the calculation of the bistable behaviour (3), it is assumed that the force on the interlocking tab is axial. In the designed interlocking connection, the acting forces in each interlocking tab are not axial. This introduces a bending moment in the tabs, making them weaker.

For instance, providing design 2 with the same rotation at failure around the suggested rotation point (see Figure 154), the points of compression are either on the top or the bottom (bottom for the right element, top for the left element). It is suggested that due to this there is an enforced rotation, introducing a bending moment. This enforced rotation is illustrated in Figure 155.

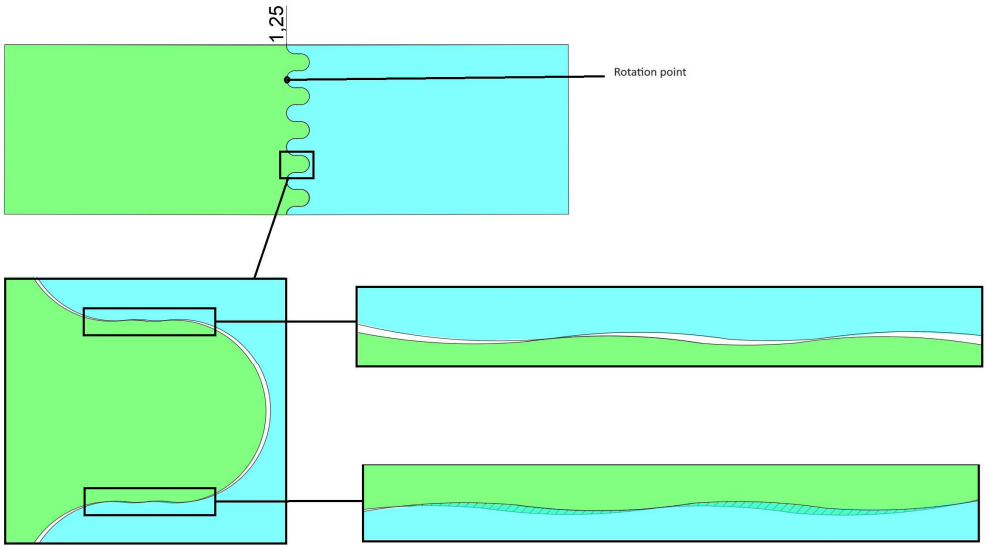

Figure 154 contact in the tabs of design 2 due to rotation only

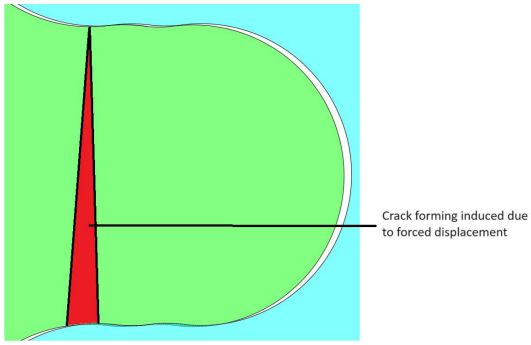

Figure 155 plastic deformation due to the enforced displacement

These enforced rotations are also evident in the numerical analyses, particularly for the design with an elongated plastic toughening phase (800% of that of UHPFRC), as illustrated in Figure 156. In this picture, the enforced rotation is introduced by the contact points marked with black squares, with the strains following this enforced rotation, indicated by the triangular cracking pattern.

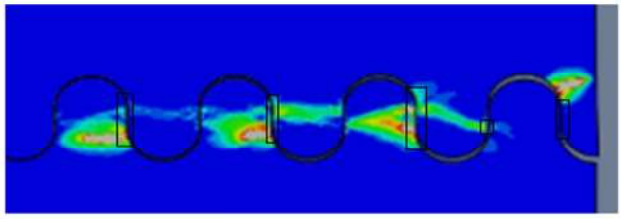

Figure 156 places where the tabs overlap if only given a rotation

This effect makes the connection fail faster, and thus less ductile. It can be argued that a better design would be a bent interlocking connection that follows this movement, so the enforced rotation does not occur. A design could be suggested where the interlocking tabs follow circles, with their centres in the rotation point of the connection, as depicted in Figure 157. The interlocking tabs do not follow the circles exactly but have small arcs that introduce friction and a contact force while they pull out. These introduced forces are seen in Figure 158.

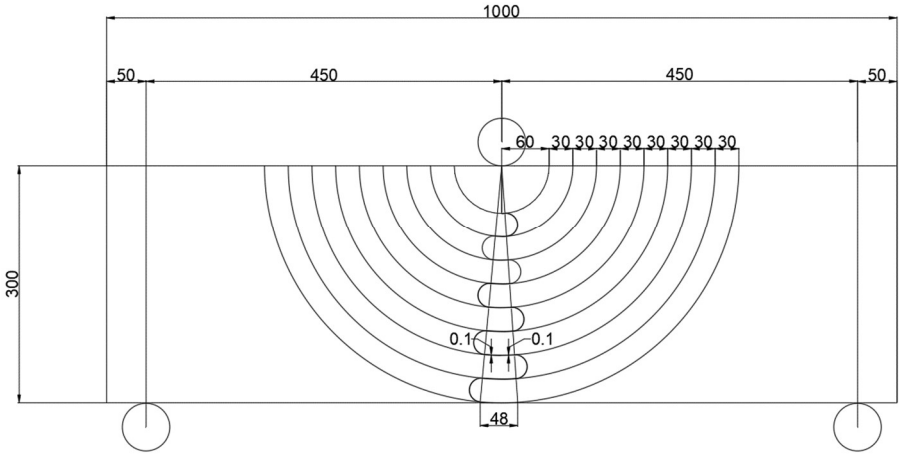

Figure 157 alternative design for an interlocking structure with a bending moment

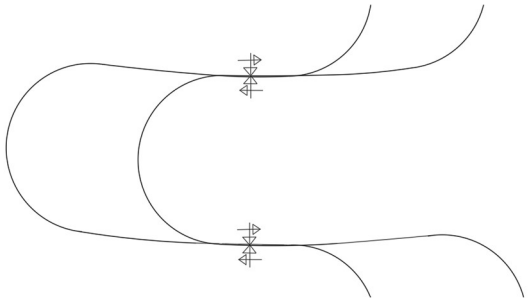

Figure 158 forces in the different design

The alternative design of Figure 157 is modelled in Abaqus, this gives the force-displacement curve of Figure 159. Here it is noted that this design fails at a higher displacement with a low impact on the total applied force. The plastic deformations are seen in Figure 160.

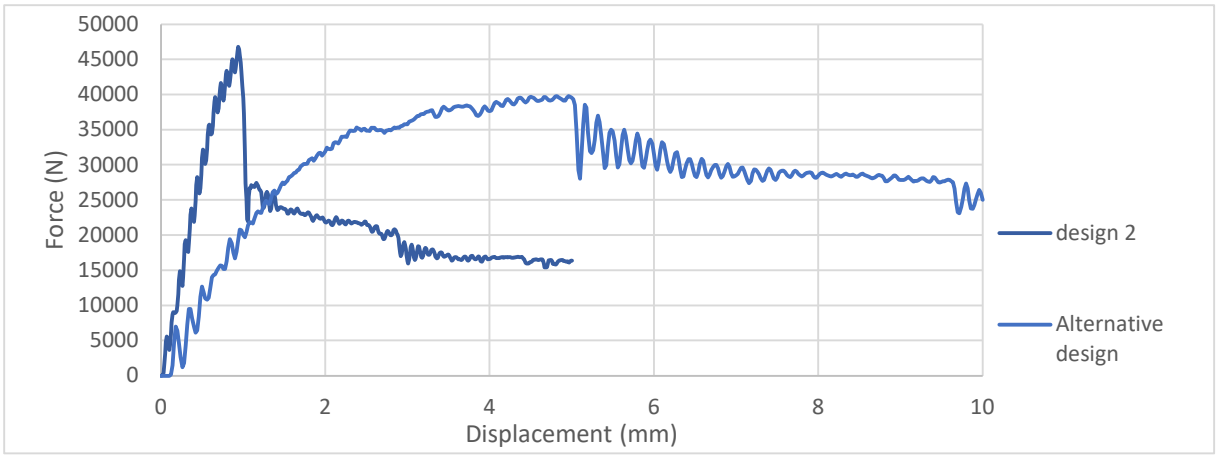

Figure 159 the force-displacement curve of design 2 and the alternative design

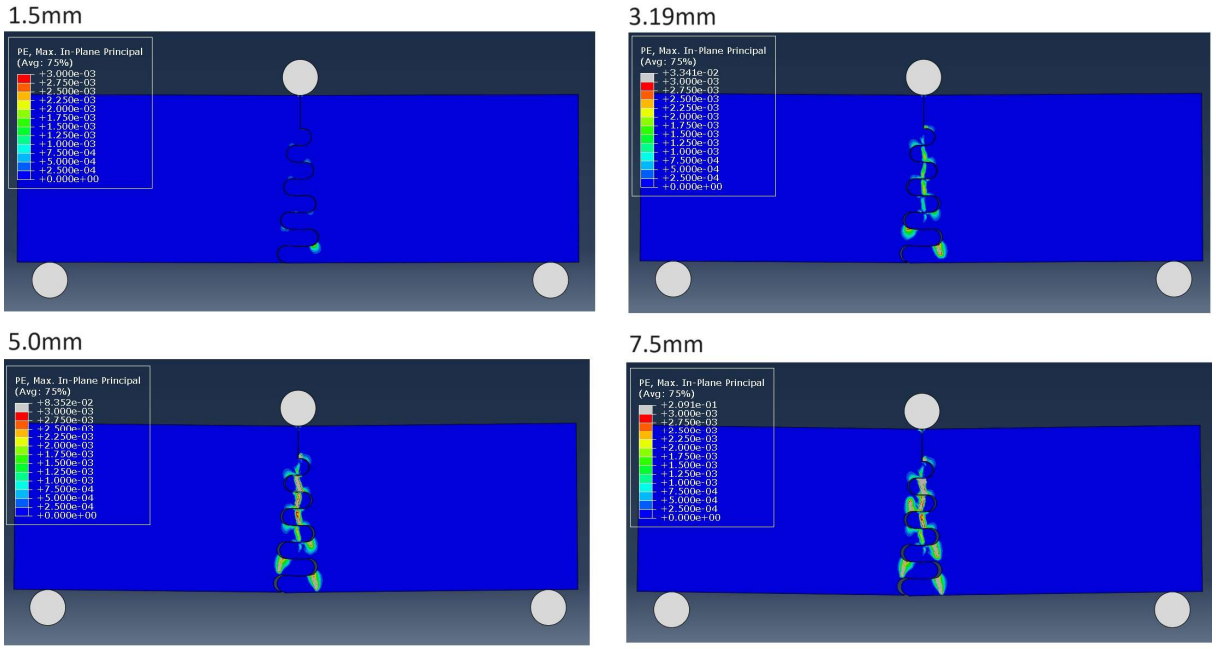

Figure 160 plastic deformation of the alternative design

In conclusion, the interlocking tabs experience minimum pullout at the peak load due to the introduction of a rotation caused by the bending moment. This rotation weakens the tabs, leading to faster failure and a less ductile response. Moreover, the choice of the material (UHPFRC) worsens the issue: Its high elastic modules makes the tabs harder to compress, and thus pullout less.

7.4. Is an analytical solution applicable in assessing the behaviour of the interlocking connection?

The analytical approach seems applicable in assessing the behaviour of the interlocking connection of the numerical model. This is for both the interlocking design with one circle and the bistable design 2 with two circles, where the compared results of design 2 are depicted in Figure 161.

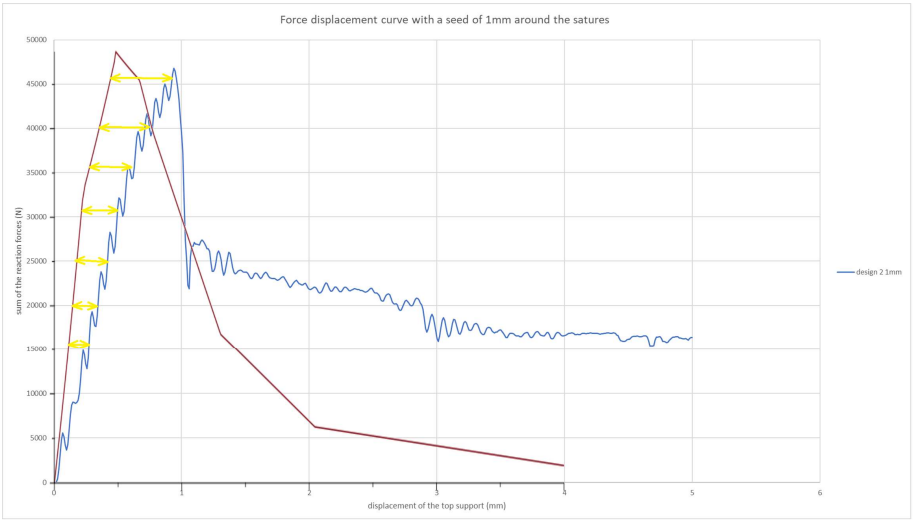

Figure 161 a comparison between the analytical approach and the numerical solution of design 2

The analytical approach deviates from the numerical results if more displacement of the top roller is observed/modelled. This could be done by decreasing the elastic modulus or increasing the tensile strength. This could be explained by that the assumption become critical with higher displacements. The made assumptions where:

1. No moments in the tabs, only a full tensional force
2. Tabs experience a linear plastic softening curve
3. Rigid body movement
4. Compressive point and the rotation points stay the same

Especially the assumptions 1 and 3 becomes a problem with higher displacements. When higher displacements are modelled the interlocking tabs need to deform a bit, introducing non-rigid movement of the interlocking tabs, accompanied by bending moments and second order effects, as seen in Figure 162.

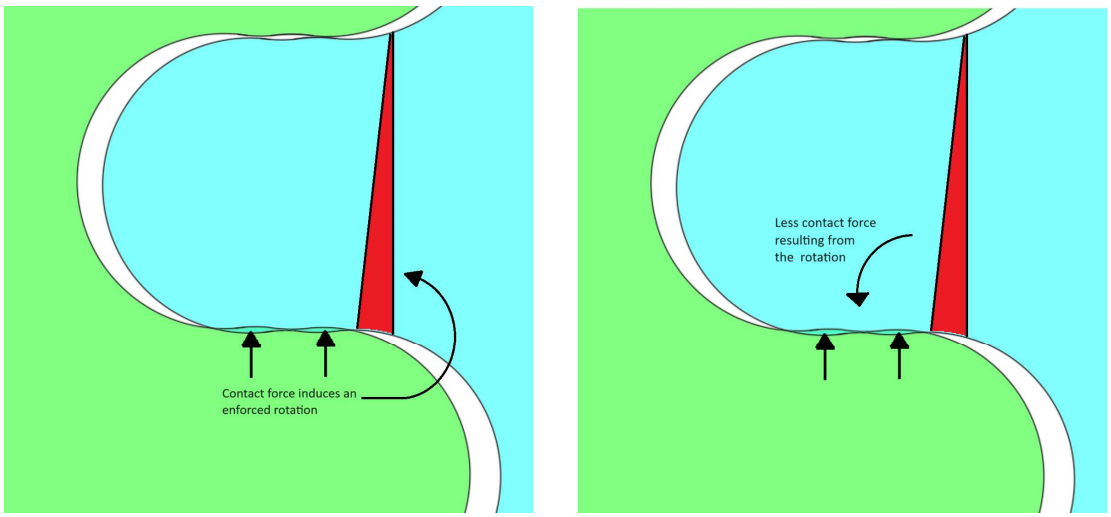

Figure 162 rotation of the interlocking tabs during pull out

It is suggested that for a better model, non-rigid movement and bending moments in the tabs should be modelled. If this would be the case, better results are expected.

8. Conclusions and recommendations

This chapter summarizes the results presented in this thesis. An answer to the main research question are formulated, based upon the acquired results. Also, practical recommendations and directions for further research is suggested.

8.1. Conclusions

The primary objective of this thesis was to investigate the performance of interlocked connections made with Ultra-High-Performance Fiber-Reinforced Concrete under a bending moment. The design of the interlocking tabs is based on a bistable design.

RQ1 What are the governing parameters that influence the ductility and strength of the interlocking connection?

- A parameter study was conducted involving 3 bistable interlocking designs. Whitin this study, the elastic modulus, plastic and elastic strength, and friction coefficient were varied. Additionally, a design with a single circle and a bistable design with a gap is researched.
- The parameter study revealed that interlocking design 2 (design 1 in the experimental results) exhibited the most ductile response among the three. This is caused by the overall smoothness of the design, making the interlocking tabs easier to pull out.
- The conducted parameter study indicates that the interlocking design exhibits greater ductility when a material is used with a lower elastic modulus, higher tensile strength, lower friction coefficient or greater plastic strain.
- With increase in ductility, the total strength of the interlocking connection decreases. A reason for this is that each tab fails individually, meaning that the peak resistance of each tab is observed at different stages. With higher displacements, the failures are more spread out, meaning that the residual strength during the plastic softening phase has less influence on the total resistance of the structure.
- Incorporating a gap in the design results in a slight increase in ductility of the connection, with a small decrease in total strength. The depth of the gap is the governing parameter for this design. Even small increments in depth significantly influence the overall behaviour of the connection, affecting both strength and ductility.

RQ2 How closely does the numerical model correlate with the experimental results?

- In the verification of the numerical study, it was observed that the numerical model correlates well with findings from prior papers. When replicating the experiments in a numerical model, the results closely align. Furthermore, the strength of the conducted numerical study of the three interlocking designs falls within the range of prior papers.
- Although the strength of UHPFRC in the experiments was higher, lower loads where observed during testing. The expected values where 15.6kN, 14.1kN and 12.7kN for design 1 , 2 and 3 respectively. However, the observed strength in the experiments where 6.0-6.6kN, 3.2-5.4kN and 2.1-6.0kN for design 1, 2 and 3 respectively. When comparing the total resistance of the connection with a monolithic connection, the strengths where approximately 9.5%, 5.0% and 3.0-7.6% for design 1, 2 and 3 respectively. In contrast, for the numerical model, it was 30-32%.
- The reduced strength observed in the experiments can be attributed to several factors. These include bad fibre distribution due to the small interlock size, reduced friction due to the application of oil, and small changes in the design during the casting of the specimens.
- The force-displacement curve of the numerical model aligns better with the experimental results when the friction coefficient is reduced, suggesting that the assumed friction of 0.3 was too high.

- The crack pattern of Design 1 aligns the numerical results, where first the lower half tab fails and then the middle tabs. Similarly, design 3 also aligns with the numerical results, with the cracks congregate near the gaps. However, design 2 deviates from the numerical results. During loading, a vertical crack was observed through both the interface and the tabs, which was not the case in the numerical model.

RQ3 Which is the type of failure mechanism that occurs?

- The loading sequence for the (bistable) interlocks with two circles in the numerical model is quite clear, first a relatively linear loading sequence occurs, where some geometric hardening behaviour (pullout of the interlocking tabs) is seen. Then, the lowest (half) tab breaks, resulting in a minor change in the curve. After reaching the peak resistance, there is a sudden drop in the resistance and the plastic softening behaviour of the material itself becomes governing.
- In both the experimental and numerical studies, it was observed that the tabs break with minimal pullout of the interlocks for two main reasons. First, the material used (UHPFRC) has a high elastic modulus compared to its tensile strength. This high elastic modulus means that more force is required to compress the interlocking tabs, resulting in high tensile stress and thus cracks with minimal pullout. Second, due to the rotation introduced by the bending moment the individual interlocking tabs experience an off-centre force, where the frictional and contact forces are higher on either the top or bottom. This introduces a bending moment in addition to the tensile force, weakening the tabs, leading to faster failure and reduced pullout.

RQ4 Is an analytical solution applicable in assessing the behaviour of the interlocking connection?

- An analytical approach was made with inspiration from the paper (16).
- The analytical approach is satisfactory in assessing the behaviour of the interlocking tabs. It is seen that the force-displacement curve plotted from this approach mimics the force-displacement curve of the numerical model with the properties of UHPFRC.
- When different material properties are used, resulting in delayed failure of the connection, bigger discrepancies between the numerical models are spotted. This is attributed to increase of the inaccuracies of the made assumptions. Correcting these assumptions will result in a more accurate model.

8.2. Recommendations for further research

- The interlocking tabs, if made with Ultra High Strength Fibre Reinforced Concrete (UHPFRC) or any other fibre material, should be bigger than those designed in this paper. It seems that the distribution of these fibres where a problem in the experimental tests.
- It has been observed that greater geometric hardening behaviour occurs in the interlocking connection when a material with a low elastic modulus compared to its tensile strength is used. However, the material used in this study (UHPFRC) lacks this characteristic. Hence, alternative materials could be suggested, including steel, changing the steel fibres to basalt fibres, plastics or other materials.
- The design of the interlocking connection does not seem to behave optimal under bending conditions. The design described in paragraph 7.3 showed promising behaviour for bending conditions and could be further researched.
- The analytical solution suggested in this report shows promising results. This model can be refined with the incorporation of non-rigid movements, bending moments in the tabs and modelling the plastic toughening stage of UHPFRC.

- For the interlocking connection, adhesion was outside of the scope of the research. Incorporating adhesion in the interlocking connection could benefit the initial strength, making it overall stronger.

9. Bibliography

1. **béton, Fédération internationale du Béton.** *Fib Model Code for Concrete Structures 2010.* s.l. : Fédération internationale du béton, 2010. ISBN 9782883940956.

2. **Ali A. Semendary, Waleed K. Hamid, Eric P. Steinberg, Issam Khoury.** *Shear friction performance between high strength concrete (HSC) and ultra high performance concrete (UHPC) for bridge connection applications.* s.l. : Engineering Structures, 2020. ISSN 0141-0296.

3. **Mohammad Mirkhalaf, Francois Barthelat.** *Design, 3D printing and testing of architectured materials with bistable interlocks.* Montreal : Extreme Mechanics Letters, 2017. ISSN 2352-4316.

4. **Brühwiller, Eugen.** *"Structural UHPRFRC" : Welcome to the post-concrete era!* Lausanne, Switserland : EPFL – Swiss Federal Institute of Technology in Lausanne, Switzerland, 2016.

5. **Lee N, Horstemeyer MF,Rhee H, Nabors B, Liao J, Williams LN.** *Hierarchical multiscale structure–property relationships of the red-bellied woodpecker (Melanerpes carolinus) beak.* s.l. : Journal of the royal society interface, 2014. ISSN 1742-5662.

6. **Erica Lin, Yaning Li, Christine Ortiz, Mary C. Boyce.** *3D printed, bio-inspired prototypes and analytical models for structured suture interfaces with geometrically-tuned deformation and failure behavior.* Massachusetts : Journal of mechanics and physics of solids, 2014. ISSN 0022-5096.

7. **Juha Song, Steffen Reichert, Ilan Kallai, Dan Gazit, Matthew Wund, Mary C. Boyce, Christine Ortiz.** *Quantitative microstructural studies of the armor of the marine threespine stickleback (Gasterosteus aculeatus).* Massachusetts : Journal of Structural Biology, 2010. ISSN 1047-8477.

8. **Cray J Jr, Mooney MP, Siegel MI.** *Timing of Ectocranial Suture Activity in Pan troglodytes as Related to Cranial Volume and Dental Eruption.* Pittsburgh : The anatomical record, 2010.

9. **Irene H. Chen, Wen Yang, Marc A. Meyers.** *Leatherback sea turtle shell: A tough and flexible biological design.* San Diego : Acta Biomaterialia, 2015. ISSN 1742-7061.

10. **Wang Hu, Yang Mengzhu, Wu Yufan.** *Closed-loop optimization and investigation of bistable interlocked structure.* Hunan : International Journal of Mechanical Sciences, 2018. ISSN 0020-7403.

11. **Idris A. Malik, Francois Barthelat.** *Bioinspired sutured materials for strength and toughness: Pullout mechanisms and geometric enrichments.* s.l. : International Journal of Solids and Structures, 2018. ISSN 0020-7683.

12. **I.A. Malik, M. Mirkhalaf, F. Barthelat.** *Bio-inspired "jigsaw"-like interlocking sutures: Modeling, optimization, 3D printing and testing`.* Montreal : Journal of the Mechanics and Physics of Solids 102, 2017. ISSN 0022-5096.

13. **K.L.Johnson.** *Contact Mechenics.* camebridge : camebridge university press, 1985.

14. **Wickramasinghe, Sachini, Do, Truong and Tran, Phuong.** *Flexural behavior of 3D printed bio-inspired interlocking suture structures.* Hanoi Vietnam : Materials Science in Additive Manufacturing, 2022.

15. **Sachini Wickramasinghe, Oraib Al-Ketan, Chenxi Peng, Yun Lu Tee, Mladenko Kajtaz & Phuong Tran.** *Influence of design parameters on the flexural properties of a bio-inspired suture structure.* Melbourne, Australia : Virtual and Physical Prototyping, 2023.

16. **Upendra Yadav, Mark Coldren, Praveen Bulusu, Trisha Sain, Susanta Ghosh.** *Interface fracture of micro-architectured glass: Inverse identification of interface properties and a novel analytical model.* Houghten : Mechanics of materials, 2019. ISSN 0167-6636.

17. **Seung Hun Park, Dong Joo Kim, Gum Sung Ryu, Kyung Taek Koh.** *Tensile behavior of Ultra High Performance Hybrid Fiber Reinforced Concrete.* s.l. : Cement and Concrete Composites, 2012. ISSN 0958-9465.

18. **J, Wuest.** *Structural behaviour in tension of Ultra-High Performance Fibre Reinforced Concrete in.* s.l. : Swiss Federal Institute of Technology Lausanne, 2007. Doctoral Thesis No. 3987.

19. **Denarié E., Brühwiler E.** *Strain Hardening of Ultra-high Performance Fibre Reinforced Concrete: Deformability versus Strength Optimization, International Journal for Restoration of Buildings and Monuments.* s.l. : Aedificatio Publishers, 2011.

20. **Jian Yang, Baochun Chen, Xiangguo Wu, Gang Xu.** *Quantitative analysis of steel fibers on UHPFRC uniaxial tensile behavior.* Hubei China : Construction and Building Materials, 2023. ISSN 0950-0618.

21. **Yitao Huang, Dawei Gu, Shozab Mustafa, Steffen Grünewald, Mladena Luković.** *Shear behaviour of reinforced concrete beams strengthened with ultra-high performance fiber reinforced concrete (UHPFRC).* s.l. : Case Studies in Construction Materials, 2023. ISSN 2214-5095.

22. **Goran H. Mahmud, Zhenjun Yang, Aram M.T. Hassan.** *Experimental and numerical studies of size effects of Ultra High Performance Steel Fibre Reinforced Concrete (UHPFRC) beams.* Hangzhou : Construction and building materials, 2013. ISSN 0950-0618.

23. **Yassiri, Ammar.** *Reinforced hyvrid concrete beams with a U-shaped SHCC mould.* Delft : TU Delft, 2020.

24. **Papoulidou, Sofia.** *Bi-stable interlocks of sutured ABS geometries- A numerical study in Abaqus.* Delft : TU-Delft, 2022.

25. **Awasthy, Nikhil.** *Development of Mechanical Experimental and Numerical.* Delft : Tu-Delft, 2019.

26. **Ritchie, Robert O.** *The conflicts between strength and toughness.* s.l. : Macmillan Publishers, 2011.

27. **M. Mirkhalaf, A. Khayer Dastjerdi, F. Barthelat.** *Overcoming the brittleness of glass through bio-inspiration and micro-architecture.* quebec : Nature communications, 2014.

Appendix A Abaqus model parameters

Parts

The Abaqus model exists of 3 parts. The left and right parts with the interlocking tabs and the roll support that is used 3 times. These parts were defined as 2D planar deformable parts. The parts were created to test the design for a bending moment. The bending moment is created by a 3-point bending test.

For each part, a section was assigned. This section contains all the information about the material type and properties. The materials and sections of the left and right parts were the same. The properties of these parts can be seen in Figure 163. The materials of the roll support differed. The properties of the rollers can be seen in Figure 164.

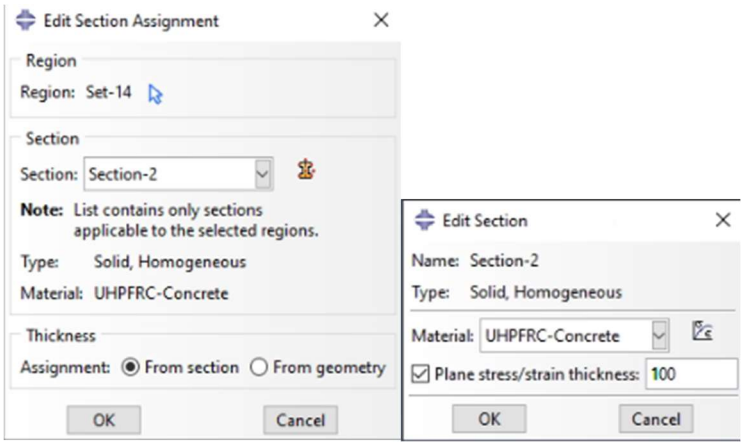

Figure 163 properties of section-2 UHPFRC-concrete

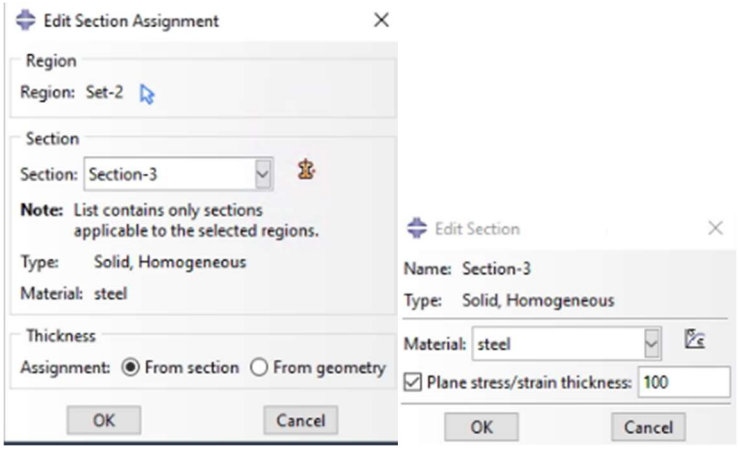

Figure 164 properties of section-3 steel rollers

Module assembly

To test the design the parts were brought together, and the instances were translated with respect to the global coordinate system and each other. The assembly of the module can be seen in Figure 165.

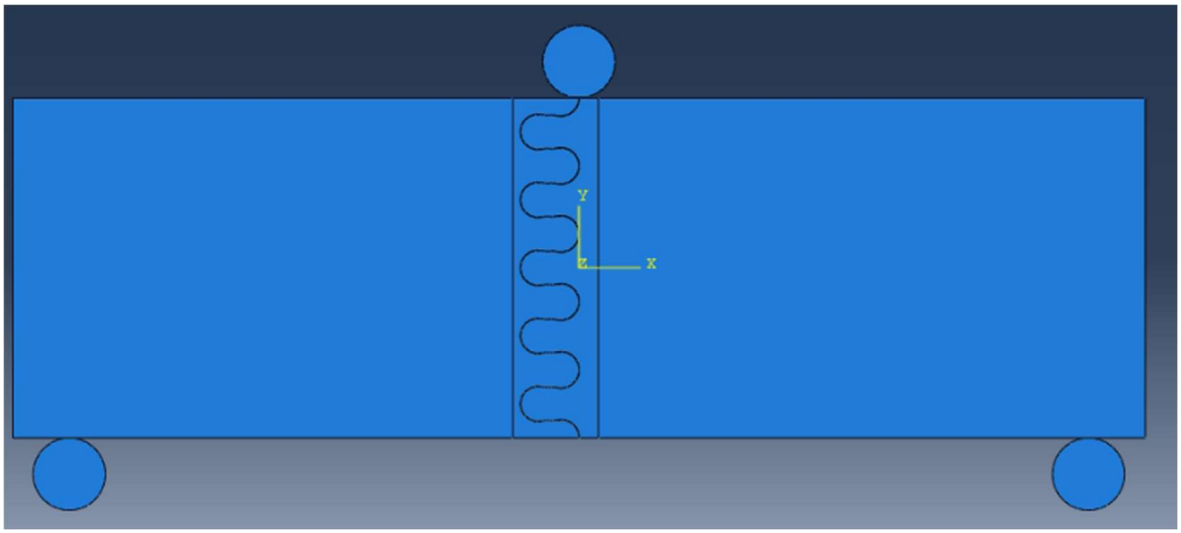

Figure 165 assembly of the parts

Module material

The stress-strain curve of UHPFRC shows a small but strong elastic regime and a long plastic regime after yielding. This is modelled with an elastic component and a “concrete damaged plasticity” component. Cracking of the concrete will not be modelled. This is fine because UHPFRC does not have a big cracking behaviour. The parameters that are in the model can be seen in Figure 166, Figure 167 and Figure 168.

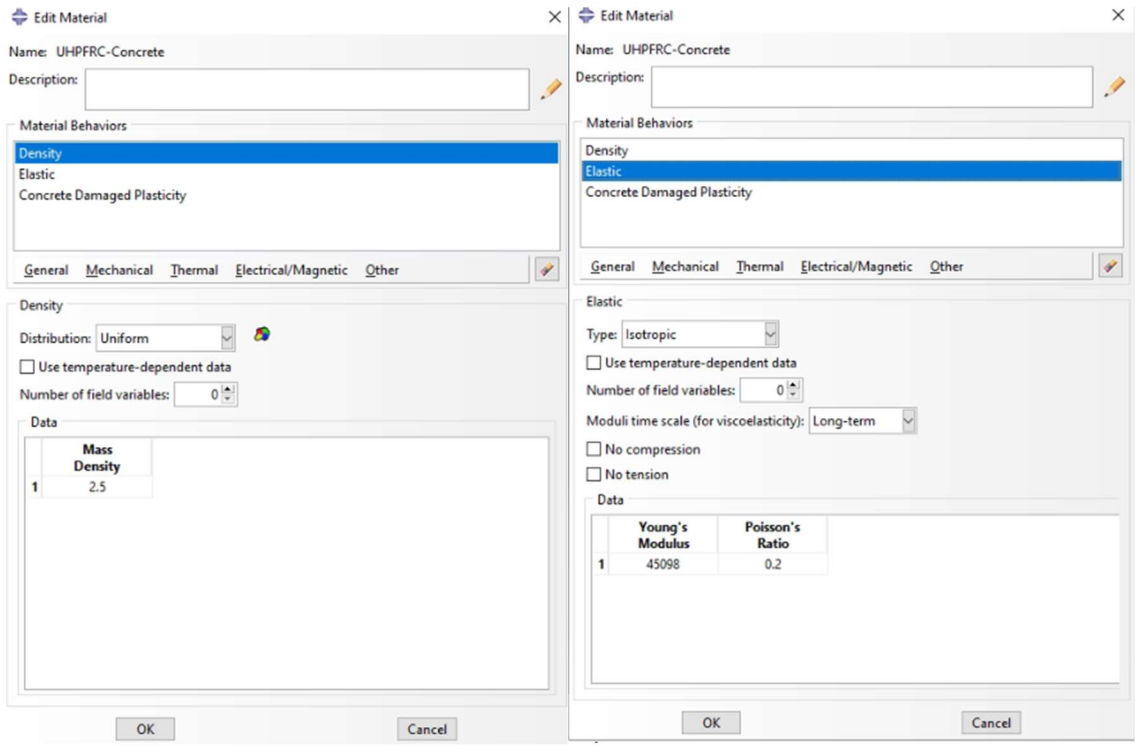

Figure 166 density and elastic properties of the UHPFRC concrete

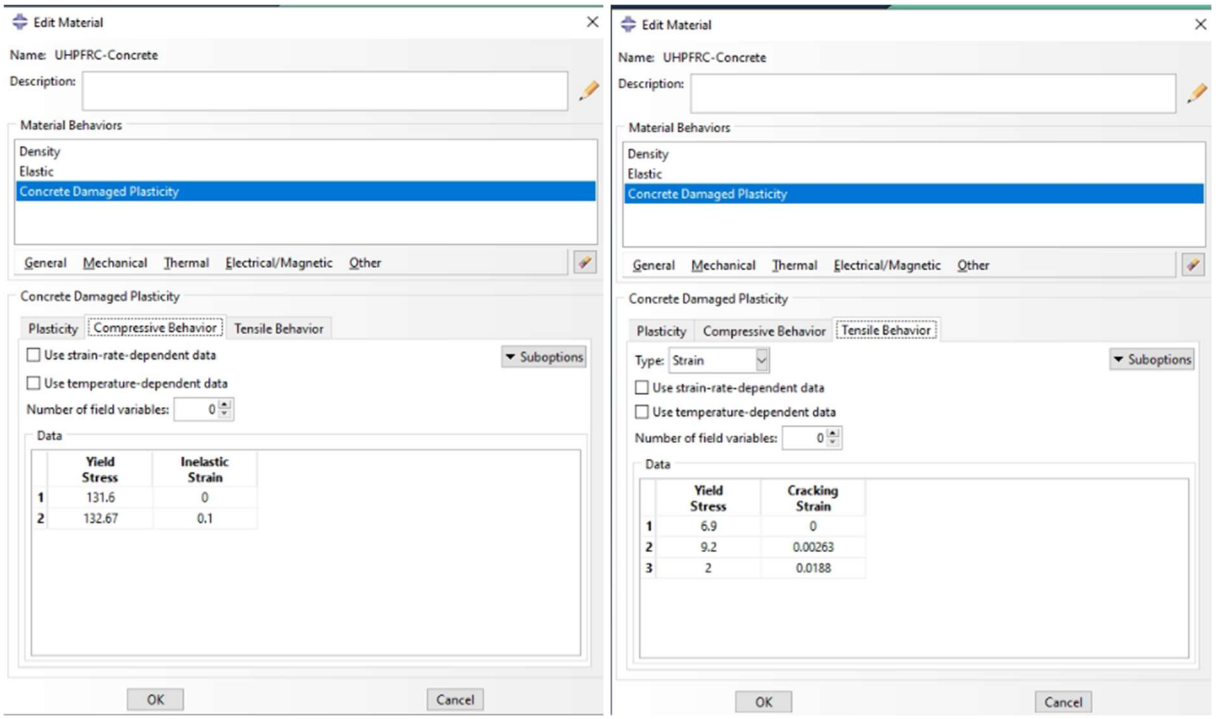

Figure 167 compressive and tensile behaviour of the UHPFRC

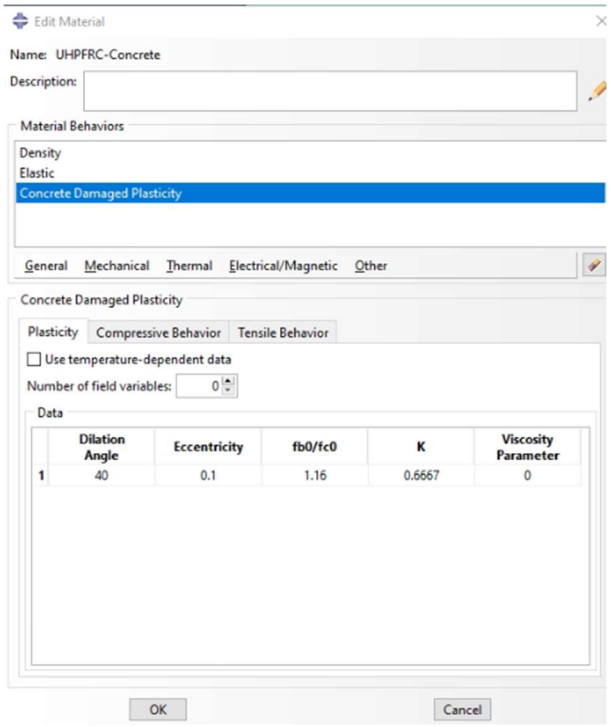

Figure 168 plasticity behaviour of the concrete

Module: mesh

The mesh was created in the module parts. The mesh is made finer near the interlocking tabs and less fine near the supports. This is done by making a partition in the element. After this the meshing command where done. These commands consisted of:

- Seed part instance
- Mesh part instance
- Element types

The seeding tools allow to adjust the mesh density in the selected regions. The seeds act like markers on the selected edges. This is done near the interlocking tabs with a density of 1mm and near the supports with a density of 20mm.

After this, the meshing commands were done. The element shape with the mesh controls where quad-dominated. The technique used was free with an advancing front algorithm (see Figure 164). The total mesh can be seen in Figure 169.

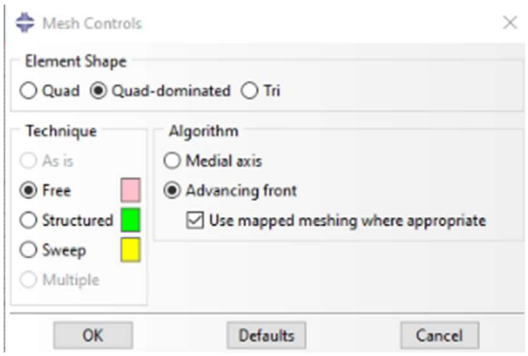

Figure 169 mesh controls

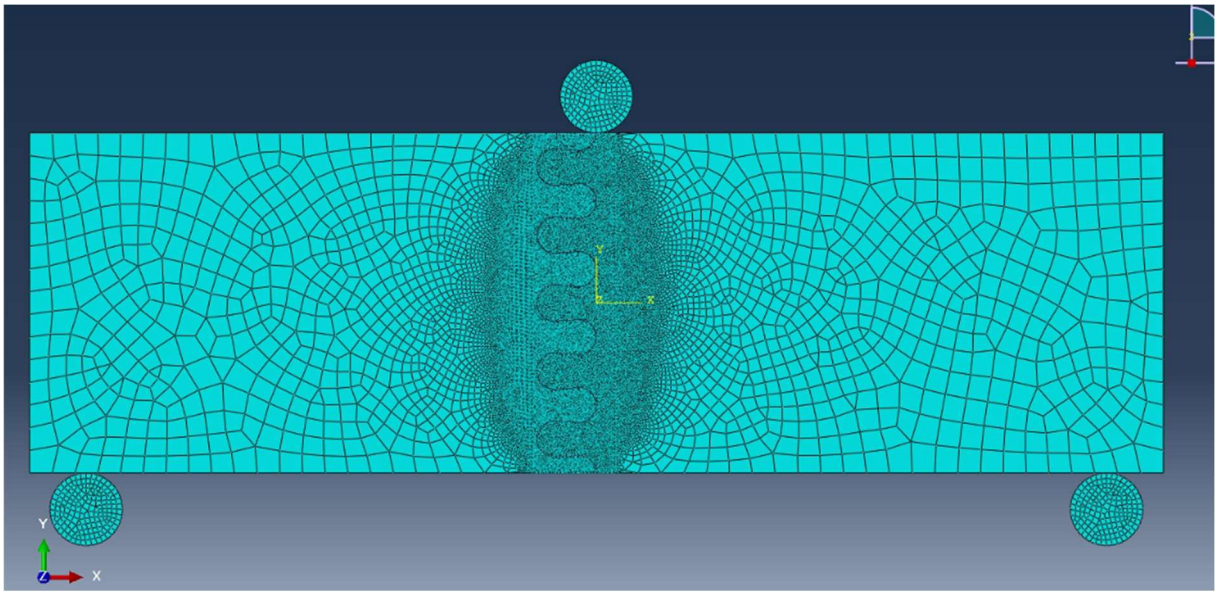

Figure 170 meshing of the Abaqus model

Plane stress elements were used for the modelling of the interlocking tabs in 2D, from the explicit library. The rest of the properties were the default options of Abaqus.

Module interaction

Interaction between the tabs and support needs to be modelled. This is done with the interaction module. For the analyses surface to surface contact was used.

The constraint formulation chosen was the penalty contact method. The sliding between the elements was chosen to be finite.

Module interaction property

When two surfaces meet there is an interaction. To model this some properties are given to these surfaces. The tangential behaviour is given with a friction coefficient in penalty formulation. The normal behaviour is defined as “hard” contact. The properties can be seen in Figure 171.

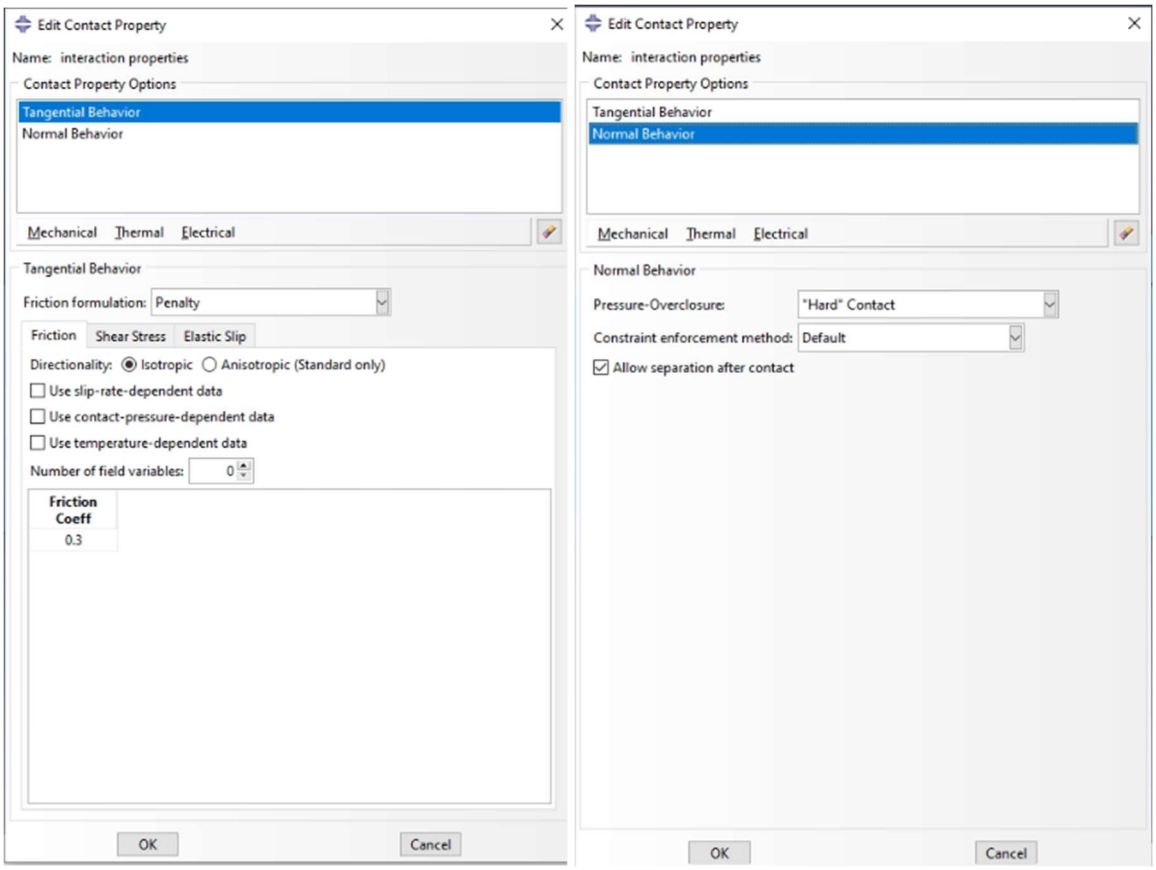

Figure 171 properties of the interactions

Module boundary conditions

For the boundary conditions, the lower supports are fully encastered. The top support gives a force in displacement control (as seen in Figure 172). This means that the beam gives a reaction force due to the displacement of the top support. For the analyses, a time period of 5000 seconds was used.

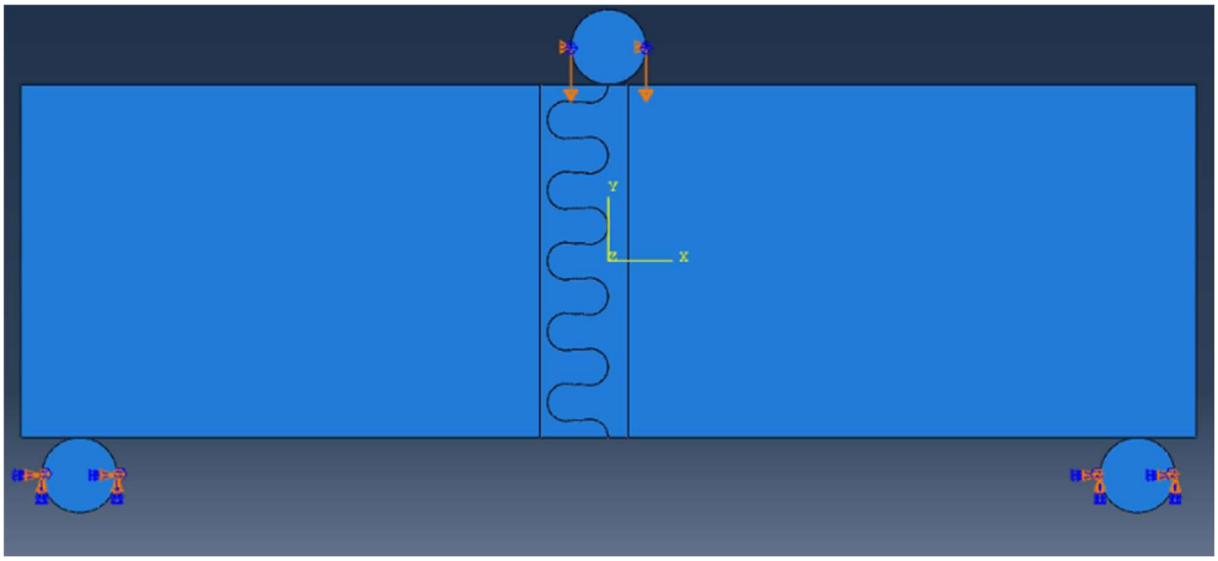

Figure 172 boundry conditions of the model

Module Steps

Two steps were included in the analysis. The initial one (static) was existent already and the interface conditions and bottom supports were defined in that step. The second step was a dynamic (explicit) step to take into account the inertia effects. The loading condition for the top support was described in this step.

Appendix B hand calculations

First, the total bending moment and force of the lowest tab is calculated. Here it is assumed that there is a force on the edge of the lowest tab. The first design is calculated with a plastic failure. And the second and third design is calculated with an elastic failure. The force will act as follows:

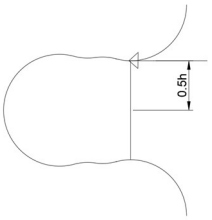

The elastic calculation is as follows:

$$sigma\_moment := \frac{\frac{1}{2}\cdot h\cdot\frac{1}{2}\cdot h\cdot F}{\frac{1}{12}\cdot b\cdot h^3} \qquad sigma\_tension := \frac{F}{h\cdot b}$$

Calculating the stress at the top of the tab

$$sigma\_moment := 0.001007387508\,F$$

$$sigma\_tension := 0.0003357958361\,F$$

Calculating the stress due to the force without moment

$$y := sigma\_moment + sigma\_tension = 6.9$$

$$y := 0.001343183344\,F = 6.9$$

The stress should be less than the max stress of 6.9

$$assign(solve(\{y\}));$$

$$F \qquad 5137.050002$$

$$\frac{1}{2}\cdot h\cdot F \qquad 76490.67455$$

The total force and moment can be calculated

The plastic failure is a bit different. This is as follows:

$$M := \frac{1}{2}\cdot h\cdot F;\ \text{sigma} := \frac{F}{h\cdot b}$$

moment and stress due to force

$$M := 1800.572480$$

$$\sigma := 0.04538025268$$

$$eq1 := \frac{\epsilon\_pl}{a}\cdot\left(\frac{(\sigma\_pl+\sigma\_el)}{2}-\text{sigma}\right) = 0.5\cdot\left(h-\frac{\epsilon\_pl}{a}\right)\cdot\left(h-\frac{\epsilon\_pl}{a}\right)\cdot a\cdot E$$

Total horizontal forces in the moment diagram should be 0. Left of the equal sign is the tensional stress and right of the equal sign is the compresive stress.

$$eq1 := \frac{2.63\,(8.050000000-0.0003357958361\,F)}{a} = 22.70\left(29.78-\frac{2.63}{a}\right)^2 a$$

$$moment := \left(\left(\frac{2}{3}\cdot\left(h-\frac{\epsilon\_pl}{a}\right)+0.5\cdot\frac{\epsilon\_pl}{a}\right)\cdot\frac{\epsilon\_pl}{a}\cdot(\sigma\_el-\text{sigma})+\left(\frac{2}{3}\cdot\left(h-\frac{\epsilon\_pl}{a}\right)+\frac{2}{3}\cdot\frac{\epsilon\_pl}{a}\right)\cdot\frac{\epsilon\_pl}{a}\cdot 0.5\cdot(\sigma\_pl-\sigma\_el)\right)\cdot b = M$$

The total moment due to the stresses should be equal to the acting moment. The moment is taken from the compresion zone

$$moment := \frac{263.00\left(19.85333333-\frac{0.4383333334}{a}\right)(6.9-0.0003357958361\,F)}{a} + \frac{6004.640665}{a} = 14.89000000\,F$$

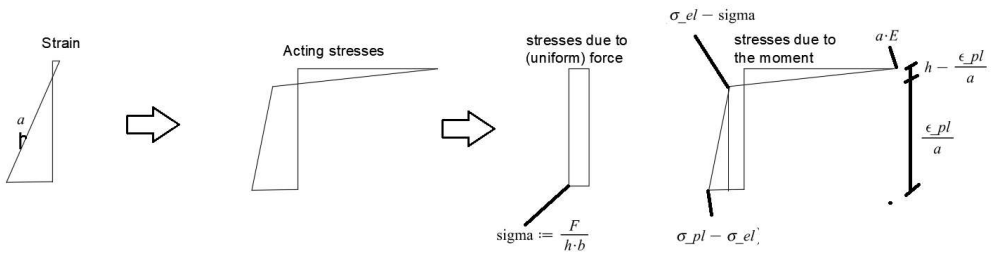

Then the total resistance of the tabs is calculated. The sketch is seen below.

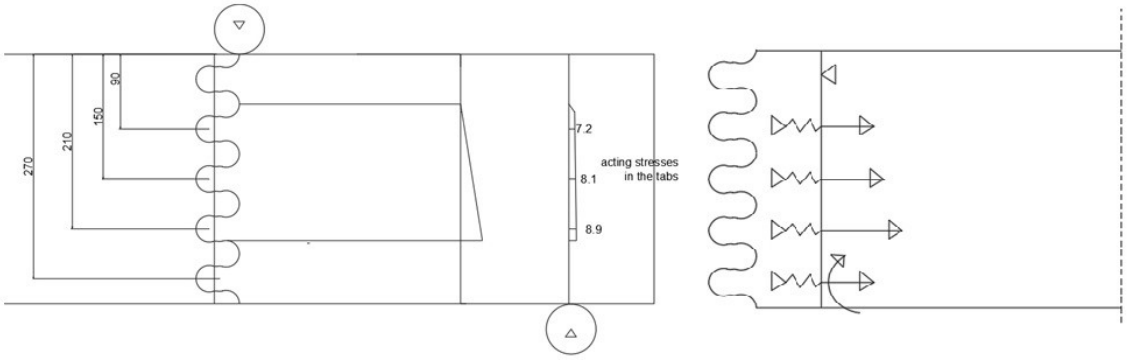

The calculation is as follows:

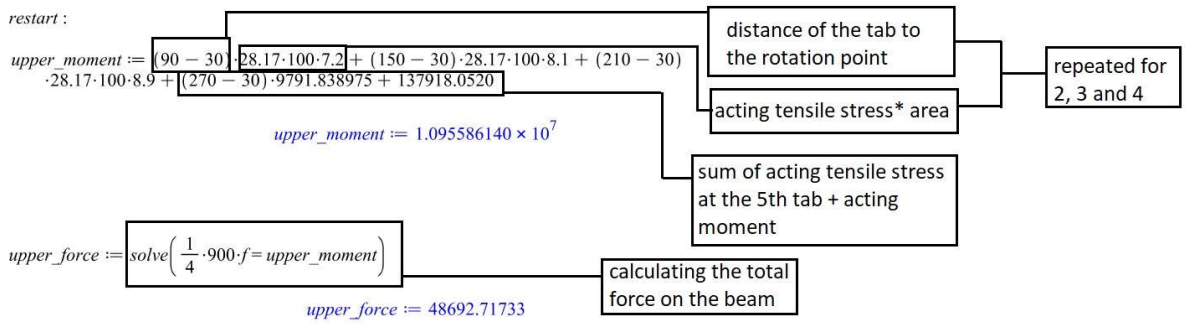

This is done for all designs and is seen below

Lower Tab first design 1

$restart;$

$\epsilon\_pl := 2.63; E := 45.4; \sigma\_pl := 9.2; h := 28.17; b := 100; \sigma\_el := 6.9$

$\epsilon\_pl := 2.63$

$E := 45.4$

$\sigma\_pl := 9.2$

$h := 28.17$

$b := 100$

$\sigma\_el := 6.9$

$$M := \frac{1}{2}\cdot h\cdot F;\ \text{sigma} := \frac{F}{h\cdot b}$$

$M := 1800.572480$

$\sigma := 0.04538025268$

$$eq1 := \frac{\epsilon\_pl}{a}\cdot\left(\frac{(\sigma\_pl+\sigma\_el)}{2}-\text{sigma}\right) = 0.5\cdot\left(h-\frac{\epsilon\_pl}{a}\right)\cdot\left(h-\frac{\epsilon\_pl}{a}\right)\cdot a\cdot E$$

$$eq1 := \frac{2.63\ (8.050000000 - 0.0003357958361\,F)}{a} = 22.70\left(29.78-\frac{2.63}{a}\right)^2 a$$

$$moment := \left(\left(\frac{2}{3}\cdot\left(h-\frac{\epsilon\_pl}{a}\right)+0.5\cdot\frac{\epsilon\_pl}{a}\right)\cdot\frac{\epsilon\_pl}{a}\cdot(\sigma\_el-\text{sigma})+\left(\frac{2}{3}\cdot\left(h-\frac{\epsilon\_pl}{a}\right)+\frac{2}{3}\cdot\frac{\epsilon\_pl}{a}\right)\cdot\frac{\epsilon\_pl}{a}\cdot 0.5\cdot(\sigma\_pl-\sigma\_el)\right)\cdot b = M$$

$$moment := \frac{263.00\left(19.85333333-\frac{0.4383333334}{a}\right)(6.9-0.0003357958361\,F)}{a} + \frac{6004.640665}{a} = 14.89000000\,F$$

$solve(\{eq1, moment\});\ assign(solve(\{eq1, moment\})[3])$

$\{F = -85562.64802, a = 0.01899480064\}, \{F = 13861.02163, a = 0.06725258543\}, \{F = 11365.76884, a = 0.1118315281\}, \{F = -1.155999786\times 10^6, a = -0.1392027109\}$

$$\frac{\epsilon\_pl}{a}$$

23.51751822

$$\frac{moment \cdot 0.5 \cdot h}{\frac{1}{12} \cdot b \cdot h^3}$$

$11.44973357 = 11.44973355$

F

11365.76884

$moment$

$169236.2982 = 169236.2980$

sigma

3.816577851

Lower tab second design 2

$restart;$

$\epsilon\_pl := 2.63; E := 45.4; \sigma\_pl := 8.05; h := 29.78; b := 100$

$\epsilon\_pl := 2.63$

$E := 45.4$

$\sigma\_pl := 8.05$

$h := 29.78$

$b := 100$

$$sigma\_moment := \frac{\frac{1}{2} \cdot h \cdot \frac{1}{2} \cdot h \cdot F}{\frac{1}{12} \cdot b \cdot h^3}; sigma\_tension := \frac{F}{h \cdot b}$$

$sigma\_moment := 0.001007387508\, F$

$sigma\_tension := 0.0003357958361\, F$

$y := sigma\_moment + sigma\_tension = 6.9$

$y := 0.001343183344\, F = 6.9$

$assign(solve(\{y\}));$

F

5137.050002

$$\frac{1}{2} \cdot h \cdot F$$

76490.67455

Lower tab Third design 3

$restart;$

$\epsilon\_pl := 2.63; E := 45.4; \sigma\_pl := 8.05; h := 33.6; b := 100$

$\epsilon\_pl := 2.63$

$E := 45.4$

$\sigma\_pl := 8.05$

$h := 33.6$

$b := 100$

$$sigma\_moment := \frac{\frac{1}{2}\cdot h\cdot\frac{1}{2}\cdot h\cdot F}{\frac{1}{12}\cdot b\cdot h^3};\ sigma\_tension := \frac{F}{h\cdot b}$$

$sigma\_moment := 0.0008928571429\,F$

$sigma\_tension := 0.0002976190476\,F$

$y := sigma\_moment + sigma\_tension = 6.9$

$y := 0.001190476190\,F = 6.9$

$assign(solve(\{y\}))$;

F

5796.000002

$\frac{1}{2}\cdot h\cdot F$

97372.80005

Total resistance first design

$restart$:

$$upper\_moment := (90-30)\cdot 28.17\cdot 100\cdot 7.2 + (150-30)\cdot 28.17\cdot 100\cdot 8.1 + (210-30)\cdot 28.17\cdot 100\cdot 8.9 + (270-30)\cdot 9791.838975 + 137918.0520$$

$upper\_moment := 1.095586140\times 10^7$

$$upper\_force := solve\left(\frac{1}{4}\cdot 900\cdot f = upper\_moment\right)$$

$upper\_force := 48692.71733$

Total resistance second design

restart;

$$upper\_moment := (90 - 30)\cdot 29.78\cdot 100\cdot 7.2 + (150 - 30)\cdot 29.78\cdot 100\cdot 8.1 + (210 - 30)\cdot 29.78\cdot 100\cdot 8.9 + (270 - 30)\cdot 5137.050002 + 76490.67455$$

$$upper\_moment := 1.026125067 \times 10^{7}$$

$$upper\_force := solve\left(\frac{1}{4}\cdot 900\cdot f = upper\_moment\right)$$

$$upper\_force := 45605.55853$$

Total resistance third design

restart;

$$upper\_moment := (90 - 30)\cdot 33.6\cdot 100\cdot 7.2 + (150 - 30)\cdot 33.6\cdot 100\cdot 8.1 + (210 - 30)\cdot 33.6\cdot 100\cdot 8.9 + (270 - 30)\cdot 5796.000002 + 97372.80005$$

$$upper\_moment := 1.158857280 \times 10^{7}$$

$$upper\_force := solve\left(\frac{1}{4}\cdot 900\cdot f = upper\_moment\right)$$

$$upper\_force := 51504.76800$$

Appendix C Analytical approximation of the interlocking connection

For the design with one circle, the resistance is calculated with inspiration from the paper “Interface fracture of micro-architectured glass: Inverse identification of interface properties and a novel analytical model” (16). The difference between this calculation and the calculation made here is that no second-order effects are modelled, the plastic and elastic deformation of the tabs themselves are ignored till failure and the rotation point stays the same.

Firstly all the parameters will be defined. Then the contact force will be approximated. This is done by polynomials. This can be seen below

$$restart;$$
$$a := \mathrm{sqrt}\left(\frac{8 \cdot p \cdot R\_fix}{\mathrm{Pi} \cdot t \cdot E}\right); R := 15.1; R\_fix := \frac{15.1}{2}; theta0 := \frac{7 \cdot \mathrm{Pi}}{180}; E := 45100; t := 100; f := 0.3; delta1 := 0.0000000001; delta2 := 0.1; delta3 := 0.2; delta4 := 0.3; delta5 := 0.4; delta6 := 0.5; delta7 := 0.6;$$

$$a := 2\sqrt{2}\sqrt{\frac{p\, R\_fix}{\pi\, t\, E}}$$

$$R := 15.1$$

$$R\_fix := 7.550000000$$

$$\theta 0 := \frac{7\,\pi}{180}$$

$$E := 45100$$

$$t := 100$$

$$f := 0.3$$

$$\delta 1 := 1. \times 10^{-10}$$

$$\delta 2 := 0.1$$

$$\delta 3 := 0.2$$

$$\delta 4 := 0.3$$

$$\delta 5 := 0.4$$

$$\delta 6 := 0.5$$

$$\delta 7 := 0.6$$

$$eq := \left(delta1 = \frac{a^2}{4 \cdot R\_fix} \cdot \left(2 \cdot \ln\left(\frac{8 \cdot R\_fix}{a}\right) - 1\right)\right) : y1 := solve(eq, p)[2] :$$
$$eq := \left(delta2 = \frac{a^2}{4 \cdot R\_fix} \cdot \left(2 \cdot \ln\left(\frac{8 \cdot R\_fix}{a}\right) - 1\right)\right) : y2 := solve(eq, p)[2] : \quad :$$

$$eq := \left(delta3 = \frac{a^2}{4 \cdot R\_fix} \cdot \left(2 \cdot \ln\left(\frac{8 \cdot R\_fix}{a}\right) - 1\right)\right) :$$
$$y3 := solve(eq, p)[2] :$$
$$eq := \left(delta4 = \frac{a^2}{4 \cdot R\_fix} \cdot \left(2 \cdot \ln\left(\frac{8 \cdot R\_fix}{a}\right) - 1\right)\right) :$$
$$y4 := solve(eq, p)[2] :$$

$$eq := \left(delta5 = \frac{a^2}{4 \cdot R\_fix} \cdot \left(2 \cdot \ln\left(\frac{8 \cdot R\_fix}{a}\right) - 1\right)\right) : y5 := solve(eq, p)[2] :$$

$$eq := \left(delta6 = \frac{a^2}{4 \cdot R\_fix} \cdot \left(2 \cdot \ln\left(\frac{8 \cdot R\_fix}{a}\right) - 1\right)\right) : \; y6 := evalf(solve(eq, p))[2] :$$

$$eq := \left(delta7 = \frac{a^2}{4 \cdot R\_fix} \cdot \left(2 \cdot \ln\left(\frac{8 \cdot R\_fix}{a}\right) - 1\right)\right) : \; y7 := evalf(solve(eq, p))[2] :$$

$$P := c1 + c2 \cdot \text{delta} + c3 \cdot \delta^2 + c4 \cdot \delta^3 + c5 \cdot \delta^4 + c6 \cdot \delta^5 + c7 \cdot \delta^6 :$$

delta := *delta1* :
eq1 := *P* = *y1* :
delta := *delta2* :
eq2 := *P* = *y2* :
delta := *delta3* :
eq3 := *P* = *y3* :
delta := *delta4* :
eq4 := *P* = *y4* :
delta := *delta5* :
eq5 := *P* = *y5* :
delta := *delta6* :
eq6 := *P* = *y6* :
delta := *delta7* :
eq7 := *P* = *y7* :

delta :='delta':

assign(*solve*([*eq1*, *eq2*, *eq3*, *eq4*, *eq5*, *eq6*, *eq7*]))

So the contact force Will be as follows:

P

$$5.912975212 \times 10^6 \, \delta^6 - 1.296006107 \times 10^7 \, \delta^5 + 1.162068858 \times 10^7 \, \delta^4 - 5.651899616 \times 10^6 \, \delta^3 + 1.985651985 \times 10^6 \, \delta^2 + 711405.3224 \, \delta - 0.00004770494858$$

plot(*P*, delta = 0 ..0.6)

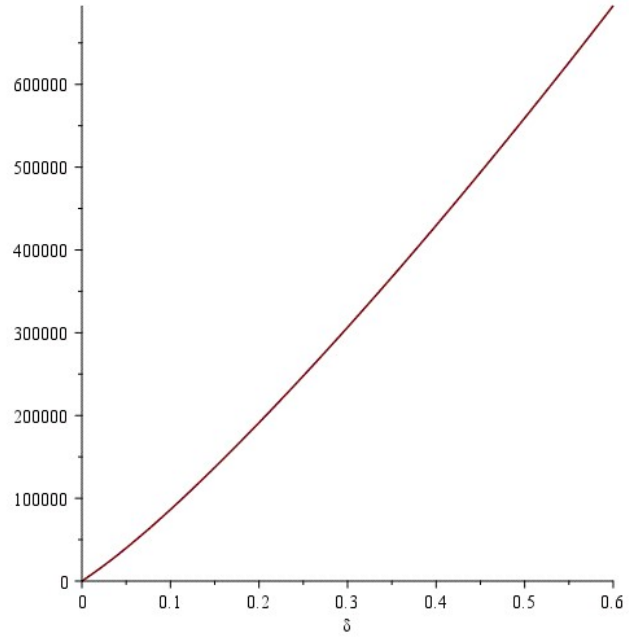

Then each contact point will be given an x and y position from the guessed rotation point. Here theta is the angle the interlocking tabs have from the rotation point.

$$c := 15 : w := 30 : x1 := w : x2 := 2\cdot w : x3 := 3\cdot w : x4 := 4\cdot w : x5 := 5\cdot w : x6 := 6\cdot w : x7 := 7\cdot w : x8 := 8\cdot w :$$
$$ytop := 18.57 : ybot := 15.1 :$$

$$x1t := \cos(\text{theta})\cdot x1 + \sin(\text{theta})\cdot ytop :$$
$$x2t := \cos(\text{theta})\cdot x2 - \sin(\text{theta})\cdot ybot :$$
$$x3t := \cos(\text{theta})\cdot x3 + \sin(\text{theta})\cdot ytop :$$
$$x4t := \cos(\text{theta})\cdot x4 - \sin(\text{theta})\cdot ybot :$$
$$x5t := \cos(\text{theta})\cdot x5 + \sin(\text{theta})\cdot ytop :$$
$$x6t := \cos(\text{theta})\cdot x6 - \sin(\text{theta})\cdot ybot :$$
$$x7t := \cos(\text{theta})\cdot x7 + \sin(\text{theta})\cdot ytop :$$
$$x8t := \cos(\text{theta})\cdot x8 - \sin(\text{theta})\cdot ybot :$$

$$y1t := \cos(\text{theta})\cdot ytop - \sin(\text{theta})\cdot x1 :$$
$$y2t := \cos(\text{theta})\cdot ybot + \sin(\text{theta})\cdot x2 :$$
$$y3t := \cos(\text{theta})\cdot ytop - \sin(\text{theta})\cdot x3 :$$
$$y4t := \cos(\text{theta})\cdot ybot + \sin(\text{theta})\cdot x4 :$$
$$y5t := \cos(\text{theta})\cdot ytop - \sin(\text{theta})\cdot x5 :$$
$$y6t := \cos(\text{theta})\cdot ybot + \sin(\text{theta})\cdot x6 :$$
$$y7t := \cos(\text{theta})\cdot ytop - \sin(\text{theta})\cdot x7 :$$
$$y8t := \cos(\text{theta})\cdot ybot + \sin(\text{theta})\cdot x8 :$$

Then the change in distance between every tab will be defined. This is how much the tab needs to be compressed.

$$delta1 := 2\,R - \text{sqrt}\left((y2t - y1t)^2 + (x2t - x1t)^2\right) :$$
$$delta2 := 2\,R - \text{sqrt}\left((y3t - y2t)^2 + (x3t - x2t)^2\right) :$$
$$delta3 := 2\,R - \text{sqrt}\left((y4t - y3t)^2 + (x4t - x3t)^2\right) :$$
$$delta4 := 2\,R - \text{sqrt}\left((y5t - y4t)^2 + (x5t - x4t)^2\right) :$$
$$delta5 := 2\,R - \text{sqrt}\left((y6t - y5t)^2 + (x6t - x5t)^2\right) :$$
$$delta6 := 2\,R - \text{sqrt}\left((y7t - y6t)^2 + (x7t - x6t)^2\right) :$$
$$delta7 := 2\,R - \text{sqrt}\left((y8t - y7t)^2 + (x8t - x7t)^2\right) :$$

$$plot\left([delta1, delta3, delta5, delta7], \text{theta} = 0 .. \frac{1 \cdot \text{Pi}}{180} \right)$$

The total amount of compression is as follows:

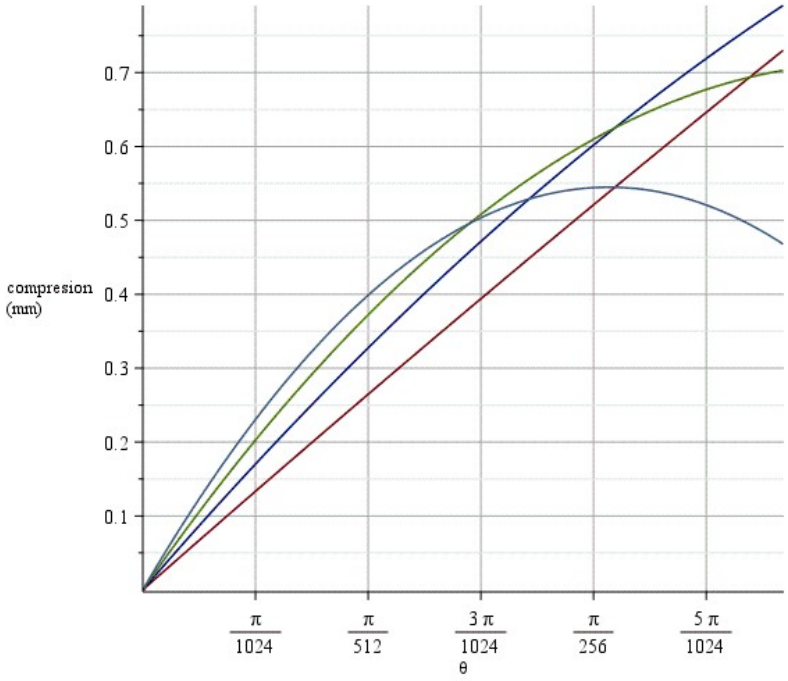

Then the local rotation can be calculated. This is for the direction of the contact force. This will only be done for the places where the connection has contact.

$$theta1 := \arctan\left(\frac{(y2t - y1t)}{(x2t - x1t)} \right) :$$

$$theta3 := \arctan\left(\frac{(y4t - y3t)}{(x4t - x3t)} \right) :$$

$$theta5 := \arctan\left(\frac{(y6t - y5t)}{(x6t - x5t)} \right) :$$

$$theta7 := \arctan\left(\frac{(y8t - y7t)}{(x8t - x7t)} \right) :$$

So the angle of the contact forces are as follows:

$$plot\left([theta1, theta3, theta5, theta7], \text{theta} = 0 .. \frac{1 \cdot \text{Pi}}{180} \right)$$

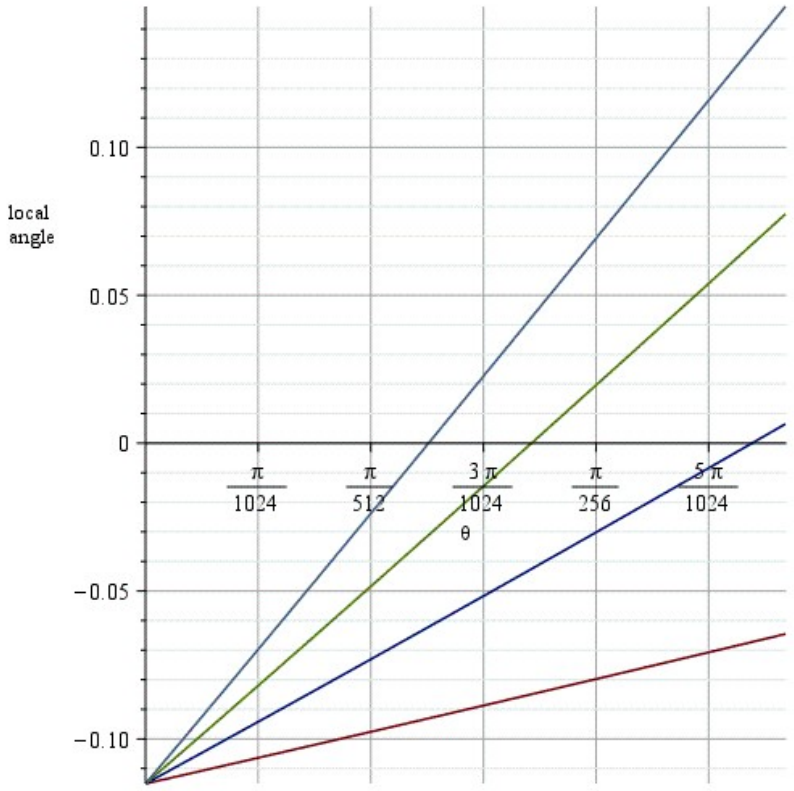

Then the compression of the force will be assigned to each tab so the acting force can be calculated.

delta := *delta1* :

$P1 := P\cdot(f\cdot\cos(theta1) + \sin(theta1))$:

delta := *delta3* :

$P2 := P\cdot(f\cdot\cos(theta3) + \sin(theta3))$:

delta := *delta5* :

$P3 := P\cdot(f\cdot\cos(theta5) + \sin(theta5))$:

delta := *delta7* :

$P4 := P\cdot(f\cdot\cos(theta7) + \sin(theta7))$: delta :='delta':

With this, the bending moment can be calculated as seen below. As seen here it is assumed that the tabs will not fail.

$M := P1\cdot(x2 - c + 30) + P2\cdot(x4 - c + 30) + P3\cdot(x6 - c + 30) + P4\cdot(x8 - c + 30)$:

$\text{theta} := \arctan\left(\frac{u}{450}\right)$:

$plot\left(\frac{M}{900}\cdot 4, u = 0..10\right)$

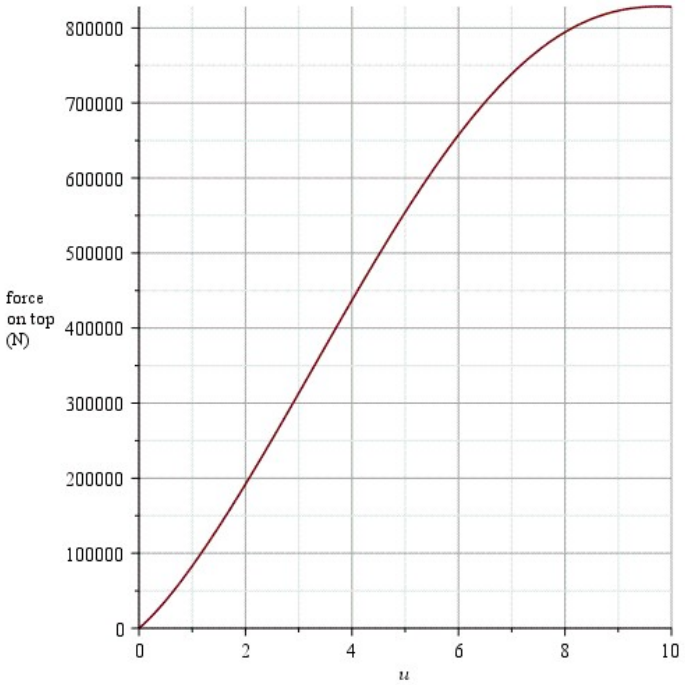

Because the tabs will fail the pullout at the max u will be read from the curve below. (analytically this is unsolvable).

$plot([P1, P2, P3, P4, 13698, 27397], u = 0..2)$

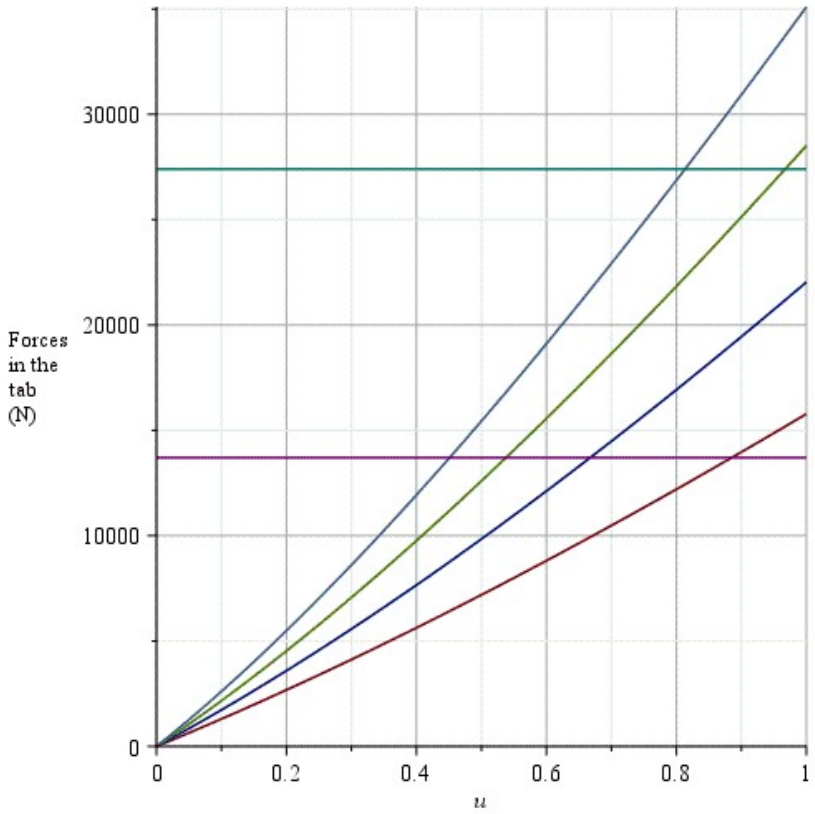

Then the failure of the tabs can be modelled with a hevyside function. Where the acting force in the tab will be 0 as soon as this max u has been reached. The results of the complete structure can be seen below.

$$tab1 := P1\cdot(x2 - c + 30) - P1\cdot(x2 - c + 30)\text{Heaviside}(-1.6 + u):$$
$$tab2 := P2\cdot(x4 - c + 30) - P2\cdot(x4 - c + 30)\text{Heaviside}(-1.2 + u):$$
$$tab3 := P3\cdot(x6 - c + 30) - P3\cdot(x6 - c + 30)\cdot\text{Heaviside}(-0.97 + u):$$
$$tab4 := P4\cdot(x8 - c + 30) - P4\cdot(x8 - c + 30)\text{Heaviside}(-0.45 + u):$$
$$M := tab1 + tab2 + tab3 + tab4:$$

$$plot\left(\frac{M}{900}\cdot 4, u = 0..2\right)$$

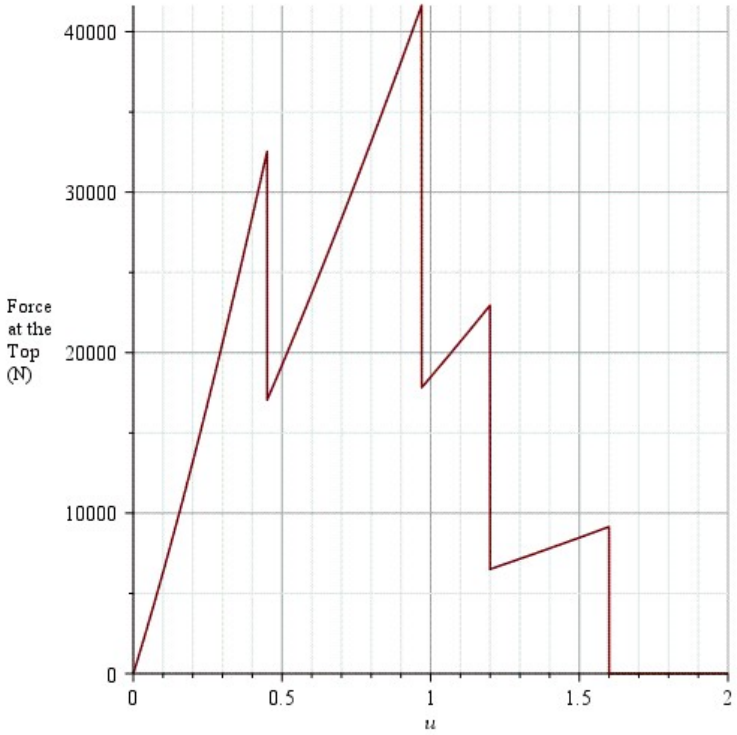

This is quite rough because no plasticity is modelled. This can be estimated with also a Heaviside function.

$$hPl := 11 \cdot 0.025 :$$

$$uPl1 := \frac{hPl}{30} \cdot 450 :$$

$$uPl2 := \frac{hPl}{90} \cdot 450 :$$

$$uPl3 := \frac{hPl}{150} \cdot 450 :$$

$$uPl4 := \frac{hPl}{230} \cdot 450 :$$

$$tab1 := P1 \cdot (x2 - c + 30) - \left(P1 - 27397 \cdot \left(1 - \frac{u - 1.6}{uPl1}\right)\right) \cdot (x2 - c + 30)\text{Heaviside}(-1.6 + u) - \left(27397 \cdot \left(1 - \frac{u - 1.6}{uPl1}\right)\right) \cdot (x2 - c + 30)\text{Heaviside}(-1.6 + u - uPl1) :$$

$$tab2 := P2 \cdot (x4 - c + 30) - \left(P2 - 27397 \cdot \left(1 - \frac{u - 1.2}{uPl2}\right)\right) \cdot (x4 - c + 30)\text{Heaviside}(-1.2 + u) - \left(27397 \cdot \left(1 - \frac{u - 1.2}{uPl2}\right)\right) \cdot (x4 - c + 30)\text{Heaviside}(-1.2 + u - uPl2) :$$

$$tab3 := P3 \cdot (x6 - c + 30) - \left(P3 - 27397 \cdot \left(1 - \frac{u - 0.97}{uPl3}\right)\right) \cdot (x6 - c + 30) \cdot \text{Heaviside}(-0.97 + u) - \left(27397 \cdot \left(1 - \frac{u - 0.97}{uPl3}\right)\right) \cdot (x6 - c + 30) \cdot \text{Heaviside}(-0.97 + u - uPl3) :$$

$$tab4 := P4 \cdot (x8 - c + 30) - \left(P4 - 13698 \cdot \left(1 - \frac{u - 0.45}{uPl4}\right)\right) \cdot (x8 - c + 30)\text{Heaviside}(-0.45 + u) - \left(13698 \cdot \left(1 - \frac{u - 0.45}{uPl4}\right)\right) \cdot (x8 - c + 30)\text{Heaviside}(-0.45 + u - uPl4) :$$

$$M := (tab1 + tab2 + tab3 + tab4) :$$

$$plot([tab1, tab2, tab3, tab4, M], u = 0..2)$$

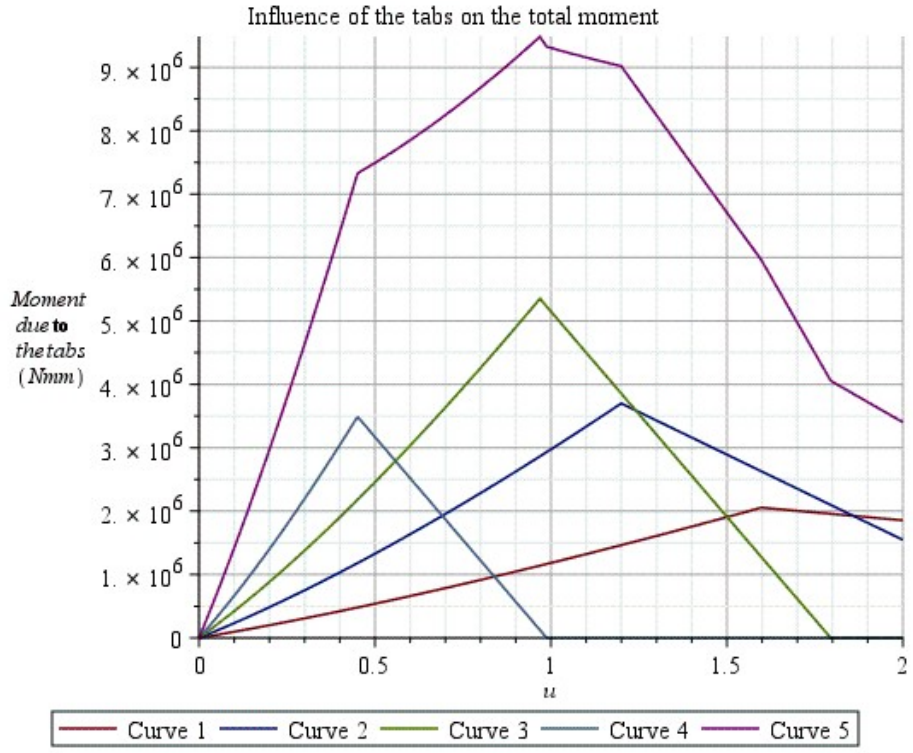

$$plot\left(\frac{M}{900}\cdot 4,\ u=0..4\right)$$

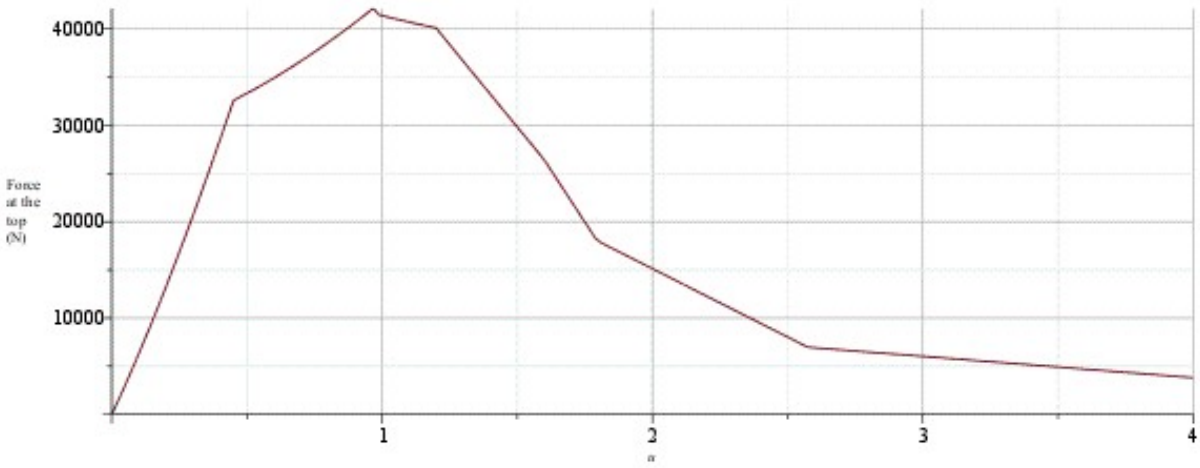

The same can be done with the design with 2 circles. The difference with this design is that there are more interaction points. In total, it has 8 interaction points instead of the 4. The total calculation is as follows:

```
restart;
a := sqrt(8·p·R_fix/(Pi·t·E)); R := 15.1; R_fix := 15.1/2; theta0 := 7·Pi/180; E := 45100; t := 100; f := 0.3;
delta1 := 0.0000000001; delta2 := 0.1; delta3 := 0.2; delta4 := 0.3; delta5 := 0.4; delta6 := 0.5;
delta7 := 0.6;
```

$$a := 2\sqrt{2}\sqrt{\frac{p\,R\_fix}{\pi\,t\,E}}$$

$$R := 15.1$$

$$R\_fix := 7.550000000$$

$$\theta 0 := \frac{7\,\pi}{180}$$

$$E := 45100$$

$$t := 100$$

$$f := 0.3$$

$$\delta 1 := 1. \times 10^{-10}$$

$$\delta 2 := 0.1$$

$$\delta 3 := 0.2$$

$$\delta 4 := 0.3$$

$$\delta 5 := 0.4$$

$$\delta 6 := 0.5$$

$$\delta 7 := 0.6$$

$$eq := \left(delta1 = \frac{a^2}{4\cdot R\_fix}\cdot\left(2\cdot\ln\left(\frac{8\cdot R\_fix}{a}\right)-1\right)\right): y1 := solve(eq,p)[2]:$$

$$eq := \left(delta2 = \frac{a^2}{4\cdot R\_fix}\cdot\left(2\cdot\ln\left(\frac{8\cdot R\_fix}{a}\right)-1\right)\right): y2 := solve(eq,p)[2]: \quad :$$

$$eq := \left(delta3 = \frac{a^2}{4\cdot R\_fix}\cdot\left(2\cdot\ln\left(\frac{8\cdot R\_fix}{a}\right)-1\right)\right):$$
$$y3 := solve(eq,p)[2]:$$
$$eq := \left(delta4 = \frac{a^2}{4\cdot R\_fix}\cdot\left(2\cdot\ln\left(\frac{8\cdot R\_fix}{a}\right)-1\right)\right):$$
$$y4 := solve(eq,p)[2]:$$

$$eq := \left(delta5 = \frac{a^2}{4\cdot R\_fix}\cdot\left(2\cdot\ln\left(\frac{8\cdot R\_fix}{a}\right)-1\right)\right): y5 := solve(eq,p)[2]:$$

$$eq := \left(delta6 = \frac{a^2}{4\cdot R\_fix}\cdot\left(2\cdot\ln\left(\frac{8\cdot R\_fix}{a}\right)-1\right)\right): y6 := evalf(solve(eq,p))[2]:$$

$$eq := \left(delta7 = \frac{a^2}{4\cdot R\_fix}\cdot\left(2\cdot\ln\left(\frac{8\cdot R\_fix}{a}\right)-1\right)\right): y7 := evalf(solve(eq,p))[2]:$$

$$P := c1 + c2\cdot\mathrm{delta} + c3\cdot\delta^2 + c4\cdot\delta^3 + c5\cdot\delta^4 + c6\cdot\delta^5 + c7\cdot\delta^6:$$

delta := *delta1* :
eq1 := *P* = *y1* :
delta := *delta2* :
eq2 := *P* = *y2* :
delta := *delta3* :
eq3 := *P* = *y3* :
delta := *delta4* :
eq4 := *P* = *y4* :
delta := *delta5* :
eq5 := *P* = *y5* :
delta := *delta6* :
eq6 := *P* = *y6* :
delta := *delta7* :
eq7 := *P* = *y7* :

delta :='delta':

assign(*solve*([*eq1*, *eq2*, *eq3*, *eq4*, *eq5*, *eq6*, *eq7*]))

P

$$5.912975212 \times 10^{6}\,\delta^{6} - 1.296006107 \times 10^{7}\,\delta^{5} + 1.162068858 \times 10^{7}\,\delta^{4} - 5.651899616 \times 10^{6}\,\delta^{3} + 1.985651985 \times 10^{6}\,\delta^{2} + 711405.3224\,\delta - 0.00004770494858$$

plot(*P*, delta = 0 ..0.6)

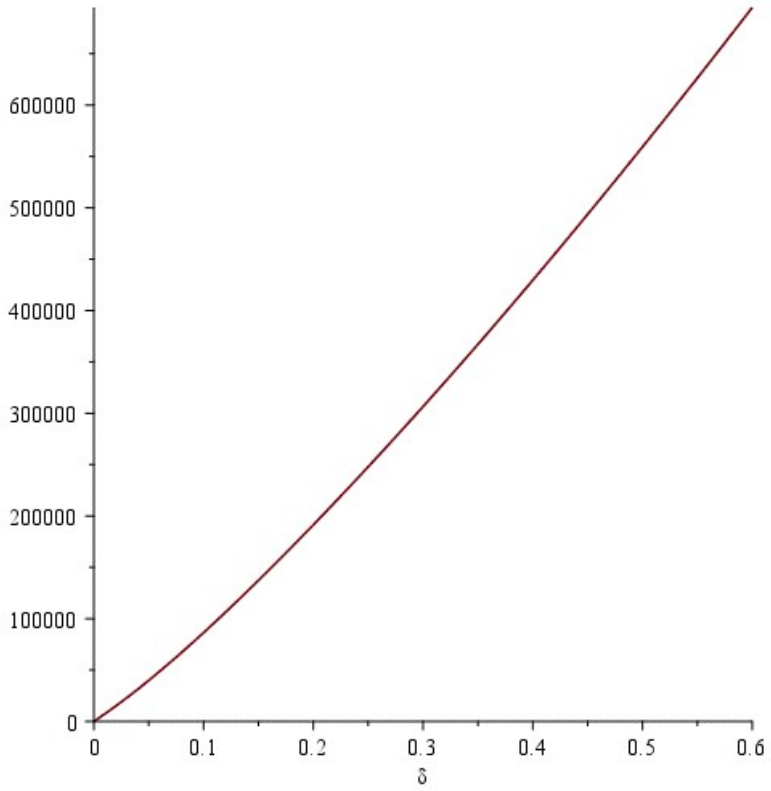

$$c := 15 : w := 30 : x1 := w : x2 := 2\cdot w : x3 := 3\cdot w : x4 := 4\cdot w : x5 := 5\cdot w : x6 := 6\cdot w : x7 := 7\cdot w : x8 := 8\cdot w : ytop := 18.57 : ybot := 15.1 : ytop2 := 25.5 : ybot2 := 22.03 :$$

$$x1t := \cos(\text{theta})\cdot x1 + \sin(\text{theta})\cdot ytop :$$
$$x2t := \cos(\text{theta})\cdot x2 - \sin(\text{theta})\cdot ybot :$$
$$x3t := \cos(\text{theta})\cdot x3 + \sin(\text{theta})\cdot ytop :$$
$$x4t := \cos(\text{theta})\cdot x4 - \sin(\text{theta})\cdot ybot :$$
$$x5t := \cos(\text{theta})\cdot x5 + \sin(\text{theta})\cdot ytop :$$
$$x6t := \cos(\text{theta})\cdot x6 - \sin(\text{theta})\cdot ybot :$$
$$x7t := \cos(\text{theta})\cdot x7 + \sin(\text{theta})\cdot ytop :$$
$$x8t := \cos(\text{theta})\cdot x8 - \sin(\text{theta})\cdot ybot :$$

$$y1t := \cos(\text{theta})\cdot ytop - \sin(\text{theta})\cdot x1 :$$
$$y2t := \cos(\text{theta})\cdot ybot + \sin(\text{theta})\cdot x2 :$$
$$y3t := \cos(\text{theta})\cdot ytop - \sin(\text{theta})\cdot x3 :$$
$$y4t := \cos(\text{theta})\cdot ybot + \sin(\text{theta})\cdot x4 :$$
$$y5t := \cos(\text{theta})\cdot ytop - \sin(\text{theta})\cdot x5 :$$
$$y6t := \cos(\text{theta})\cdot ybot + \sin(\text{theta})\cdot x6 :$$
$$y7t := \cos(\text{theta})\cdot ytop - \sin(\text{theta})\cdot x7 :$$
$$y8t := \cos(\text{theta})\cdot ybot + \sin(\text{theta})\cdot x8 :$$

$$delta1 := 2R - \text{sqrt}\left((y2t - y1t)^2 + (x2t - x1t)^2\right) :$$
$$delta3 := 2R - \text{sqrt}\left((y4t - y3t)^2 + (x4t - x3t)^2\right) :$$
$$delta5 := 2R - \text{sqrt}\left((y6t - y5t)^2 + (x6t - x5t)^2\right) :$$
$$delta7 := 2R - \text{sqrt}\left((y8t - y7t)^2 + (x8t - x7t)^2\right) :$$

Defining more contact points:

$$x1t2 := \cos(\text{theta})\cdot x1 + \sin(\text{theta})\cdot ytop2 :$$
$$x2t2 := \cos(\text{theta})\cdot x2 - \sin(\text{theta})\cdot ybot2 :$$
$$x3t2 := \cos(\text{theta})\cdot x3 + \sin(\text{theta})\cdot ytop2 :$$
$$x4t2 := \cos(\text{theta})\cdot x4 - \sin(\text{theta})\cdot ybot2 :$$
$$x5t2 := \cos(\text{theta})\cdot x5 + \sin(\text{theta})\cdot ytop2 :$$
$$x6t2 := \cos(\text{theta})\cdot x6 - \sin(\text{theta})\cdot ybot2 :$$
$$x7t2 := \cos(\text{theta})\cdot x7 + \sin(\text{theta})\cdot ytop2 :$$
$$x8t2 := \cos(\text{theta})\cdot x8 - \sin(\text{theta})\cdot ybot2 :$$

$$y1t2 := \cos(\text{theta})\cdot ytop2 - \sin(\text{theta})\cdot x1 :$$
$$y2t2 := \cos(\text{theta})\cdot ybot2 + \sin(\text{theta})\cdot x2 :$$
$$y3t2 := \cos(\text{theta})\cdot ytop2 - \sin(\text{theta})\cdot x3 :$$
$$y4t2 := \cos(\text{theta})\cdot ybot2 + \sin(\text{theta})\cdot x4 :$$
$$y5t2 := \cos(\text{theta})\cdot ytop2 - \sin(\text{theta})\cdot x5 :$$
$$y6t2 := \cos(\text{theta})\cdot ybot2 + \sin(\text{theta})\cdot x6 :$$
$$y7t2 := \cos(\text{theta})\cdot ytop2 - \sin(\text{theta})\cdot x7 :$$
$$y8t2 := \cos(\text{theta})\cdot ybot2 + \sin(\text{theta})\cdot x8 :$$

$$delta12 := 2R - \text{sqrt}\left((y2t2 - y1t2)^2 + (x2t2 - x1t2)^2\right) :$$
$$delta32 := 2R - \text{sqrt}\left((y4t2 - y3t2)^2 + (x4t2 - x3t2)^2\right) :$$
$$delta52 := 2R - \text{sqrt}\left((y6t2 - y5t2)^2 + (x6t2 - x5t2)^2\right) :$$
$$delta72 := 2R - \text{sqrt}\left((y8t2 - y7t2)^2 + (x8t2 - x7t2)^2\right);$$

$$plot\left([delta1, delta3, delta5, delta7, delta12, delta32, delta52, delta72], \text{theta} = 0 .. \frac{1 \cdot Pi}{180}, gridlines = true, labels = [\text{"Compresion (mm)"}, \text{"θ"}] \right)$$

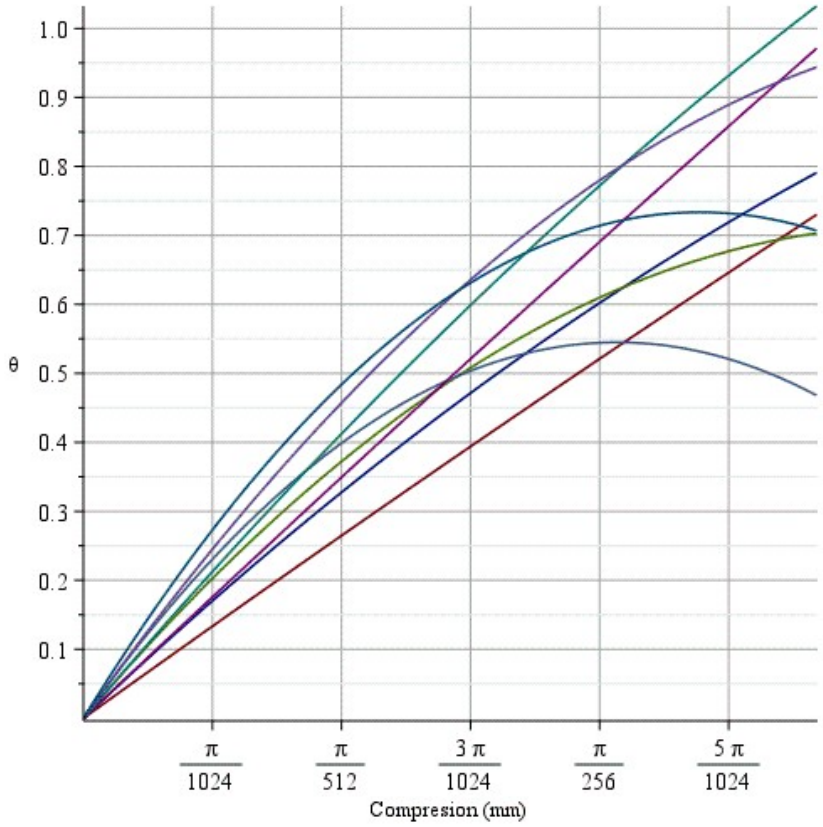

$$theta1 := \arctan\left(\frac{(y2t - y1t)}{(x2t - x1t)} \right) :$$

$$theta3 := \arctan\left(\frac{(y4t - y3t)}{(x4t - x3t)} \right) :$$

$$theta5 := \arctan\left(\frac{(y6t - y5t)}{(x6t - x5t)} \right) :$$

$$theta7 := \arctan\left(\frac{(y8t - y7t)}{(x8t - x7t)} \right) :$$

$$theta12 := \arctan\left(\frac{(y2t2 - y1t2)}{(x2t2 - x1t2)} \right) :$$

$$theta32 := \arctan\left(\frac{(y4t2 - y3t2)}{(x4t2 - x3t2)} \right) :$$

$$theta52 := \arctan\left(\frac{(y6t2 - y5t2)}{(x6t2 - x5t2)} \right) :$$

$$theta72 := \arctan\left(\frac{(y8t2 - y7t2)}{(x8t2 - x7t2)} \right) :$$

$$plot\left([theta1, theta3, theta5, theta7, theta12, theta32, theta52, theta72], \text{theta} = 0 .. \frac{1 \cdot Pi}{180}, gridlines = true, labels = [\text{"θ"}, \text{"Local angle"}] \right)$$

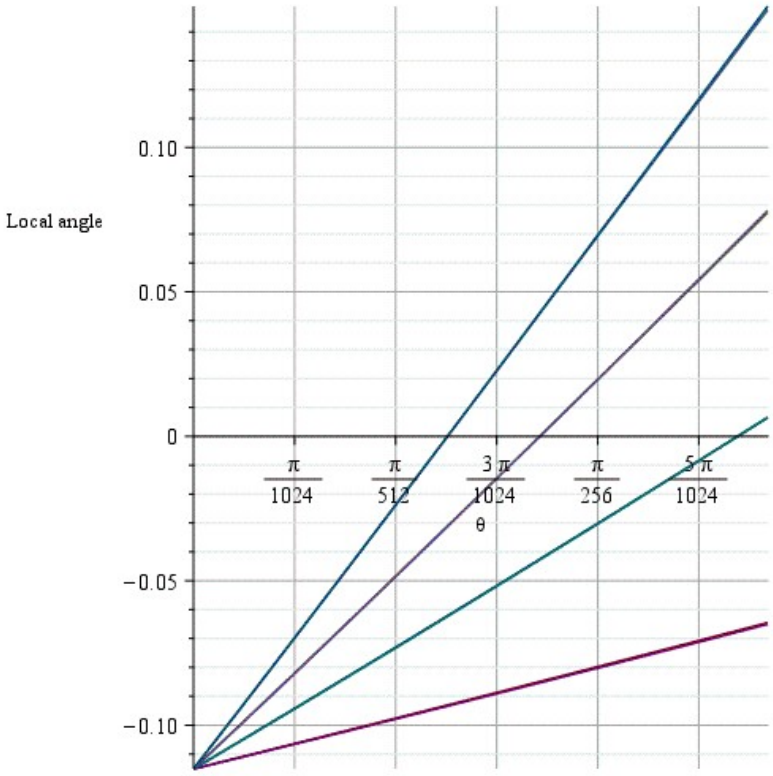

delta := *delta1* : *P11* := *P*·(*f*·cos(*theta1*) + sin(*theta1*)) :

delta := *delta12* : *P12* := *P*·(*f*·cos(*theta12*) + sin(*theta12*)) : *P1* := *P11* + *P12* :

delta := *delta3* :

P21 := *P*·(*f*·cos(*theta3*) + sin(*theta3*)) : delta := *delta3* :

P22 := *P*·(*f*·cos(*theta32*) + sin(*theta32*)) : *P2* := *P21* + *P22* :

delta := *delta5* :

P31 := *P*·(*f*·cos(*theta5*) + sin(*theta5*)) :

delta := *delta52* :

P32 := *P*·(*f*·cos(*theta52*) + sin(*theta52*)) : *P3* := *P31* + *P32* :

delta := *delta7* :

P41 := *P*·(*f*·cos(*theta7*) + sin(*theta7*)) :

delta := *delta72* :

P42 := *P*·(*f*·cos(*theta72*) + sin(*theta72*)) : *P4* := *P41* + *P42* : delta :='delta':

M := *P1*·(*x2* − *c* + 30) + *P2*·(*x4* − *c* + 30) + *P3*·(*x6* − *c* + 30) + *P4*·(*x8* − *c* + 30) :

$$\text{theta} := \arctan\left(\frac{u}{450}\right) :$$

$$plot\left(\frac{M}{900}\cdot 4,\ u = 0\ ..10,\ gridlines = true,\ labels = [\text{"u"},\ \text{"Force on top (N)"}]\right)$$

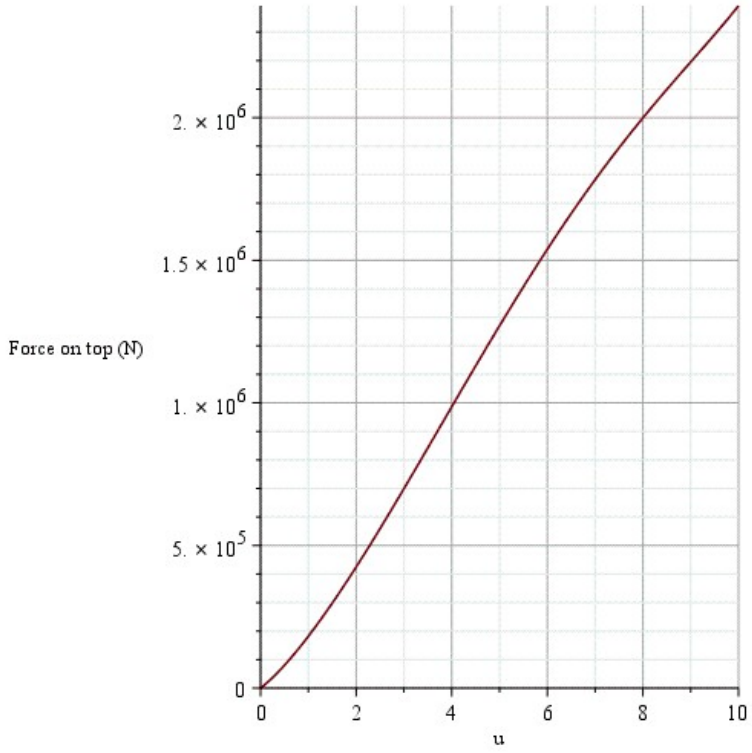

plot([*P1*, *P2*, *P3*, *P4*, 13698, 27397], *u* = 0 ..1, *gridlines* = *true*, *labels* = ["u", "Forces in each tab"])

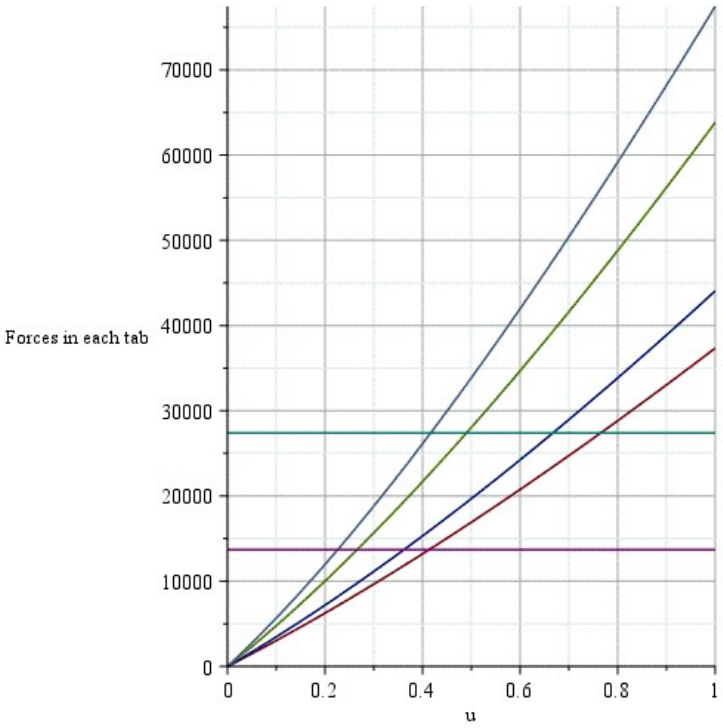

$c\_1 := -0.76; c\_2 := -0.67; c\_3 := -0.48; c\_4 := -0.23;$

$$c\_1 := -0.76$$

$$c\_2 := -0.67$$

$$c\_3 := -0.48$$

$$c\_4 := -0.23$$

$$tab1 := P1\cdot(x2 - c + 30) - P1\cdot(x2 - c + 30)\text{Heaviside}(c\_1 + u):$$
$$tab2 := P2\cdot(x4 - c + 30) - P2\cdot(x4 - c + 30)\text{Heaviside}(c\_2 + u):$$
$$tab3 := P3\cdot(x6 - c + 30) - P3\cdot(x6 - c + 30)\cdot\text{Heaviside}(c\_3 + u):$$
$$tab4 := P4\cdot(x8 - c + 30) - P4\cdot(x8 - c + 30)\text{Heaviside}(c\_4 + u):$$
$$M := tab1 + tab2 + tab3 + tab4:$$

$$plot\left(\frac{M}{900}\cdot 4,\ u = 0..1,\ gridlines = true,\ labels = [\text{"u"},\ \text{"Force on top (N)"}]\right)$$

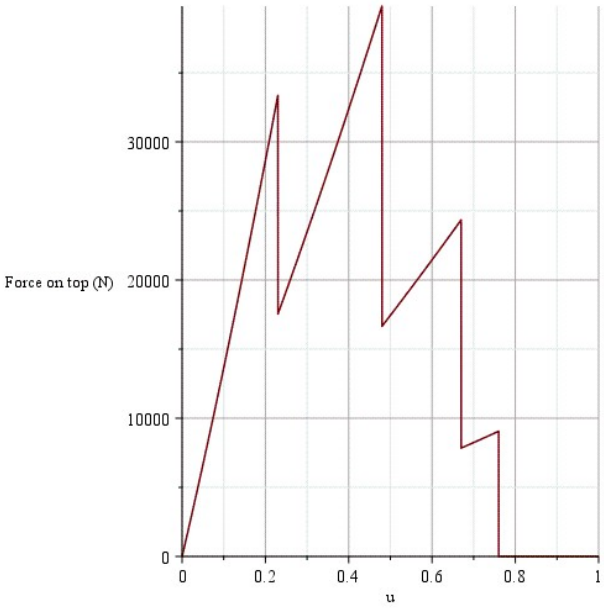

$$P\_max := 27397:$$
$$hPl := 11\cdot(0.025):$$
$$uPl1 := \frac{hPl}{30}\cdot 450:$$
$$uPl2 := \frac{hPl}{90}\cdot 450:$$
$$uPl3 := \frac{hPl}{150}\cdot 450:$$
$$uPl4 := \frac{hPl}{230}\cdot 450:$$
$$tab1 := P1\cdot(x2 - c + 30) - \left(P1 - P\_max\cdot\left(1 - \frac{u + c\_1}{uPl1}\right)\right)\cdot(x2 - c + 30)\text{Heaviside}(c\_1 + u)$$
$$- \left(P\_max\cdot\left(1 - \frac{u + c\_1}{uPl1}\right)\right)\cdot(x2 - c + 30)\text{Heaviside}(c\_1 + u - uPl1):$$
$$tab2 := P2\cdot(x4 - c + 30) - \left(P2 - P\_max\cdot\left(1 - \frac{u + c\_2}{uPl2}\right)\right)\cdot(x4 - c + 30)\text{Heaviside}(c\_2 + u)$$
$$- \left(P\_max\cdot\left(1 - \frac{u + c\_2}{uPl2}\right)\right)\cdot(x4 - c + 30)\text{Heaviside}(c\_2 + u - uPl2):$$
$$tab3 := P3\cdot(x6 - c + 30) - \left(P3 - P\_max\cdot\left(1 - \frac{u + c\_3}{uPl3}\right)\right)\cdot(x6 - c + 30)\cdot\text{Heaviside}(c\_3 + u)$$
$$- \left(P\_max\cdot\left(1 - \frac{u + c\_3}{uPl3}\right)\right)\cdot(x6 - c + 30)\cdot\text{Heaviside}(c\_3 + u - uPl3):$$
$$tab4 := P4\cdot(x8 - c + 30) - \left(P4 - \frac{1}{2}\cdot P\_max\cdot\left(1 - \frac{u + c\_4}{uPl4}\right)\right)\cdot(x8 - c + 30)\text{Heaviside}(c\_4$$
$$+ u) - \left(\frac{1}{2}\cdot P\_max\cdot\left(1 - \frac{u + c\_4}{uPl4}\right)\right)\cdot(x8 - c + 30)\text{Heaviside}(c\_4 + u - uPl4):$$
$$M := (tab1 + tab2 + tab3 + tab4):$$

plot([*tab1*, *tab2*, *tab3*, *tab4*, *M*], *u* = 0 ..5, *y* = 0 ..13000000, *gridlines* = *true*, *labels* = ["Top Displacement (mm)", "Moment (Nmm)"], *legend* = ["Tab 1", "Tab 2", "Tab 3", "Tab 4", "Total"])

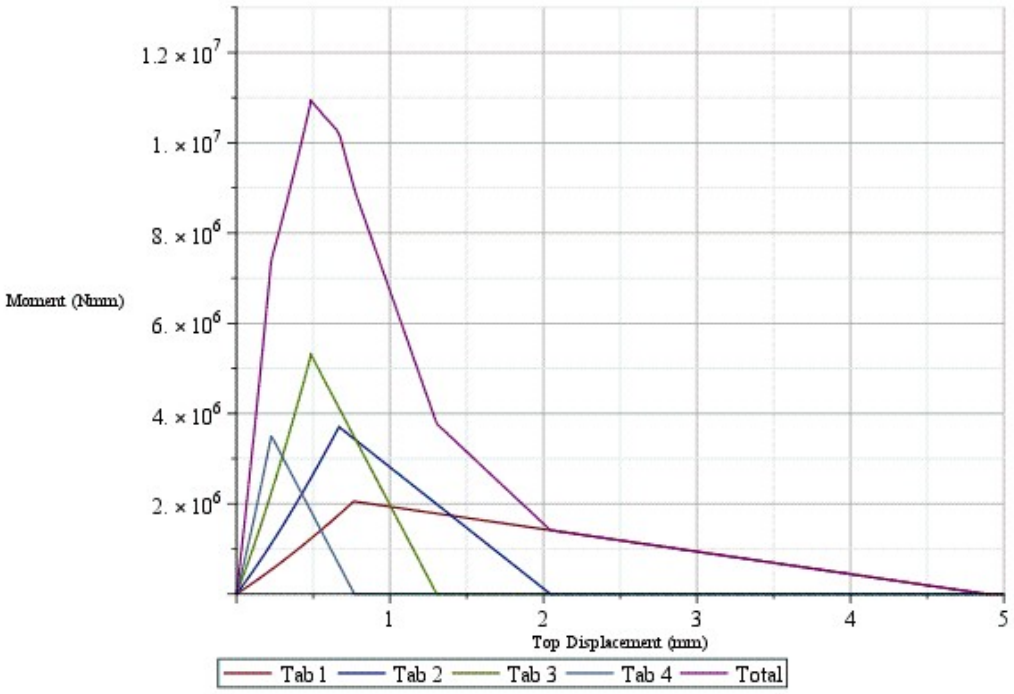

plot($\frac{M}{900} \cdot 4$, *u* = 0 ..6, *gridlines* = *true*, *labels* = ["Top Displacement (mm)", "Force (N)"])

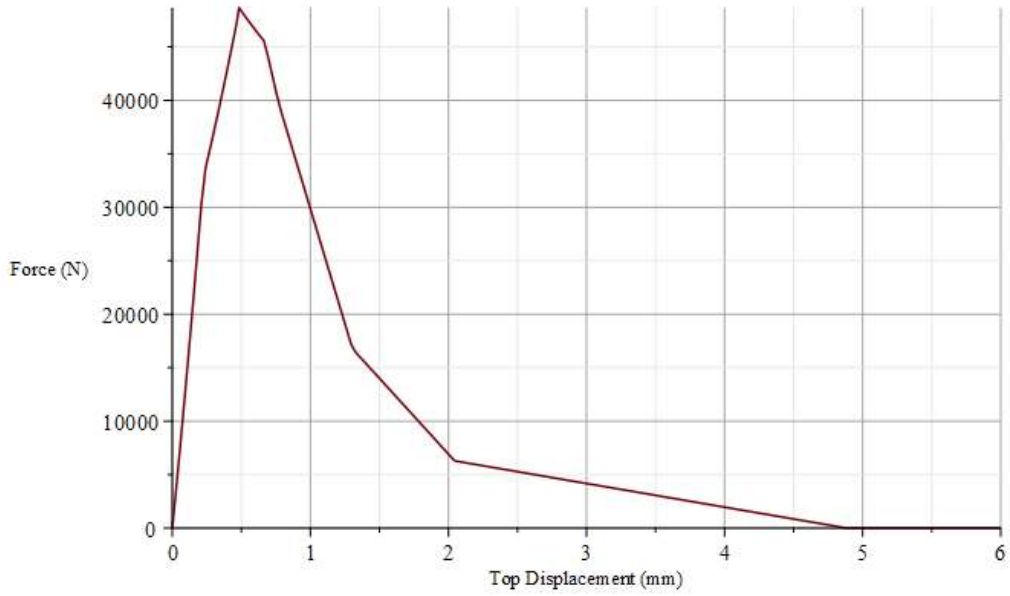

For the calculation with an elastic modulus of 0.25:

```
restart;
a := sqrt(8·p·R_fix/(Pi·t·E)); R := 15.1; R_fix := 15.1/2; theta0 := 7·Pi/180; E := 45100/4; t := 100; f := 0.3;
delta1 := 0.0000000001; delta2 := 0.1; delta3 := 0.2; delta4 := 0.3; delta5 := 0.4; delta6 := 0.5;
delta7 := 0.6;
```

$$a := 2\sqrt{2}\sqrt{\frac{p\,R\_fix}{\pi\,t\,E}}$$

$$R := 15.1$$

$$R\_fix := 7.550000000$$

$$\theta 0 := \frac{7\,\pi}{180}$$

$$E := 11275$$

$$t := 100$$

$$f := 0.3$$

$$\delta 1 := 1. \times 10^{-10}$$

$$\delta 2 := 0.1$$

$$\delta 3 := 0.2$$

$$\delta 4 := 0.3$$

$$\delta 5 := 0.4$$

$$\delta 6 := 0.5$$

$$\delta 7 := 0.6$$

```
eq := (delta1 = a^2/(4·R_fix)·(2·ln(8·R_fix/a) − 1)): y1 := solve(eq, p)[2]:
eq := (delta2 = a^2/(4·R_fix)·(2·ln(8·R_fix/a) − 1)): y2 := solve(eq, p)[2]: :

eq := (delta3 = a^2/(4·R_fix)·(2·ln(8·R_fix/a) − 1)):
y3 := solve(eq, p)[2]:
eq := (delta4 = a^2/(4·R_fix)·(2·ln(8·R_fix/a) − 1)):
y4 := solve(eq, p)[2]:

eq := (delta5 = a^2/(4·R_fix)·(2·ln(8·R_fix/a) − 1)): y5 := solve(eq, p)[2]:

eq := (delta6 = a^2/(4·R_fix)·(2·ln(8·R_fix/a) − 1)): y6 := evalf(solve(eq, p))[2]:

eq := (delta7 = a^2/(4·R_fix)·(2·ln(8·R_fix/a) − 1)): y7 := evalf(solve(eq, p))[2]:

P := c1 + c2·delta + c3·δ^2 + c4·δ^3 + c5·δ^4 + c6·δ^5 + c7·δ^6:
```

```
delta := delta1 :
 eq1 := P = y1 :
 delta := delta2 :
 eq2 := P = y2 :
 delta := delta3 :
 eq3 := P = y3 :
 delta := delta4 :
 eq4 := P = y4 :
delta := delta5 :
 eq5 := P = y5 :
 delta := delta6 :
 eq6 := P = y6 :
 delta := delta7 :
 eq7 := P = y7 :


delta :='delta':

assign(solve([eq1, eq2, eq3, eq4, eq5, eq6, eq7]))

P
```

$$1.478243983 \times 10^6\,\delta^6 - 3.240015465 \times 10^6\,\delta^5 + 2.905172188 \times 10^6\,\delta^4 - 1.412974889 \times 10^6\,\delta^3 + 496412.9907\,\delta^2 + 177851.3311\,\delta - 0.00001192623719$$

```
plot(P, delta = 0 ..0.6)
```

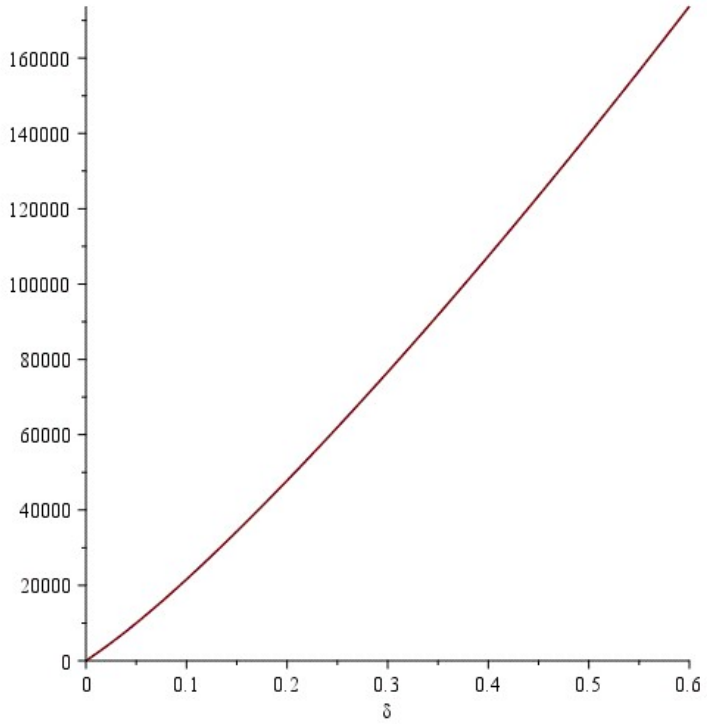


```
c := 15 : w := 30 : x1 := w : x2 := 2·w : x3 := 3·w : x4 := 4·w : x5 := 5·w : x6 := 6·w : x7 := 7·w :
    x8 := 8·w : ytop := 18.57 : ybot := 15.1 : ytop2 := 25.5 : ybot2 := 22.03 :
```

$$x1t := \cos(\text{theta})\cdot x1 + \sin(\text{theta})\cdot ytop :$$
$$x2t := \cos(\text{theta})\cdot x2 - \sin(\text{theta})\cdot ybot :$$
$$x3t := \cos(\text{theta})\cdot x3 + \sin(\text{theta})\cdot ytop :$$
$$x4t := \cos(\text{theta})\cdot x4 - \sin(\text{theta})\cdot ybot :$$
$$x5t := \cos(\text{theta})\cdot x5 + \sin(\text{theta})\cdot ytop :$$
$$x6t := \cos(\text{theta})\cdot x6 - \sin(\text{theta})\cdot ybot :$$
$$x7t := \cos(\text{theta})\cdot x7 + \sin(\text{theta})\cdot ytop :$$
$$x8t := \cos(\text{theta})\cdot x8 - \sin(\text{theta})\cdot ybot :$$

$$y1t := \cos(\text{theta})\cdot ytop - \sin(\text{theta})\cdot x1 :$$
$$y2t := \cos(\text{theta})\cdot ybot + \sin(\text{theta})\cdot x2 :$$
$$y3t := \cos(\text{theta})\cdot ytop - \sin(\text{theta})\cdot x3 :$$
$$y4t := \cos(\text{theta})\cdot ybot + \sin(\text{theta})\cdot x4 :$$
$$y5t := \cos(\text{theta})\cdot ytop - \sin(\text{theta})\cdot x5 :$$
$$y6t := \cos(\text{theta})\cdot ybot + \sin(\text{theta})\cdot x6 :$$
$$y7t := \cos(\text{theta})\cdot ytop - \sin(\text{theta})\cdot x7 :$$
$$y8t := \cos(\text{theta})\cdot ybot + \sin(\text{theta})\cdot x8 :$$

$$delta1 := 2R - \text{sqrt}\left((y2t - y1t)^2 + (x2t - x1t)^2\right) :$$
$$delta3 := 2R - \text{sqrt}\left((y4t - y3t)^2 + (x4t - x3t)^2\right) :$$
$$delta5 := 2R - \text{sqrt}\left((y6t - y5t)^2 + (x6t - x5t)^2\right) :$$
$$delta7 := 2R - \text{sqrt}\left((y8t - y7t)^2 + (x8t - x7t)^2\right) :$$

$$x1t2 := \cos(\text{theta})\cdot x1 + \sin(\text{theta})\cdot ytop2 :$$
$$x2t2 := \cos(\text{theta})\cdot x2 - \sin(\text{theta})\cdot ybot2 :$$
$$x3t2 := \cos(\text{theta})\cdot x3 + \sin(\text{theta})\cdot ytop2 :$$
$$x4t2 := \cos(\text{theta})\cdot x4 - \sin(\text{theta})\cdot ybot2 :$$
$$x5t2 := \cos(\text{theta})\cdot x5 + \sin(\text{theta})\cdot ytop2 :$$
$$x6t2 := \cos(\text{theta})\cdot x6 - \sin(\text{theta})\cdot ybot2 :$$
$$x7t2 := \cos(\text{theta})\cdot x7 + \sin(\text{theta})\cdot ytop2 :$$
$$x8t2 := \cos(\text{theta})\cdot x8 - \sin(\text{theta})\cdot ybot2 :$$

$$y1t2 := \cos(\text{theta})\cdot ytop2 - \sin(\text{theta})\cdot x1 :$$
$$y2t2 := \cos(\text{theta})\cdot ybot2 + \sin(\text{theta})\cdot x2 :$$
$$y3t2 := \cos(\text{theta})\cdot ytop2 - \sin(\text{theta})\cdot x3 :$$
$$y4t2 := \cos(\text{theta})\cdot ybot2 + \sin(\text{theta})\cdot x4 :$$
$$y5t2 := \cos(\text{theta})\cdot ytop2 - \sin(\text{theta})\cdot x5 :$$
$$y6t2 := \cos(\text{theta})\cdot ybot2 + \sin(\text{theta})\cdot x6 :$$
$$y7t2 := \cos(\text{theta})\cdot ytop2 - \sin(\text{theta})\cdot x7 :$$
$$y8t2 := \cos(\text{theta})\cdot ybot2 + \sin(\text{theta})\cdot x8 :$$

$$delta12 := 2R - \text{sqrt}\left((y2t2 - y1t2)^2 + (x2t2 - x1t2)^2\right) :$$
$$delta32 := 2R - \text{sqrt}\left((y4t2 - y3t2)^2 + (x4t2 - x3t2)^2\right) :$$
$$delta52 := 2R - \text{sqrt}\left((y6t2 - y5t2)^2 + (x6t2 - x5t2)^2\right) :$$
$$delta72 := 2R - \text{sqrt}\left((y8t2 - y7t2)^2 + (x8t2 - x7t2)^2\right);$$

$$plot\left([delta1, delta3, delta5, delta7, delta12, delta32, delta52, delta72], \text{theta} = 0 .. \frac{1\cdot \text{Pi}}{180}, gridlines = true, labels = [\text{"Compresion (mm)"}, \text{"}\theta\text{"}]\right)$$

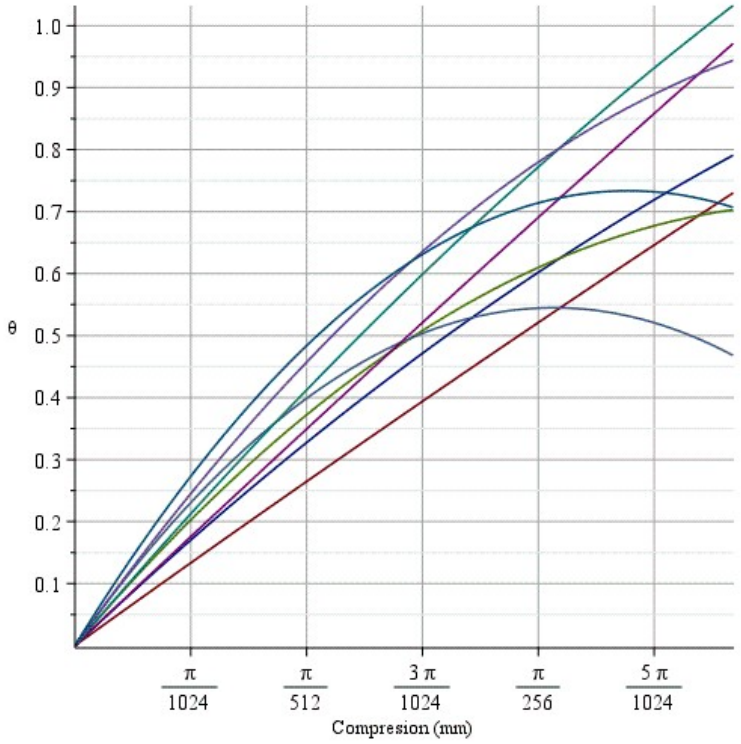

$$theta1 := \arctan\left(\frac{(y2t - y1t)}{(x2t - x1t)}\right):$$

$$theta3 := \arctan\left(\frac{(y4t - y3t)}{(x4t - x3t)}\right):$$

$$theta5 := \arctan\left(\frac{(y6t - y5t)}{(x6t - x5t)}\right):$$

$$theta7 := \arctan\left(\frac{(y8t - y7t)}{(x8t - x7t)}\right):$$

$$theta12 := \arctan\left(\frac{(y2t2 - y1t2)}{(x2t2 - x1t2)}\right):$$

$$theta32 := \arctan\left(\frac{(y4t2 - y3t2)}{(x4t2 - x3t2)}\right):$$

$$theta52 := \arctan\left(\frac{(y6t2 - y5t2)}{(x6t2 - x5t2)}\right):$$

$$theta72 := \arctan\left(\frac{(y8t2 - y7t2)}{(x8t2 - x7t2)}\right):$$

$$plot\left([theta1, theta3, theta5, theta7, theta12, theta32, theta52, theta72], \text{theta} = 0 .. \frac{1 \cdot \text{Pi}}{180}, gridlines = true, labels = [\text{"θ"}, \text{"Local angle"}]\right)$$

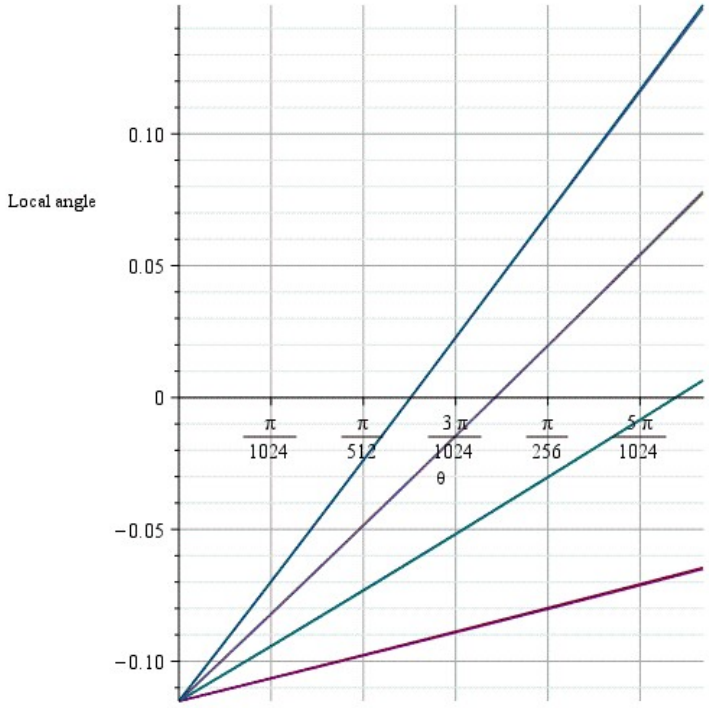

delta := *delta1* : *P11* := *P*·(*f*·cos(*theta1*) + sin(*theta1*)) :

delta := *delta12* : *P12* := *P*·(*f*·cos(*theta12*) + sin(*theta12*)) : *P1* := *P11* + *P12* :

delta := *delta3* :

P21 := *P*·(*f*·cos(*theta3*) + sin(*theta3*)) : delta := *delta3* :

P22 := *P*·(*f*·cos(*theta32*) + sin(*theta32*)) : *P2* := *P21* + *P22* :

delta := *delta5* :

P31 := *P*·(*f*·cos(*theta5*) + sin(*theta5*)) :

delta := *delta52* :

P32 := *P*·(*f*·cos(*theta52*) + sin(*theta52*)) : *P3* := *P31* + *P32* :

delta := *delta7* :

P41 := *P*·(*f*·cos(*theta7*) + sin(*theta7*)) :

delta := *delta72* :

P42 := *P*·(*f*·cos(*theta72*) + sin(*theta72*)) : *P4* := *P41* + *P42* : delta :='delta':

M := *P1*·(*x2* − *c* + 30) + *P2*·(*x4* − *c* + 30) + *P3*·(*x6* − *c* + 30) + *P4*·(*x8* − *c* + 30) :

$$\text{theta} := \arctan\left(\frac{u}{450}\right) :$$

$$plot\left(\frac{M}{900}\cdot 4,\ u = 0\ ..10,\ gridlines = true,\ labels = [\text{"u"},\ \text{"Force on top (N)"}]\right)$$

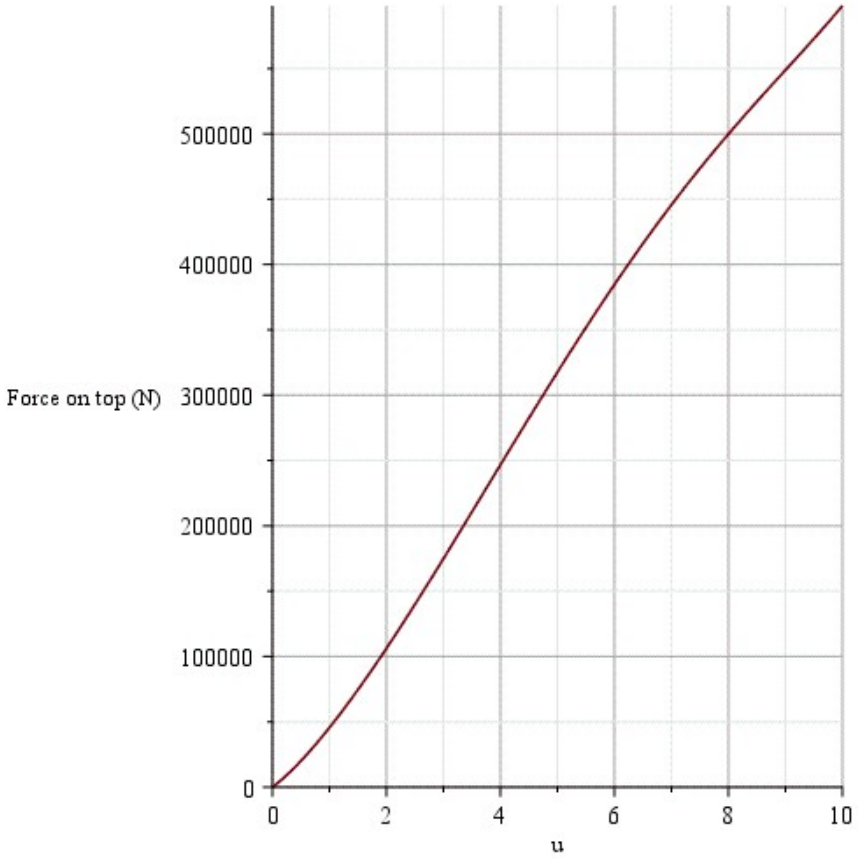

plot([*P1*, *P2*, *P3*, *P4*, 13698, 27397], *u* = 0 ..3, *gridlines* = *true*, *labels* = ["u", "Forces in each tab"])

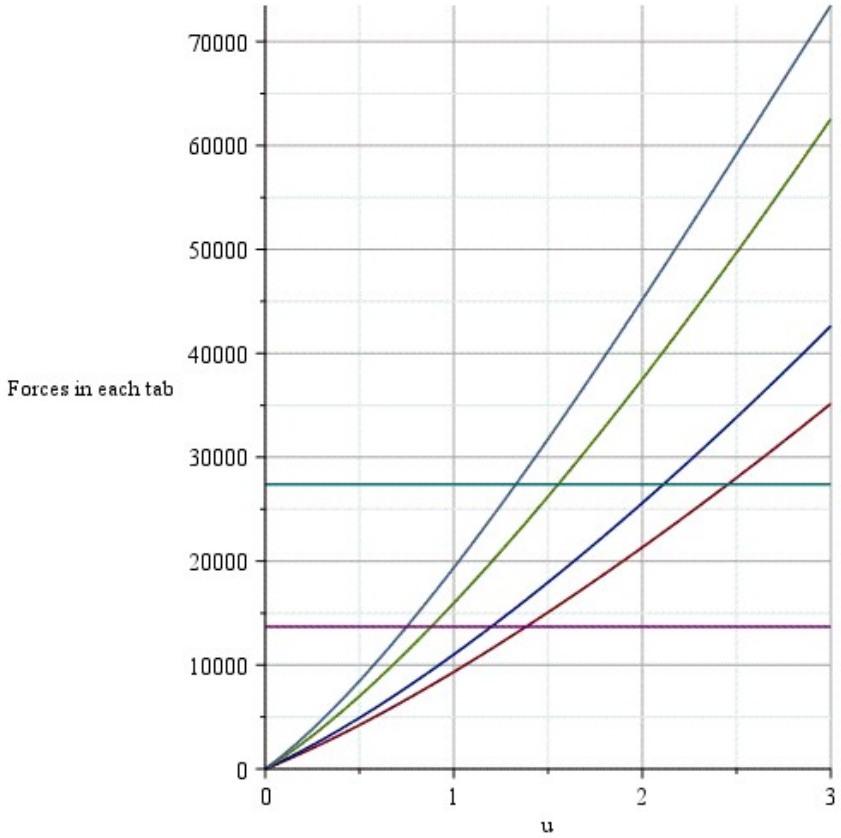

$c\_1 := -2.45; c\_2 := -2.1; c\_3 := -1.55; c\_4 := -0.75;$

$tab1 := P1 \cdot (x2 - c + 30) - P1 \cdot (x2 - c + 30)\text{Heaviside}(c\_1 + u):$
$tab2 := P2 \cdot (x4 - c + 30) - P2 \cdot (x4 - c + 30)\text{Heaviside}(c\_2 + u):$
$tab3 := P3 \cdot (x6 - c + 30) - P3 \cdot (x6 - c + 30) \cdot \text{Heaviside}(c\_3 + u):$
$tab4 := P4 \cdot (x8 - c + 30) - P4 \cdot (x8 - c + 30)\text{Heaviside}(c\_4 + u):$
$M := tab1 + tab2 + tab3 + tab4:$

$$plot\left(\frac{M}{900} \cdot 4, u = 0..5, gridlines = true, labels = [\text{"u"}, \text{"Force on top (N)"}]\right)$$

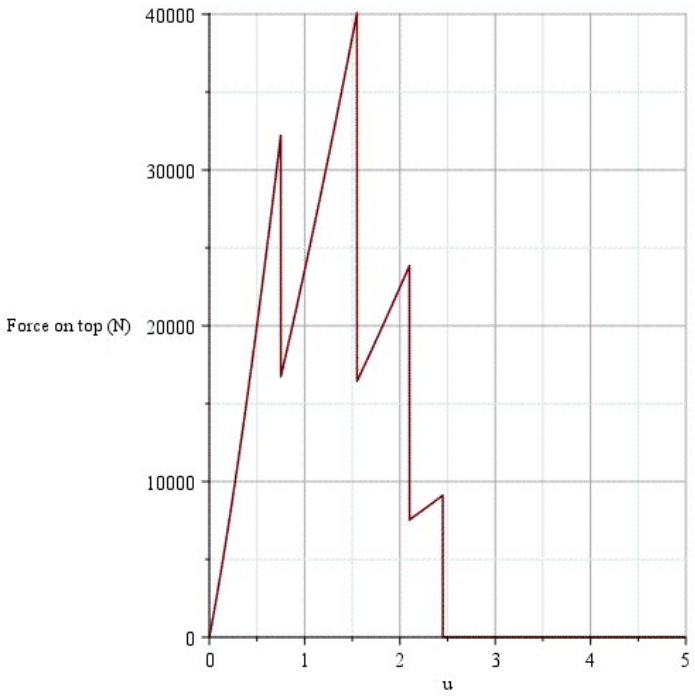

$P\_max := 27397$:

$hPl := 11 \cdot (0.025)$:

$uPl1 := \frac{hPl}{30} \cdot 450$:

$uPl2 := \frac{hPl}{90} \cdot 450$:

$uPl3 := \frac{hPl}{150} \cdot 450$:

$uPl4 := \frac{hPl}{230} \cdot 450$:

$$tab1 := P1 \cdot (x2 - c + 30) - \left(P1 - P\_max \cdot \left(1 - \frac{u + c\_1}{uPl1}\right)\right) \cdot (x2 - c + 30)\,\text{Heaviside}(c\_1 + u) - \left(P\_max \cdot \left(1 - \frac{u + c\_1}{uPl1}\right)\right) \cdot (x2 - c + 30)\,\text{Heaviside}(c\_1 + u - uPl1) :$$

$$tab2 := P2 \cdot (x4 - c + 30) - \left(P2 - P\_max \cdot \left(1 - \frac{u + c\_2}{uPl2}\right)\right) \cdot (x4 - c + 30)\,\text{Heaviside}(c\_2 + u) - \left(P\_max \cdot \left(1 - \frac{u + c\_2}{uPl2}\right)\right) \cdot (x4 - c + 30)\,\text{Heaviside}(c\_2 + u - uPl2) :$$

$$tab3 := P3 \cdot (x6 - c + 30) - \left(P3 - P\_max \cdot \left(1 - \frac{u + c\_3}{uPl3}\right)\right) \cdot (x6 - c + 30) \cdot \text{Heaviside}(c\_3 + u) - \left(P\_max \cdot \left(1 - \frac{u + c\_3}{uPl3}\right)\right) \cdot (x6 - c + 30) \cdot \text{Heaviside}(c\_3 + u - uPl3) :$$

$$tab4 := P4 \cdot (x8 - c + 30) - \left(P4 - \frac{1}{2} \cdot P\_max \cdot \left(1 - \frac{u + c\_4}{uPl4}\right)\right) \cdot (x8 - c + 30)\,\text{Heaviside}(c\_4 + u) - \left(\frac{1}{2} \cdot P\_max \cdot \left(1 - \frac{u + c\_4}{uPl4}\right)\right) \cdot (x8 - c + 30)\,\text{Heaviside}(c\_4 + u - uPl4) :$$

$M := (tab1 + tab2 + tab3 + tab4)$:

plot([*tab1*, *tab2*, *tab3*, *tab4*, *M*], *u* = 0 ..5, *y* = 0 ..13000000, *gridlines* = *true*, *labels* = ["Top Displacement (mm)", "Moment (Nmm)"], *legend* = ["Tab 1", "Tab 2", "Tab 3", "Tab 4", "Total"])

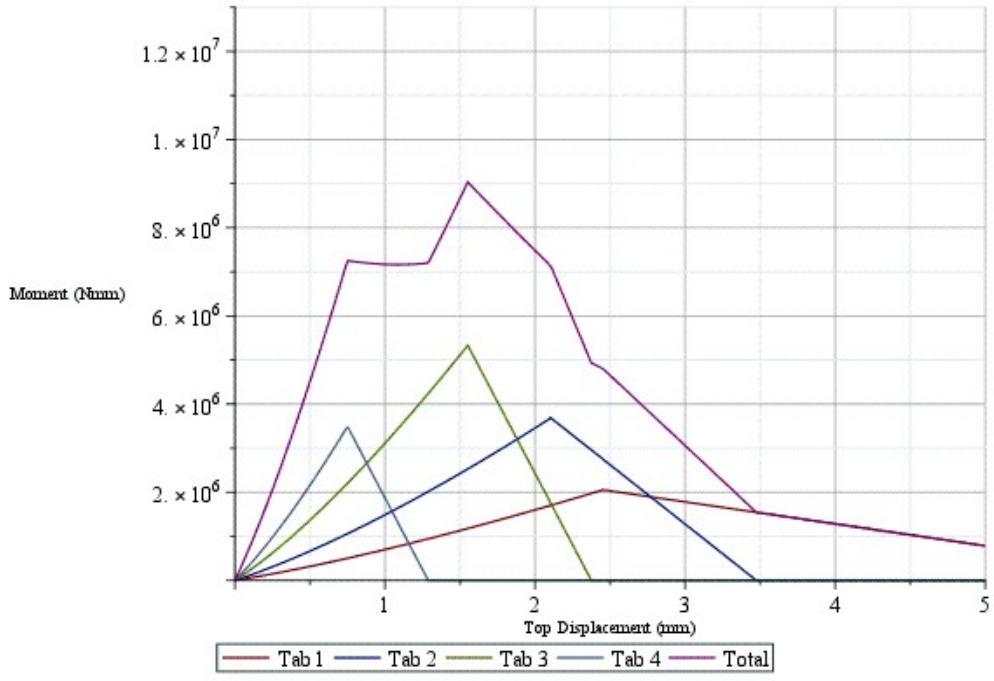

$$plot\left(\frac{M}{900}\cdot 4,\ u = 0\ ..6,\ gridlines = true,\ labels = [\text{"Top Displacement (mm)"},\ \text{"Force (N)"}]\right)$$

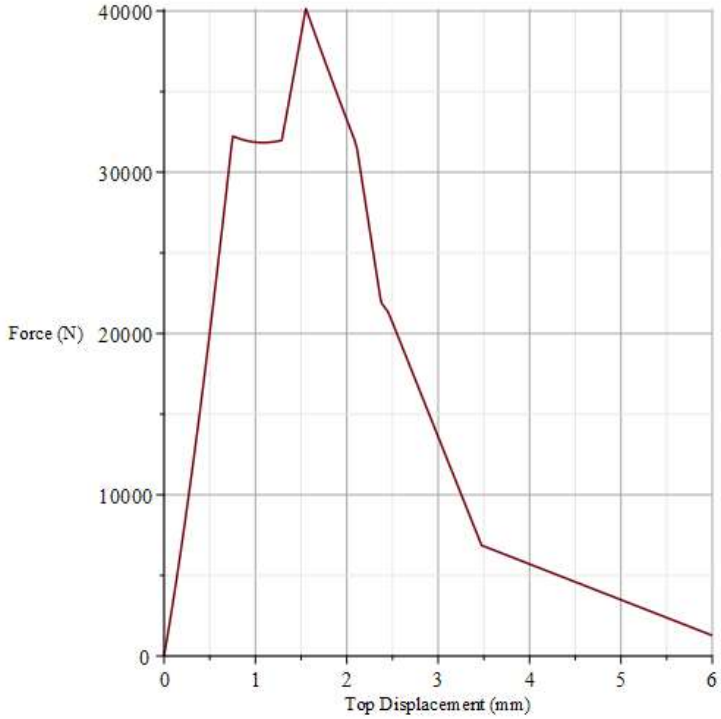

Appendix D Bending resistance calculation

BEAM INPUT

Δh	=	0.05	mm	neutral axis steps
l_1	=	50	mm	distance between force and support
h	=	40	mm	height of the beam
n	=	100		number of layers (start from bottom)
t	=	0.4	mm	thickness of layer
b	=	40	mm	width of the beam
Δκ	=	1.00E-06	mm^{-1}	curvature steps
n.a.	=	20.00	mm	**initial** location neutral axis from bottom

MATERIALS		E N/mm^2	f_1 N/mm^2	ε_1 [-]	f_2 N/mm^2	ε_2 [-]	f_3 N/mm^2	ε_3 [-]	ρ kg/m^3
Concrete	+	45000	8.9	0.000198	14.8	0.00263	0	0.01	2400
	-	45000	227	0.005044	130	0.0035	0	0.05	
SHCC	+	18000	3	0.000167	3.4	0.015			2000
	-	18000	44	0.002444	36	0.0035			
Steel	+	200000	550	0.00275	650	0.05			7850
	-	200000	550	0.00275	650	0.05			

LAYER SPECS	t mm	E N/mm^2	ρ kg/m^3
Top layer	40	45000	2400
Bottom layer	0	18000	2000
Web (U-shape)	0	18000	2000

Points	170
RUN	
Progress	100.0%

DRYING SHRINKAGE

drying time after curing (days): NONE

CRACK INPUT

	Input?	l_{tot} mm	$w_{c,2}$ mm	f_2 N/mm^2	ε_2 [-]	$w_{c,3(NO)}$ mm	$f_{3(NO)}$ N/mm^2	$\varepsilon_{3(NO)}$ [-]
Concrete	NO	~~62.5~~	~~0.09~~	~~12.3~~	~~0.00407~~	~~0.23~~	0	~~0.00631~~
SHCC	NO	5	0.09	3.4	~~0.033~~	0.11	2.8	~~0.037~~

REINFORCEMENT		Bottom		Top		
ϕ	=	8	mm	8	mm	bar diameter
c	=	31	mm	38	mm	concrete cover
#	=	0		0		number of bars
y	=	35	mm	-2	mm	location bar centre

DEFLECTION

test type		3-point		type of bending test
$\#_{ext}$	=	10		segments (#LE) in load-support region
b_{seg}	<	4.99	mm	width of each segment

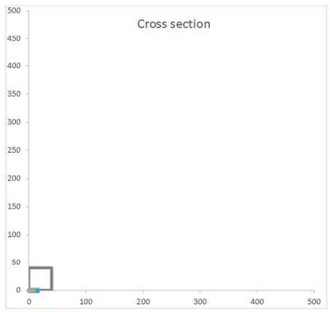

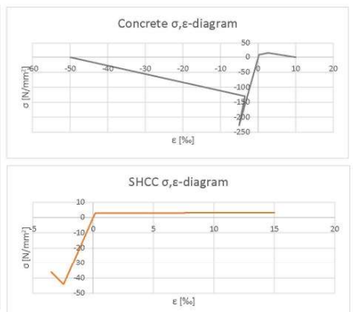

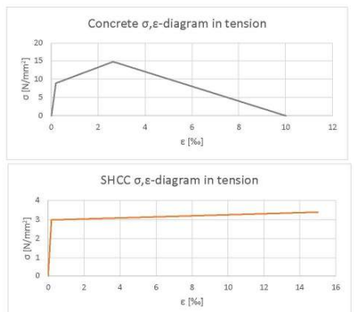

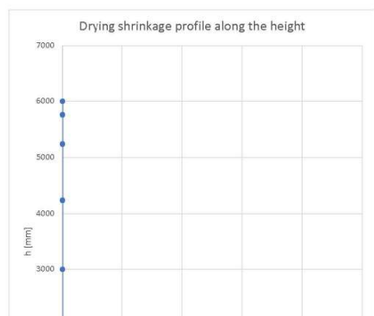

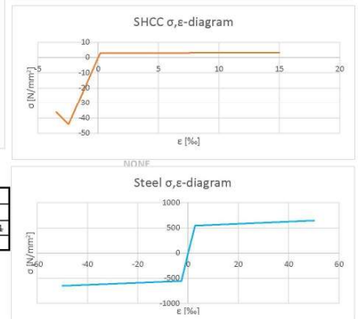

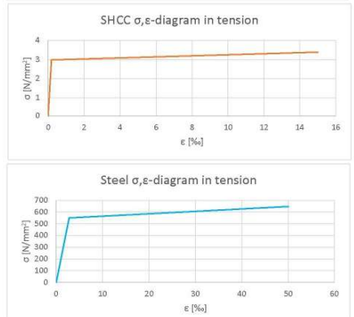

		1	2	3	4	5	6	7	8	9	10	11	12	13	14	15	16	17	18	19	20	21	22	23	24	25	26	27	28	29	30	31	32	33	34	35	36	37	38
N_{steel}		0	0	0	0	0	0	0	0	0	0	0	0	0	0	0	0	0	0	0	0	0	0	0	0	0	0	0	0	0	0	0	0	0	0	0	0	0	0
δ	6.11E-06	0.0069172	0.006566	0.006429	0.00644	0.00651	0.006628	0.00678	0.006917	0.007155	0.007317	0.007572	0.007759	0.00795	0.008204	0.008404	0.00861	0.008813	0.009019	0.009223	0.009547	0.009749	0.009911	0.010123	0.010324	0.010651	0.010816	0.0111	0.01126	0.011589	0.011819	0.012041	0.012213	0.012473	0.012684	0.012984	0.013225	0.013447	0.013736	0.014007
n.a.	20	20	20	20.00676	20.0824	20.2049	20.36204	20.53704	20.72321	20.91543	21.11177	21.30977	21.50144	21.69375	21.881	22.06225	22.23993	22.42099	22.58032	22.74532	22.90246	23.05563	23.20414	23.34742	23.49081	23.62004	23.75932	23.88502	24.00863	24.1289	24.24535	24.36009	24.4697	24.57793	24.68118	24.78301	24.88177	24.97751	25.07111	25.16337
M	0	79992	89576	99093	107516	115015	121685	127748	133292	138406	142944	147465	151633	155485	159144	162656	165984	169112	172205	175136	177976	180698	183365	185952	188427	190984	193244	195544	197797	200023	202217	204332	206429	208481	210540	212535	214496	216446	218347	220269
F	0	3203.8261	3587.954	3969.397	4306.992	4607.554	4874.888	5117.894	5340.099	5545.069	5726.952	5908.155	6075.209	6229.598	6376.251	6517.012	6650.399	6775.77	6899.738	7017.213	7131.041	7240.139	7347.033	7450.72	7549.918	7652.403	7742.984	7835.169	7925.469	8014.688	8102.624	8187.393	8271.441	8353.686	8436.211	8516.171	8594.768	8672.924	8749.117	8826.151
$\Sigma N_{[min]}$	0	0	0	-5	19	-18	-6	22	13	7	3	2	9	8	13	21	25	25	-11	-18	-9	-4	2	9	9	27	15	35	-34	-30	-25	-23	-15	-13	-5	-3	2	7	11	13
$\Sigma N_{[max]}$	0			32	-20	22	36	-22	-34	-38	-38	-48	-45	-44	-38	-35	-31	-41	48	42	54	59	-65	-58	-59	-38	-55	-37	38	44	51	55	63	66	72	79	-79	-75	-75	-71	
κ	0	8.333E-06	9.33E-06	1.03E-05	1.13E-05	1.23E-05	1.33E-05	1.43E-05	1.53E-05	1.63E-05	1.73E-05	1.83E-05	1.93E-05	2.03E-05	2.13E-05	2.23E-05	2.33E-05	2.43E-05	2.53E-05	2.63E-05	2.73E-05	2.83E-05	2.93E-05	3.03E-05	3.13E-05	3.23E-05	3.33E-05	3.43E-05	3.53E-05	3.63E-05	3.73E-05	3.83E-05	3.93E-05	4.03E-05	4.13E-05	4.23E-05	4.33E-05	4.43E-05	4.53E-05	4.63E-05
Start	L.E.	56.53834	56.53834	56.53834	56.53834	56.53834	56.53834	56.53834	56.53834	56.53834	56.53834	56.53834	56.53834	56.53834	56.53834	56.53834	56.53834	56.53834	56.53834	56.53834	56.53834	56.53834	56.53834	56.53834	56.53834	56.53834	56.53834	56.53834	56.53834	56.53834	56.53834	56.53834	56.53834	56.53834	56.53834	56.53834	56.53834	56.53834	56.53834

Layer	y-location	drying ε
1	0.2	0
2	0.6	0
3	1	0
4	1.4	0
5	1.8	0
6	2.2	0
7	2.6	0
8	3	0
9	3.4	0
10	3.8	0
11	4.2	0
12	4.6	0
13	5	0
14	5.4	0
15	5.8	0
16	6.2	0
17	6.6	0
18	7	0
19	7.4	0
20	7.8	0
21	8.2	0
22	8.6	0
23	9	0
24	9.4	0
25	9.8	0
26	10.2	0
27	10.6	0
28	11	0
29	11.4	0
30	11.8	0
31	12.2	0
32	12.6	0
33	13	0
34	13.4	0
35	13.8	0
36	14.2	0
37	14.6	0
38	15	0
39	15.4	0
40	15.8	0
41	16.2	0
42	16.6	0
43	17	0
44	17.4	0
45	17.8	0
46	18.2	0
47	18.6	0
48	19	0
49	19.4	0
50	19.8	0
51	20.2	0
52	20.6	0
53	21	0
54	21.4	0
55	21.8	0
56	22.2	0